Patterning and characterization of graphene nano-ribbon by electron beam induced etching

Sébastien Linas

Université de Toulouse

THÈSE

En vue de l'obtention du

DOCTORAT DE L'UNIVERSITÉ DE TOULOUSE

Délivré par :

Université Toulouse 3 Paul Sabatier (UT3 Paul Sabatier)

Présentée et soutenue par :
LINAS Sébastien

le mercredi 19 décembre 2012

Titre :

Fabrication et caractérisation de nano-rubans de graphène
par gravure électronique directe.

École doctorale et discipline ou spécialité :

ED SDM : Nano-physique, nano-composants, nano-mesures - COP 00

Unité de recherche :

Centre d'Elaboration de Matériaux et d'Etudes Structurales. CEMES CNRS UPR8011

Directeur(s) de Thèse :

DUJARDIN Erik

Jury :

BANHART Florian (IPCMS, Strasbourg), Rapporteur
BOUCHIAT Vincent (Inst. Néel, Grenoble), Rapporteur

SERP Philippe (LCC, Toulouse), Président

MLAYAH Adnen (CEMES, Toulouse), Examinateur
PAILLET Matthieu (L2C-UM2, Montpellier), Examinateur

Remerciements.

Mes premiers remerciements vont à mon amoureuse Céline et notre Paul qui ont supporté mes absences ces trois années durant. Je leur doit beaucoup, ce travail n'aurait pas abouti sans eux.

Mes premiers remerciements professionnels vont à mon directeur de thèse, monsieur Dujardin Erik qui m'a permis d'effectuer cette thèse en me recrutant et en me fournissant tout au long de ce travail un soutien technique nécessaire à l'aboutissement de ce travail. Sous sa direction j'ai pu me familiariser avec de nombreuses techniques de caractérisation ainsi qu'acquérir rigueur et autonomie nécessaires au métier de chercheur.

Je tiens à remercier chaleureusement les membres du jury qui ont évalué ce travail. Messieurs Banhart Florian et Bouchiat Vincent pour leur rapport, monsieur Serp philippe, président de ce jury ainsi que messieurs Mlayah Adnen et Paillet Matthieu en tant qu'examinateurs. Leur commentaires et remarques ont permis d'améliorer la qualité de ce manuscrit.

Je souhaite également remercier toutes les personnes qui font tourner le laboratoire sans pour autant être mis en avant. Merci à tous les ingénieurs de recherche, d'étude et techniciens, et notamment les personnes qui m'ont assisté dans mon travail, Philippe Salles pour le FIB, Antoine Zwick, Frédéric Neumayer et Sébastien Moyano pour le service spectroscopie, Florent Houdellier et Sébastien Joulié pour la MET, Laure Noé pour le four, Christophe Deshayes pour le MEB, Christine Viala et bien sur Isabelle Labau, bibliothécaire émérite. Je tiens également à remercier ceux qui contribuent à l'entretien des locaux.

Remerciements.

Je souhaite également remercier messieurs David Martrou (pour lll également) et Sébastien Gauthier qui m'ont aidé, six mois durant à me familiariser avec l'AFM non contact et l'ultra haut vide. Merci à monsieur Ondarçuhu Thierry pour son aide sur le mouillage en AFM. Je remercie également monsieur Gatel Cristophe pour ses routines de traitement d'images TEM.

Je remercie spécialement Antoine Hinaut et Laure Fabié qui ont longuement partagé un bureau avec moi. Je remercie Gurunatha Kargal-Laxminarayana dont j'ai beaucoup apprécié les conversations. Merci également aux camarades Olivier Couturaud dont j'ai faillit boire les paroles et Miguel Rubio-Roy. Je remercie Marc Nuñez que j'ai co-encadré deux fois lors de ses stages et qui continue le travail au quel j'ai participé trois ans durant. Merci également à Alexandre ainsi qu'à toutes les personnes que j'ai rencontré au cours de mon séjour au laboratoire.

Sébastien Linas

Acronyms.

AFM	Atomic force microscopy
2D	Two dimensions
A_0	Free amplitude
a-C	Amorphous carbon
AGNR	Armchair graphene nano-ribbon (GNR with armchair edges)
AM-AFM	Amplitude modulation atomic force microscopy
A_{SP}	Amplitude set point
CNT	Carbon nano-tube
CVD	Chemical vapor deposition
DFT	Density functional theory
e-beam	Electron beam
EBIE	Electron beam induced etching
FET	Field-emission transistor
FIB	Focused ion beam
FLG	Few layer graphene
GIS	Gas injection system
GL	Graphene layer
GNR	Graphene nano-ribbon
HBC	Hexabenzocoronene

Acronyms.

HRTEM	High resolution transmission electron microscopy
IPA	Isopropanol
MWCNT	Multiwall carbon nano-tube
NC-AFM	Non contact atomic force microscopy
NEMS	Nanoelectro-mechanical system
PMMA	Polymethyl methacrylate
PmPV	Poly(m-phenylenevinylene-co-2,5-dioctoxy-p-phenylenevinylene)
RH	Relative humidity
RMS	Root mean square
RT	Room temperature
SACTEM	Spherical aberration corrected transmission electron microscopy
SAED	Selected area electron diffraction
SEM	Scanning electron microscopy
STM	Scanning tunneling spectroscopy
SWCNT	Single walled carbon nano-tube
TEM	Transmission electron microscopy
UHV	Ultra high vacuum
VLSI	Very large scale integration
ZGNR	Zig-zag graphene nano-ribbon (GNR with Zig-zag edges)

Table of content.

Table of content.

Table of content.

Table of content.

Introduction.

Etudié théoriquement depuis près d'un siècle et identifié expérimentalement depuis les années 1960 en microscopie électronique puis dans les années 1990 en microscopie en champ proche, le graphène a définitivement regagné de l'intérêt par la découverte en 2004 d'une méthode simple pour le déposer sur un substrat arbitraire. [1] Depuis huit ans, une vaste communauté s'est penchée sur l'exploration des méthodes de production, la caractérisation de ses propriétés et l'exploitation technologique du graphène. Parmi les domaines scientifiques variés dans lesquels le graphène est désormais considéré comme pertinent, citons, par exemple, l'analyse des acides nucléiques [2] pour la biolo-

Theoretically studied for almost one century and experimentally since the 60's by electron microscopists and in the 90's for near-field microscopists, graphene has definitely regained importance since the discovery in 2004 of a simple method to deposit it on an arbitrary substrate. [1] For eight years, a vast community has explored the production methods, characterization of its properties and technological applications of graphene. Among the scientific domains for which graphene is now considered as promising, one can cite the nucleic acid analysis [2] for biology or the use of its chemicals properties for ca-

gie ou l'utilisation de ses propriétés chimiques pour la catalyse. [3] Toutefois, ce sont les propriétés physiques du graphène qui sont les plus explorées à la fois pour la nouvelle science fondamentale à laquelle il donne accès et pour d'éventuelles applications qu'il rend envisageables. Sa quasi-transparence optique dans le visible [4], associée à sa conductivité élevée, en fait un bon candidat de remplacement de l'oxyde d'indium et d'étain (ITO) pour la fabrication d'électrodes transparentes, qui seraient de surcroit flexibles, de cellules photovoltaïques ou d'écrans à cristaux liquides. [5-8]

Les propriétés mécaniques du graphène sont comparables à celles du graphite mais l'épaisseur monoatomique du graphène le rend attractif comme matériau de renfort incorporé dans une matrice pour former des matériaux composites. [9, 10] Cette épaisseur ultime et sa robustesse en font aussi un matériau de choix comme substrat pour la microscopie électronique en transmission. [11-13] Enfin, la combinaison de ses propriétés optiques, mécaniques et électroniques permettent d'envisager son utilisation pour des dispositifs nano-électromécaniques. [14, 15]

Bien que le graphène soit considéré comme

talysis. [3] However, the physical properties of graphene are the most explored ones for the new fundamental scientific perspectives or for the potential applications it may enable. Its optical transparency in the visible range, [4] associated with a high conductivity make graphene a good candidate for the replacement of indium thin oxide (ITO) as transparent electrode in solar or liquid crystals cells, which could moreover be rendered flexible. [5-8]

The mechanical properties of graphene are similar those of graphite but the monoatomic thickness of graphene make it attractive as reinforcement material incorporated in a matrix to form composites materials. [9, 10] This ultimate thickness and mechanical robustness make graphene an ideal substrate for transmission electron microscopy. [11-13] Finally the combination of its optical, mechanical and electronic properties makes graphene a good candidate for nano-electro-mechanical devices. [14, 15]

Although graphene is considered as

un matériau propice aux applications en micro et nanoélectronique, la fabrication de composants comme des transistors à effet de champ, requiert qu'une bande interdite soit ouverte dans la dispersion linéaire et continue de ce semi-métal à gap nul. Plusieurs voies sont envisageables pour ouvrir un tel gap et parmi celles-ci, nous nous sommes intéressés au confinement latéral du graphène. Il a été montré théoriquement que lorsque le graphène est confiné en forme de ruban, un gap peu être ouvert dans lequel des états discrets peuvent subsister qui sont alors essentiellement délocalisés sur les bords du ruban. Le transport électronique dans les nanorubans de graphène est donc extrêmement sensible à l'état des bords de graphène, de sorte que lors de la gravure il est essentiel de préserver une grande qualité cristallographique de ces bords, pour exploiter cette propriété du graphène confiné. Les techniques de gravures ioniques comme la gravure par plasma à oxygène effectuée après une étape de lithographie électronique ou la gravure directe par faisceau d'ions focalisés causent d'importants dégâts dans la structure du graphène. [16, 17] A l'inverse, il a été montré que la gravure électronique [18-21] du graphène à haute tension d'accélération dans un microscope

a material suited for applications in micro and nano-electronics, fabrication of devices, such as field-effect transistors, require a band gap to be opened in the dispersion band of graphene. Several techniques have been explored to open such a gap, among which we considered the lateral confinement of graphene. It has been theoretically shown that when graphene is patterned in shape of graphene nanoribbons (GNR), a gap can be opened inside which discrete states can survive and are essentially delocalized on the edges of the GNRs. The electronic transport inside GNRs is thus extremely sensitive to the edges states. The ribbon etching technique should preserve the crystallinity of the material and of its edges to exploit the properties of the confined graphene. Patterning techniques using ions like oxygen plasma preceded by an electron beam (e-beam) lithography step or the direct etching by a focused ion beam create damages in the structure of graphene. [16, 17] On the contrary, it has been shown that the e-beam etching of graphene [18-21] at high acceleration volt-

électronique à transmission (MET) a produit des bords de découpe droits à l 'échelle atomique et peu endommagés. [19, 21] Cependant la forme de découpe est difficile à contrôler et le MET impose une configuration suspendue difficilement compatible avec des dispositifs de mesure de transport électronique.

L'objectif de ce travail est la mise au point d'une méthodologie de gravure permettant une structuration multi-échelle, du micromètre à l'échelle atomique, produisant des formes arbitraires tout en limitant l'amorphisation et la contamination du graphène. Un objectif en découlant est la caractérisation structurale du graphène pour mesurer la qualité des gravures. La technique de gravure développée ici sera appliquée sur du graphène déposé sur un substrat et contacté par des électrodes métalliques en vue de mesures de transport électronique. Au cours du travail décrit dans ce manuscrit, nous montrerons que la gravure par un faisceau électronique focalisé de microscope électronique à balayage assistée par la présence de vapeur d'eau permet d'associer la qualité de gravure des phénomènes observés en MET, tout en gardant un contrôle sur la forme de gravure.

Le premier chapitre de ce manuscrit pré-

ages in a transmission electron microscope (TEM) produces well ordered and atomically smooths edges. [19, 21] However, the shape of the etched patterns is difficult to control and the TEM imposes a suspended configuration hardly compatible with electric transport measurement devices.

The aim of this work is to develop an etching technique allowing a multiscale structuration of graphene from micrometer to the atomic scale producing an arbitrary shape while limiting graphene contamination. A subsequent objective is the structural characterization of graphene to assess the quality of the etching. The etching technique developed here will be applied to graphene deposited on a substrate and contacted by metallic electrodes for electronic measurements. In this manuscript we will show that the etching by a focalized electron beam of a scanning electron microscope assisted by the presence of water vapor allows to associate the quality of etching shown in TEM and keeping a control on the shape of the etching.

The first chapter of this manuscript

sente les caractéristiques essentielles du graphène et du graphène confiné. Les techniques permettant de l'identifier et de le caractériser sont d'abord présentées, puis les différentes méthodes de fabrication du graphène sont exposées: exfoliation micromécanique, croissance épitaxiale, voies de synthèse chimique de graphène et nanorubans de graphène. Finalement les principales techniques de gravure du graphène sont présentées, en soulignant leurs avantages et leurs inconvénients, avant de présenter la gravure directe par faisceau d'électrons (EBIE, Electron Beam Induced Etching).

Le deuxième chapitre rassemble les détails techniques des instruments et méthodes utilisés au cours de cette thèse.

Afin de mesurer l'amorphisation induite par la gravure du graphène, le troisième chapitre présente des développements techniques visant à identifier et caractériser le graphène ainsi que ses défauts. Dans une première partie, nous montrons que la dispersion des hauteurs apparente du mono-feuillet de graphène rapporté dans la littérature à partir de mesures en microscopie à force atomique (AFM) en conditions ambiante résulte de l'adsorption d'une couche d'eau et de

presents the essential characteristics of graphene and confined graphene. Techniques allowing to identify and characterize graphene are presented first, followed by several production techniques of graphene: micromechanical exfoliation, epitaxial growth and chemical synthesis of graphene and GNRs. Finally the main known techniques of etching of graphene are presented, underlining their advantages and disadvantages before presenting direct etching by a focalized electron beam (EBIE, *electron beam induced etching*).

The second chapter will expose technical details of instruments and methods used during this work.

In order to measure the amorphisation of the edges of graphene etched by EBIE, the third chapter presents developments of techniques aiming to identify and characterize graphene and its defects. In a first part, we will show that the dispersion of apparent thickness of monolayer graphene reported in the literature from atomic force microscopy (AFM) in ambient conditions is the results

conditions d'imagerie métastables qui conduisent à une surestimation de l'épaisseur du graphène de presque 1 nm. Nous montrerons que cet artefact peut être supprimé par l'ajustement des paramètres d'imagerie. La spectroscopie Raman permet de détecter les défauts présents dans le graphène cependant, l'intensité du signal pour le graphène à faible densité de défauts est quasi nulle. Pour diminuer le seuil de détectabilité des défauts du graphène par spectroscopie Raman, des colloïdes cristallins d'or sont déposés sur du graphène pour exalter l'intensité du signal des pics Raman du graphène. Cette exaltation offrirait ainsi une technique macroscopique et non destructive permettant de caractériser la qualité structurale du graphène. L'AFM non contact en modulation de fréquence est une technique à sonde locale permettant d'imager des surfaces isolantes ou des molécules sur surface isolante avec une résolution atomique ou submoléculaire. Pour le graphène sur substrat isolant, cette technique permettrait d'imager des bords découpé avec potentiellement une résolution atomique afin d'en caractériser les défauts. Les contraintes notamment au niveau du substrat imposées par cette technique sont présentées.

of the absorption of a water layer and metastable imaging conditions that lead to overestimation of the apparent thickness of graphene of about 1 nm. We will show that this artifact can be suppressed by adjusting the imaging conditions. Raman spectroscopy allows detecting defects in graphene but the signal intensity of the D-peak with a low density of defects is almost null. To reduce the detection threshold, gold crystalline colloids are deposited on graphene to enhance the intensity of its Raman signal. This exaltation would provide a non destructive and macroscopic technique for characterizing the structural quality of graphene. Non-contact AFM in frequency modulation is a local probe technique allowing to image insulating surfaces or molecules on insulating surface with an atomic or sub-molecular resolution. For graphene deposited on an insulating substrate, this technique would permit to image the etched edges with potentially an atomic resolution allowing a characterization of the edges quality. The constraints on the nature of the substrate imposed by this technique are pre-

Le quatrième chapitre présente la gravure directe du graphène par un faisceau électronique (EBIE) ainsi que l'étude structurale de graphène découpé par cette technique. Après avoir présenté les échantillons utilisés pour l'étude structurale – du graphène déposé sur des grilles de microscopie électronique en transmission – les différents paramètres influençant l'EBIE sont présentés avant d'étudier la gravure de ligne puis de rubans dans le graphène. La rugosité des bords de découpes simples ainsi que la zone amorphisée par les gravures sont étudiées par une imagerie à la résolution atomique avec un microscope électronique en transmission équipé d'un correcteur d'aberrations sphériques.

Le cinquième chapitre vise à appliquer la gravure du graphène par EBIE à du graphène déposé sur des substrats Si/SiO_2 en vue de mesures de transport électronique. Dans un premier temps, nous étudions les modifications entrainées par la présence d'un substrat sous le graphène. Ces modifications impliquent de suspendre le graphène localement. La gravure du graphène par EBIE révèle que, dans cette configuration, le graphène est contraint par des tensions mécaniques qui élargissent significative-

sented.

The fourth chapter presents the direct etching of graphene by an electron beam (EBIE) and a structural study of graphene cut by this technique. After presenting the samples used for the structural study - graphene deposited on TEM grids – different parameters influencing EBIE are presented before studying lines and ribbon etching in graphene. The edge roughness of the etched graphene and the amorphized area near the cut area are studied by atomic resolution imaging using a TEM equipped with a spherical aberration corrector.

The fifth chapter shows the application of EBIE to graphene deposited on Si/SiO_2 substrate for electronic transport measurement. In a first paragraph, a modification induced by the presence of the substrate under the graphene is evidenced. This modification implies that graphene must be locally suspended. Etching of graphene by EBIE reveals that in this configuration, graphene is under mechanical strains that enlarge signifi-

ment les traits de découpes. Après relaxation de ces contraintes des rubans de graphène monocouche contactés par des électrodes sont fabriqués avec succès.

cantly the width of the cuts. After releasing the strains, graphene nano-ribbons contacted by metallic electrodes are successfully fabricated.

References

[1] Novoselov, K. S.; Geim, A. K.; Morozov, S. V.; Jiang, D.; Zhang, Y.; Dubonos, S. V.; Grigorieva, I. V.; Firsov, A. A. "**Electric field effect in atomically thin carbon films**". *Science* (**2004**) *Vol. 306*, p. 666-669.

[2] Venkatesan, B. M.; Bashir, R. "**Nanopore sensors for nucleic acid analysis**". *Nat. Nanotechnol.* (**2011**) *Vol. 6*, p. 615-624.

[3] Machado, B. F.; Serp, P. "**Graphene-based materials for catalysis**". *Catal. Sci. Technol.* (**2012**) *Vol. 2*, p. 54-75.

[4] Nair, R. R.; Blake, P.; Grigorenko, A. N.; Novoselov, K. S.; Booth, T. J.; Stauber, T.; Peres, N. M. R.; Geim, A. K. "**Fine Structure Constant Defines Visual Transparency of Graphene**". *Science* (**2008**) *Vol. 320*, p. 1308.

[5] Eda, G.; Fanchini, G.; Chhowalla, M. "**Large-area ultrathin films of reduced graphene oxide as a transparent and flexible electronic material**". *Nat Nano* (**2008**) *Vol. 3*, p. 270-274.

[6] Blake, P.; Brimicombe, P. D.; Nair, R. R.; Booth, T. J.; Jiang, D.; Schedin, F.; Ponomarenko, L. A.; Morozov, S. V.; Gleeson, H. F.; Hill, E. W.; Geim, A. K.; Novoselov, K. S. "**Graphene-based liquid crystal device**". *Nano Lett.* (**2008**) *Vol. 8*, p. 1704-1708.

[7] Wang, X.; Zhi, L. J.; Mullen, K. "**Transparent, conductive graphene electrodes for dye-sensitized solar cells**". *Nano Lett.* (**2008**) *Vol. 8*, p. 323-327.

[8] Chen, J. H.; Ishigami, M.; Jang, C.; Hines, D. R.; Fuhrer, M. S.; Williams, E. D. "**Printed graphene circuits**". *Adv. Mater.* (**2007**) *Vol. 19*, p. 3623-3627.

[9] Lee, C.; Wei, X.; Kysar, J. W.; Hone, J. "**Measurement of the Elastic Properties and Intrinsic Strength of Monolayer Graphene**". *Science* (**2008**) *Vol. 321*, p. 385-388.

[10] Stankovich, S.; Dikin, D. A.; Dommett, G. H. B.; Kohlhaas, K. M.; Zimney, E. J.; Stach, E. A.; Piner, R. D.; Nguyen, S. T.; Ruoff, R. S. "**Graphene-based composite materials**". *Nature* (**2006**) *Vol. 442*, p. 282-286.

[11] Meyer, J. C.; Girit, C. O.; Crommie, M. F.; Zettl, A. "**Imaging and dynamics of light atoms and molecules on graphene**". *Nature* (**2008**) *Vol. 454*, p. 319-322.

[12] Nair, R. R.; Blake, P.; Blake, J. R.; Zan, R.; Anissimova, S.; Bangert, U.; Golovanov, A. P.; Morozov, S. V.; Geim, A. K.; Novoselov, K. S.; Latychevskaia, T. "**Graphene as a transparent conductive support for studying biological molecules by transmission electron microscopy**". *Appl. Phys. Lett.* (**2010**) *Vol. 97*, p. 3.

[13] Pantelic, R. S.; Meyer, J. C.; Kaiser, U.; Stahlberg, H. "**The application of graphene as a sample support in transmission electron microscopy**". *Solid State Communications* (**2012**) *Vol. 152*, p. 1375-1382.

[14] Bunch, J. S.; van der Zande, A. M.; Verbridge, S. S.; Frank, I. W.; Tanenbaum, D. M.; Parpia, J. M.; Craighead, H. G.; McEuen, P. L. "**Electromechanical resonators from graphene sheets**". *Science* (**2007**) *Vol. 315*, p. 490-493.

[15] Reserbat-Plantey, A.; Marty, L.; Arcizet, O.; Bendiab, N.; Bouchiat, V. "**A local optical probe for measuring motion and stress in a nanoelectromechanical system**". *Nat Nano* (**2012**) *Vol. 7*, p. 151-155.

[16] Han, M. Y.; Brant, J. C.; Kim, P. "**Electron Transport in Disordered Graphene Nanoribbons**". *Phys. Rev. Lett.* (**2010**) *Vol. 104*, p. 4.

[17] Dayen, J. F.; Mahmood, A.; Golubev, D. S.; Roch-Jeune, I.; Salles, P.; Dujardin, E. "**Side-gated transport in focused-ion-beam-fabricated multilayered graphene nanoribbons**". *Small* (**2008**) *Vol. 4*, p. 716-720.

[18] Albrecht, T. R.; Dovek, M. M.; Kirk, M. D.; Lang, C. A.; Quate, C. F.; Smith, D. P. E. "**Nanometer-scale hole formation on graphite using a scanning tunneling microscope**". *Appl. Phys. Lett.* (**1989**) *Vol. 55*, p. 1727-1729.

[19] Girit, C. O.; Meyer, J. C.; Erni, R.; Rossell, M. D.; Kisielowski, C.; Yang, L.; Park, C. H.; Crommie, M. F.; Cohen, M. L.; Louie, S. G.; Zettl, A. "**Graphene at the Edge: Stability and Dynamics**". *Science* (**2009**) *Vol. 323*, p. 1705-1708.

[20] Biro, L. P.; Lambin, P. "**Nanopatterning of graphene with crystallographic orientation control**". *Carbon* (**2011**) *Vol. 48*, p. 2677-2689.

[21] Song, B.; Schneider, G. F.; Xu, Q.; Pandraud, G.; Dekker, C.; Zandbergen, H. "**Atomic-Scale Electron-Beam Sculpting of Near-Defect-Free Graphene Nanostructures**". *Nano Letters* (**2011**) *Vol. 11*, p. 2247-2250.

CHAPTER 1

Properties, production and patterning of graphene.

Ce chapitre présente l'état de l'art sur l'identification, la production et la mise en forme du graphène jusqu'à l'échelle atomique à partir d'une sélection de travaux.

La première partie présente la structure cristallographique du graphène ainsi que la structure de bande qui en découle. Les propriétés électroniques et notamment la mobilité des porteurs de charge à température ambiante sont exposés. Les propriétés du graphène unidimensionnel, appelé nano ruban de graphène y sont traités, comme l'ouverture d'un gap par confinement latéral du graphène.

This chapter presents the state-of-the-art on the identification, production and patterning of graphene down to the atomic.

The first part describes the crystallographic structure of graphene and its band structure. The electronic properties including the charges carrier mobility at room temperature are presented. The properties of uni-dimensionnal graphene, graphene nanoribbon (GNR), are treated, with a particular emphasis on the opening of a gap by lateral confinement of graphene.

Dans une deuxième partie, des techniques permettant d'identifier le graphène et notamment le nombre de couches dont il est constitué sont exposées. La microscopie optique, est d'abord présentée, la nécessité de techniques d'identification plus fiables nous conduit ensuite à exposer la spectroscopie Raman qui outre une identification rapide du graphène, est riche en informations sur sa structure cristallographique. L'AFM, qui est une technique de microscopie à sonde locale peut aussi être utilisée pour l'identification du graphène. La MET propose différentes techniques pour identifier et caractériser le graphene, comme l'imagerie à faible grandissement, la diffraction électronique et l'imagerie à fort grandissement avec correcteur d'aberrations sphériques. La MET permet une identification univoque du graphène suspendu.

La troisième partie traitera de la production du graphène en commençant par la technique d'exfoliation micromécanique du graphite. Cette technique produit jusqu'à ce jour le graphène de meilleure qualité mais est difficilement adaptable à la production de masse. La sublimation de carbures ou la croissance CVD sur substrats métalliques sont ensuite présentées, ces techniques produisent du graphène à grande échelle. Finalement

In a second part, the techniques allowing to identify graphene and its number of are exposed. Optical microscopy and Raman spectroscopy provide a fast identification of graphene and a comprehensive information on its crystallographic structure. AFM, a local probe microscopy technique, is also used for identifying graphene. TEM comprises a number of techniques that allow the unambiguous identification of suspended graphene and its structural characterization: bright and dark field imaging, electron diffraction and high magnification imaging with aberrations correction. TEM.

The third part summarizes the methods of production of graphene. The micromechanical exfoliation technique produces until now the best quality graphene for electronic physics but is not suitable for large scale production. Carbides sublimation or CVD growth on metallic surfaces can produce large scale graphene. Finally the chemical synthesis

la synthèse chimique de nano graphène et de rubans de graphène présentant des bords atomiquement droits est présentée.

La quatrième partie de ce chapitre présente des techniques de gravure du graphène pour sa mise en forme en s'attachant à présenter leurs effets sur la qualité cristallographique du graphène et la rugosité de ses bords découpés. Les techniques sont regroupées en trois catégories: les techniques de gravure ioniques, électroniques et celles dirigées par la cristallographie du graphène. Les gravures ioniques rassemblent la lithographie électronique suivie d'une gravure par plasma d'oxygène et la gravure directe par faisceau focalisé d'ion (FIB) gallium ou hélium. Les techniques électroniques présentées sont les lithographies à sonde locale et la gravure directe par faisceau d'électrons focalisé. Les techniques de gravures dirigées par la cristallographie du graphène sont l'ouverture de nanotubes de carbone par oxydation chimique ou sonication intense, la fabrication de nanorubans de graphène par déchirement mécanique (sonication) ainsi que l'hydrogénation du graphène catalysé par des nanoparticules métalliques.

of nano-graphene and GNR with atomically smooth edges is presented.

The fourth part of this chapter focuses on the graphene patterning techniques by etching. Their effects on the crystallinity of graphene and the roughness of the cut edges are examined. These techniques are classified in three categories: the ion-based etching, the electron-based etching and the chemical etching. Ion-based techniques comprise e-beam lithography followed by an oxygen plasma etching and direct etching by a focused Ga^{3+} or He^{+} ion beam (FIB). The electronic techniques are tunneling lithography and direct focused electron beam etching. Chemical etching presents the peculiarity of cutting graphene along crystallographic orientations. One can mention the opening of carbon nanotube (CNT) by chemical oxidation or intense sonication, the mechanical tearing (sonication) of graphene into GNRs and the catalytic hydrogenation of graphene by running metallic nanoparticles.

1.1 Properties of graphene.

1.1.1 Graphene, a no gap semi conductor.

Graphene is a single atom thick sheet in which carbon atom are arranged in a honeycomb lattice (Figure 1.1). The distance between two nearest atoms is a=1.42 Å. The unit cell of graphene is formed by the two vectors $\mathbf{a}_1$ and $\mathbf{a}_2$.

$$\boldsymbol{a_1} = \frac{a}{2}\begin{pmatrix} 3 \\ \sqrt{3} \end{pmatrix} \text{ and } \boldsymbol{a_2} = \frac{a}{2}\begin{pmatrix} 3 \\ -\sqrt{3} \end{pmatrix} \text{ in the base } \begin{pmatrix} \boldsymbol{e_x} \\ \boldsymbol{e_y} \end{pmatrix}$$

The primitive cell of graphene contains two carbon atoms: α and β (Figure 1.1) that are distinguishable by their environment. The C-C bonds are rotated by 60° giving two non equivalent atoms in the primitive cell of graphene. Graphite is the stacking of graphene layers linked by Van Der Waals interactions and spaced by 0.335 nm. [1, 2] In an AB stacking (Bernal stacking), graphene plane are superposed in the order ABABABAB... B is a graphene plane translated with respect to the A graphene plane by the vector $\boldsymbol{\delta_1} = \frac{a}{2}\,(\boldsymbol{e_x} + \sqrt{3}\,\boldsymbol{e_y})$. In turbostratic graphite the stacking of the graphene layers is rotationally random around an axis perpendicular to the graphene plane. Thin graphite composed of less than about 10 graphene layers is called few layer graphene (FLG).

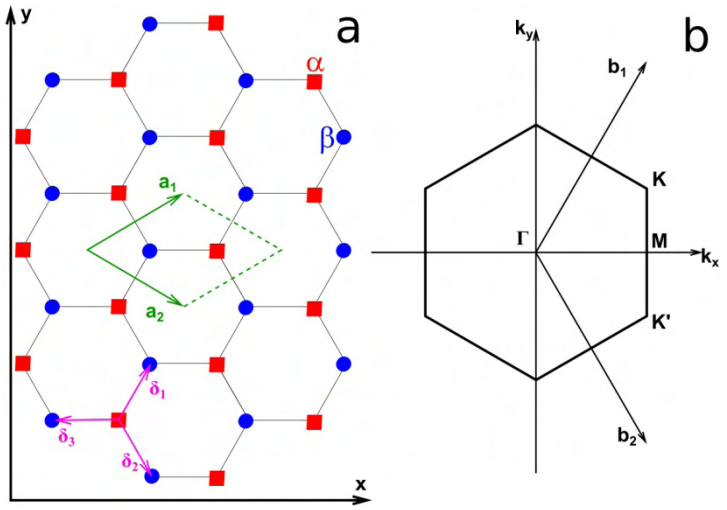

Figure 1.1. *Graphene lattice. (a) Schematics of the direct space, black lines representing C-C bonds, red squares and blue disks represent carbon atoms α and β. $\mathbf{a_1}$ and $\mathbf{a_2}$ are the primitive cell unit vectors. $\boldsymbol{\delta_1}$, $\boldsymbol{\delta_2}$ and $\boldsymbol{\delta_3}$ are the nearest neighbor vectors. (b) First Brillouin zone with reciprocal vectors $\mathbf{b_1}$ and $\mathbf{b_2}$. High symmetry points are indicated (Γ, K, K' and M).*

The vectors of the reciprocal base $\begin{pmatrix}\boldsymbol{k_x}\\ \boldsymbol{k_y}\end{pmatrix}$ are defined by:

$$\boldsymbol{e_i}.\boldsymbol{k_i} = \frac{2\pi}{(\boldsymbol{e_x}\times\boldsymbol{e_y}).\boldsymbol{e_z}}(\boldsymbol{e_i}\times\boldsymbol{e_j}).\boldsymbol{e_k} \text{ with (i, j, k) a circular permutation of (x, y, z)}$$

The reciprocal lattice is defined by the ensemble of **K** vectors verifying:

$$e^{i\boldsymbol{K}.\boldsymbol{R}} = 1$$

For all the position vectors **R** of the direct lattice.

The reciprocal vectors in the base $\begin{pmatrix}\boldsymbol{k_x}\\ \boldsymbol{k_y}\end{pmatrix}$ are:

$$\boldsymbol{b_1} = \frac{2\pi}{3a}\begin{pmatrix}1\\ \sqrt{3}\end{pmatrix} \text{ and } \boldsymbol{b_2} = \frac{2\pi}{3a}\begin{pmatrix}1\\ -\sqrt{3}\end{pmatrix}$$

K and K′ are the Dirac points, located on the corners of the first Brillouin zone. Their coordinates in the base $\begin{pmatrix}\boldsymbol{k_x}\\ \boldsymbol{k_y}\end{pmatrix}$ are:

$$K = \frac{2\pi}{3a}\begin{pmatrix}1\\ \frac{1}{\sqrt{3}}\end{pmatrix} \text{ and } K' = \frac{2\pi}{3a}\begin{pmatrix}1\\ -\frac{1}{\sqrt{3}}\end{pmatrix}.$$

The band structure is calculated in a first approximation using the tight binding Hamiltonian and resolving the Schrödinger equation. [3] The energy dispersion in the momentum space is:

$$E(\boldsymbol{k_x}, \boldsymbol{k_y}) \propto \pm\sqrt{1 + 4\cos\left(\frac{\sqrt{3}a\boldsymbol{k_x}}{2}\right)\left(\cos\left(\frac{3a\boldsymbol{k_y}}{2}\right) + 1\right)} \quad (1.1)$$

The energy band is plotted in Figure 1.2a. For an undoped graphene the Fermi energy is situated where the valence and the conduction band meet. These six meeting points are situated on the K and K′ points of the first Brillouin zone.

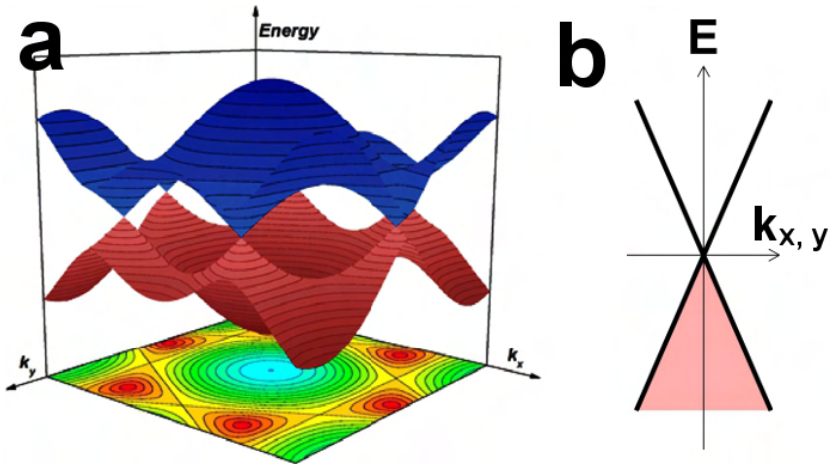

Figure 1.2. *Band structure of graphene. (a) 3D first Brillouin zone adapted from [4]. (b) Projected first Brillouin zone around K and K' points. The conductive band is displayed in blue and the valence band in red..*

For a momentum vector $\mathbf{k}$ which is close to $\mathbf{\Gamma K}$: $||\mathbf{q}|| << ||\mathbf{\Gamma K}||$ with $\boldsymbol{q} \equiv \boldsymbol{k} - \mathbf{\Gamma K}$, the energy can be approximated to:

$$E(\boldsymbol{k}) \sim \pm v_F ||\boldsymbol{q}|| + o\left(\frac{||\boldsymbol{q}||}{||\mathbf{K}||}\right)^2 \quad (1.2)$$

In the vicinity of K and K' points, dispersion band is linear in first approximation (Figure 1.2b). The two dispersion bands meet each other producing a conical-shaped valley. This dependence is unusual and implies unique properties for graphene. Carriers in graphene can be treated as massless Dirac fermions with an effective "speed of light" $c^*=10^6$ m.s^{-1}. [5-7]

1.1.2 Electronic properties.

In the Drude model, the mobility of the carriers is defined as $\mu = \frac{1}{en\rho}$ where e is the charge of an electron, n the carrier density and ρ the sheet resistivity. In graphene, at room temperature, electron mobility exceeds 2,000 cm^2.V^{-1}.s^{-1} for any micromechanically deposited graphene, providing access to high temperature quantum hall effect. [5, 6] The simultaneous observation of high mobility, sensibility to field effect and large lateral extension, implying an ease for contacting made possible the exploration of graphene as a potential alternative to carbon nanotubes (CNT) for field-effect transistors (FET) devices. [8, 9]

The dominant scattering mechanism that limits carrier mobility in graphene is related to graphene defects. [5, 10] Performing a current annealing in graphene remove adsorbates and allowed to reach motilities of more than 25,000 $cm^2.V^{-1}.s^{-1}$. [11] For oxide supported graphene, the optical phonons of the oxide set a theoretical limit to the carrier mobility which is 40,000 $cm^2.V^{-1}.s^{-1}$ at room temperature. [12] Carrier mobility increases by one order of magnitude if the underlying substrate is removed: graphene is deposited by micromechanical exfoliation technique and contacted by metallic electrodes, the silica surface underneath is etched, resulting in the suspension of graphene (Figure 1.3a). [11] In this suspended device, carrier mobility exceeds 200,000 $cm^2.V^{-1}.s^{-1}$ after annealing (Figure 1.3b).

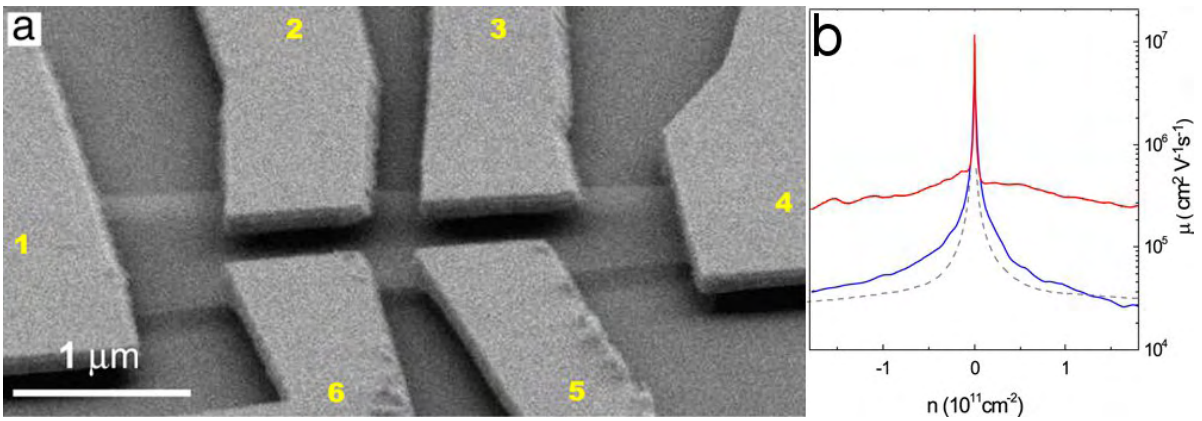

Figure 1.3. *Suspended graphene device. (a) SEM image of a typical suspended six-probes graphene device taken at 15° with respect to the sample plane. (b) Mobility μ as a function of carrier density n for a suspended graphene before (blue) and after (red) current annealing. Dotted line is the same measurement for the annealed supported sample. Adapted from [11].*

1.1.3 Graphene nanoribbons.

A graphene nano ribbon (GNR) is graphene for which one of its two dimensions is reduced to a few benzene rings and is considered as 1D graphene. There are two types of idealized GNR, (i) armchair graphene nanoribbon (AGNR), is infinite along one direction and terminated by two parallel armchair edges along the second direction (Figure 1.4a). (ii) Zig-zag graphene nanoribbon (ZGNR) is infinite along one direction and is terminated by two parallel zig-zag edges along the second direction (Figure 1.4b). A narrow band of

graphene (few nanometers in width) is called GNR, the edges of which can be a random mixture of zig-zag and armchair edges.

This lateral confinement of graphene modifies its pristine dispersion bands. Tight binding calculation has been performed to plot the energy band of AGNR and ZGNR (Figure 1.4c and d). For ZGNRs, valence and conduction bands are flattened with respect to the bands of the 2D graphene but it is still semi-metallic. AGNRs can be semi-metallic or semiconducting depending on their widths. [13]

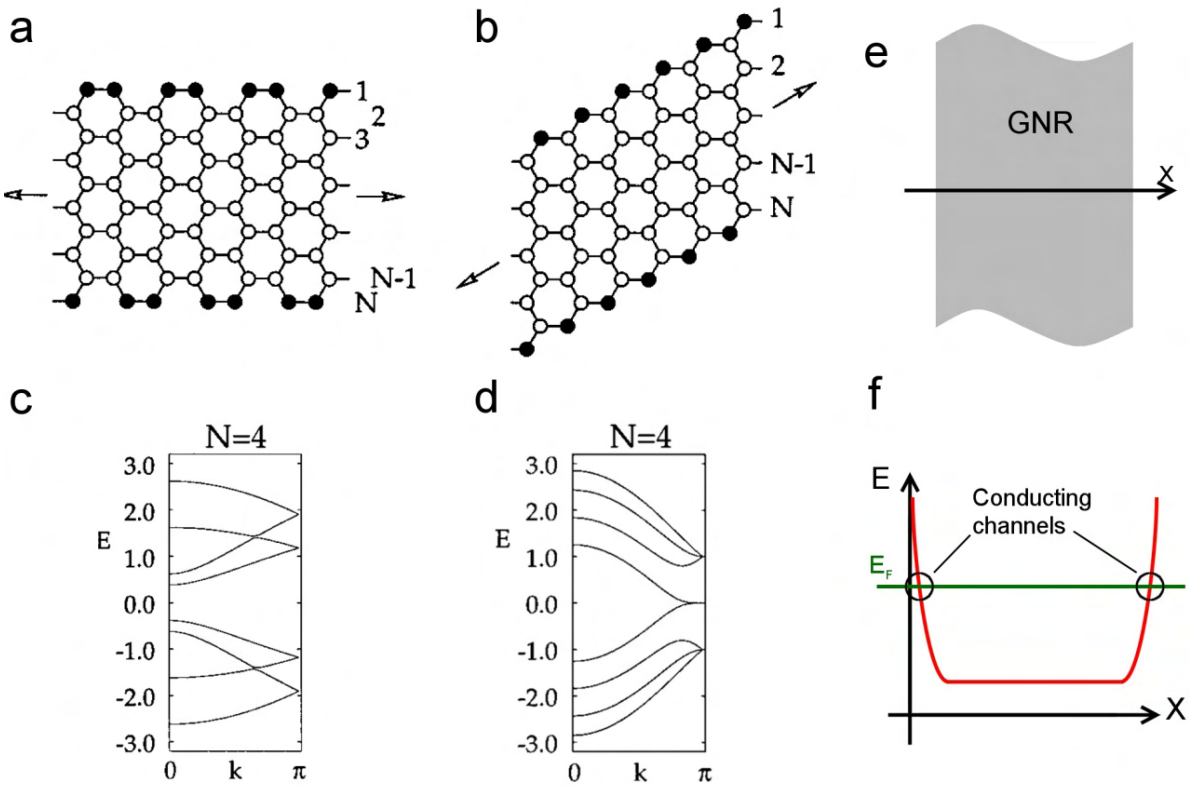

Figure 1.4. *Schematics representing (a) an Armchair graphene nanoribbon and (b) a Zig-zag graphene nanoribbon. Calculated band structure of (c) an AGNR and (d) a ZGNR. Adapted from [13]. (e) "x" is the transverse axis of a GNR. (f) Energy of the valence band of a GNR versus the position along the transverse axis "x".*

Figure 1.4f plots the energy of the valence band of a GNR with a gap versus its transverse axis "x". In the middle of the GNR, the valence band is below the Fermi energy, no conduction occurs. On the edges of the GNR, the valence band continuously increases to reach the energy level of the insulator surrounding the GNR. Where the valence band cross-

es the Fermi level, it creates two conducting channels on the edges of the GNR. The electronic transport is thus mainly carried by the edges of the GNRs which implies that the quality of the edges has a major influence on the electronic transport behavior.

Lateral confinement of graphene is one technique allowing to open a gap in the graphene band to produce a FET out of graphene. [13-15] It has been predicted that electrical properties of GNR can be tuned from perfectly metallic for ZGNR to semiconducting for AGNR, the gap of which varies with the ribbon width. [16]

1.2 Identification of graphene.

1.2.1 Optical characterization.

A technique allowing a quick determination of the number of graphene layers is optical microscopy associated with a specific substrate. The structure of Si/SiO_2 substrate with a thin oxide layer grown on silicon act as a Fabry-Perrot cavity. Graphene deposited on this substrate adds a small optical path to the Fabry-Perrot cavity [17] which increases the contrast of graphene and makes it visible with an optical microscope despite it is a single atom thick crystal (Figure 1.5a). The optical contrast of graphene versus the oxide thickness and the wavelength of the incident light is shown in Figure 1.5b. At the maximum sensitivity of the human eye, [8] at the wavelength λ=550 nm, the maximum optical contrast for graphene is obtained for 90 and 285 nm oxide thicknesses. Alternative substrates were also explored to enhance the optical contrast of graphene, for example, Si_3N_4, PMMA [17] or Al_2O_3 on silicon wafer. [18] Optical identification of graphene allows to rapidly identify the thinnest flakes of a substrate but until now, it cannot unambiguously attribute the number of layer of a graphene flake and should be associated with another characterization technique.

1.2.2 Raman spectroscopy.

Raman spectroscopy is a non destructive characterization technique. A photon beam interacts with a material to be analyzed. Incidents photons excite electrons from the valence to the conduction band, excited electrons can interact with phonons of the solid. The pho-

tons emitted from the de-excitation have a different energy than the incident photons. This energy difference is the Raman shift and provides information on the phonons of the crystal.

This non destructive and macroscopic technique is sensitive to the number of graphene layers of a flake or its crystalline quality. With a laser excitation of 514 nm, the Raman spectrum of graphene has peaks with a Raman shift comprise between 1,300 and 3,000 cm^{-1} (Figure 1.5d).

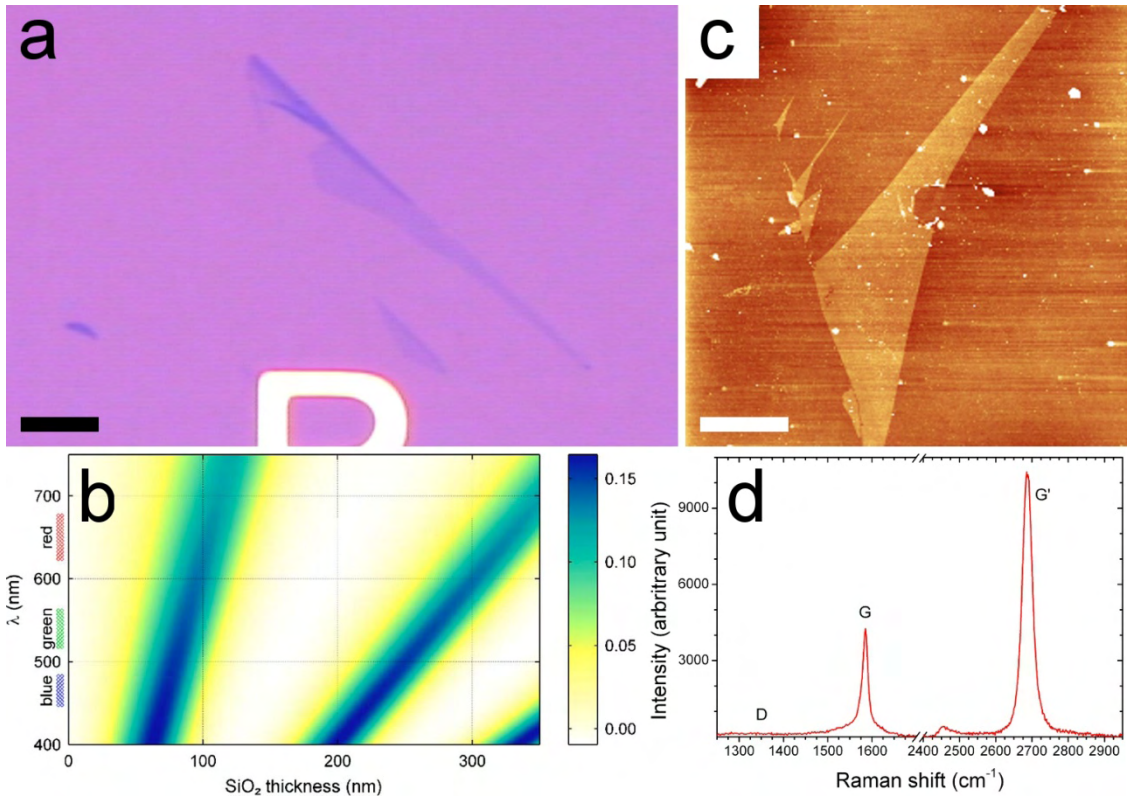

Figure 1.5. *Identification of graphene (a) Optical image of a graphene flake deposited on a Si/SiO_2 substrate with an oxide thickness of 285 nm. (b) Graphene monolayer contrast with respect to the silica as a function of wavelength and SiO_2 thickness, adapted from [17]. (c) AFM image of a graphene flake. (d) Raman spectrum of a micromechanically exfoliated graphene monolayer. Vertical scale color: 15 nm. Scale bars: 10 µm.*

The G peak around 1,560 cm^{-1} corresponds to a first order Raman process implying phonons mode of symmetry E_{2G} at the center of the Brillouin zone (Γ point). The G band intensity is proportional to the probed volume and thus, for a constant area illuminated by the laser, to the number of graphene layer. [19, 20]

The two other main peaks in the Raman spectrum of graphene are second order processes, they are called D and G′. The D peak originates from an E_{2G} symmetry phonon mode and a defect, it is centered around 1,350 cm^{-1}. The D band is active in presence of defects, including graphene edges. [21, 22] The D peak intensity is related to the density of defects in the probed area. For micromechanically exfoliated graphene, the D peak intensity is often null, only on the edges of the flake, [23] indicating the high quality of this type of graphene. The intensity of the D peak is dependent on the laser polarization, being maximum (minimum) for a polarization parallel (perpendicular) to the edge. [23-25] The Raman D peak intensity give information on the type of graphene edges in theory, pure zig-zag edges does not contribute to the D peak while pure armchair edges does. [26, 27] This behavior is well observed for graphite [19] or for pure zig-zag edges. [28] But the edges of micromechanically exfoliated graphene are too rough to be able to identify the edge average arrangement (zig-zag or armchair). [23, 24]

The G′ band originates from two E_{2G} symmetry phonon modes. G′ peak is also called 2D since its Raman shift is about twice the one of the D peak, however, this two-phonon band is allowed in the second order Raman spectra of graphene without any kind of disorder or defects. In order to prevent any misleading connection of this feature with disorder or defects, and to avoid confusion between the designation of ``2D'' to denote two dimensionality, we will use here the conventional notation ``G′-band'' as is used in the graphite and nanotube literature. [20] For a monolayer graphene or non AB stacked graphite (AA stack, turbostratic, decoupled graphene layers) it is a single Lorentzian peak. For a monolayer graphene it is centered around 2680 cm^{-1} (514nm laser wavelength). [29, 30]. For AB stacked FLG, the G′ peak is a combination of several Lorentzian peaks around 2,700 cm^{-1}. [20]

1.2.3 Atomic force microscopy characterization.

AFM is a scanning probe microscopy technique in which a cantilever scans a surface. This technique maps the topography of a surface. A tip is in interaction with a surface and gives information on the topography of the scanned object. Different modes are available, in

contact mode, the cantilever is in permanent contact with the surface, the position of the tip is regulated by the deviation of the cantilever, recorded by a laser. In intermittent or tapping mode the tip oscillates and is regulated by its amplitude. The intermittent mode reduces modification of the surface induced by the cantilever with respect to the contact mode.

Figure 1.5c shows an AFM height image of a graphene monolayer flake. The average of height profiles of the graphene-silica step measures the thickness of a graphene flake. However, attributing a number of layers to a certain apparent height is not obvious because of a low reproducibility of the height measurement. The thickness of a graphene flake on top of HOPG or FLG is measured with an intermittent mode AFM at 0.4 nm.[19] This value is close to the interplanar van der Waals spacing in graphite (i.e. 0.35 nm [1, 2]). For graphene on top of a SiO_2 surface, the AFM apparent height is measured between 0.5 and 1.0 nm. [8, 19, 31-33] The number of layer of these flakes has been confirmed by complementary characterizations like studying self folded sheets [34] or Raman spectroscopy. [19] The origin of the apparent height of graphene on silica remains unclear since Van Der Waals interaction between graphene and silica cannot explain such a high value.

1.2.4 Transmission electron microscopy.

TEM offers a unique characterization technique from large scale to the atomic scale for suspended graphene. The identification of the number of layers of a suspended graphene flake with a conventional TEM can be achieved by different approaches: imaging a folded part of graphene, the folds brings it locally parallel to the electron beam and reveals dark lines corresponding to each graphene sheets, [35-38] the number of dark lines corresponding to the number of graphene layer. However, a graphene scroll exhibits a large number of dark lines even for a graphene monolayer. [38] This technique is complemented by an electron diffraction analysis,[36] the diffraction pattern of graphene exhibit two hexagons, corresponding to the 2.13 Å spacing (inner hexagon) and the 1.23 Å spacing (outer hexagon) of graphene direct lattice. [35] In the case of AB-stacked FLG of two or more layers, the intensity of the diffraction peaks of the outer hexagon is higher than the intensity of the diffraction

peaks of the inner hexagon. It is the contrary for a monolayer graphene. [36] However, for AA stacking the previous technique can be wrong, and an unambiguous identification of single versus multilayer sample is possible by looking at the variation of diffraction intensity with respect to the tilt angle of the sample. For a monolayer graphene, the diffraction intensity varies very few with the tilt angle while a multilayer graphene lead to stronger variations. [36]

Aberration corrected TEM images of graphene with atomic resolution makes possible to determine the number of layer of a FLG flake with the contrast of carbon atoms. [35, 36, 39] Furthermore this technique allows the characterization of defects of graphene and CNT. [40, 41] Atomic resolution of suspended graphene provides the unique opportunity of studying the crystallographic quality of the edges of graphene. [37, 38, 42]

1.3 Graphene production.

1.3.1 Micromechanical exfoliation of graphite.

Van Der Waals interactions, which link graphene layers in graphite, are weak. [43] By attaching graphite micro pillars on an AFM tip and rubbing it against a silica surface a value of 300 nN.μm^2 has been found for the graphene interlayer adhesion force. [43, 44] This technique provides in-situ deposition of FLG but it never leads to flakes thinner than a few nanometers. [4]

Seeking for an electron beam transparent and uniform substrate, microscopists did extract 5 nm thick (~15 layers) graphene sheets from graphite crystals by micromechanical exfoliation. [45] This technique led to the isolation of monolayer graphene in 2004 when Novoselov and Geim [8, 46] used a common adhesive tape to repeatedly peeling a HOPG and thins it from about few micrometers to a graphene monolayer. The adhesive tape is then rubbed against a Si/SiO_2 substrate depositing flakes of various thicknesses.

This technique produces monolayer graphene flakes of tens of micrometers in lateral size. Figure 1.5a shows a micromechanically exfoliated graphene flake on a Si/SiO_2 substrate

with an oxide thickness of 285 nm. Figure 1.5b shows a Raman spectrum of a graphene monolayer, the absence of D peak is a signature of low defects density. It reflects the unique crystallographic quality of this graphene source.

Micromechanical exfoliation remains the best method for producing high electrical and structural quality graphene because it benefits from the high quality of the starting single crystalline graphite source. The size of the deposit is also appreciable and it is compatible with standard lithography techniques. However it will be challenging to bring this approach to large scale production.

1.3.2 Epitaxial graphene.

Epitaxial growth produces wafer scale graphene, it can be performed by mainly two techniques, sublimation of carbides or CVD growth on a metallic substrate.

Sublimation of silicon carbides occurs at 1300°C by the sublimation of silicon atoms, leaving the rich carbon surface reorganizing by graphitization. [47] The thermal decomposition of the C-terminated face produces loose stacked multilayer graphene. The stack of this multilayer is not Bernal and its single Lorentzian G' peak misled to conclude that it was monolayer. Later, Raman and STM studies revealed the multilayer nature of this graphene. [30, 48] Sublimation of silicon needs high temperatures which makes difficult to control the graphitization process. A compromise has been found by adjusting the pressure to decrease the silicon sublimation temperature. The graphitization of Si-terminated face of SiC(0001) under 900 mbar argon atmosphere produces wafer-scale monolayer graphene. [49]

Another technique to produce supported graphene is chemical vapor deposition (CVD) growth on a metallic substrate. CVD of "single layer graphite" has been reported very early on Pt(111), [50] monolayers of small lateral size (few tens of nanometers) have been produced. Larger (more than 100 μm) crystalline domains are grown on Ru(0001) by CVD with ethylene. [51] The first graphene layer is in strong interaction (chemisorption) with the metal, which limits the size and alters the study of the electronic transport in graphene. A

growth leading to physisorbed graphene like low pressure CVD of ethylene on Ir(111) [52] produces graphene monolayer exhibiting full coherence over step edges on a few micrometer scale area. However, the prohibiting cost of iridium limits its use to very specific needs.

Polycrystalline nickel films can be used as a template for CVD growth of centimeter sized continuous FLG films. [53] However the high solubility of carbon in nickel (10^{-1} at. % at 900°C) [54] prevent a precise control of the graphene thickness. The lower solubility of carbon in copper (10-3 at. % at 900°C) [55] allows to produce large scale (50x50 cm^2) graphene monolayer by CVD. [56, 57] Figure 1.6a shows graphene grown by CVD on copper and transferred on a glass slide, its size is 1x1 cm^2. An optical image of CVD graphene transferred onto a Si/SiO_2 substrate is shown in figure 1.6b. The resulting film is a graphene monolayer covered by small bi-layer or FLG islands (figure 1.6b), the thickness is confirmed by Raman spectroscopy in figure 1.6c. Graphene is found to cover about 95% of the sample. The Raman spectrum shown in figure 1.6c does not exhibit D peak for the monolayer, which is an evidence of a good crystallography quality.

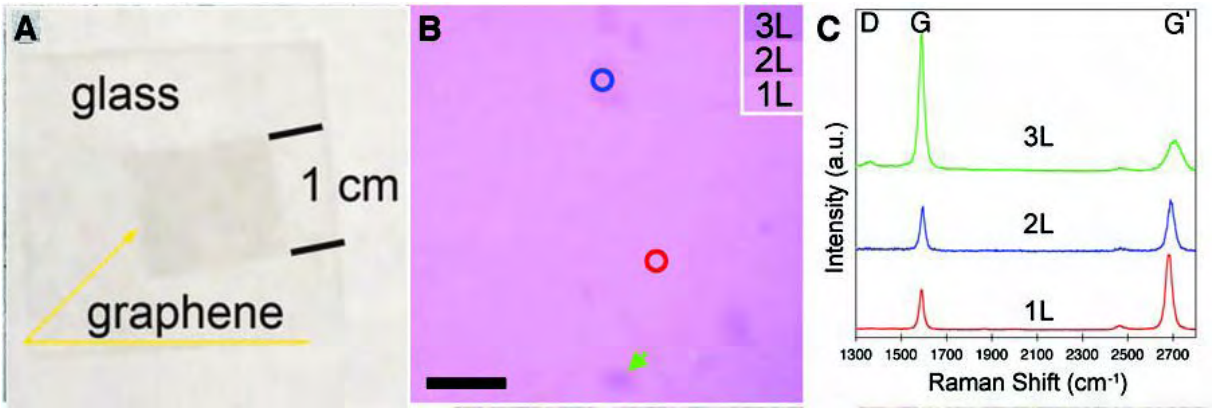

***Figure 1.6**. CVD graphene grown on copper foil and transferred on (a): a glass slide or (b): a Si/SiO_2 substrate. (c) Raman spectrum is taken on the blue and red circle and on the flake shown by green arrow. Scale bar is 5 μm. adapted from [56].*

Copper and nickel can easily be solved in etching bath, offering the opportunity to transfer CVD graphene on any substrate. A transfer technique uses PMMA which is spun to cover the graphene surface, then the metal/graphene/PMMA is plunged in a metal etchant.

The graphene covered with PMMA can be transferred to any substrate including insulating substrate and TEM grid. [56]

1.3.3 Molecular approaches.

Bottom-up chemicals routes to produce graphene offer an opportunity to control the edge crystallography of graphene. When graphene domains sizes exceed a few hundred of nanometers, its properties are well described by mesoscopic condensed matter. When its size decrease, as it is intrinsically composed of a 2D pavement of organic molecular entities -benzene rings- its properties are sensitive to the arrangement of molecular rings and edges atomic chains. In order to investigate the nanometer-scale properties of graphene, bottom-up approaches to produce graphene have been explored.

The hexabenzocoronene (HBC), which consist of thirteen fused benzene rings, become a building block for synthesis of larger molecules. Graphene molecules containing 90 [58] and up to 222 [58] carbon atoms have been synthesized. One dimensional fusion of polyaromatic precursor could be a rigorous approach for the synthesis of graphene nanoribbons with controlled edges configuration. [59] A first step in this direction was the synthesis of dehydrogenated polyphenylenes polymers which produced 2.9 nm wide ribbons having length of 8-12 nm. [60] Starting from 10,10′-dibromo-9,9′-bianthryl precursor monomer, Cai et al. [61] produced AGNRs wide of 3 benzene rings (~0.7 nm) the length of which is a few tens of nanometers. They also synthesized chevron-type GNR or C_3 symmetry structures. [61] These ribbons have atomically smooth edges but they are limited to STM studies.

1.4 Graphene patterning techniques.

Besides the direct production of GNRs by chemical bottom-up techniques, [61] graphene nanoribbons can be engineered via etching techniques. Ion or electron based techniques can produce arbitrary shaped graphene. For the narrowest GNRs (less than 50 nm) the preservation of the crystallinity quality and the edges smoothness become a major pa-

rameters for preserving a good carrier transport in GNR. Patterning techniques based on direct electron etching are less destructive than ion based techniques because they avoid the contamination of graphene by resist residue or ion implantation. Patterning techniques driven by the crystallography of graphene based on chemical etching or mechanical tearing of graphene are discussed here.

1.4.1 Ion-based patterning.

In a work by Han et al., [62] GNRs are produced by etching graphene that is not protected with hydrogen silisesquioxane (HSQ) resist with an oxygen plasma. GNRs with a minimum width of 15 nm and a length of 1 to 2 μm have been produced. [62, 63] GNRs had various widths and various crystallographic orientations, contacted and electrically measured. Examples of these GNRs are shown in figure 1.7.

The size of the band gap is obtained from the nonlinear conductance at low temperature. The inverse of the energy of the gap is plotted in figure 1.7c and varies linearly with the GNRs width.

Han et al. [62] compared their results with density functional theory calculations [64, 65] which predict that the energy gap of a GNR scale inversely with its width. This comparison suggests that a gap is opened by lateral confinement of the 2D electron gas. However the fact that no dependence is found for the energy of the gap with the GNR orientation is in contradiction with theoretical studies [65, 66]

A study of Sols et al. [67] calculates the energy of the gap opened by GNRs with rough edges (Figure 1.7d). The standard theory of Coulomb blockade effect is used for the calculation. These GNRs have an edge roughness and width that lead to ”necks” along the ribbon edges (Figure 1.7d). Theses constrictions cause an abrupt reduction in the number of conducting channels and thus an increase of the impedance along the GNRs. The results are an electric insulation of “nano-dots” where electrons become temporary confined. Coulomb

blockade results from the electron transport from dot to dot through graphene necks by tunnel effect.

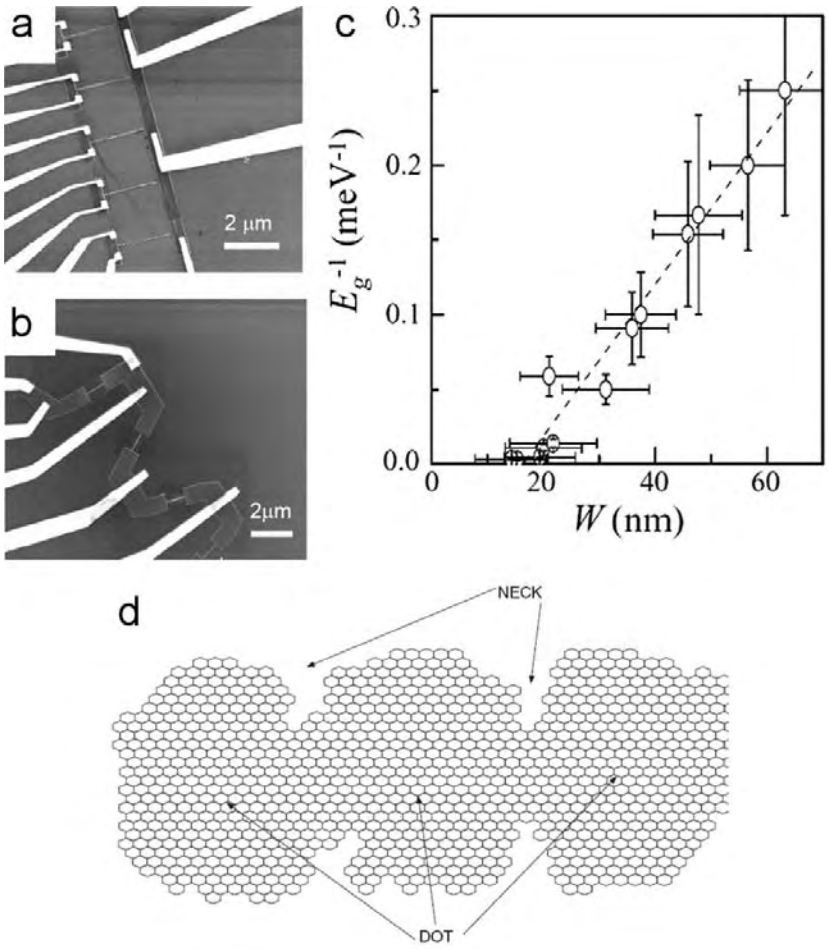

Figure 1.7. *. (a) SEM image of parallel GNRs with varying width. (b) SEM image of GNR with varying orientations. (c) Inverse of band gap energy versus GNRs width. Dashed line is a linear fit. (a-c) Adapted from [62]. (d) Schematics of a graphene ribbon with a disordered edge leading to the formation of necks and dots along the ribbon.. Adapted from [67].*

The conclusion of this work is that the oxygen plasma etching of GNRs produces edges with a high disorder. The energy gap opened in these ribbons is not due to lateral confinement but to Coulomb blockade originated from edges disorder induced in GNRs by the patterning technique.[68-70] The disorder may also originates from contamination of graphene by resist residue, [71-73] ion implantation or amorphization of.

A resist-free technique, focused ion beam (FIB) induced etching avoids alteration of graphene electronic properties by resist contamination. A work by Dayen et al. [44] study electronic transport in GNRs etched by FIB. FLG micro-disks have been extracted from HOPG and deposited onto pre-patterned microelectrodes. Electrical contacts have been produced by FIB assisted deposition of platinum and GNR have been etched by FIB (Ga^+). A side gate has been performed out of the graphene disk (see Figure 1.8a).

SEM and AFM analysis reveal that an amorphous zone of 65 nm is created around the FIB cut edges. Source and drain electrodes were used to plot I-V characteristics in graphite nanoribbons for various biases in the lateral gate voltage. Experimental results are represented by disks in Figure 1.8b. Solid lines are numerical fits of the experimental values with a model based on Coulomb blockade in a 1D array of N tunnel junctions. The value of the fitting parameter N lead to graphene dots of about 30 nm in size.

Electronic transport measurement on 100 nm wide ribbon etched by FIB shows that they behave as a 1D array of 30 nm graphene quantum dots. The process is entirely resist-less but disorder has been induced in GNR by irregularities in the edges cut by FIB, intercalated Ga^+ ions and/or random defects.

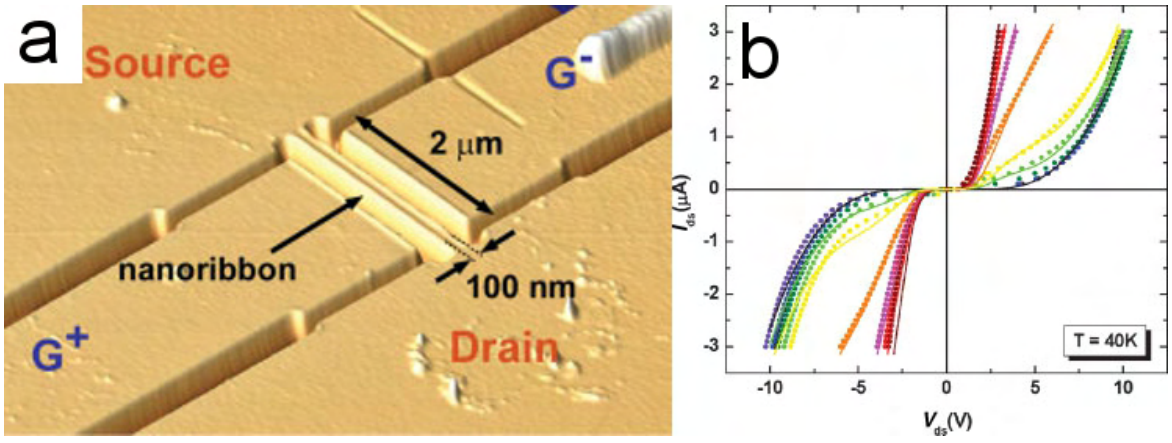

Figure 1.8. *(a) 3D rendering of an AFM image of a side-gated sub-100 nm wide graphite nanoribbon. (b) I–V characteristics of a 50x2 mm², FLG ribbon at T=40 K. Applied side-gate voltages are 0; 2; 4; 6; 8; 10; 15; 20; 25; and 30 V, displayed in a black-to-red rainbow color scheme. Open circles are experimental data and continuous lines are fits using a 1D quantum dot array model. Adapted from [44].*

In an attempt of reducing the ion dose during FIB milling, Archanjo et al. [74] found that the minimum ion dose that can insulate graphene is $3x10^{15}$ ions.cm^{-2}. At this ion dose, the lateral damaged width analyzed with the D band of Raman spectroscopy is 90 nm. A graphene sample has been contacted with metallic electrodes, shaped in a Hall bar measurement devices by EBL and irradiated with a low ion dose of $4x10^{13}$ ions.cm^{-2}. Raman D-peak shows damages on the irradiated area and even far from the bombarded area. The damages of the non irradiated area are explained by electron beam imaging or non focused ions. Electrical measurement before and after irradiation shows a dramatic decrease of the conductivity and thus the mobility drop from 1,200 to 120 cm^2.V^{-1}.s^{-1}.

Helium ion lithography takes the advantage of a lower mass of the He^+ ions in comparison with Ga^+. Using the software TRIM, Bell et al. [75] have shown that for graphene on Si/SiO_2 substrate gallium ions interact mainly with the upper most part of the material resulting in features size larger than the ion beam diameter. On the contrary, helium ions pass through graphene with very few interactions resulting in an etching size similar to the FIB probe size. The helium ion lithography has a smaller interaction volume with graphene, and hence a higher resolution and a potentially smaller milling feature size compared to gallium ion lithography.

Helium ion lithography of graphene on a Si/SiO_2 substrate produces sub-20 nm features size with an arbitrary pattern. However for the highest ion doses used, the substrate swell by effect of the knock-on damage of the underlying silicon. [75] By suspending graphene, Lemme et al. produced cut of 10 nm feature size with helium beam lithography. [76] Damages induced by the beam to graphene can be further reduced by using electron instead of ions.

1.4.2 Direct electron beam patterning of graphene.

Graphene patterning techniques using electrons can be divided in two groups: At very low voltage (2-10 V), current flows from a biased STM or AFM tip to the graphene sample

and etch it by local anodic oxidation. At larger voltage (80-300 kV) the focused electron beam of the TEM etches graphene by physical removal of carbon atoms.

Few years after STM invention, [77] it has been used to locally etch a graphite surface. [78-80] A tip is biased with a pulse voltage of 2.4 to 8 V [78-80] of maximum amplitude for a current of 0.1 to 0.5 nA. [78, 79] The etching process is related to the presence of water, in UHV the etching of graphite has been reported for a bias higher or equal to 8.5 V. [81] At low voltage, no etching is either observed in pure nitrogen or oxygen atmosphere. [78] The mechanical etching is excluded because no etching occurs with low bias voltage and high current (50-500 mV and 1-4 nA) while the tip is closer to the surface in this conditions than in the etching conditions (higher bias). [79]

The depth of the etching can be monolayer [79] or more than two layers of graphene [78] by adjusting the STM parameters (bias 2.8 V and current 0.25 nA). Various shapes have been achieved on HOPG, the smallest reported width of a trench is 2 nm,[78] squares of 25x25 to 300x300 nm^2 one-monolayer deep or 10 nm wide lines which is long of 750 nm [79] have been also reported. A GNR produced by local anodic oxidation of a HOPG surface has been studied by STM. [80] The lithography parameters are 2.4 V bias potential and 1-2 $nm.s^{-1}$ of etching speed, resulting in a 10 nm wide GNR over a length of 120 nm (see figure 1.9).

The edge maximum roughness is defined as the distance between two parallel lines in which fit the edge. For nanometric wide ribbons, edge roughness is an important parameter to assess the quality of a GNR. The 10 nm ribbon shown in figure 1.9 has a maximum edge roughness of 2 nm over a length of 20 nm, this represent about 10 benzene rings. The RMS roughness of these edges is 0.3 nm.

To date no etching of graphene on an insulating substrate and electrically contacted has been reported by STM local anodic oxidation. In the literature, GNRs are made on bulk

HOPG or on Au/SiO_2/Si substrates. [82] However, graphene deposited on an insulating substrate and electrically contacted has been etched by AFM local anodic oxidation. [82-85]

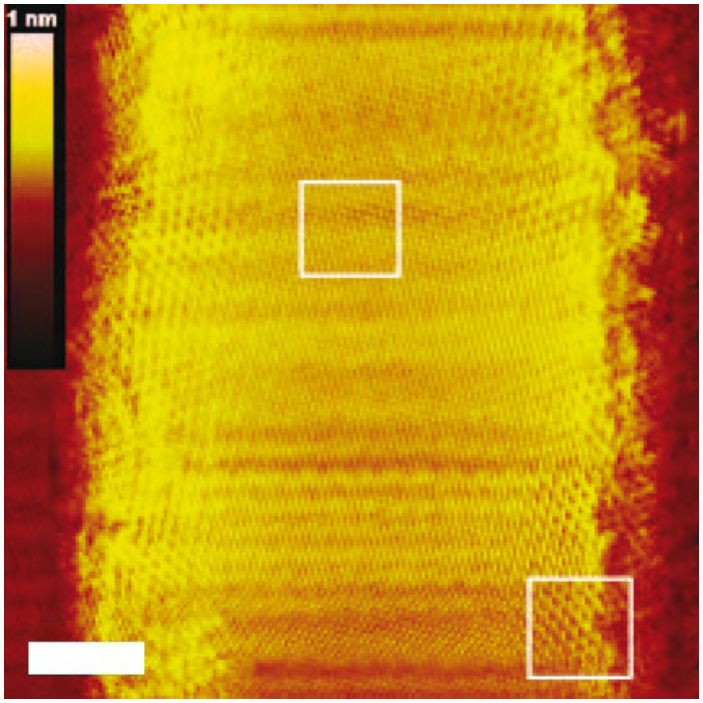

Figure 1.9. *STM image of a 15-nm-wide GNR etched by local anodic oxidation. Scale bar: 2 nm. adapted from [80].*

Scanning probe lithography on graphene deposited on a Si/SiO_2 substrate by micromechanical exfoliation has been done with AFM biased tip. The bias voltage is increased by one order of magnitude with respect to STM lithography, 15-35 V. [83-85] For contact mode AFM, the bias is pulsed, [84] but AFM also operates in intermittent mode with a constant bias. [83, 85] The relative humidity is maintained between values from 40 to 50% [84, 85] and the etching velocity is about 10 to 200 $nm.s^{-1}$. [83, 84] The lateral minimum size of GNR is 25 nm in width over a length of 800 nm. [85]

Direct electron beam patterning techniques of graphene using higher energy electrons (80-300 kV) are performed in TEM. At these energies, the main effect that can cause an electron irradiation on graphene is knock-on atom displacement. [86] Atom displacement by an electron can be treated by a simple Coulomb potential. An electron with an incident energy

E and a mass m hit a nucleus with a mass M which is deviated by an angle θ with the incident electron direction. The angular dependence of the energy T that the electron can transfer to the nucleus is given by:

$$T(\theta) = T_{max} cos^2(\theta). \quad (1.3)$$

Where T_{max} is the maximum energy transferred by a head-on collision (θ =0).

For a relativistic electron (m<<M and E<<Mc²):

$$T_{max} = \frac{2E(E+2mc^2)}{Mc^2}. \quad (1.4)$$

T_d is the threshold energy required to remove an atom. E_d is the corresponding electron energy. For a carbon atom in graphene, T_d=17 eV, meaning that an electron beam with energy equal or higher than E_d=86 keV can create a hole in graphene by knock-on displacement of carbon atoms. For an atom at the edge of a graphene sheet, T_d is only 15 eV and E_d=74 keV. A 60 keV or lower energy of the electron beam cannot etch graphene directly. However, a 60 keV electrons can etch graphene by knock-on displacement of lighter atom of an impurity (e.g. hydrogen) followed by the collision of the light atom with a carbon atom of graphene

These energies are standard for TEM which can be used for electron beam induced etching (EBIE) of graphene. Indeed, carbon allotropes can be etched [87, 88] or damaged [89] by an electron beam of sufficient energy. For example a 5 nm wide FLG nanoribbon or 3 nm in diameter nanopores have been etched by a Focused TEM beam of 200 keV. [88]

By setting the energy of the electrons at 80 keV, the TEM beam can enlarge a preexisting hole without creating a new one. By using this energy, Girit et al. [90] have enlarged a hole in a monolayer graphene membrane. The edges of this hole, as shown in figures 1.10a and b, exhibit long range atomic order of "zig-zag" or "armchair" configuration. A DFT calculation has shown that the energy barrier for migration of a carbon atom to various nearby vacant sites is between 0.3 and 6.6 eV. [90] This energy is well below the threshold required

to extract a carbon atom in an edge (Td=15 eV). A carbon atom is thus more likely to rearrange on the edge of the hole than to be ejected. The hole is overall growing but rearrangements of the atoms on the edges of graphene are stimulated by electron irradiation, leading to edges with long range order at the atomic scale. During the growth of the hole, "zig-zag" shaped edges are favored with respect to "armchair" ones. [90]

By irradiating graphene membranes with a focused electron beam accelerated at 300 kV, Song et al. [91] shown that among the etching of graphene, the surrounding area is severely amorphized at room temperature. By studying the e-beam induced amorphization with respect to the sample temperature, they observed that if graphene is completely amorphous at room temperature, it is polycrystalline at 500°C under the same irradiation conditions and single crystalline at 700°C. Two processes are in competition, self repairing of graphene due to increased temperature and amorphization of graphene by the electron beam. Increasing the temperature favor repairing of graphene, in consequence, under 400°C graphene is amorphized under the electron beam accelerated at 300 kV, while over 600°C graphene is still crystalline. [91] Decreasing the electron energy reduces the amorphization, that is why Girit et al. [90] do not observe severe amorphization of the surrounding graphene at room temperature with an electron beam accelerated at 80 kV (Figure 1.10a and b).

With a TEM beam accelerated at 300 kV at temperature 700°C, Song et al. [91] performed 2 nm diameter holes and 2 nm wide AGNR (Figure 1.10c). The GNR has perfect armchair edges. The hole also exhibit long range order edges with "armchair" configuration. Nanopores as small as 10 hexagons (e.g. 7 Å) have been produced. All the edges cut by this technique with long range order are "armchair".

The control of the shape of the nanostructures achieved by EBIE in a TEM is performed by irradiating an elongated area (astigmatic beam) or by manually moving the e-beam. [91] Potentially a servo e-beam could pattern graphene in an arbitrary shape but this is not a standard feature of a TEM beam.

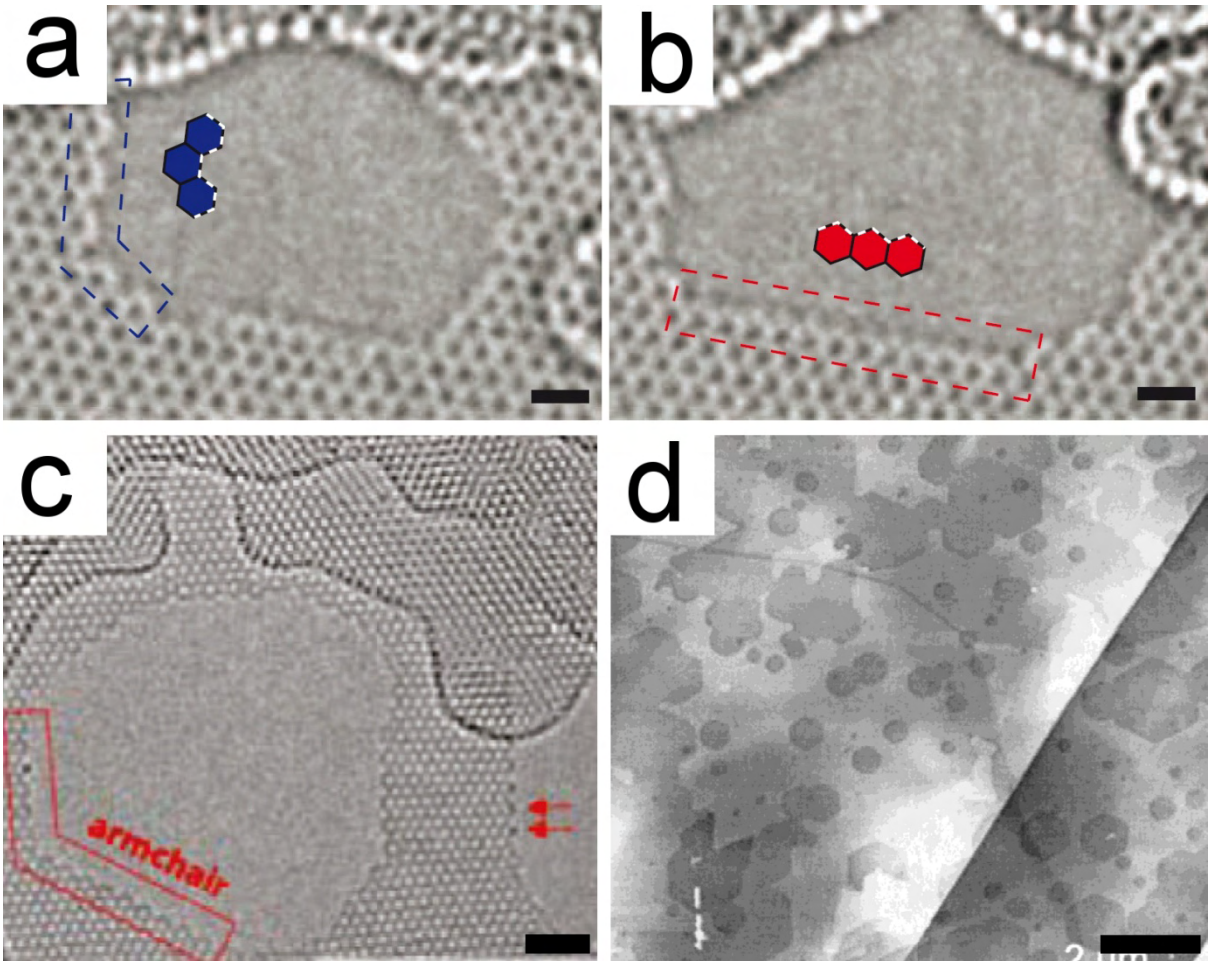

Figure 1.10. *(a) Armchair and (b) zigzag configuration of carbon atoms at the edge of a hole in graphene. (c) AGNR made from a single layer of graphene. (d) STM image of geometrical flat bottomed microholes in HOPG after electron beam exposure. Adapted from: (a) and (b) [90]; (c) [91] (d) [92]. Scale bars: (a) and (b) 0.5 nm, (c) 1 nm and (d) 2 µm.*

For STM lithography, a chemical reagent (water) can lower the bias tension necessary for etching graphene. [78, 81] In the case of direct irradiation with an e-beam, it behaves the same way. Indeed, Hiura [92] has exposed an HOPG surface to the irradiation of an e-beam with electrons accelerated at 4 kV. The energy of the electron is well below the knock-on threshold energy to displace a carbon atom on the edge of graphene (74 keV) However, this irradiation leads to the formation of microholes on the surface of graphite, as shown in figure 1.10d. All the holes are deep of one monolayer of graphene only. The shape of the holes is circular for small holes (diameter less than 500 nm) and become hexagonal for bigger holes (diameter greater than 500 nm). The direction of any side of the hexagons is parallel to

a symmetrical axis of the graphite sheet where the holes are located. Hiura interpreted the formation of these holes by residual oxygen in the vacuum chamber (10^{-7} mbar). Holes start to grow at point defects in graphite and become greater via the oxidation by the residual O_2. The association of low energy electron beam with a chemical reagent leads to the formation of crystallographically orientated and faceted holes on graphite.

1.4.3 Catalytic patterning of graphene by metal nanoparticles.

Besides electron beam irradiation of graphene in presence of O_2, other patterning techniques benefits from graphene crystallinity even at the sub-nanometric size for etching this material with smooth edges. Longitudinal unzipping of carbon nanotube is one of these techniques. [93-95] Single or multiwall carbon nanotube (SWCNT and MWCNT) are unzipped and dispersed in a solution of potassium permanganate [93] or lithium and ammonia. [95] These solutions based on oxidation process lead to long (few micrometers and narrow, few tens of nanometers) GNRs. [93, 95] These nanoribbons are oxidized, terminated by carboxyl groups. [93]

A later process, involving sonochemical unzipping of MWCNTs also produce micrometer long GNR with a minimum width of 10 to 30 nm. [96] MWCNTs are grown by arc discharge and calcinated in air at 500°C. CNTs are then dispersed in a 1,2-dichloroethane organic solution of poly(m-phenylenevinylene-co-2,5-dioctoxy-p-phenylenevinylene) (PmPV) by sonication. TEM analysis of these GNR reveals that the maximum edge roughness is 1 nm over a 20 nm length. [94] Electrical transport measurement of a GNR wide of 14 nm has been performed, electrons travelled over a length of 200 nm and shown very good transport properties. [96] The ribbon is metallic with a high conductance (4 e^2/h) at low temperature. Electrons in the ribbon show coherent phase transport, the electronic properties confirm the high quality of the ribbons.

Graphite has been exfoliated by high temperature, plunged in a PmPV solution and intensively sonicated. [97] This technique produces GNRs of various widths, from 50 to sub-10 nm with a micrometer length. The mechanism of fabrication of these ribbons is

thought to be chemical and mechanical, due to sonication in PmPV. A theoretical study by Kawai et al. [98] has shown that GNR formed by mechanical tearing of graphene exhibit armchair edge structure, independently from the tearing direction. The smooth edge of these ribbon is confirmed by Poumirol et al., [99] GNRs have been produced by sonochemical exfoliation of graphite [97] and dispersed on a Si/SiO_2 substrate. The magneto-current flowing in those ribbons has been measured under high magnetic field (0-60 T). They found that the edges of these narrow ribbons are smooth and the major source of scattering is trapped charges in the substrate.

These chemical and mechanical techniques are able to produce GNRs with a minimum width of sub-10 nm with edges almost atomically smooth. GNRs are obtained by suspension and can thus be deposited on almost any substrates. However the shape cannot be controlled and is mainly a simple rectangular.

The catalytic hydrogenation of graphene consists in depositing metallic nanoparticles (Fe, [100-103] Ni [100, 104-106] and Co [107, 108]) on graphene and heating the sample at 700 to 1100°C in an Ar/H_2 or He/H_2 atmosphere during few minutes. These particles while diffusing on the graphite surface etch it. The trenches formed are straight and parallel to graphite crystallographic orientation. These channels usually bend at 60 or 120° (Figure 1.11a). [100] Datta et al. [101] have analyzed the length of these channels versus their orientation with an AFM on a FLG cut by catalytic hydrogenation, they observed that particles mainly travelled along a privileged direction with other preferred directions at ±60° relative to this. Slightly less preferred direction at 30° are observed and almost none at random direction. This privileged direction related to graphene lattice originates from the chemical etching mechanism and the graphene lattice orientation.

This technique allows the formation of various but not controlled shapes. Remarkably, when two particles are parallel, they form graphene nanoribbon, for example Campos et al. [106] observed that on monolayer graphene deposited on a silica surface, nanoparticles that are moving toward an already existing cut are deviated just before reaching it and can

form 10 nm wide GNR (Figure 1.11b). Equilateral triangles or parallelograms are also observed. [106]

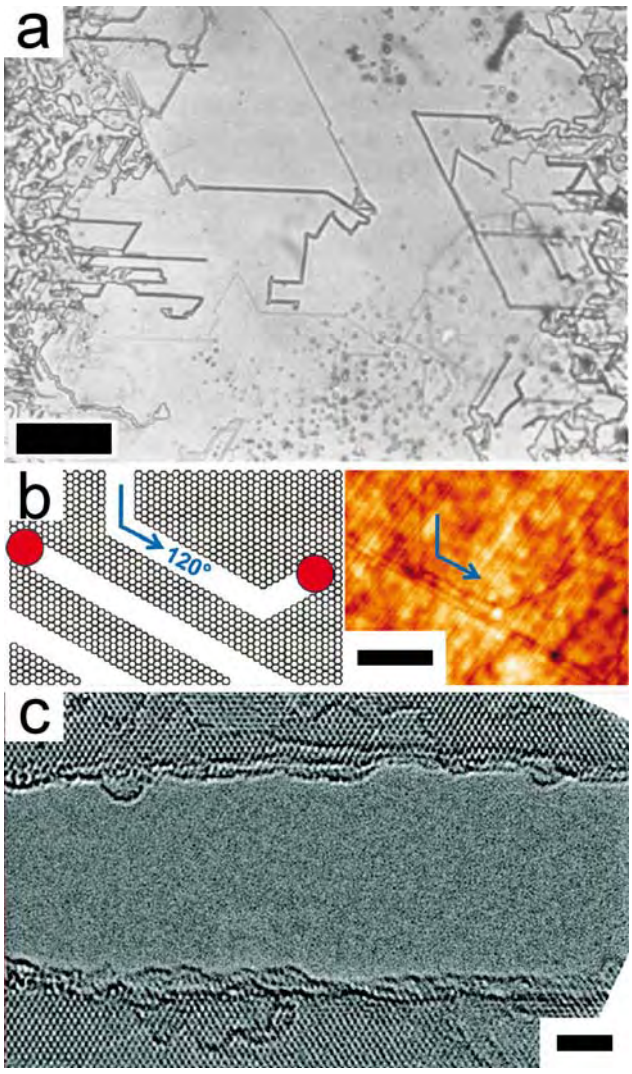

Figure 1.11. *(a) Optical image of straight trenches formed by catalytic hydrogenation of graphite. adapted from [100]. (b) Drawing and AFM image of a ribbon created by a nanoparticle which turns twice, forming two angles of 120°. Adapted from [106]. (c) TEM image of a trench in FLG by a catalytic hydrogenation of graphene. Adapted from [108]. Scale bars: (a) 20 µm, (b) 100 nm and (c) 2 nm.*

Cut made by catalytic hydrogenation of graphene are straight and preferentially parallel to the graphene lattice orientations, a HRTEM study characterized the quality of their edge at the atomic scale. [108] Schäffel observed that edges cut by catalytic hydrogenation of few graphene layers (see Figure 1.11c) have a maximum roughness between 1 and 1.5 nm

over a length of 25 nm. The maximum edge roughness of the best edge is only 0.6 nm. The respective RMS roughnesses are 0.3 and 0.2 nm. The crystallinity of graphene is even preserved near the cut, visible in the direct TEM image (Figure 1.11c).

This technique provides good etching quality but a full control of the shape of the etching has not been demonstrated even if some experiments show a partial control of the shape. Tsukamoto et al. [102, 103] have deposited graphene on crystalline sapphire. It is possible to drive metallic nanoparticles and thus the trenches direction by step edges of a sapphire. This shows the possibility of a partial control of the etching direction but not the capability of etching graphene with an arbitrary shape.

1.5 Perspectives.

Dans cette thèse, nous allons étudier une technique de structuration du graphène, la gravure directe par faisceau électronique focalisée (EBIE) assistée de vapeur d'eau. Cette technique combine des électrons de faible énergie (2 à 20 keV) et une gravure chimique (vapeur d'eau) sensible à la cristallographie du graphène. La faible énergie des électrons devrait éviter l'amorphisation du graphène et la rugosité des bords de gravure devrait bénéficier de la gravure électronique et chimique qui ont déjà fait la preuve de bords très droit jusqu'à l'échelle atomique.

Pour étudier cette technique de gravure, le graphène a été déposé sur deux types de supports, des grilles MET et des substrats

In this thesis, we will study an patterning technique of graphene, the electron beam induced etching (EBIE) assisted by water vapor. This technique combines low energy electrons (2 to 20 keV) and a chemical etching (water vapor) sensitive to the crystallography of graphene. The low energy of the electrons should limit the amorphisation of graphene and the roughness of the edges cut by this technique should benefit from the chemical and electron-based approach, which taken independently have shown the production of very smooth edges.

To study this etching technique, graphene has been deposited on two types of substrate, TEM grids and Si/SiO_2 substrates.

Si/SiO_2. Le graphène suspendu sur grille MET a été identifié par diffraction électronique, la mise au point de la technique de gravure a été effectuée sur ce graphène. Un MET avec correcteur d'aberrations sphériques pour l'image a été utilisée pour l'analyse structurale des découpes EBIE. Cet outil permet notamment de mesurer la rugosité des bords et d'évaluer l'amorphisation du graphène. Le graphène déposé par exfoliation micromécanique sur substrat Si/SiO_2 a été contacté électriquement et gravé par la technique EBIE. Cette configuration facilitera les mesures de transport électronique.

Graphene suspended on TEM grids have been identified by electronic diffraction, the development of the etching technique has been done on this graphene. A spherical aberration corrected TEM (SACTEM) has been used for a structural analysis of the EBIE cuts. This tool allows to measure the edges roughness and to evaluate the amorphisation of graphene at the cutting edge. Graphene deposited by micromechanical exfoliation on Si/SiO_2 substrates has been contacted and etched by the EBIE technique. This configuration will facilitate the electronic transport measurements.

1.6 References.

[1] Hoerni, J. "**Diffraction of Electrons in Graphite**". *Nature* (**1949**) *Vol. 164*, p. 1045-1046.

[2] Bernal, J. D. "**The Structure of Graphite**". *Proceedings of the Royal Society of London. Series A* (**1924**) *Vol. 106*, p. 749-773.

[3] Wallace, P. R. "**The Band Theory of Graphite**". *Physical Review* (**1947**) *Vol. 71*, p. 622-634.

[4] Soldano, C.; Mahmood, A.; Dujardin, E. "**Production, properties and potential of graphene**". *Carbon* (**2010**) *Vol. 48*, p. 2127-2150.

[5] Novoselov, K. S.; Geim, A. K.; Morozov, S. V.; Jiang, D.; Katsnelson, M. I.; Grigorieva, I. V.; Dubonos, S. V.; Firsov, A. A. "**Two-dimensional gas of massless Dirac fermions in graphene**". *Nature* (**2005**) *Vol. 438*, p. 197-200.

[6] Zhang, Y. B.; Tan, Y. W.; Stormer, H. L.; Kim, P. "**Experimental observation of the quantum Hall effect and Berry's phase in graphene**". *Nature* (**2005**) *Vol. 438*, p. 201-204.

[7] Nomura, K.; MacDonald, A. H. "**Quantum transport of massless dirac fermions**". *Phys. Rev. Lett.* (**2007**) *Vol. 98*, p. 4.

[8] Novoselov, K. S.; Geim, A. K.; Morozov, S. V.; Jiang, D.; Zhang, Y.; Dubonos, S. V.; Grigorieva, I. V.; Firsov, A. A. "**Electric field effect in atomically thin carbon films**". *Science* (**2004**) *Vol. 306*, p. 666-669.

[9] Zhang, Y.; Small, J. P.; Amori, M. E. S.; Kim, P. "**Electric Field Modulation of Galvanomagnetic Properties of Mesoscopic Graphite**". *Phys. Rev. Lett.* (**2005**) *Vol. 94*, p. 176803.

[10] Morozov, S. V.; Novoselov, K. S.; Katsnelson, M. I.; Schedin, F.; Elias, D. C.; Jaszczak, J. A.; Geim, A. K. "**Giant intrinsic carrier mobilities in graphene and its bilayer**". *Phys. Rev. Lett.* (**2008**) *Vol. 100*, p. 4.

[11] Bolotin, K. I.; Sikes, K. J.; Jiang, Z.; Klima, M.; Fudenberg, G.; Hone, J.; Kim, P.; Stormer, H. L. "**Ultrahigh electron mobility in suspended graphene**". *Solid State Commun.* (**2008**) *Vol. 146*, p. 351-355.

[12] Chen, J.-H.; Jang, C.; Xiao, S.; Ishigami, M.; Fuhrer, M. S. "**Intrinsic and extrinsic performance limits of graphene devices on SiO2**". *Nat Nano* (**2008**) *Vol. 3*, p. 206-209.

[13] Nakada, K.; Fujita, M.; Dresselhaus, G.; Dresselhaus, M. S. "**Edge state in graphene ribbons: Nanometer size effect and edge shape dependence**". *Physical Review B* (**1996**) *Vol. 54*, p. 17954-17961.

[14] Fujita, M.; Wakabayashi, K.; Nakada, K.; Kusakabe, K. "**Peculiar localized state at zigzag graphite edge**". *J. Phys. Soc. Jpn.* (**1996**) *Vol. 65*, p. 1920-1923.

[15] Ando, T. "**Physics of Graphene - Zero-Mode Anomalies and Roles of Symmetry**". *Progress of Theoretical Physics Supplement* (**2008**) *Vol.* 203-226.

[16] Barone, V. n.; Hod, O.; Scuseria, G. E. "**Electronic Structure and Stability of Semiconducting Graphene Nanoribbons**". *Nano Letters* (**2006**) *Vol. 6*, p. 2748-2754.

[17] Blake, P.; Hill, E. W.; Neto, A. H. C.; Novoselov, K. S.; Jiang, D.; Yang, R.; Booth, T. J.; Geim, A. K. "**Making graphene visible**". *Appl. Phys. Lett.* (**2007**) *Vol. 91*, p. 3.

[18] Gao, L.; Ren, W.; Li, F.; Cheng, H.-M. "**Total Color Difference for Rapid and Accurate Identification of Graphene**". *ACS Nano* (**2008**) *Vol. 2*, p. 1625-1633.

[19] Gupta, A.; Chen, G.; Joshi, P.; Tadigadapa, S.; Eklund, P. C. "**Raman scattering from high-frequency phonons in supported n-graphene layer films**". *Nano Letters* (**2006**) *Vol. 6*, p. 2667-2673.

[20] Malard, L. M.; Pimenta, M. A.; Dresselhaus, G.; Dresselhaus, M. S. "**Raman spectroscopy in graphene**". *Phys. Rep.-Rev. Sec. Phys. Lett.* (**2009**) *Vol. 473*, p. 51-87.

[21] Thomsen, C.; Reich, S. "**Double Resonant Raman Scattering in Graphite**". *Phys. Rev. Lett.* (**2000**) *Vol. 85*, p. 5214-5217.

[22] Ferrari, A. C.; Robertson, J. "**Resonant Raman spectroscopy of disordered, amorphous, and diamondlike carbon**". *Physical Review B* (**2001**) *Vol. 64*, p. 075414.

[23] Casiraghi, C.; Hartschuh, A.; Qian, H.; Piscanec, S.; Georgi, C.; Fasoli, A.; Novoselov, K. S.; Basko, D. M.; Ferrari, A. C. "**Raman Spectroscopy of Graphene Edges**". *Nano Letters* (**2009**) *Vol. 9*, p. 1433-1441.

[24] Gupta, A. K.; Russin, T. J.; Gutierrez, H. R.; Eklund, P. C. "**Probing Graphene Edges via Raman Scattering**". *ACS Nano* (**2009**) *Vol. 3*, p. 45-52.

[25] You, Y. M.; Ni, Z. H.; Yu, T.; Shen, Z. X. "**Edge chirality determination of graphene by Raman spectroscopy**". *Appl. Phys. Lett.* (**2008**) *Vol. 93*, p. 3.

[26] Cancado, L. G.; Pimenta, M. A.; Neves, B. R. A.; Dantas, M. S. S.; Jorio, A. "**Influence of the atomic structure on the Raman spectra of graphite edges**". *Phys. Rev. Lett.* (**2004**) *Vol. 93*, p. 4.

[27] Cancado, L. G.; Pimenta, M. A.; Neves, B. R. A.; Medeiros-Ribeiro, G.; Enoki, T.; Kobayashi, Y.; Takai, K.; Fukui, K.; Dresselhaus, M. S.; Saito, R.; Jorio, A. "**Anisotropy of the Raman spectra of nanographite ribbons**". *Phys. Rev. Lett.* (**2004**) *Vol. 93*, p. 4.

[28] Krauss, B.; Nemes-Incze, P.; Skakalova, V.; Biro, L. P.; von Klitzing, K.; Smet, J. H. "**Raman Scattering at Pure Graphene Zigzag Edges**". *Nano Letters* (**2010**) *Vol. 10*, p. 4544-4548.

[29] Mafra, D. L.; Samsonidze, G.; Malard, L. M.; Elias, D. C.; Brant, J. C.; Plentz, F.; Alves, E. S.; Pimenta, M. A. "**Determination of LA and TO phonon dispersion relations of graphene near the Dirac point by double resonance Raman scattering**". *Physical Review B* (**2007**) *Vol. 76*, p. 233407.

[30] Faugeras, C.; Nerriere, A.; Potemski, M.; Mahmood, A.; Dujardin, E.; Berger, C.; de Heer, W. A. "**Few-layer graphene on SiC, pyrolitic graphite, and graphene: A Raman scattering study**". *Appl. Phys. Lett.* (**2008**) *Vol. 92*, p. 3.

[31] Chen, Z.; Lin, Y.-M.; Rooks, M. J.; Avouris, P. "**Graphene nano-ribbon electronics**". *Physica E: Low-dimensional Systems and Nanostructures* (**2007**) *Vol. 40*, p. 228-232.

[32] Sidorov, A. N.; Yazdanpanah, M. M.; Jalilian, R.; Ouseph, P. J.; Cohn, R. W.; Sumanasekera, G. U. "**Electrostatic deposition of graphene**". *Nanotechnology* (**2007**) *Vol. 18*, p. 4.

[33] Nemes-Incze, P.; Osvath, Z.; Kamaras, K.; Biro, L. P. "**Anomalies in thickness measurements of graphene and few layer graphite crystals by tapping mode atomic force microscopy**". *Carbon* (**2008**) *Vol. 46*, p. 1435-1442.

[34] Li, L. X.; Liu, R. P.; Chen, Z. W.; Wang, Q.; Ma, M. Z.; Jing, Q.; Li, G.; Tian, Y. "**Tearing, folding and deformation of a carbon-carbon sp2-bonded network**". *Carbon* (**2006**) *Vol. 44*, p. 1544-1547.

[35] Meyer, J. C.; Geim, A. K.; Katsnelson, M. I.; Novoselov, K. S.; Booth, T. J.; Roth, S. "**The structure of suspended graphene sheets**". *Nature* (**2007**) *Vol. 446*, p. 60-63.

[36] Meyer, J. C.; Geim, A. K.; Katsnelson, M. I.; Novoselov, K. S.; Obergfell, D.; Roth, S.; Girit, C.; Zettl, A. "**On the roughness of single- and bi-layer graphene membranes**". *Solid State Commun.* (**2007**) *Vol. 143*, p. 101-109.

[37] Liu, Z.; Suenaga, K.; Harris, P. J. F.; Iijima, S. "**Open and Closed Edges of Graphene Layers**". *Phys. Rev. Lett.* (**2009**) *Vol. 102*, p. 015501.

[38] Warner, J. H.; Ruemmeli, M. H.; Bachmatiuk, A.; Buechner, B. "**Examining the stability of folded graphene edges against electron beam induced sputtering with atomic resolution**". *Nanotechnology* (**2010**) *Vol. 21*, p. 325702.

[39] Warner, J. H. "**The influence of the number of graphene layers on the atomic resolution images obtained from aberration-corrected high resolution transmission electron microscopy**". *Nanotechnology* (**2010**) *Vol. 21*, p. 5.

[40] Hashimoto, A.; Suenaga, K.; Gloter, A.; Urita, K.; Iijima, S. "**Direct evidence for atomic defects in graphene layers**". *Nature* (**2004**) *Vol. 430*, p. 870-873.

[41] Meyer, J. C.; Kisielowski, C.; Erni, R.; Rossell, M. D.; Crommie, M. F.; Zettl, A. "**Direct Imaging of Lattice Atoms and Topological Defects in Graphene Membranes**". *Nano Letters* (**2008**) *Vol. 8*, p. 3582-3586.

[42] Warner, J. H.; Schäffel, F.; Rümmeli, M. H.; Büchner, B. "**Examining the Edges of Multi-Layer Graphene Sheets**". *Chemistry of Materials* (**2009**) *Vol. 21*, p. 2418-2421.

[43] Zhang, Y. B.; Small, J. P.; Pontius, W. V.; Kim, P. "**Fabrication and electric-field-dependent transport measurements of mesoscopic graphite devices**". *Appl. Phys. Lett.* (**2005**) *Vol. 86*, p. 3.

[44] Dayen, J. F.; Mahmood, A.; Golubev, D. S.; Roch-Jeune, I.; Salles, P.; Dujardin, E. "**Side-gated transport in focused-ion-beam-fabricated multilayered graphene nanoribbons**". *Small* (**2008**) *Vol. 4*, p. 716-720.

[45] Fernandez-Moran, H. "**Single crystals of graphite and mica as specimen support for electron microscopy**". *Journal of applied physics* (**1960**) *Vol. 31*, p. 1844.

[46] Novoselov, K. S.; Jiang, D.; Schedin, F.; Booth, T. J.; Khotkevich, V. V.; Morozov, S. V.; Geim, A. K. "**Two-dimensional atomic crystals**". *Proc. Natl. Acad. Sci. U. S. A.* (**2005**) *Vol. 102*, p. 10451-10453.

[47] Forbeaux, I.; Themlin, J. M.; Debever, J. M. "**High-temperature graphitization of the 6H-SiC (000(1)) face**". *Surf. Sci.* (**1999**) *Vol. 442*, p. 9-18.

[48] Hass, J.; Varchon, F.; Millan-Otoya, J. E.; Sprinkle, M.; Sharma, N.; de Heer, W. A.; Berger, C.; First, P. N.; Magaud, L.; Conrad, E. H. "**Why Multilayer Graphene on 4H-SiC(0001) Behaves Like a Single Sheet of Graphene**". *Phys. Rev. Lett.* (**2008**) *Vol. 100*, p. 125504.

[49] Emtsev, K. V.; Bostwick, A.; Horn, K.; Jobst, J.; Kellogg, G. L.; Ley, L.; McChesney, J. L.; Ohta, T.; Reshanov, S. A.; Rohrl, J.; Rotenberg, E.; Schmid, A. K.; Waldmann, D.; Weber, H. B.; Seyller, T. "**Towards wafer-size graphene layers by atmospheric pressure graphitization of silicon carbide**". *Nat. Mater.* (**2009**) *Vol. 8*, p. 203-207.

[50] Land, T. A.; Michely, T.; Behm, R. J.; Hemminger, J. C.; Comsa, G. "**STM investigation of single layer graphite structures produced on Pt(111) by hydrocarbon decomposition**". *Surf. Sci.* (**1992**) *Vol. 264*, p. 261-270.

[51] Sutter, P. W.; Flege, J.-I.; Sutter, E. A. "**Epitaxial graphene on ruthenium**". *Nat Mater* (**2008**) *Vol. 7*, p. 406-411.

[52] Coraux, J.; N'Diaye, A. T.; Busse, C.; Michely, T. "**Structural coherency of graphene on Ir(111)**". *Nano Letters* (**2008**) *Vol. 8*, p. 565-570.

[53] Reina, A.; Jia, X. T.; Ho, J.; Nezich, D.; Son, H. B.; Bulovic, V.; Dresselhaus, M. S.; Kong, J. "**Large Area, Few-Layer Graphene Films on Arbitrary Substrates by Chemical Vapor Deposition**". *Nano Letters* (**2009**) *Vol. 9*, p. 30-35.

[54] J. J. Lander, H. E. K., and A. L. Beach "**Solubility and Diffusion Coefficient of Carbon in Nickel: Reaction Rates of Nickel-Carbon Alloys with Barium Oxide** ". *Journal of applied physics* (**1952**) *Vol. 23*, p. 5.

[55] McLellan, R. B. "**The solubility of carbon in solid gold, copper, and silver**". *Scripta Metallurgica* (**1969**) *Vol. 3*, p. 389-391.

[56] Li, X. S.; Cai, W. W.; An, J. H.; Kim, S.; Nah, J.; Yang, D. X.; Piner, R.; Velamakanni, A.; Jung, I.; Tutuc, E.; Banerjee, S. K.; Colombo, L.; Ruoff, R. S. "**Large-Area Synthesis of High-Quality and Uniform Graphene Films on Copper Foils**". *Science* (**2009**) *Vol. 324*, p. 1312-1314.

[57] Bae, S.; Kim, H.; Lee, Y.; Xu, X. F.; Park, J. S.; Zheng, Y.; Balakrishnan, J.; Lei, T.; Kim, H. R.; Song, Y. I.; Kim, Y. J.; Kim, K. S.; Ozyilmaz, B.; Ahn, J. H.; Hong, B. H.; Iijima, S. "**Roll-to-roll production of 30-inch graphene films for transparent electrodes**". *Nat. Nanotechnol.* (**2010**) *Vol. 5*, p. 574-578.

[58] Wu, J.; Tomovic, Z.; Enkelmann, V.; Müllen, K. "**From Branched Hydrocarbon Propellers to C3-Symmetric Graphite Disks**". *The Journal of Organic Chemistry* (**2004**) *Vol. 69*, p. 5179-5186.

[59] Wu, J.; Gherghel, L.; Watson, M. D.; Li, J.; Wang, Z.; Simpson, C. D.; Kolb, U.; Müllen, K. "**From Branched Polyphenylenes to Graphite Ribbons**". *Macromolecules* (**2003**) *Vol. 36*, p. 7082-7089.

[60] Yang, X.; Dou, X.; Rouhanipour, A.; Zhi, L.; Räder, H. J.; Müllen, K. "**Two-Dimensional Graphene Nanoribbons**". *Journal of the American Chemical Society* (**2008**) *Vol. 130*, p. 4216-4217.

[61] Cai, J. M.; Ruffieux, P.; Jaafar, R.; Bieri, M.; Braun, T.; Blankenburg, S.; Muoth, M.; Seitsonen, A. P.; Saleh, M.; Feng, X. L.; Mullen, K.; Fasel, R. "**Atomically precise bottom-up fabrication of graphene nanoribbons**". *Nature* (**2010**) *Vol. 466*, p. 470-473.

[62] Han, M. Y.; Ozyilmaz, B.; Zhang, Y. B.; Kim, P. "**Energy band-gap engineering of graphene nanoribbons**". *Phys. Rev. Lett.* (**2007**) *Vol. 98*, p. 4.

[63] Chen, Z. H.; Lin, Y. M.; Rooks, M. J.; Avouris, P. "**Graphene nano-ribbon electronics**". *Physica E* (**2007**) *Vol. 40*, p. 228-232.

[64] Son, Y.-W.; Cohen, M. L.; Louie, S. G. "**Energy Gaps in Graphene Nanoribbons**". *Phys. Rev. Lett.* (**2006**) *Vol. 97*, p. 216803.

[65] Barone, V.; Hod, O.; Scuseria, G. E. "**Electronic structure and stability of semiconducting graphene nanoribbons**". *Nano Letters* (**2006**) *Vol. 6*, p. 2748-2754.

[66] Ezawa, M. "**Peculiar width dependence of the electronic properties of carbon nanoribbons**". *Physical Review B* (**2006**) *Vol. 73*, p. 045432.

[67] Sols, F.; Guinea, F.; Neto, A. H. C. "**Coulomb blockade in graphene nanoribbons**". *Phys. Rev. Lett.* (**2007**) *Vol. 99*, p. 4.

[68] Stampfer, C.; Güttinger, J.; Hellmüller, S.; Molitor, F.; Ensslin, K.; Ihn, T. "**Energy Gaps in Etched Graphene Nanoribbons**". *Phys. Rev. Lett.* (**2009**) *Vol. 102*, p. 056403.

[69] Han, M. Y.; Brant, J. C.; Kim, P. "**Electron Transport in Disordered Graphene Nanoribbons**". *Phys. Rev. Lett.* (**2010**) *Vol. 104*, p. 4.

[70] Gallagher, P.; Todd, K.; Goldhaber-Gordon, D. "**Disorder-induced gap behavior in graphene nanoribbons**". *Physical Review B* (**2010**) *Vol. 81*, p. 115409.

[71] Ishigami, M.; Chen, J. H.; Cullen, W. G.; Fuhrer, M. S.; Williams, E. D. "**Atomic Structure of Graphene on SiO2**". *Nano Lett.* (**2007**) *Vol. 7*, p. 1643-1648.

[72] Moser, J.; Barreiro, A.; Bachtold, A. "**Current-induced cleaning of graphene**". *Appl. Phys. Lett.* (**2007**) *Vol. 91*, p. 3.

[73] Lin, Y. C.; Lu, C. C.; Yeh, C. H.; Jin, C. H.; Suenaga, K.; Chiu, P. W. "**Graphene Annealing: How Clean Can It Be?**". *Nano Lett.* (**2012**) *Vol. 12*, p. 414-419.

[74] Archanjo, B. S.; Barboza, A. P. M.; Neves, B. R. A.; Malard, L. M.; Ferreira, E. H. M.; Brant, J. C.; Alves, E. S.; Plentz, F.; Carozo, V.; Fragneaud, B.; Maciel, I. O.; Almeida, C. M.; Jorio, A.; Achete, C. A. "**The use of a Ga+ focused ion beam to modify graphene for device applications**". *Nanotechnology* (**2012**) *Vol. 23*, p. 255305.

[75] Bell, D. C.; Lemme, M. C.; Stern, L. A.; Rwilliams, J.; Marcus, C. M. "**Precision cutting and patterning of graphene with helium ions**". *Nanotechnology* (**2009**) *Vol. 20*, p. 5.

[76] Lemme, M. C.; Bell, D. C.; Williams, J. R.; Stern, L. A.; Baugher, B. W. H.; Jarillo-Herrero, P.; Marcus, C. M. "**Etching of Graphene Devices with a Helium Ion Beam**". *ACS Nano* (**2009**) *Vol. 3*, p. 2674-2676.

[77] Binnig, G.; Rohrer, H. "**Scanning tunneling microscopy**". *IBM J. Res. Dev.* (**1986**) *Vol. 30*, p. 355-369.

[78] Albrecht, T. R.; Dovek, M. M.; Kirk, M. D.; Lang, C. A.; Quate, C. F.; Smith, D. P. E. "**Nanometer-scale hole formation on graphite using a scanning tunneling microscope**". *Appl. Phys. Lett.* (**1989**) *Vol. 55*, p. 1727-1729.

[79] McCarley, R. L.; Hendricks, S. A.; Bard, A. J. "**Controlled nanofabrication of highly orientated pyrolitic-graphite with the scanning tunneling microscope**". *Journal of Physical Chemistry* (**1992**) *Vol. 96*, p. 10089-10092.

[80] Tapaszto, L.; Dobrik, G.; Lambin, P.; Biro, L. P. "**Tailoring the atomic structure of graphene nanoribbons by scanning tunnelling microscope lithography**". *Nat. Nanotechnol.* (**2008**) *Vol. 3*, p. 397-401.

[81] Kondo, S.; Lutwyche, M.; Wada, Y. "**Nanofabrication of layered materials with the scanning tunneling microscope**". *Applied Surface Science* (**1994**) *Vol. 75*, p. 39-44.

[82] Biro, L. P.; Lambin, P. "**Nanopatterning of graphene with crystallographic orientation control**". *Carbon* (**2011**) *Vol. 48*, p. 2677-2689.

[83] Masubuchi, S.; Ono, M.; Yoshida, K.; Hirakawa, K.; Machida, T. "**Fabrication of graphene nanoribbon by local anodic oxidation lithography using atomic force microscope**". *Appl. Phys. Lett.* (**2009**) *Vol. 94*, p. 3.

[84] Giesbers, A. J. M.; Zeitler, U.; Neubeck, S.; Freitag, F.; Novoselov, K. S.; Maan, J. C. "**Nanolithography and manipulation of graphene using an atomic force microscope**". *Solid State Commun.* (**2008**) *Vol. 147*, p. 366-369.

[85] Weng, L. S.; Zhang, L. Y.; Chen, Y. P.; Rokhinson, L. P. "**Atomic force microscope local oxidation nanolithography of graphene**". *Appl. Phys. Lett.* (**2008**) *Vol. 93*, p. 3.

[86] Banhart, F. "**Irradiation effects in carbon nanostructures**". *Rep. Prog. Phys.* (**1999**) *Vol. 62*, p. 1181-1221.

[87] Rodriguez-Manzo, J. A.; Krasheninnikov, A. V.; Banhart, F. "**Engineering the Atomic Structure of Carbon Nanotubes by a Focused Electron Beam: New Morphologies at the Sub-Nanometer Scale**". *ChemPhysChem* (**2012**) *Vol. 13*, p. 2596-2600.

[88] Fischbein, M. D.; Drndic, M. "**Electron beam nanosculpting of suspended graphene sheets**". *Appl. Phys. Lett.* (**2008**) *Vol. 93*, p. 3.

[89] Krasheninnikov, A. V.; Banhart, F. "**Engineering of nanostructured carbon materials with electron or ion beams**". *Nat Mater* (**2007**) *Vol. 6*, p. 723-733.

[90] Girit, C. O.; Meyer, J. C.; Erni, R.; Rossell, M. D.; Kisielowski, C.; Yang, L.; Park, C. H.; Crommie, M. F.; Cohen, M. L.; Louie, S. G.; Zettl, A. "**Graphene at the Edge: Stability and Dynamics**". *Science* (**2009**) *Vol. 323*, p. 1705-1708.

[91] Song, B.; Schneider, G. F.; Xu, Q.; Pandraud, G.; Dekker, C.; Zandbergen, H. "**Atomic-Scale Electron-Beam Sculpting of Near-Defect-Free Graphene Nanostructures**". *Nano Letters* (**2011**) *Vol. 11*, p. 2247-2250.

[92] Hiura, H. "**Generation of circular and hexagonal microholes in a graphite surface**". *J. Mater. Res.* (**2001**) *Vol. 16*, p. 1287-1292.

[93] Kosynkin, D. V.; Higginbotham, A. L.; Sinitskii, A.; Lomeda, J. R.; Dimiev, A.; Price, B. K.; Tour, J. M. "**Longitudinal unzipping of carbon nanotubes to form graphene nanoribbons**". *Nature* (**2009**) *Vol. 458*, p. 872-877.

[94] Xie, L. M.; Wang, H. L.; Jin, C. H.; Wang, X. R.; Jiao, L. Y.; Suenaga, K.; Dai, H. J. "**Graphene Nanoribbons from Unzipped Carbon Nanotubes: Atomic Structures, Raman Spectroscopy, and Electrical Properties**". *Journal of the American Chemical Society* (**2011**) *Vol. 133*, p. 10394-10397.

[95] Cano-Marquez, A. G.; Rodriguez-Macias, F. J.; Campos-Delgado, J.; Espinosa-Gonzalez, C. G.; Tristan-Lopez, F.; Ramirez-Gonzalez, D.; Cullen, D. A.; Smith, D. J.; Terrones, M.; Vega-Cantu, Y. I. "**Ex-MWNTs: Graphene Sheets and Ribbons Produced by Lithium Intercalation and Exfoliation of Carbon Nanotubes**". *Nano Letters* (**2009**) *Vol. 9*, p. 1527-1533.

[96] Jiao, L. Y.; Wang, X. R.; Diankov, G.; Wang, H. L.; Dai, H. J. "**Facile synthesis of high-quality graphene nanoribbons**". *Nat. Nanotechnol.* (**2011**) *Vol. 5*, p. 321-325.

[97] Li, X. L.; Wang, X. R.; Zhang, L.; Lee, S. W.; Dai, H. J. "**Chemically derived, ultrasmooth graphene nanoribbon semiconductors**". *Science* (**2008**) *Vol. 319*, p. 1229-1232.

[98] Kawai, T.; Okada, S.; Miyamoto, Y.; Hiura, H. "**Self-redirection of tearing edges in graphene: Tight-binding molecular dynamics simulations**". *Physical Review B* (**2009**) *Vol. 80*, p. 033401.

[99] Poumirol, J.-M.; Cresti, A.; Roche, S.; Escoffier, W.; Goiran, M.; Wang, X.; Li, X.; Dai, H.; Raquet, B. "**Edge magnetotransport fingerprints in disordered graphene nanoribbons**". *Physical Review B* (**2010**) *Vol. 82*, p. 041413.

[100] Tomita, A.; Tamai, Y. "**Optical microscopic study on catalytic-hydrogenation of graphite**". *Journal of Physical Chemistry* (**1974**) *Vol. 78*, p. 2254-2258.

[101] Datta, S. S.; Strachan, D. R.; Khamis, S. M.; Johnson, A. T. C. "**Crystallographic etching of few-layer graphene**". *Nano Letters* (**2008**) *Vol. 8*, p. 1912-1915.

[102] Tsukamoto, T.; Ogino, T. "**Graphene etching controlled by atomic structures on the substrate surface**". *Carbon* (**2011**) *Vol. 50*, p. 674-679.

[103] Tsukamoto, T.; Ogino, T. "**Control of Graphene Etching by Atomic Structures of the Supporting Substrate Surfaces**". *Journal of Physical Chemistry C* (**2012**) *Vol. 115*, p. 8580-8585.

[104] Ci, L.; Xu, Z. P.; Wang, L. L.; Gao, W.; Ding, F.; Kelly, K. F.; Yakobson, B. I.; Ajayan, P. M. "**Controlled Nanocutting of Graphene**". *Nano Res.* (**2008**) *Vol. 1*, p. 116-122.

[105] Ci, L. J.; Song, L.; Jariwala, D.; Elias, A. L.; Gao, W.; Terrones, M.; Ajayan, P. M. "**Graphene Shape Control by Multistage Cutting and Transfer**". *Advanced Materials* (**2009**) *Vol. 21*, p. 4487.

[106] Campos, L. C.; Manfrinato, V. R.; Sanchez-Yamagishi, J. D.; Kong, J.; Jarillo-Herrero, P. "**Anisotropic Etching and Nanoribbon Formation in Single-Layer Graphene**". *Nano Letters* (**2009**) *Vol. 9*, p. 2600-2604.

[107] Schaffel, F.; Warner, J. H.; Bachmatiuk, A.; Rellinghaus, B.; Buchner, B.; Schultz, L.; Rummeli, M. H. "**Shedding Light on the Crystallographic Etching of Multi-Layer Graphene at the Atomic Scale**". *Nano Res.* (**2009**) *Vol. 2*, p. 695-705.

[108] Schaffel, F.; Wilson, M.; Bachmatiuk, A.; Rummeli, M. H.; Queitsch, U.; Rellinghaus, B.; Briggs, G. A. D.; Warner, J. H. "**Atomic Resolution Imaging of the Edges of Catalytically Etched Suspended Few-Layer Graphene**". *ACS Nano* (**2011**) *Vol. 5*, p. 1975-1983.

CHAPTER 2

Materials, techniques and instruments.

Dans ce chapitre, les aspects techniques des matériels, instruments et techniques utilisées pour réaliser le travail de cette thèse sont rassemblées.

Dans un premier temps sont présentés les produits chimiques utilisés, les substrats pour déposer le graphène, les procédures de nettoyage de recuit et de dépôt du graphène sur substrat Si/SiO_2. Le transfert de graphène cru par CVD sur des grilles TEM est également traité.

Dans une deuxième partie sont rassemblées les caractéristiques techniques des différentes techniques de caractérisation utilisées au cours de cette thèse : la microscopie optique, la spectroscopie Raman et la microscopie à force atomique. Le MEB

In this chapter, the different technical aspects of the materials and techniques used to realize the work of this thesis are presented.

In a first part, the chemicals, the substrates used to deposit graphene, the cleaning, annealing and deposit procedure of graphene on Si/SiO_2 substrates are presented. The transfer of CVD graphene on TEM grids is also treated.

In a second part the specifications of the different techniques used during this thesis are presented: optical, AFM and TEM microscopy, Raman spectroscopy. The SEM used for etching and imaging

utilisé pour graver et imager les découpes dans le graphène est présenté ainsi que les METs qui ont permis de réaliser ce travail.

graphene is also presented.

2.1 Materials and techniques.

2.1.1 Chemicals, solvent and gases.

The electronic grade chemicals were used as received for the cleaning of substrates. The list includes extra pure (96%) sulfuric acid, and hydrogen peroxide (35 wt.% solution in water) from Sigma Aldrich. Solvent of Very Large Scale Integration grade (VLSI) obtained from Panreac are 1-Methyl-2-Pyrrolidinone (NMP), Acetone and 2-Propanol (IPA). De-ionized (DI) water of 18 MΩ.cm resistivity was obtained from Veolia Purelab water purifier. Dry nitrogen gas was used with high purity level lesser than: H_2O: 3 ppm, O_2: 2 ppm and C_nH_m: 0.5 ppm.

2.1.2 Si/SiO_2 substrates.

Si/SiO_2 substrates are cut in 8x8 mm^2 and 500 μm thick chips from thermally oxidized silicon wafer (degenerately doped with n-type impurities ~10^{18} cm^{-3}). Oxide thickness was 285 nm. Each substrate bears a 26x26 array of (15 μm x 15 μm) labeled gold crosses, with a 200 μm pitch as shown in figure 2.1.

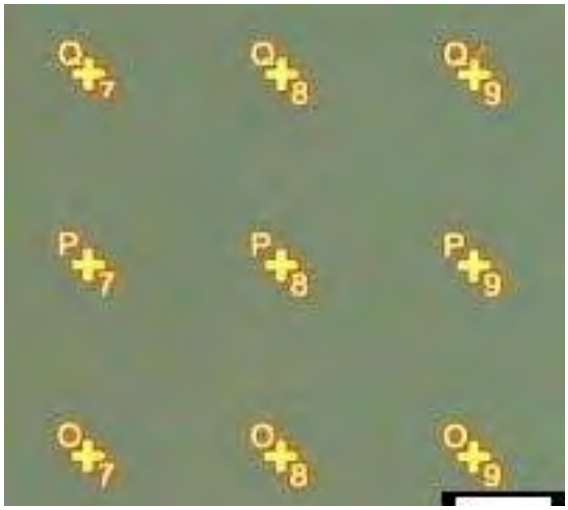

Figure 2.1: *Optical image of a Si/SiO_2 substrate with photolithography pre-patterned numbered metal crosses. Scale bar is 100 μm.*

2.1.3 Si/SiO_2 substrates cleaning.

Si/SiO_2 substrates were cleaned by two methods:

Chips are first sonicated in NMP, then in acetone and finally in IPA (15 minutes each), for a total number of three times in each solvent successively. During the transfer from NMP to acetone (or from acetone to IPA), the oxide face is rinsed with fresh acetone (or IPA respectively). Substrates are not allowed to dry during this transfer. If necessary, samples are stored in IPA before drying under N_2 flux.

The second method consists in one sonication in NMP, then in acetone and finally in IPA (15 minutes each). Substrates are then transferred in DI water twice and put for 2 h in a hot piranha bath (1/3 volume of sulfuric acid and 2/3 volume of hydrogen peroxide). Substrates are then rinsed twice in DI water and stored in IPA before drying under N_2 flux.

Finally, the substrates are cleaned in a dioxygen / Argon plasma chamber for a duration of 3 minutes, immediately before depositing graphene.

2.1.4 Annealing and storage.

Samples are annealed in an oven, the temperature is regulated by a West 6100 electronic. The temperature increasing rate is $300°C.min^{-1}$ and the cooling is performed naturally. The sample is placed in a cylindrical tube of 3 cm in diameter and 95 cm in length. One entrance of the tube is connected to a flow of a mixture of Ar and H_2 whom the flux is controlled by a Tylan RO-28. The outgas of the tube is plunged in a water tank. Typical fluxes used are 300 $cm^3.min^{-1}$ for Ar and 50 to 100 $cm^3.min^{-1}$ for H_2. Temperatures used are between 100 and 500°C.

2.1.5 Mechanical exfoliation deposition of graphene.

Mechanical exfoliation of graphite, [1, 2] is performed in a clean room, approximately 3 to 4 cm wide stripes of clean room adhesive tape are prepared. Natural graphite flakes are placed on a corner of one adhesive tape. By sticking the tape against itself 10 to 20 times, graphite is exfoliated until the whole tape surface is covered. The tape is then examined with

an optical microscope at low magnification (50x). Graphite exfoliated flakes are transferred to a second adhesive tape which is stuck against itself once or twice to refresh graphite flakes. The second tape is inspected with the binocular microscope and the substrate is placed on the tape, in an area with the highest density of graphite, oxide face against the tape. Chip and tape are pressed together between two fingers, avoiding any shearing movements. Finally samples are carefully removed from the tape and inspected with an optical microscope.

2.1.6 Graphene on TEM grid.

Several type of TEM grids were used to study graphene. In all case, graphene was grown by CVD on a metal and transferred on TEM grids.

The first type of sample has been purchased from Graphene Supermaket. The grid is a copper 2,000 mesh. Graphene is grown by CVD on a nickel surface and then transferred on the grid by a resist-free technique. [3] The grids are covered with FLG that are certified to be 1 to 10 graphene layer thick.

The other samples were prepared by us or the group of Bouchiat in Neel institute (Grenoble, France). TEM grids were either gold quantifoil or Si_3N_4 membranes. Gold quantifoil grids purchased from EMS, consist of a gold 300 mesh TEM grid covered with an amorphous carbon thin film perforated with 1 μm diameter holes. Si_3N_4 membranes are purchased from EMS, they are thin membrane of Si_3N_4 perforated with hole of 1 μm in diameter and supported by a silicon substrate. Graphene is grown by CVD on a copper surface by the group of Bouchiat in Neel institute (Grenoble, France) or purchased to Graphene Supermarket.

This graphene is transferred to a TEM grid by one of two techniques. The first one, PMMA is spun on the graphene, the sandwich copper, graphene and PMMA is placed on a 10^{-1} mol.L^{-1} $(NH_3)_4S_2O_8$ solution to solve copper in about 3 h. When all the metal has been etched, the PMMA and graphene are placed on a substrate and plunged in a NMP solution at 80°C for 15', and cooled down to room temperature. Then it is placed in an acetone solu-

tion at room temperature for 10', transferred to an IPA solution at 80°C, just below its boiling point and the substrate is dried by removing it vertically from the IPA.

In the second transfer technique, graphene and copper are placed in a $(NH_4)_2S_2O_8$ solution concentrated at $2x10^{-2}$ mol.L ^{1} until all the copper is gently etched which typically take 48h. The graphene released from the metal floats on the sulfite solution where it can be taken directly with a substrate or a grid, dried on a hot plate at 40°C, washed in DI water and let dried in air.

2.2 Instruments.

2.2.1 Optical microscopy.

Optical microscope was an Olympus B60 microscope with white reflected light. Ocular has a x10 magnification and objectives have x5, x10, x50 and x100 magnifications. Green filter can be introduced in the optical path.

2.2.2 Raman spectroscopy.

Two spectrometers have been used. A Renishaw RM1000B equipped with a low pass filter and a 1,800 line.mm^{-1} grating. An Argon gas laser at a 514.5 nm wavelength have been used. The spectrometer is coupled with an optical microscope Olympus BH-2. The other setup is an XploRA-MV2000 from Horiba coupled with an Olympus BX-51 optical microscope. Three semiconductor lasers are available with wavelength and power of 532 nm, 15.2 mW; 638 nm, 14.7 mW and 785 nm, 40 mW. 4 gating are available: 300, 600, 1800 and 2400 l.mm^{-1}. A power filter can reduces the incident laser beam power by 0.1, 1, 10, 25, 50 or 100%. Polarizer and analyzer are available. Objectives are x10, x50 and x100 magnification.

2.2.3 AFMs.

AFM imaging was performed on a Veeco DI3000 or on a Veeco multimode Picoforce microscope (Figure 2.2). DI3000 is associated with a Nanoscope III-A controller. Multimode Picoforce is associated with a Nanoscope IV controller. It is equipped with a Picoforce scanner dedicated to force spectroscopy studies. Both microscopes are mounted on a vibration

isolation table with integrated acoustic hoods. They are also equipped with an optical camera to approach the tip on the surface. They were used in intermittent mode.

The tips used (Bruker, OTESPA) are made of silicon. They are terminated by rectangular cantilever silicon, the thickness is between 3.6 and 5.6 μm, and length between 140 and 180 μm. The rear face of the cantilever is covered with a 50 nm aluminum layer reflective. The resonance frequency of these tips is between 290 kHz and 345 kHz and their spring constant between 12 and 103 Nm^{-1}.

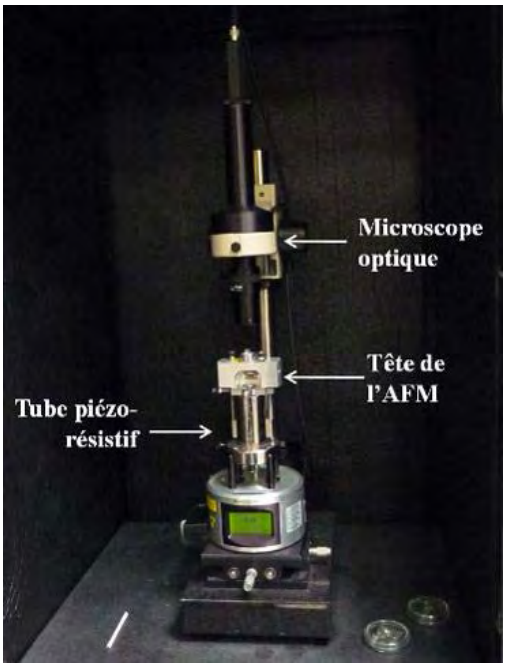

Figure 2.2. *Picoforce AFM.*

A homemade humidity control system is adapted to the multimode Picoforce. A plastic bell is placed over the AFM head, it is not hermetic and air can escape. A humidity sensor is introduced near the AFM head to measure the relative humidity (RH). For relative humidity higher than the ambient one, a nitrogen flux is introduced in a bubble system plunged in DI water. The water is contained by a hermetic bottle, its outgas gas feed a second bottle whom outgas is injected in the bell. The outgas of the second bottle has a stable RH, the value of which depends directly on the nitrogen flux. If the RH is lower than the ambient one, the

sample is annealed on hot plate in air to desorb water. It is then placed as soon as possible in the AFM system and pure nitrogen is directly injected in the bell. The RH is stable and depends on the nitrogen flux.

2.2.4 SEM-EBIE.

SEM is a 1540 XB from Zeiss (Figure 2.3). Electrons are emitted from a field emission gun (FEG) their acceleration tension can be set from 1 to 30 kV. Typical electronic current at 20 kV acceleration has been measured with a faraday cup, it is 280 pA. Primary or secondary electron detectors are available. The typical vacuum level is 0.5 to $1x10^{-6}$ mbar.

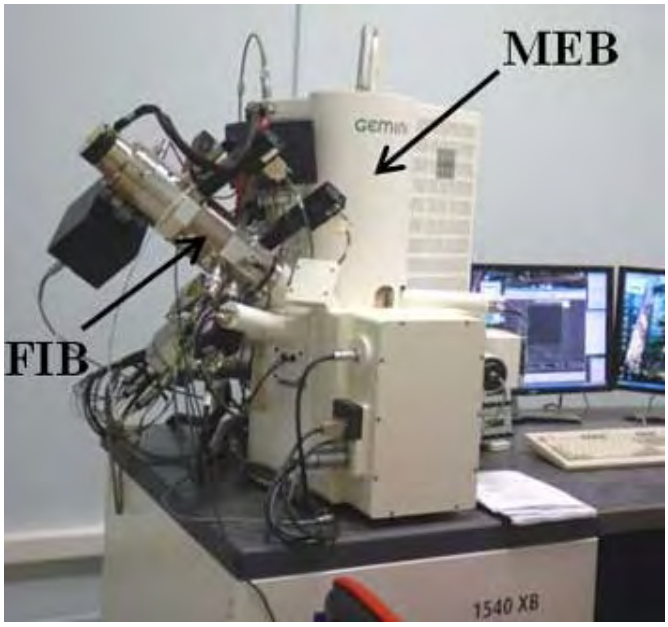

Figure 2.3. *Zeiss 1540XB FIB-SEM equipped with a GIS.*

2.2.5 TEM

The electron beam can be controlled by a software so that arbitrary shaped irradiation can be done. Associated with a gas injection system that can inject water vapor on the sample. TEM.

SACTEM analysis of graphene were conducted on a FEI TecnaiF20 (Figure 2.4) equipped with a spherical aberration corrector for the image. Electrons are emitted by a FEG

at 100 kV for imaging graphene. The microscope is equipped with a Gatan USC 2k2k camera.

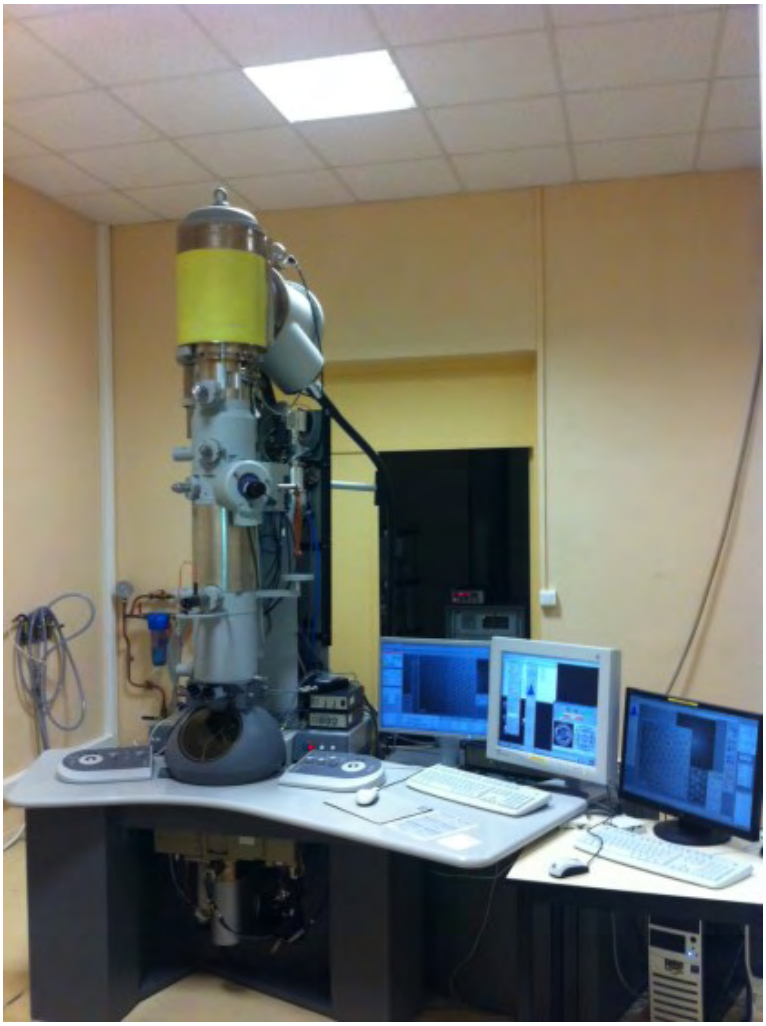

Figure 2.4. *SACTEM FEI TECNAIF20*

Conventional TEM images were carried out on a PHILIPS CM20 or CM30 operating at 80 and 100 kV accelerating voltage respectively. The filament source is a LaB_6 filament. The microscope is equipped with a home made 2k2k CCD camera for CM20 and a Gatan MSC 1k1k camera for CM30.

Microscope images were recorded on Gatan Digital Micrograph software. Images were flattened with a homemade software made by Christophe Gatel.

2.3 References.

[1].Novoselov, K. S.; Geim, A. K.; Morozov, S. V.; Jiang, D.; Zhang, Y.; Dubonos, S. V.; Grigorieva, I. V.; Firsov, A. A. "**Electric field effect in atomically thin carbon films**". *Science* (**2004**) *Vol. 306*, p. 666-669.

[2].Novoselov, K. S.; Jiang, D.; Schedin, F.; Booth, T. J.; Khotkevich, V. V.; Morozov, S. V.; Geim, A. K. "**Two-dimensional atomic crystals**". *Proc. Natl. Acad. Sci. U. S. A.* (**2005**) *Vol. 102*, p. 10451-10453.

[3].Regan, W.; Alem, N.; Aleman, B.; Geng, B. S.; Girit, C.; Maserati, L.; Wang, F.; Crommie, M.; Zettl, A. "**A direct transfer of layer-area graphene**". *Appl. Phys. Lett.* (**2010**) *Vol. 96*, p. 3.

CHAPTER 3

Morphological and structural characterization of graphene on SiO_2 by AFM and Raman spectroscopy.

La production de graphène par exfoliation et transfert sur SiO_2 est une des méthodes les plus simples et les plus usitées. L'identification de la monocouche de graphène est possible en combinant microscopie optique, AFM et spectroscopie Raman. La littérature regorge d'images AFM de la monocouche de graphène sur SiO_2 dont la hauteur apparente présente d'importantes variations, entre 0,5 et 1,0 nm.

Dans une première partie, nous nous sommes employés à trouver les paramètres permettant la mesure de la hauteur apparente

The production of graphene by exfoliation and transfer on SiO_2 is one of the most simple and most used techniques. The identification of a graphene monolayer is possible by combining optical microscopy, AFM and Raman spectroscopy. The literature provides a wide set of AFM images of graphene on SiO_2, the apparent thickness of which presents large variations from 0.5 to 1.0 nm.

In a first part, we have explored the parameters allowing the most reproducible possible measure of the apparent height of

du graphène par AFM la plus reproductible possible. Une étude en atmosphère contrôlée met en évidence le rôle du taux d'humidité. Par ailleurs, dans des conditions d'humidité fixées, la consigne d'amplitude d'oscillation de la pointe AFM en mode intermittent est responsable d'une surépaisseur artificielle qui a été identifiée et peu être corrigée afin d'aboutir à des conditions d'imagerie stables et reproductibles.

graphene by AFM. A study in controlled atmosphere evidences the role of the relative humidity. Furthermore, in fixed humidity conditions the amplitude set point of the AFM is responsible of an apparent height overestimation which has been identified and can be corrected leading to stable and reproducible imaging conditions.

En amont des chapitres 4 et 5 qui sont consacrés à la structuration du graphène et donc à la création intentionnelle de découpe et de défauts, nous avons caractérisé le matériau initial par spectroscopie Raman, d'une part, l'intensité intégrée du pic G du graphène permet de déterminer sans ambigüité le nombre de couches d'un dépôt de graphène. D'autre part, nous avons exploré la possibilité d'exalter le signal Raman intrinsèquement faible des défauts par couplage du graphène avec des structures plasmoniques colloïdales. Le pic D du graphène est sensible aux défauts présents dans son réseau atomique. Exalter ce signal permettrait de détecter une plus faible quantité de défauts et par exemple de mieux caractériser spectroscopiquement la structure des bords de ru-

Before chapters 4 and 5 which will study the patterning and thus an intentional creation of defect in graphene, we characterized the starting material by Raman spectroscopy. On one hand, the integrated intensity of the G peak of graphene allows to unambiguously determine the number of layer of a graphene flake. On the other hand, we have explored the exaltation of the intrinsically low Raman signal of defects in graphene by a coupling between graphene and surface plasmons of metallic colloids. The D peak of graphene is sensitive to its quantity of defects. Enhancing this signal would allow to detect a lower quantity of defects and, for example, to better characterize spectrocopically the structure of the edg-

ban de graphène.

Enfin, l'objectif de cette thèse étant de faire converger des techniques permettant la structuration du graphène jusqu'à l'échelle atomique sur un substrat isolant et atomiquement plan, il a semblé important d'évaluer la capacité d'imager le graphène par AFM non-contact (NC-AFM) en modulation de fréquence qui est la seule technique actuelle permettant d'imager sur un substrat isolant avec une résolution atomique. [1-5] La fin de ce chapitre rassemble nos tentatives d'imagerie en NC-AFM sous UHV.

es of graphene.

Finally, the objective of this thesis is the patterning of graphene until the atomic scale on an atomically flat insulating substrate by the convergent combination of several techniques. It seemed important to evaluate the capability of non contact AFM (NC-AFM) in frequency modulation to image graphene. This technique is the only one allowing to image an insulating substrate or a molecule on an insulating substrate with an atomic of sub molecular resolution. [1-5] The end of this chapter gathers our attempts of imaging graphene in UHV NC-AFM.

3.1 AFM imaging of graphene in ambient conditions.

Historically, apparent height of graphene measured by AFM has been one of the first techniques capable of identifying the number of layers of a graphene flakes. AFM imaging has a better spatial resolution than Raman spectroscopy and is convenient for any kind of substrates for supported graphene in contrast with optical contrast of graphene which is restricted to a few numbers of substrates.

The apparent thickness of graphene depends on the true sample thickness, the tip-substrate interaction and the possible presence of adsorbates. The number of graphene layers can thus be deduced by using the following relationship:

$$h_n = h_1 + (n-1) \times g \text{ [6]} \quad (3.1)$$

h_n is the thickness of a n graphene layer (nGL) measured by AFM and g is the separation between two graphene layers in graphite and is 0.35 nm.

Surprisingly, the reported values of AFM thickness for a monolayer graphene (h_1) are quite dispersed (table 3.1) and no consensus is achieved. This remarkable scattering of data pointed us to conduct experiments on the AFM apparent height of graphene in order to identify the origin of the dispersion.

Measured AFM thickness h_1 (nm).	**References**
0.5 to 1.0	[7]
0.7	[6]
0.5	[8]
0.4 to 0.8	[9]
0.7	[10]

Table 3.1. *Thicknesses of graphene measured by AFM. The substrates are Si/SiO_2.*

3.1.1 Graphene thickness overestimation.

For this study, amplitude modulated atomic force microscope (AM-AFM) has been used in intermittent mode and in ambient conditions, with AFM tips having a typical resonance frequency of 300 kHz (Olympus, OTESPA tips). Graphene has been deposited by micromechanical exfoliation on Si/SiO_2 substrates with an oxide thickness of 285 nm. The AFM images were flattened using SPM software Gwyddion or WSXM. [11] Apparent AFM heights have been measured on averaged (~50) height profiles.

An AFM image of a graphene flake is shown in Figure 3.1a. Three different apparent AFM heights could be identified. The height between the graphene flake and the SiO_2 surface on the left (1.3 nm) and the right (2.5 nm) side of the flake were different. The one between the folded portion of the graphene flake and the graphene flake itself (0.7 nm) was also different (Figure 3.1a and b).

The thickness of the self-folded piece is 0.7 nm, corresponding to twice the Van-Der-Vaals gap in bulk graphite (i.e. 0.35 nm), therefore n = 2. [12, 13] The linear relationship between h_n and n (equation 3.1) found by Gupta et al. [6] implies that h_1 can be deduced from h_2 by the formula $h_1 = h_2 - g$.

The measured thickness for the left side of the flake shown in Figure 3.1a corresponds to h_1=1.0 nm, which is in good agreement with the values found in the literature (see table 3.1). However for the right side of the flake the thickness corresponds to h_1=2.2 nm, which is larger than the thickness found for the left side of the flake and the values found in the literature (see table 3.1). This thickness is interpreted as an overestimation due to the AFM imaging conditions. The schematic in Figure 3.1d represents an AFM tip scanning a FLG sample. In the case of this bilayer flake the overestimation is found to be of the order of 1.2 nm. This AFM artifact affects the reproducibility of the measurements. In the following, the influence of the AFM amplitude set point (A_{SP}) on the thickness of a graphene flake measured by AFM will be investigated.

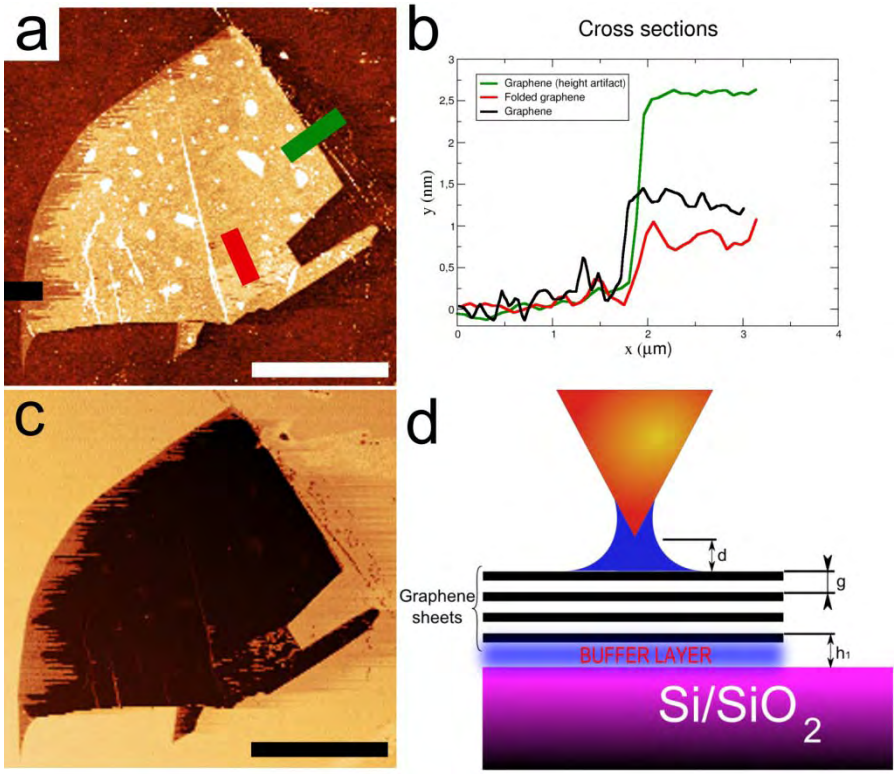

Figure 3.1. *(a) AFM image of a bilayer graphene flake left to right scanning direction and (b), the corresponding cross sections. The green and black cross sections represent a step from silica to graphene on the left (black) and the right side (green) of the graphene flake. The red cross-section represents the step between the graphene flake and a folded portion. (c) AFM phase image of Figure 3.1a. (d) is a schematic of an AFM tip scanning a FLG. h_1 is the thickness of the first graphene layer, g is the interspacing between two graphene layers in graphite and d is the overestimation due to an AFM artifact. Z color scale are (a): 4 nm and (c) 100°. Scale bars are 5 µm.*

The free amplitude (A_0) is the amplitude of oscillation of the AFM tip which has no interaction with the surface of the sample, the tip being far from the surface. The Amplitude set point (A_{SP}) is the target oscillation amplitude of the AFM cantilever for the feedback loop during the imaging. The distance between the AFM tip and the sample is adjusted by the piezo tube so that the amplitude of oscillation of the tip is equal to A_{SP}. The A_{SP} is thus related to the force applied by the tip on the surface, it has been investigated to assess whether or not, if this tip-sample interaction has an influence on the apparent AFM height. A_{SP} can be adjusted at any time by the operator while A_0 is set when choosing the free oscillations conditions before scanning.

Several AFM images of a bilayer graphene flake have been taken for different values of A_{SP}. The thickness of graphene for each A_{SP} value is measured on several areas all around the flake by a consistent protocol (flattening, sampling, averaging). Figure 3.2a shows the thickness plotted versus A_{SP} (black disks). Two extreme regimes are identified, separated by an unstable regime. For an A_{SP} exceeding 0.75V, the graphene thickness is h_2=2.5±0.3 nm. For an A_{SP} below 0.62V, the thickness is h_2=1.3±0.2 nm which is in good agreement with the literature (h_1=0.95 nm). For an A_{SP} comprised between 0.62 and 0.65 V, the graphene thickness is either the high value or the low value (Figure 3.1a). Interestingly, the thickness of the self-folded graphene piece (red squares) remains unchanged and is 0.7 nm for the entire A_{SP} range.

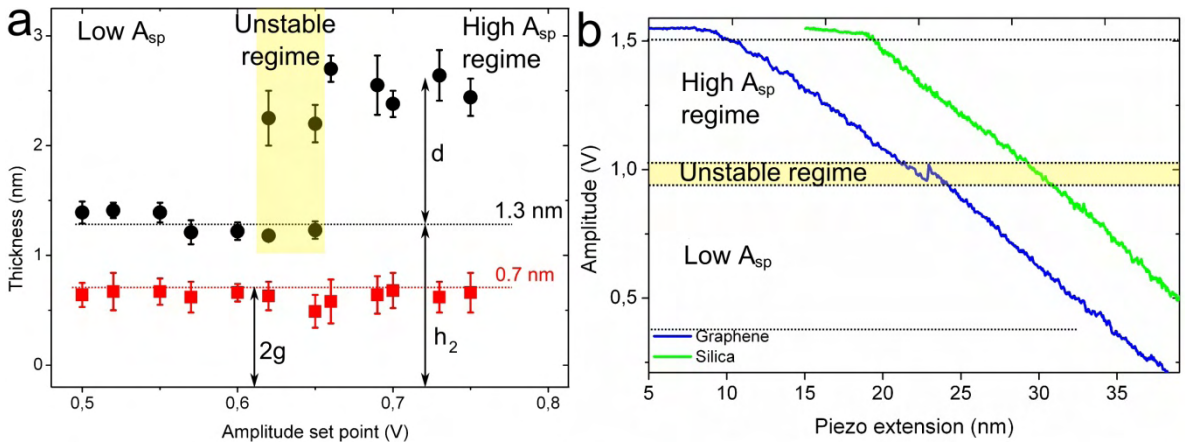

Figure 3.2. *Graphene bilayer apparent height variation with the A_{SP}. (a): Graphene bilayer thickness versus A_{SP}. The thickness is the height difference in AFM image between: bilayer graphene and SiO_2 surface (black disks) and between the folded bilayer and the rest of the flake (red squares). The colors correspond with the cross sections in Figure 3.1a. (b) Approaching curves which correspond to the amplitude of oscillation of the cantilever versus the piezo extension. Approaching curves are recorded other graphene (blue line) and SiO_2 (green line).*

We believe that these two extreme regimes correspond to different tip-sample interactions originated from a water meniscus forming between the tip and the surface. In order to understand this behavior, approaching curve experiments over the graphene and the silica surface have been performed. An approaching curve experiment in intermittent AFM mode records the tip oscillation amplitude a phase shift between excitation and oscillation while

the tip is approaching the surface. The free amplitude was A_0=30 nm, these curves are shown in Figure 3.2b.

The three regimes identified in Figure 3.2a are also observed in the approaching curves. When approaching toward silica, the amplitude decreases smoothly and almost linearly, no specific feature is observed. On the contrary, when approaching over graphene, the monotonous decrease of amplitude is suddenly discontinued with a small jump to a larger amplitude than before and resuming the same monotonous decrease.

For the low A_{SP} regime, the oscillation amplitude is low, a stable water meniscus joins the tip and the surface. The meniscus effect is an attractive tip-sample interaction, the piezo extension is high (Figure 3.2b), the tip is close to the surface. The situation is the same over silica. For the high A_{SP} regime, the oscillation amplitude is higher, the meniscus does not form or is unstable, the attractive interaction of it is reduced the piezo extension thus reduces in comparison with the low A_{SP} regime (Figure 3.2b) and thus the tip is more far from the surface than with a stable meniscus. However, as silica is hydrophilic, the meniscus remains stable at such a high A_{SP}. In consequence the tip is close to the silica surface and far from the graphene surface, the apparent AFM height is thus overestimated. For the measurement on the self-folded piece, the two corresponding amplitude approaching curves would be the amplitude curve of graphene (Figure 3.2b) shifted along the piezo extension axis. For any A_{SP}, the tip-sample interaction is the same on the folded graphene and on the graphene, there is no overestimation.

An approaching or retracting curve can also record the phase shift of the tip. Phase is rich in information about the tip-surface interaction. Noticeably, a negative phase shift is the signature to an overall repulsive tip-sample interaction (averaged over an entire oscillation cycle) while a positive phase shift reveal an attractive interaction. [14] In Figure 3.3, a jump in the phase approaching curve corresponds to the jump of the amplitude approaching curve. For low A_{SP}, the phase shift is positive and thus the tip-sample interaction is overall

attractive while for high A_{SP}, the phase shift is negative and the interaction repulsive. The phase also agrees the hypothesis of the water meniscus.

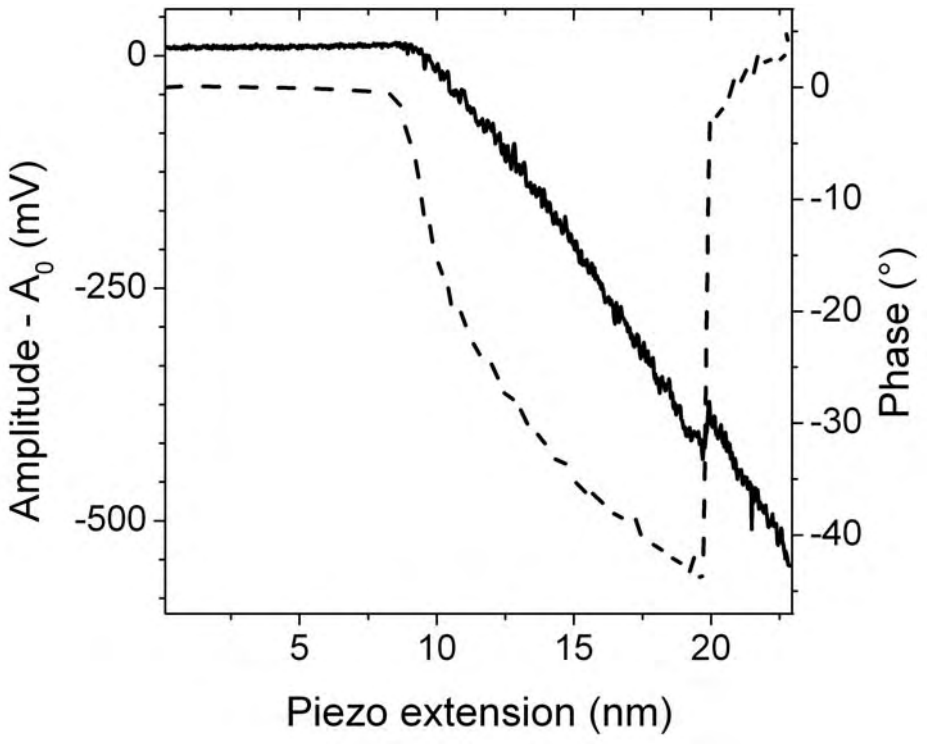

Figure 3.3. *Amplitude (solid line) and phase (dashed line) approaching curve over graphene monolayer.*

For the unstable regime, in Figure 3.1a, while the tip scan the silica, a meniscus is formed, the interaction is attractive. The tip scan the surface and reach a graphene step, the interaction remain attractive until the second edge of the meniscus reach the graphene step or a defect induces the breaking of the meniscus, the interaction become thus repulsive and the height is overestimated. In summary, a band of graphene has a low apparent height and the rest of the flake has an overestimated height. This is exactly what is observed in the AFM image of Figure 3.1a. The jump in the phase between the two regimes is also visible in Figure 3.1c. The radius of the water meniscus is thus estimated to be a few micrometers.

In order to explore the influence of water on the apparent height of graphene an experiment has been designed to control the relative humidity (RH).

3.1.2 Influence of the relative humidity.

Graphene has been deposited on a Si/SiO_2 substrate by the micromechanical technique. The sample and the AFM head have been placed in a home-made bell to control the relative humidity (RH) (see chapter 2). The samples have been annealed at 200°C for one hour on a hot plate before introducing it in the AFM if the RH was lower than the ambient one. The AFM apparent height of monolayer graphene versus the A_{SP} have been measured for a range of RH from 5 to 70%, the results are plotted in Figure 3.4.

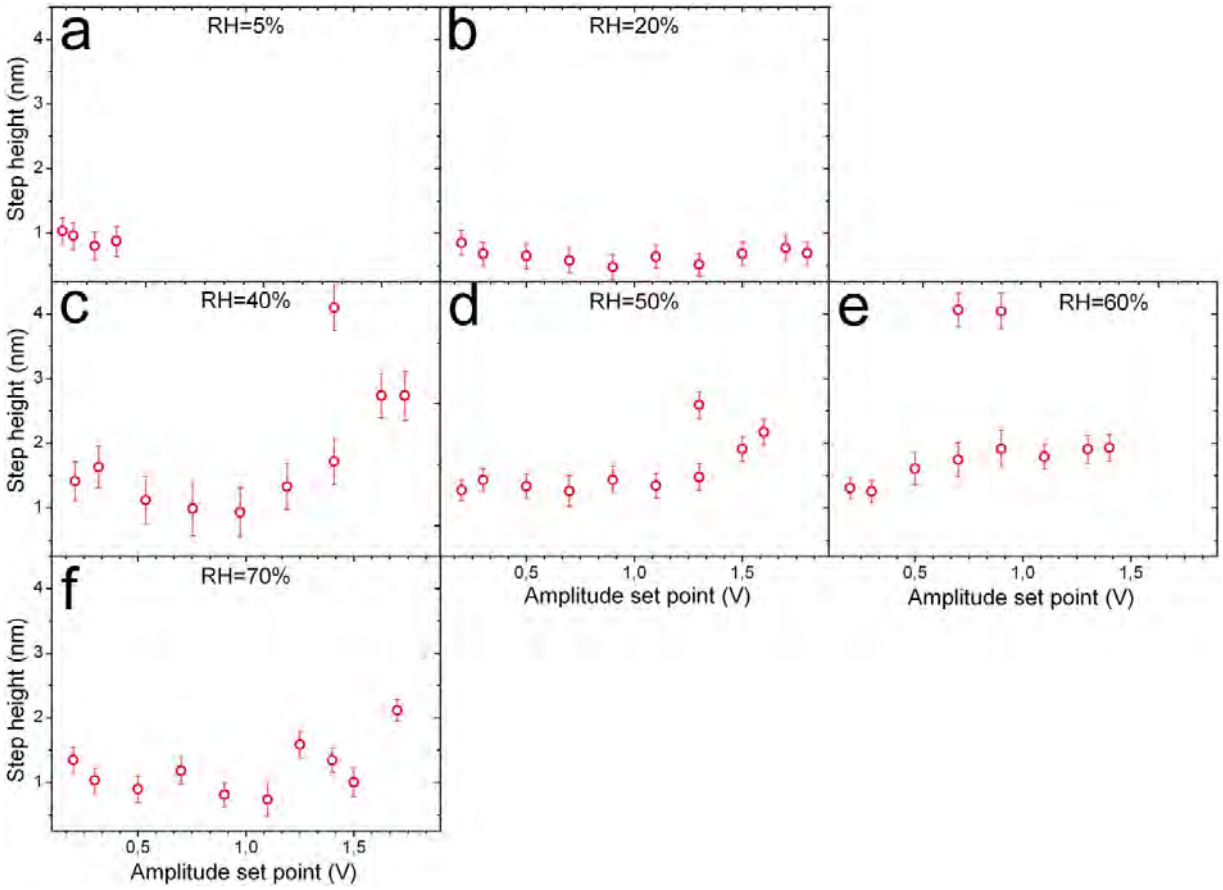

Figure 3.4. *Apparent height of graphene under AFM imaging versus the amplitude set point for dry regime (a-b); medium humidity regime (c-e) and wet regime (f). RH are (a) 5%, (b) 20%, (c) 40%, (d) RH=50%, (e) RH=60% and (f) RH=70%.*

Three domains of humidity are identified, (a-b) dry condition (0%<RH<30%), (c-e) intermediate conditions (30%<RH<60%) and (f) wet condition with RH>60%. Unstable A_{SP} with a jump in the thickness vs. A_{SP} plot and the overestimation of graphene thickness are

only observed for the intermediate RH conditions. For 40, 50, 60 and 70% RH, the apparent height at low A_{SP} are 1.3±0.5, 1.3±0.2, 1.4±0.4 and 1.2±0.5 nm respectively. For RH=40, 50,60 and 70% the apparent height for high A_{SP} are 2.6 ±0.1, 2.0±0.3, 1.9±0.1 and 1.2±0.5 nm respectively.

For extreme dry (RH=5, 20%) and wet (RH=70%) conditions, no jump is observed in the approaching curve and the apparent height of graphene is independent of the A_{SP}. The average step height is 0.7±0.2 nm for dry conditions (RH=5 and 20%).

These results are interpreted by the presence of a water meniscus, for intermediate RH conditions, the meniscus break later with an increasing RH over the graphene, and the overestimation of the apparent height of graphene decreases with the RH. At the wet regime limit, the meniscus does not break any more and there is no overestimation. For dry humidity conditions, the meniscus does not form and since, the imaging conditions are the same over the two materials, the thickness is measured reliably. To avoid overestimation of the apparent height of graphene, the RH conditions should be set to less than 30%, but the control of the RH is not available on all AFM. As a consequence in ambient RH (typically between 40 and 60%), the overestimation can be suppressed by searching the A_{SP} threshold below which the flake height is stable again (Figure 3.1a).

3.1.3 Conclusion.

The apparent AFM height of graphene has a high dispersion in the literature, searching for the causes of it, an AFM artifact has been observed. Under certain conditions, the thickness of graphene is overestimated by 0.7 to 1.2 nm. This overestimation has been interpreted as the breaking of a water meniscus over graphene for high oscillation amplitude of the tip. This artifact has been only observed for medium relative humidity (between 40 and 60%). During imaging, if the A_{SP} is set below a threshold, which allow imaging in stable conditions. These conditions can help in reducing the dispersion of the AFM thickness of graphene.

3.2 Raman scattering for characterizing thickness and crystalline quality of graphene.

3.2.1 Graphene thickness identification using Raman scattering.

Raman spectroscopy is an efficient non destructive probe to characterize graphene mono and multilayer, the complete spectrum of graphene is shown in Figure 3.5a. In particular, the shape of the Raman G'-peak can distinguish between graphene monolayer and AB stacked FLG. [15, 16] The G'-peak of a graphene monolayer is composed of a unique Lorentzian while AB stacked FLG is composed of 2 or more Lorentzians. Figure 3.5b shows a G'-peak of a graphene monolayer and its Lorentzian fit. This identification technique cannot unambiguously discriminate mono from multilayer graphene since the G' Raman peak of a misoriented or turbostratic multilayer graphene has the same shape than the one of a monolayer graphene. [17, 18] Another technique is needed to confirm the identification of graphene monolayer. It has been proposed to consider the ratio between the G'-peak intensity and the G-peak intensity ($\frac{I_{G'}}{I_G}$) is greater than 1 for monolayer graphene while it is lower than 1 for multilayer [16, 19]. The Raman spectrum of a graphene monolayer shown in Figure 3.5a exhibits this characteristic. However, this $\frac{I_{G'}}{I_G}$ ratio is dependent on defects and doping of graphene [20, 21] which can vary independently from the number graphene layers and therefore does not provide an accurate technique of identification of graphene monolayer

The G-peak integrated intensity of graphene is proportional to the volume of graphene probed by the laser beam. [6, 16] If we assume that the surface probed by the laser focal point is constant, the G-peak integrated intensity of graphene is proportional to the thickness of the sample. Therefore the integrated intensity of the G-peak can in principle give the exact number of layers of a graphene flake. The following analysis has been done under the guidance of Paillet M., Hutzinger J.R. and Tiberij A. (L2C, Montpellier). Experimentally, we will focus on the reproducibility of the technique on 10 samples. The G-peak integrated intensity of graphene flakes are normalized by the G-peak integrated intensity of a freshly

cleaved HOPG measured before each experiment. The graphene samples have been deposited on Si/SiO_2 substrates with an oxide thickness of 285 nm by the mechanical exfoliation technique. The thinnest samples have been identified using optical microscopy and Raman spectra have been acquired on a XploRA spectrometer (Horiba). For each spectrum, the optical focus is set so that the G-peak intensity is maximized. The excitation wavelength was 532 nm, the power intensity set to 10% and the exposure time was 10 s. the gating was 1,800 stripes, with a hole size of 500 and a slit of 200.

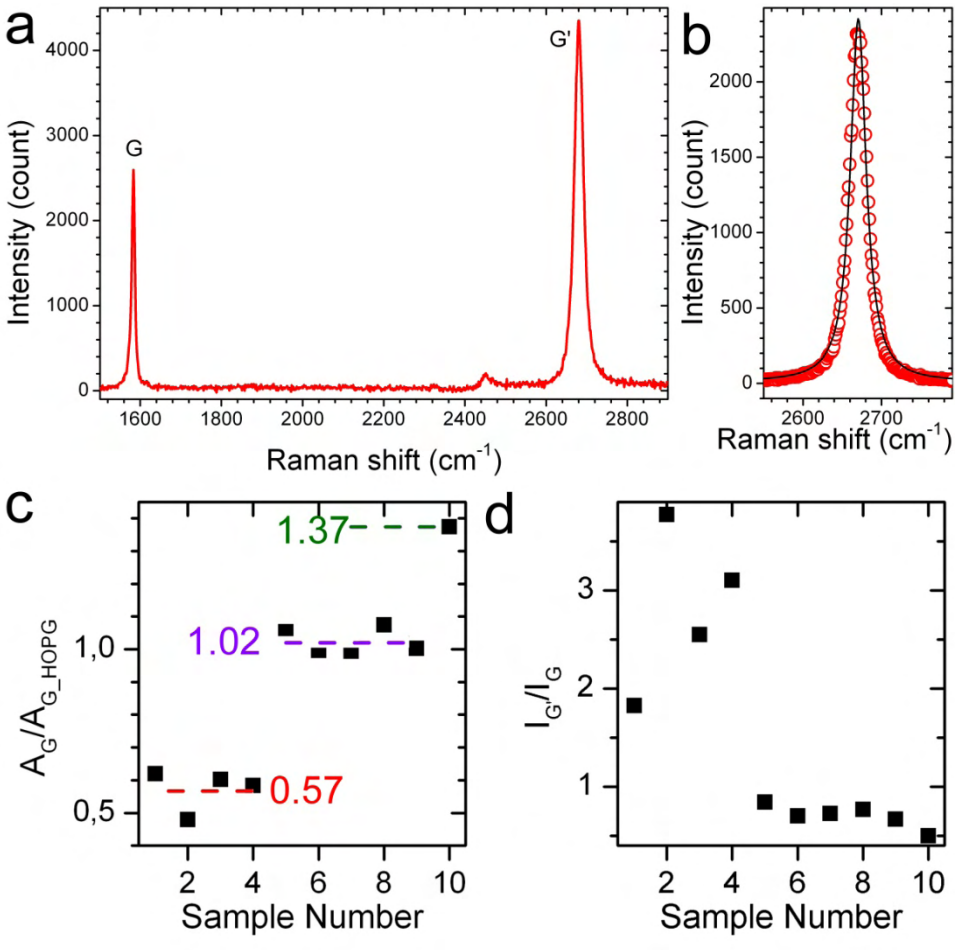

Figure 3.5. *(a) Raman spectrum of a graphene monolayer supported by a silicon/silicon oxide substrate. The two main peaks of graphene (G and G') are labeled. (b) is a Raman spectrum of a graphene monolayer G'-peak (red circles) and its Lorentzian fit (solid black line). (c) is a plot of the G-peak integrated intensity of graphene flakes normalized by the G-peak integrated intensity of a freshly cleaved HOPG. (d) is the $I_{G'}/I_G$ ratio for several graphene flakes.*

The samples are labeled from 1 to 10. The contrast in optical microscopy and the shape of the G'-peak allow a first identification of samples thicknesses 1 to 4 as monolayer and samples 5 to 10, are multilayer graphene. For all samples, the ratio between the integrated intensity of the G-peak of the sample and the integrated intensity of the G-peak of a HOPG is plotted in Figure 3.5c. For samples 1 to 4 the averaged G-peak intensity $A_G/A_{G,\,HOPG}$ is 0.6. For samples 5 to 9, it is 1 and for sample 10 it is 1.4. The clear quantification of these values led us to assume that samples 1 to 4 were monolayer, sample 5 to 9 bilayer and sample 10 was a tri-layer. The relevant parameter then appears to be $A_G/nxA_{G,\,HOPG}$ which would be constant for the entire dataset. Indeed, the average $I_G/nxI_{G,\,HOPG}$ ratio is 0.57 with a standard deviation of 0.05 (i.e. 8%). We can therefore consider that the number of layer of graphene can be experimentally determined with the G-peak integrated intensity technique $n=A_G/0.57A_{G,\,HOPG}$ (±8%).

Figure 3.5d shows the ratio $\frac{I_{G'}}{I_G}$ for sample 1 to 10. Even if there is a clear difference between monolayer $I_{G'}/I_G$ =2.9±1.0 and bi or tri layers (0.8±0.1), the deviation from the mean value is very high. Additionally with this technique it is impossible to distinguish between bi and tri or more graphene layers.

3.2.2 Graphene G-peak exaltation by colloidal gold colloids.

While the exploitation of G and G' is not impacted by the weakness of signals in graphene, the Raman spectrum can also be used to determine the presence of defects by exploiting the D peak at 1350 cm^{-1}. It appears that this peak has a rather small intensity which makes it difficult to characterize low density of defects by Raman. One useful phenomenon is the enhancement of the Raman signal in the presence of noble metals. The Raman signal can be enhanced by plasmon or doping of the metal. The enhancement by plasmon is due to the local enhancement of the electric field by the collective oscillations of the electrons, the Raman signal is enhanced because it is proportional to the square of the electric field.

Graphene Raman signal has been enhanced in the presence of lithographically defined Cr/Au nanodisks, with diameter comprised between 100 and 200 nm. [22] The enhancement

factor of the G peak near the gold structure compared to areas of graphene far from metallic disks is more than 20 and reaches 30 for the G'-peak. [22] However, enhancement factor is not spatially homogeneous, and it varies from 5 to 15. [22] When a thin layer of gold is deposited on graphene, enhancement factors up to 120 for G-peak and 60 for G'-peak are even found. [23] These disks and films have variable shape and crystalline quality, their deposition process can damage the underlying graphene. Additionally we are interested in the specific enhancement of the D peak. In the following, we have used gold bi-crystalline nanoprism [24] and single crystalline nanorods [25] to study enhancement of the Raman signal of the graphene. This work has been done with M. Nuñez during its master 1 training.

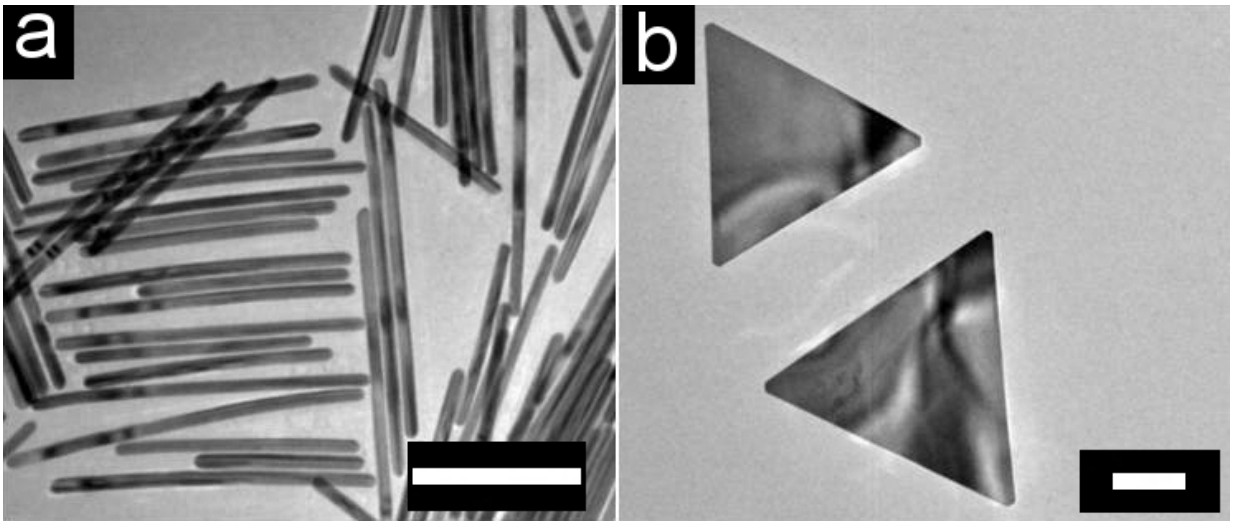

Figure 3.6. *TEM images of (a) gold nanorods and (b) Au nanoplatelets. Scale bar are 200 nm. Courtesy of J. Sharma.*

The intensity map of the Raman G, G' and D-peak are shown in Figure 3.7b-d, the excitation wave length was 532 nm, with a circular polarization. The signal is higher on the central red spot, which is the area on a nanoprism, than on the surrounding graphene by a factor 2 to 15. Two spectra acquired on the particle and on the bare FLG surrounding the particle are shown in Figure 3.7b, the G-peak intensity is about 610 counts above the prism while only 195 counts on the bare FLG, corresponding to an enhancement factor of about 3. There is also an enhancement of the D (1.4) and G' (2.5) peak.

One should notice that the graphene used in this experience was grown by CVD on nickel and has the same domain size than the nickel grains composing the film. Due to the small size of these domains, the Raman D-peak intensity varies with the position of the laser beam and so the measured enhancement for the D-peak on these samples is thus not reproducible.

Gold nanorods typically 400x20 nm (Figure 3.6a) prepared by J. Sharma have been dispersed on a Si/SiO_2 substrate before depositing graphene by the mechanical exfoliation technique. Raman map has been acquired of a graphene flake deposited on gold nanorods (Figure 3.7a). The maps of the G, G' and D peak intensity are shown in Figures 3.7b, c and d respectively.

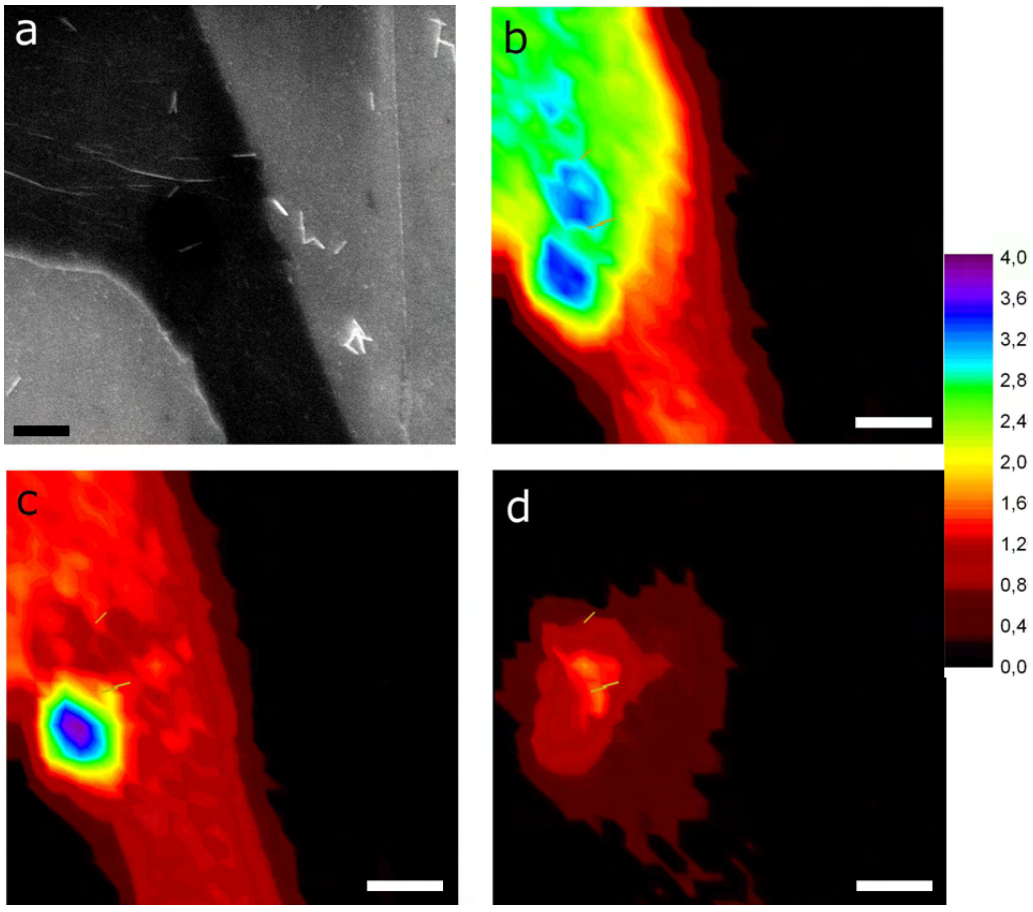

Figure 3.7. *Raman signal of graphene enhanced by gold nanorods.. (a) A SEM image of a graphene flake deposited on gold nanorods. Raman map of the intensity of the (b)G peak, (c) G'-peak and (d) D peak at 532 nm of excitation wavelength of the same graphene flake.. Color scale bar is normalized by the second order Raman peak of the Si [100]. Scale bars are 1 µm*

G and G' peak are enhanced by factors of 1.5 and 3.5 respectively. The D-peak map shows that there is signal only over the nanorods. The nanorods enhance the Raman D peak although the factor is not measurable since the D-peak is null elsewhere.

The best contrast has been obtained for the G'-peak intensity, for this parameter a polarization and wavelength dependence study have been conducted. Figures 3.8a to d are the Raman map intensity of the G'-peak at two polarization and two wavelengths.

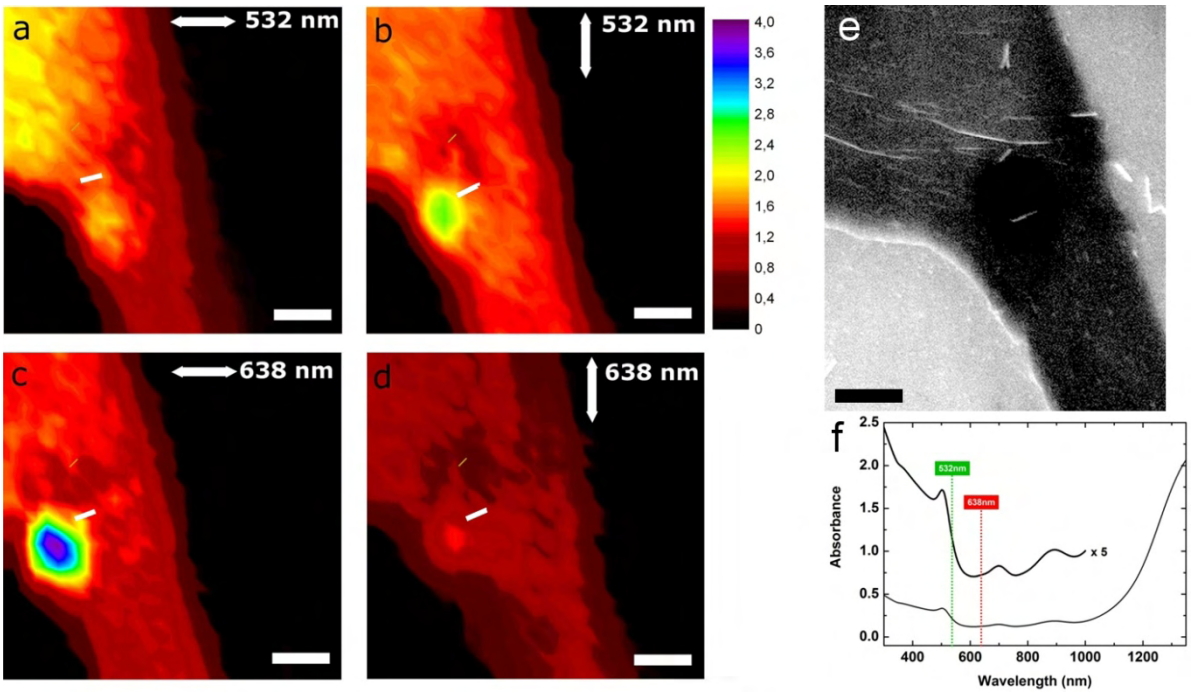

Figure 3.8. *Polarization and wavelength dependence of the enhancement of the Raman G'-peak of graphene by gold nanorods. (a-d) Raman maps of the G'-peak intensity with (a, c) horizontal polarization and (b, d) vertical polarization. The excitation wavelength are (a, b) 532 nm and (c, d) 638 nm. (e) SEM image of the graphene and nanorods. (f) Absorbance spectrum of gold nanorods. Color scale bar is normalized by the second order Raman peak of the Si [100]. Scale bars are 1 µm.*

The 538 nm wavelength is close to the transverse resonance of the Plasmon of the gold nanorods (Figure 3.8f). This is in accordance with the Raman map of Figures 3.8a and b, no exaltation is visible if the polarization of the laser is perpendicular to the nanorod and an exaltation of a factor 2 is visible if the polarization of the laser is perpendicular to the nanorod.

The 638 nm wavelength is close to a longitudinal resonance of the Plasmon of the nanorod, which is in accordance with the Raman maps of Figures 3.8c and d where a enhancement factor higher than 4 is found for a longitudinal excitation while it is only 1.2 for a transverse excitation. This behavior is an evidence that the exaltation is partially due to the Plasmon of the nanorod. The following paragraph will focus on the exaltation of the D peak intensity to improve Raman spectroscopy as a defect characterization technique.

3.2.3 Enhancement of graphene D-peak intensity by colloidal gold nanorod.

Gold nanorods typically 400x20 nm (Figure 3.6a) prepared by J. Sharma have been dispersed on a Si/SiO_2 substrate before depositing graphene by the mechanical exfoliation technique. Two Raman maps of the D-peak intensity have been acquired, Figure 3.9b for the horizontal polarization and 3.8c for the vertical polarization. The excitation wavelength is 532 nm.

The Figure 3.9a is a SEM image, showing the graphene flake deposited on top of gold nanorods. The edges of graphene contribute to the D peak while the center of graphene does not. It seems that the D peak signal of the edges is dependent on the polarization, the D peak of edges parallel to the polarization is more intense than the edges perpendicular to the polarization. Some nanorods have been labeled in Figure 3.9a, the same area are circled in the Raman maps. For A and B nanorods, there is a very small signal enhancement because they are next to the graphene, not under it. The plasmon enhancement of the local field or the doping of graphene are local effects, which need a close contact. As the structures can be a few nanometers away from graphene, they do not enhance the D peak of the edge. For C and D nanorods, they are far from graphene edge, at their position, the D peak of graphene would exhibit no signal if the particle was not under the graphene. On the localization of the nanorod, there is a clear D-peak signal far from a graphene edge. It is not possible to calculate an enhancement factor since the graphene around the particle has no D-peak signal but the D peak intensity is enhanced by the presence of the nanorods.

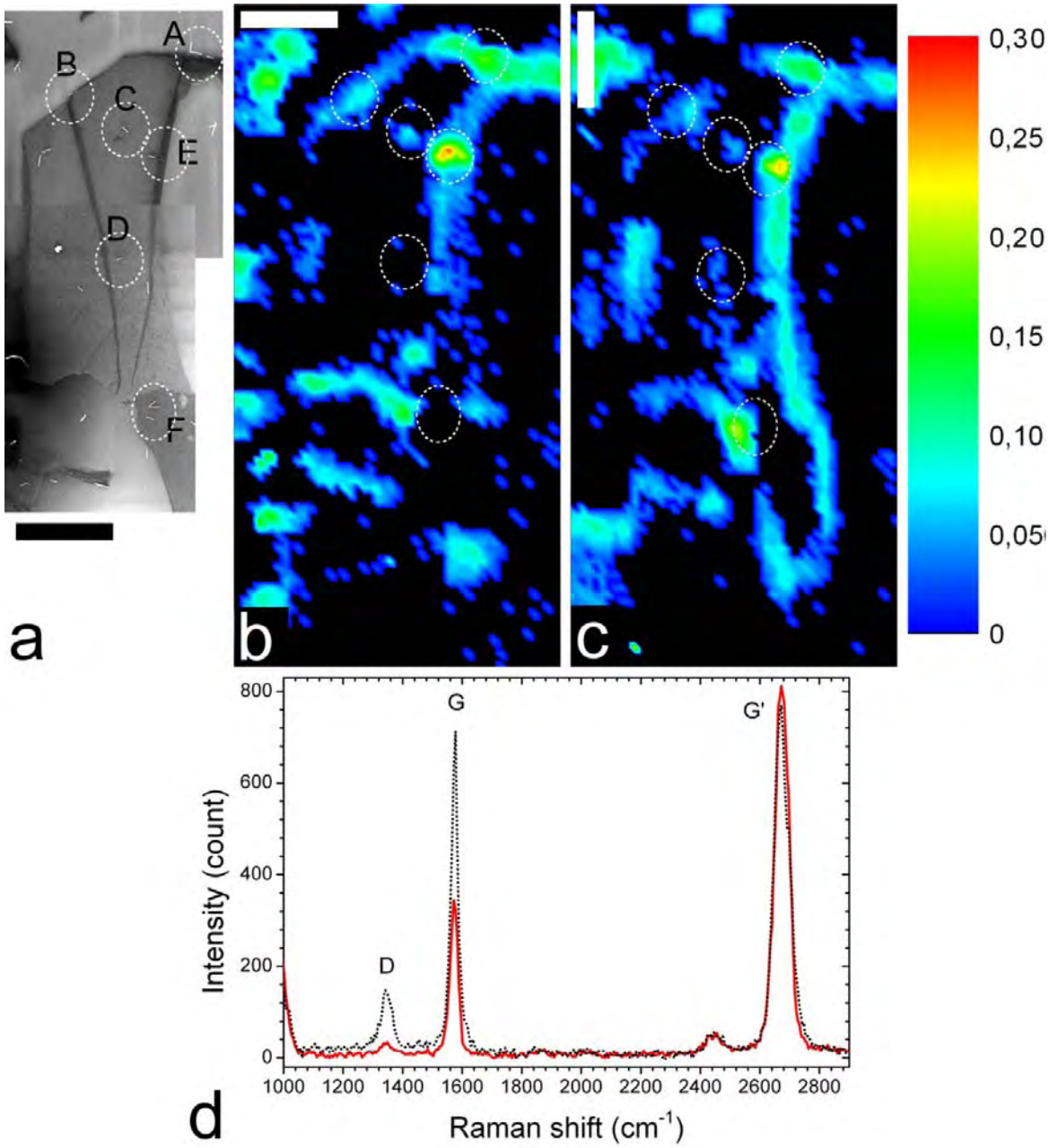

***Figure 3.9**. Exaltation of graphene D-peak by gold nanorods. (a) is a SEM image of a graphene flake on a Si/SiO_2 substrate. (b) and (c) are Raman maps of the D-peak intensity of graphene with an excitation wave-length of 532 nm with a horizontal and vertical polarization, respectively. Color scale shows the D-peak intensity counts normalized by the second order of Si[100]. (d) Raman spectra acquired on the nanorod E and on the edge next to it for the horizontal polarization. Scale bars: 3 µm.*

A clear enhancement of the D-peak is visible, Figure 3.9d shows two Raman spectra acquired on the "E" nanorod and on the graphene edge next to it. The D-peak enhancement factor is 5. A careful examination of the SEM image shows a tearing of the graphene sheet

around the rod, the enhancement observed is a combination of plasmon-induced enhancement, edges created by the tearing and defect of graphene.

For the nanorods in F, their structure is a V-shape. These coupled nanorods have a plasmon resonance modified from the pristine nanorod. On the vertical polarization Raman map (Figure 3.9c), this structure enhances the D-peak by a factor of about 2.5, but there is no enhancement for the vertical polarization. This enhancement is perpendicular to the axis of the V-shape structure, this observation could be interpreted by a tip effect phenomenon. [26]

3.2.4 Graphene irradiation effect in the presence of gold colloidal nanoprism.

Prismatic Au platelets (Figure 3.6b) with lateral size ranging between 0.5 and 1.0 μm have been produced by a new one-pot method based on the direct reduction of Au precursors by polyvinylpyrrolidone (PVP) in alkaline conditions at room temperature, the details of which will be reported elsewhere. Once the reaction is complete, the nanoprisms suspension is naturally settled, decanted and redispersed into 18 MΩ deionized water without any further purification steps. This suspension has been prepared by J. Sharma and drop-casted on Si/SiO_2 substrates before graphene deposition by micromechanical exfoliation technique. The Raman map of the D-peak intensity of this suspended graphene has been acquired, the sample has been imaged in a SEM with electrons accelerated at 5 kV and a second D-peak Raman map has been acquired. In the map acquired before irradiation, shown in Figure 3.10a, the D-peak intensity is almost zero. The spectra on and next to gold nanoprisms are very similar and do not present decrease or enhancement of their intensity. After irradiation, the intensity of the D-peak Raman map of Figure 3.10c shows an increase to about 30 counts on the bare graphene, far from any nanoprism. For a spectrum acquired on a nanoprism, D-peak intensity is 150 counts, as shown in Figure 3.10d. There is also a decrease of the G and G'-peaks intensity with respect to the spectrum acquired on bare FLG (red solid line of Figure 3.10d)

Outside the nanoprism, primary and backscattered electron (BSE) irradiation of graphene induce defects [27] and lead to an increase of the Raman D-peak intensity to about 30 counts, while it was not detectable before electron irradiation. Over a nanoprism, the D-peak is 5 times more intense than on the bare FLG. We interpret that by an increase of the electronic dose induced by BSE produced in the nanoprism, resulting in a more intense amorphization of graphene. The increase of the amorphization is shown by the quenching of G and G'-peak as well as the I_D/I_G ratio. [28] This additional amorphisation is due to a local increase of the electronic dose because the gold surface create more BSE than the SiO_2 ($Z_{Au}>Z_{Si}$).

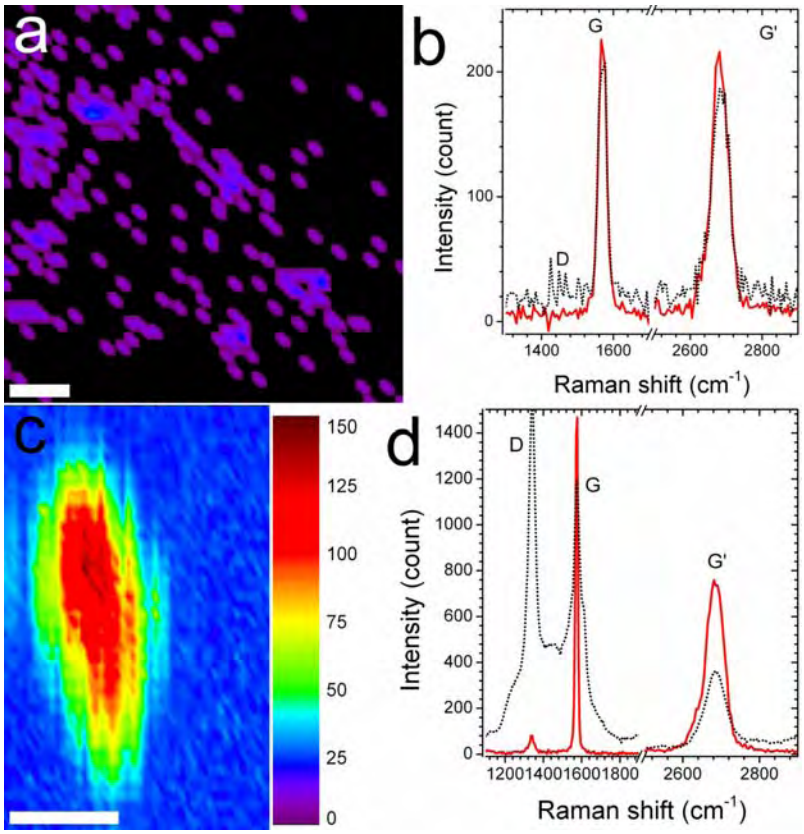

Figure 3.10. *Electron irradiation effect on graphene D-peak. (a) D-peak Raman map of an Au nano-platelet under graphene before electron irradiation. (b) two spectra of the (a) map, on the location of the nanoprism (black dotted line) and on the multilayer graphene far from the nanoprism (red solid line). (c) D-peak map of an Au nano-platelet under graphene after electron irradiation (5 kV). (d) Two spectra of the (c) map that has been acquired on the location of the nanoprism (black dotted line) and on the multilayer graphene far from the nanoprism (red solid line). Scale bars are (a): 3 µm, (c): 1 µm. (a) and (c) color scale are in counts.*

This experiment points out the care that must be taken while imaging graphene with electronic microscopy techniques. In the two previous studies (paragraph 3.2.2 and 3.2.3), Raman map have been acquired before SEM imaging. The role of back-scattered electrons is arising in this experiment, it will be discussed in more detail in the chapter 5 during etching of supported graphene by electron beam induced etching.

3.2.5 Conclusion.

This Raman signal enhancement by nanoprism has to be rationalized because the examples shown here are not observed for all similar systems. The case of Au platelet on nickel grown graphene is the less reproducible, it can be explained by the contamination of graphene by carbonaceous material (see chapter 4) and eventually polymer covering the platelets. In chapter 4 some experiments will be presented that aims to produce clean monolayer graphene on TEM grid, this Raman study would also benefit of better samples.

Nanorods deposited on Si/SiO_2 and covered by mechanically exfoliated graphene exhibit more reproducible results. It has been found that the nanostructures enhance the Raman D-peak signal of graphene. There is a dependence on the polarization, of the exaltation of the G'-peak agreeing with the absorbance of the plasmon of the nanorods. This polarization dependence is an evidence of the role of the Plasmon of the nanorod in the exaltation of the signal.

Further study of this enhancement could be to deposit nanorods on clean graphene monolayer and etch the graphene close to nanorods by EBIE which would provide experiment for studying the enhancement of D-peak by nanorod and provide a macroscopic and non destructive technique to study defects in graphene.

3.3 NC-AFM imaging of graphene.

3.3.1 Graphene over silica.

Non-contact AFM (NC-AFM) is a technique allowing to reach atomic and sub-molecular resolution on insulating substrates. We have used this technique to assess wheth-

er graphene on an insulating substrate and specially graphene edges can be imaged with an atomic resolution. Such a technique would provide information on structural defects of graphene in a device configuration. Preliminary results on the modification of the substrates and requirements for UHV and NC-AFM are presented here.

Micromechanically exfoliated graphene has been deposited on oxidized silicon wafer (285 nm oxide thickness). The source was natural graphite. Graphene flakes were identified by optical microscopy. The samples were then stuck on an OMICRON holder with EPOTEK glue and dried in an oven (120°C during 1h in ambient air). After introduction in the UHV DUF, the sample was annealed at 200°C in UHV (10^{-9} to 10^{-11} mbar) during 2 hours. Graphene has been then imaged in non-contact mode AFM (NC-AFM) in frequency modulation mode. A PPP-NCH tip (f_0=319 kHz, quality factor Q=23 500) has been used to perform the imaging. Further imaging was carried out with a contact tip (OMCL-TR800PB: f_0=74 kHz, Q=1 543) with the same imaging conditions. Finally the sample has been again imaged in ambient condition in intermittent mode AM-AFM.

Figure 3.11a is an optical image of a graphene flake, the AFM image in ambient condition is shown in Figure 3.11b. The thickness of this flake has been measured at 0.72 nm, consistent with a graphene monolayer. During the scan with a PPP-NCH tip, imaging conditions were unstable and it was impossible to acquire an image. Using a tip with a lower resonance frequency and a lower spring constant, an OMCL-TR800PB allowed to acquire a NC-AFM image that is shown in Figure 3.11c. An AM-AFM image acquired in ambient condition is shown in Figure 3.11d. A green arrow shows a defect in silica, proving that the zone imaged in Figures 3.11b, c and d are the same.

Figures 3.11c and d, show that the graphene flake has been partially destroyed. This can explain why the graphene could not be imaged with the PPP-NCH tip, the interaction of this tip in non contact mode in UHV is higher than the cohesion between graphene and silica. In non-contact mode, the tip-surface interaction is always attractive, the tip pull the graphene while in intermittent mode the tip press the graphene. If the attractive interaction

graphene-substrate is lower than the graphene-tip interaction, the tip will attract and tear the graphene, this is what has been observed. The contact tip (OMCL-TR800PB) has a resonance frequency and so a spring constant quite lower than the PPP-NCH tip. The interaction between graphene and the tip is thus reduced, which allows imaging the graphene without destroying it. However, NC-AFM is regulated by the oscillation frequency of the cantilever, it requires thus a high quality factor of the tip oscillation to be able to reach atomic resolution (Q>10,000). The contact tips have a too low quality factor and cannot reach atomic resolution. It is thus necessary change the substrate to increase the graphene-surface interaction. As thermal Silica is rough (~0.5-1 nm), the graphene is not in contact with all the surface which decreases the cohesions forces. An atomically flat substrate as for example KBr would increase the contact area and thus the adhesion force which would enable to image graphene with a PPP-NCH tip.

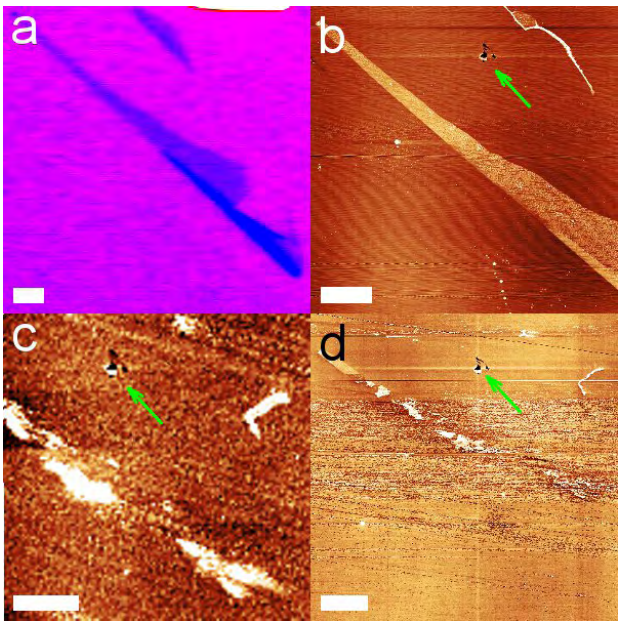

Figure 3.11 *: Graphene flake deposited on a Si/SiO_2 substrate. Optical (a) and AFM (b) image of a graphene flake just after its fabrication. The area has then been imaged in NC-AFM in frequency modulation with a PPP-NCH tip without being able to image it. (c) A NC-AFM in frequency modulation image has been taken with a contact tip: OMCL-TR800PB-1. The substrate has been then taken out of the UHV chamber and imaged in ambient condition in an intermittent mode AFM. The three green arrows show a defect in the silica. Scale bars: 5 µm. Vertical color scale: (b) 10 nm, (c) and (d) 5 nm.*

3.3.2 Choice of substrates and deposition technique of graphene.

Three substrates have been studied to try to image graphene in NC-AFM. All these substrates are atomically flat: KBr, Mica and monocrystalline sapphire. Graphene has been deposited on them by the micromechanical technique (Figure 3.12). Optical contrast of graphene on these transparent substrates is very small, nevertheless it was possible to found monolayer graphene flake. Several attempts to image in NC-AFM a graphene flake on these substrates were unsuccessful because the optical system of the NC-AFM is a simple optical camera. It was not possible to localize graphene flake because of a too poor resolution of the optical camera, a pixel size of 10 µm, in the order of the size of the graphene flakes.

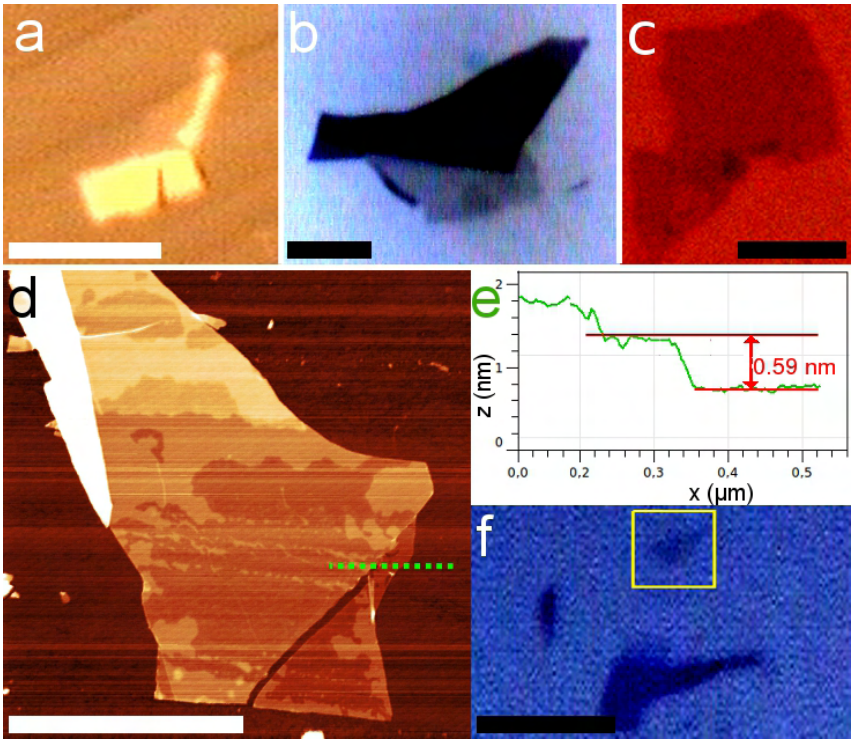

Figure 3.12. *Optical images of micromechanically exfoliated graphene deposited on (a) KBr, (b) mica and (c) alumina. (d) AFM image of a mono or bi layer graphene on mica. Vertical color scale is 10 nm (e) cross section along the green dashed line in (d). (f) optical image of the flake shown in (d). Scale bars are (a)(b)(c)(f), 10 µm and (d) 1 µm.*

In order to grow graphene on a wafer scale, its production technique has been changed, graphene grown on SiC by molecular beam epitaxy (MBE) has been prepared by E.

Moreau [29] and imaged by NC-AFM. Due to a sample preparation issue, we were unable to image the graphene with an atomic resolution. A mechanical abrasion of the SiC created morphological defects on the substrate, making impossible to image the atomic flat terraces of the SiC and preventing atomically resolved images of graphene. However a change in the sample preparation or, cleaner technique of transfer of graphene grown by CVD (chapter 4) will be attempted to try to image graphene by NC-AFM.

3.4 References.

[1] Bammerlin, M.; Luthi, R.; Meyer, E.; Baratoff, A.; Lu, J.; Guggisberg, M.; Loppacher, C.; Gerber, C.; Guntherodt, H. J. "**Dynamic SFM with true atomic resolution on alkali halide surfaces**". *Appl. Phys. A-Mater. Sci. Process.* (**1998**) *Vol. 66*, p. S293-S294.

[2] Hoffmann, R.; Lantz, M. A.; Hug, H. J.; van Schendel, P. J. A.; Kappenberger, P.; Martin, S.; Baratoff, A.; Güntherodt, H. J. "**Atomic resolution imaging and force versus distance measurements on KBr (0 0 1) using low temperature scanning force microscopy**". *Applied Surface Science* (**2002**) *Vol. 188*, p. 238-244.

[3]Hinaut, A. **Etude par microscopie à force atomique en mode non contact et par microscopie à sonde de Kelvin de dérivés du Triphénylène sur KBr(001) dans l'ultra vide**. PhD thesis, (**2012**).

[4] Hinaut, A.; Lekhal, K.; Aivazian, G.; Bataille, S.; Gourdon, A.; Martrou, D.; Gauthier, S. "**NC-AFM Study of the Adsorption of Hexamethoxytriphenylene on KBr(001)**". *J. Phys. Chem. C* (**2011**) *Vol. 115*, p. 13338-13342.

[5] Gross, L.; Mohn, F.; Moll, N.; Liljeroth, P.; Meyer, G. "**The Chemical Structure of a Molecule Resolved by Atomic Force Microscopy**". *Science* (**2009**) *Vol. 325*, p. 1110-1114.

[6] Gupta, A.; Chen, G.; Joshi, P.; Tadigadapa, S.; Eklund, P. C. "**Raman scattering from high-frequency phonons in supported n-graphene layer films**". *Nano Lett.* (**2006**) *Vol. 6*, p. 2667-2673.

[7] Novoselov, K. S.; Geim, A. K.; Morozov, S. V.; Jiang, D.; Zhang, Y.; Dubonos, S. V.; Grigorieva, I. V.; Firsov, A. A. "**Electric field effect in atomically thin carbon films**". *Science* (**2004**) *Vol. 306*, p. 666-669.

[8] Chen, Z.; Lin, Y.-M.; Rooks, M. J.; Avouris, P. "**Graphene nano-ribbon electronics**". *Physica E: Low-dimensional Systems and Nanostructures* (**2007**) *Vol. 40*, p. 228-232.

[9] Sidorov, A. N.; Yazdanpanah, M. M.; Jalilian, R.; Ouseph, P. J.; Cohn, R. W.; Sumanasekera, G. U. "**Electrostatic deposition of graphene**". *Nanotechnology* (**2007**) *Vol. 18*, p. 4.

[10] Nemes-Incze, P.; Osvath, Z.; Kamaras, K.; Biro, L. P. "**Anomalies in thickness measurements of graphene and few layer graphite crystals by tapping mode atomic force microscopy**". *Carbon* (**2008**) *Vol. 46*, p. 1435-1442.

[11] Horcas, I.; Fernandez, R.; Gomez-Rodriguez, J. M.; Colchero, J.; Gomez-Herrero, J.; Baro, A. M. "**WSXM: A software for scanning probe microscopy and a tool for nanotechnology**". *Rev. Sci. Instrum.* (**2007**) *Vol. 78*, p. 8.

[12] Bernal, J. D. "**The Structure of Graphite**". *Proceedings of the Royal Society of London. Series A* (**1924**) *Vol. 106*, p. 749-773.

[13] Hoerni, J. "**Diffraction of Electrons in Graphite**". *Nature* (**1949**) *Vol. 164*, p. 1045-1046.

[14] Zitzler, L.; Herminghaus, S.; Mugele, F. "**Capillary forces in tapping mode atomic force microscopy**". *Phys. Rev. B* (**2002**) *Vol. 66*, p. 8.

[15] Ferrari, A. C.; Meyer, J. C.; Scardaci, V.; Casiraghi, C.; Lazzeri, M.; Mauri, F.; Piscanec, S.; Jiang, D.; Novoselov, K. S.; Roth, S.; Geim, A. K. "**Raman spectrum of graphene and graphene layers**". *Phys. Rev. Lett.* (**2006**) *Vol. 97*, p. 4.

[16] Malard, L. M.; Pimenta, M. A.; Dresselhaus, G.; Dresselhaus, M. S. "**Raman spectroscopy in graphene**". *Phys. Rep.-Rev. Sec. Phys. Lett.* (**2009**) *Vol. 473*, p. 51-87.

[17] Faugeras, C.; Nerriere, A.; Potemski, M.; Mahmood, A.; Dujardin, E.; Berger, C.; de Heer, W. A. "**Few-layer graphene on SiC, pyrolitic graphite, and graphene: A Raman scattering study**". *Appl. Phys. Lett.* (**2008**) *Vol. 92*, p. 3.

[18] Poncharal, P.; Ayari, A.; Michel, T.; Sauvajol, J. L. "**Effect of rotational stacking faults on the Raman spectra of folded graphene**". *Phys. Rev. B* (**2009**) *Vol. 79*, p. 4.

[19] Li, X. S.; Cai, W. W.; An, J. H.; Kim, S.; Nah, J.; Yang, D. X.; Piner, R.; Velamakanni, A.; Jung, I.; Tutuc, E.; Banerjee, S. K.; Colombo, L.; Ruoff, R. S. "**Large-Area Synthesis of High-Quality and Uniform Graphene Films on Copper Foils**". *Science* (**2009**) *Vol. 324*, p. 1312-1314.

[20] Das, A.; Chakraborty, B.; Sood, A. K. "**Raman spectroscopy of graphene on different substrates and influence of defects**". *Bull. Mat. Sci.* (**2008**) *Vol. 31*, p. 579-584.

[21] Das, A.; Pisana, S.; Chakraborty, B.; Piscanec, S.; Saha, S. K.; Waghmare, U. V.; Novoselov, K. S.; Krishnamurthy, H. R.; Geim, A. K.; Ferrari, A. C.; Sood, A. K. "**Monitoring dopants by Raman scattering in an electrochemically top-gated graphene transistor**". *Nat. Nanotechnol.* (**2008**) *Vol. 3*, p. 210-215.

[22] Schedin, F.; Lidorikis, E.; Lombardo, A.; Kravets, V. G.; Geim, A. K.; Grigorenko, A. N.; Novoselov, K. S.; Ferrari, A. C. "**Surface-Enhanced Raman Spectroscopy of Graphene**". *ACS Nano* (**2010**) *Vol. 4*, p. 5617-5626.

[23] Lee, J.; Shim, S.; Kim, B.; Shin, H. S. "**Surface-Enhanced Raman Scattering of Single- and Few-Layer Graphene by the Deposition of Gold Nanoparticles**". *Chem.-Eur. J.* (**2011**) *Vol. 17*, p. 2381-2387.

[24]Sharma, j.; Dujardin, E., To be published. In 2012.

[25] Murphy, C. J.; San, T. K.; Gole, A. M.; Orendorff, C. J.; Gao, J. X.; Gou, L.; Hunyadi, S. E.; Li, T. "**Anisotropic metal nanoparticles: Synthesis, assembly, and optical applications**". *J. Phys. Chem. B* (**2005**) *Vol. 109*, p. 13857-13870.

[26]Sanchot, A. **Propriétés de nanostructures plasmoniques auto-assemblées: vers la plasmonique moléculaire**. PhD thesis, Université paul sabatier, (**2011**).

[27] Teweldebrhan, D.; Balandin, A. A. "**Modification of graphene properties due to electron-beam irradiation**". *Appl. Phys. Lett.* (**2009**) *Vol. 94*, p. 3.

[28] Ferrari, A. C.; Robertson, J. "**Resonant Raman spectroscopy of disordered, amorphous, and diamondlike carbon**". *Phys. Rev. B* (**2001**) *Vol. 64*, p. 075414.

[29]Moreau, E. **Elaboration de graphène par épitaxie par jets moleculaires et caracterisation**. PhD thesis, Institut d'Electronique, de Micro et Nanotechnologies, (**2011**).

CHAPTER 4

Graphene Nano-Ribbons:

Electron beam induced etching and structural analysis.

Dans ce chapitre, la structuration directe du graphène sous un faisceau électronique ("Electron beam induced etching", EBIE) jusqu'à quelques nanomètres est détaillée. Cette structuration permet de réaliser des motifs arbitraires, sur plusieurs échelles de taille depuis le micromètre jusqu'à quelques nanomètres. L'avantage essentiel de notre approche est de limiter les sources de contamination et d'amorphization afin de préserver la structure et les propriétés du graphène natif.

Le graphène peut être structuré par plusieurs techniques dont nous rappelons ici les avantages et limitations afin d'établir les objectifs et critères que nous nous proposons d'at-

In this chapter, the patterning of graphene by EBIE is exposed. This structuration allows to realize arbitrary shapes, on several length scales, from the micrometer down to the nanometer scale. The main advantage of this technique is to limit the contamination sources and the amorphization to preserve the structure and the properties of pristine graphene.

Graphene has recently been patterned by several techniques, the main advantages and limitations of which are first summarized here. This survey will

teindre par EBIE. Elles peuvent être regroupées en trois catégories. Tout d'abord, les approches lithographiques (optique ou électronique) suivies d'une étape de gravure par un plasma oxygène permettent de graver le graphène suivant un motif arbitraire atteignant une résolution de quelques dizaines de nanomètres. [1-3] Cependant, l'utilisation d'une résine contribue à la contamination du graphène. [4-6] De plus, la gravure par plasma ionique amorphize le graphène et implante des ions. [7, 8] La technique de gravure par faisceau d'ion focalisé (Focused Ion Beam, FIB) évite l'utilisation de résine mais résulte en une amorphization et implantation ionique importante pour le graphène supporté par le substrat. [9-11]

Un deuxième groupe de techniques consistent à modifier directement le graphène par interaction avec un faisceau électronique. A très basse tension d'accélération (0.01-30 V), les lithographies en champ proche (STM, AFM) permettent une gravure du graphène avec une forme arbitraire sur des distances d'au plus quelques centaines de nanomètres. [12-16] Dans le cas du STM, la tension de polarisation nécessaire en ultravide (supérieure à 8.5 V [12, 15]),

enable us to list the challenges and criteria to be achieved by EBIE. These existing techniques can be separated in three categories. Firstly, the ion-based techniques. Lithography (optic or electronic) followed by a reactive oxygen plasma etching is able to patterned graphene into arbitrary shapes and reaches a feature resolution size of a couple of tens of nanometers. [1-3] However the use of a resist tends to contaminates the surface of graphene. [4-6] Furthermore the ionic etching amorphize the graphene and contaminates it by ion implantation. [7, 8] FIB obviates the use of a resist but supported graphene is amorphized and ions are implanted. [9-11]

A second group of techniques consists in modifying directly the graphene by interaction with a focused electron beam. At very low acceleration voltages (0.01 to 30 V), local probe lithography techniques (STM lithography, AFM anodic oxidation) allow etching with arbitrary shape over a few hundreds of nanometer. [12-16] In the case of the STM, the polarization bias required in UHV

peut être abaissée parla présence d'eau (conditions ambiantes) à typiquement 3 V. [12, 13, 16] A des énergies d'accélération d'environ 100 keV, le faisceau électronique d'un TEM permet de graver le graphène avec des bords ("zig-zag" ou "armchair") atomiquement droits. [17, 18] Cependant, le pilotage de microscopes électronique en transmission pour la lithographie reste un défi.

Les techniques du dernier groupe reposent sur la rupture chimique ou mécanique des liaisons C-C et sont donc intimement dépendantes de la cristallographie intrinsèque du graphène. La sonication intensive d'une suspension de particules de graphite produit des rubans de quelques centaines de nanomètres de long et aussi fins que 10 nm de large. [19] Les bords de ces rubans ont un très faible désordre et sont préférentiellement orienté suivant les directions "armchair". [20, 21] De la même manière, l'hydrogénation du graphène catalysée par des nanoparticules métalliques qui diffusent à sa surface produit des découpes suivant des directions cristallographiques privilégiées. [22, 23] En outre les bords de ces découpes sont également très ordonnés avec une fluctuation de quelques cycles benzéniques (~1.5 nm). [24] Ces

(higher than 8.5V [12, 15]), can be reduced to typically 3-4 V when water is present (ambient conditions). [12, 13, 16] At energies of about 100 keV, the e-beam of a TEM can etch graphene with atomically smooth (zig-zag or armchair) edges. [17, 18] However, the control of the beam of a TEM is not a standard feature.

The last group is composed of techniques which are based on the chemical or mechanical breaking of the C-C bound and are thus sensitive on the intrinsic crystallography of graphene. Intense sonication of a suspension of graphite produces ribbons of few hundred of nanometer in length and thinner than 10 nm in width. [19] These ribbons have presented a limited edge disorder and are preferentially orientated along the "armchair" directions. [20, 21] Similarly, the hydrogenation of graphite by metallic nanoparticles, which diffuse at its surface, produces trenches with an edge roughness of less than few benzenic rings (~1.5 nm). [24] However these two approaches do not ensure any control on

deux approches n'assurent cependant aucun contrôle précis de la forme de la gravure.

Nous proposons donc d'associer la gravure chimique, qui semble permettre de contrôler précisément la rugosité des bords de découpe, avec l'activation de la réaction par un faisceau électronique focalisé et pilotable dans un SEM.. La tension d'accélération disponible avec un SEM (1-30 kV) est inférieure à celle d'un TEM, mais la présence d'un réactif, l'eau, permet d'abaisser l'énergie d'activation pour la rupture de la liaison C-C (Figure 4.1).

La première partie de ce chapitre décrit les échantillons dont la préparation anticipe la caractérisation structurale en microscopie électronique en transmission après gravure en MEB. Les échantillons seront du graphène suspendu sur des grilles TEM (Figure 4.1a). La deuxième partie est consacrée à la gravure directe du graphène sous faisceau électronique de basse énergie. Les principes de l'EBIE sont présentés avant d'exposer les caractéristiques des gravures. Les paramètres importants au contrôle du processus de gravure EBIE du graphène seront examinés :

the shape of the etching.

We propose to combine the chemical etching, which fosters smooth edges, with an e-beam-induced activation of the reaction in an SEM in order to have control over the focal point where the etching reaction is triggered. The acceleration tension available in a SEM (1 to 30 kV) is lower than the one of a TEM but the presence of a reactant (water) will lower the activation energy to break the C-C bond (Figure 4.1).

The first part of this chapter describes the sample preparation in anticipation of the structural characterization in TEM. The samples will be graphene suspended on TEM grids (Figure 4.1a).

The second part is dedicated to the low energy electron etching of graphene. The principle of EBIE is presented before showing the characteristics of the etching. The important parameters for the control of the EBIE process are examined and applied to simple line. Next the etch-

Les paramètres pour des gravures simples étant établis, nous envisageons la gravure de motifs complexes (Figure 4.1b) qui comportent un certain nombre d'étapes clés. Un ruban de graphène sera continument connecté à deux électrodes métalliques par des constrictions triangulaires de graphène. L'angle entre le ruban et les constrictions est fixé à 45°. L'influence de l'orientation de la gravure par rapport aux directions cristallographiques du graphène est évoquée. La gravure d'une longue découpe, permettant d'isoler un ruban du reste du feuillet de graphène est montrée. La connexion entre deux découpes contigües avec un angle de 45° est étudiée. Enfin nous examinons l'influence de l'épaisseur du graphite avant de réaliser la gravure de rubans de graphène par deux découpes parallèles.

La dernière partie de ce chapitre étudie la qualité structurale des bords de gravures simples effectuées par EBIE sur du graphene. L'étude est menée avec un MET avec correcteur d'aberrations sphériques ("spherical aberation corrected TEM" SACTEM). Le désordre des bords à courte distance est d'abord étudié. La distance maximale de la zone amorphisée par la gravure est ensuite mesurée. La rugosité sur une longue distance est ensuite mesurée et commen-

ing of more complex shapes is considered (Figure 4.1b) that contains some crucial steps. A nano-ribbon of graphene will be continuously connected to metallic electrodes by two triangular graphene constrictions. The angle between the ribbon and the constrictions is fixed to 45°. The influence of the orientation of the etching with respect to the crystallographic orientation of graphene is discussed. The etching of a long cut, allowing to insulate a ribbon from the rest of the flake is shown. The junction between to cuts with an angle of 45° is studied. Finally we will examine the influence of the thickness of graphite before realizing an etching of GNRs by two parallel cuts.

The final part of this chapter studies by a SACTEM the structural quality of the edges of single cuts made by EBIE on graphene. . The disorder of the edges at small distance is first studied. The maximum amorphisation length is then measured. The long range roughness is finally measured and discussed. Finally are studied the contamination of graphene by carbonaceous species and

tée. Finalement, La contamination du graphène par des matières carbonées et son nettoyage sont étudiés.

the cleaning of graphene.

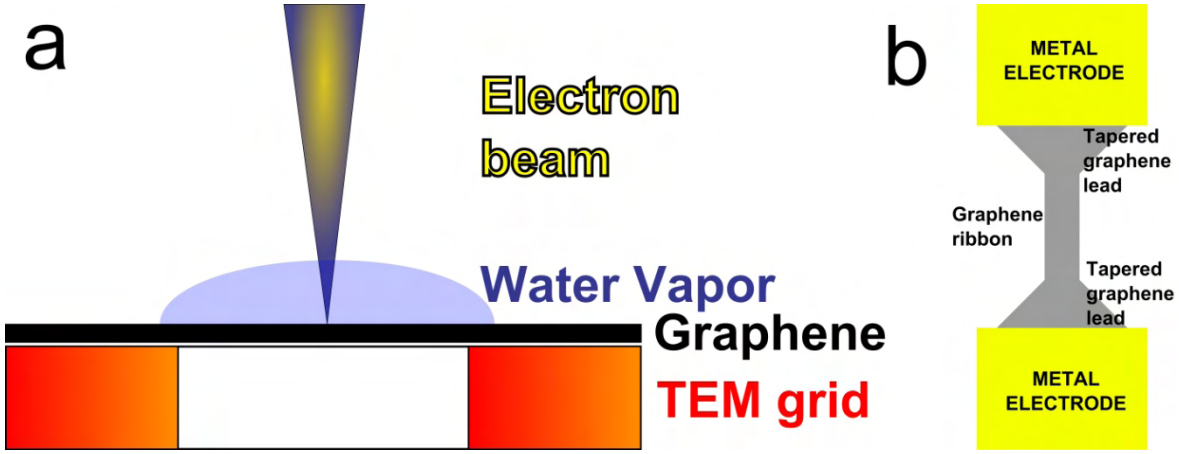

Figure 4.1. *(a) Schéma de l'EBIE assisté par de la vapeur d'eau sur du graphène suspendu. (b) schéma d'un dispositif de mesure électrique en deux point d'un ruban de graphène.*

Figure 4.1. *(a) Schematics of water assisted EBIE on suspended graphene. (b) Schematic of an electronic transport measurement device made with graphene.*

4.1 Sample preparation.

4.1.1 CVD graphene on Ni transferred onto copper TEM grid.

FLG (1 to 10 graphene layers) is grown on a nickel surface by chemical vapor deposition (CVD). The thin layer is transferred on a 2000 mesh TEM copper grid by a resist free technique. [25] An IPA droplet is deposited over the grid set on the Ni/CVD graphite surface. While the droplet is drying, the grid sticks to the graphite. The nickel is etched leaving the TEM grid covered with thin graphite. On the grid, large particles or defects are used to locate a specific area of interest. This localization technique allows to relocate a trench performed by EBIE in the TEM.

The coverage of the grid with graphene is very high, Figure 4.2a shows a large scale SEM image of a grid where almost all the 7x7 μm^2 squares are covered with thin graphite. Graphite films are composed of a large variety of thicknesses identifiable by their difference

in contrast in the SEM (Figure 4.2b) and TEM (Figure 4.2c) images. The size of the domains of constant thickness varies from about 1 to 10 µm.

A SAED (Figure 4.2d) shows a diffraction pattern of thin graphite, the selected area is 0.13 µm². The inner hexagon correspond to a spacing of 2.13 Å related to the $[0\bar{1}10]$ direction, the diffraction peaks of the $[1\bar{2}10]$ direction are also visible. A cross section along the yellow dashed line in Figure 4.2d is plotted in Figure 4.2e. The intensity ratio $\frac{I_{[0\bar{1}10]}}{I_{[1\bar{2}10]}}$ is smaller than one, indicating that this sample is a FLG of two or more graphene layers.[26]

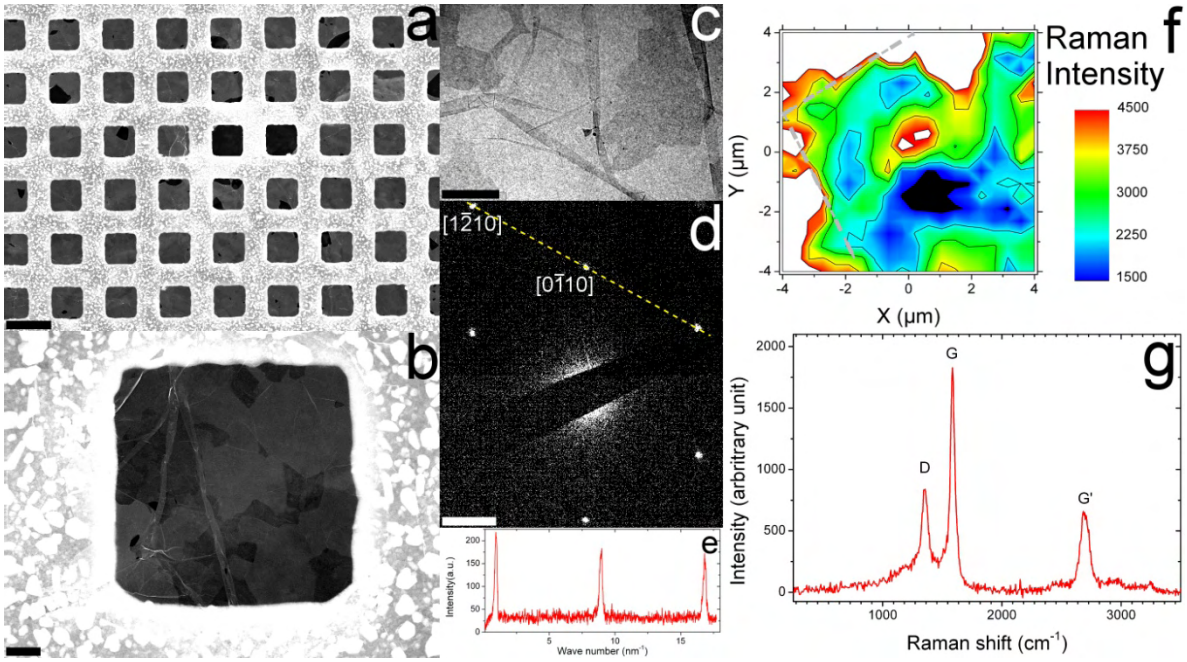

Figure 4.2. *Nickel grown CVD graphene on a copper TEM grid. (a) and (b): SEM images of a copper TEM grid covered with graphite. (c) Bright field TEM image of thin suspended graphite. (e) cross section following the yellow dashed line in (d): SAED of a thin graphite, the diaphragm diameter is 200 nm. (f) is a Raman map of the G peak intensity of graphene recorded over a suspended graphite. Dashed gray lines represent the edges of the copper grid. (g) is a Raman spectrum of a thin suspended graphite. Scale bars: (a) 10 µm, (b) and (c) 1 µm and (d) 2 nm^{-1}. The excitation wavelength for (f) and (g) is 532 nm.*

The Raman map of the G peak in Figure 4.2f shows an edge of the Copper support of the grid (white in the map) and a suspended FLG. The G peak intensity varies from 1,500 to 5,000 counts, confirming a large variety of thicknesses (the G peak intensity is proportional to the volume of FLG scanned and thus to its number of layers). Raman map has too poor a

resolution to clearly distinguish the border of equal thicknesses domains. Since the laser spot is larger than the typical size of FLG domains which prevents the monolayer identification. It probes several thickness domains at each acquisition, Figure 4.2g shows a Raman spectrum of a suspended FLG, the G' is constituted of more than one Lorentzian, suggesting that there is at least one domain with 2 or more layers of graphene under the laser beam. The spectrum also shows a D peak at 1354 cm^{-1}. This peak reveals defects in the FLG lattice and/or domains boundaries.

4.1.2 CVD Graphene grown on copper transferred with PMMA on Si_3N_4 membranes.

CVD graphene grown on a copper foil is transferred on Si_3N_4 membranes perforated with 1 μm holes of 1 μm in diameter over which graphene is suspended. A PMMA layer is spun onto graphene. The copper foil supporting graphene is then placed on a copper etchant bath (0.1 $g.ml^{-1}$ $Na_2S_2O_8$ solution). After dissolution of the copper, the graphene supported by PMMA is directly transferred on a Si_3N_4 membrane and the PMMA is dissolved in acetone. These samples have been prepared in the group of V. Bouchiat in Grenoble.

A SEM image of the membrane reveals that almost all the membrane is covered after the transfer (Figure 4.3a). Only few areas (dark in the Figure 4.3a), let the bare Si_3N_4 membrane visible. A TEM image in Figure 4.3b confirms that the holes are covered with a thin film. In several areas in Figure 4.3b the film is partially folded, a difference in the contrast is visible. These folded areas can be used, as well as some dust particles, to identify a specific location on the Si_3N_4 membrane.

TEM image in Figure 4.3c shows suspended graphene. Adsorbates visible on the surface are attributed to PMMA. [6] Nevertheless there are uniforms regions where the graphene is less contaminated. The diffraction pattern in Figure 4.3d is typical of a graphene monolayer lattice. As shown in the Figure 4.3e where $\frac{I_{[0\bar{1}10]}}{I_{[1\bar{2}10]}}$ is greater than 1. According to the diffraction patterns, the sizes of the mono-crystals domains are higher than 0.5 μm^2.

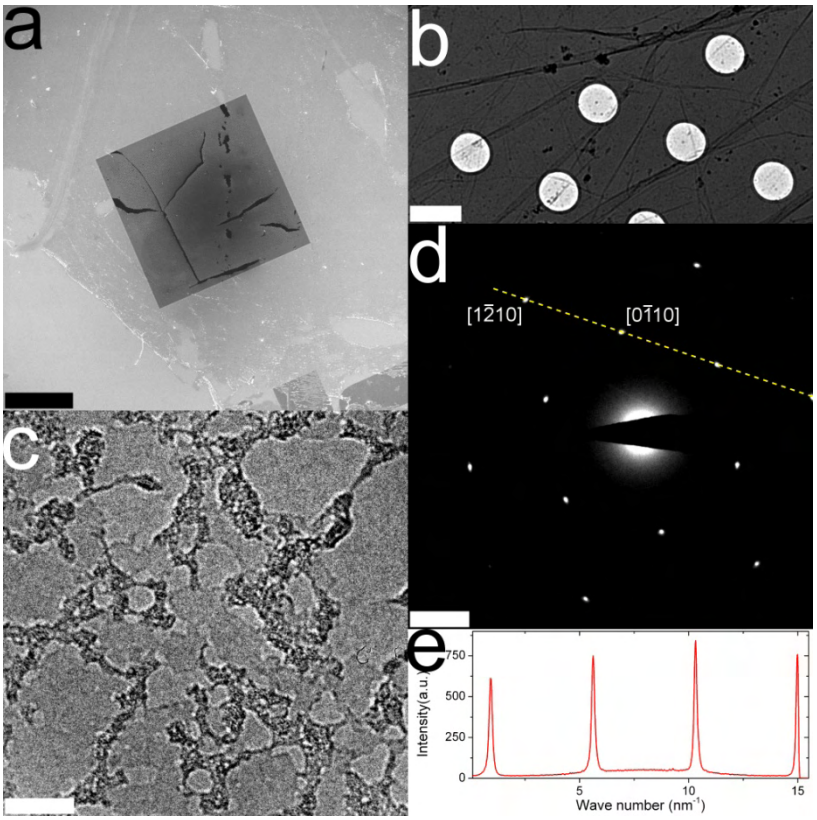

Figure 4.3. *Si_3N_4 membrane covered with CVD graphene. A SEM image (a) showing the membrane and its silicon nitride support. The darker stripes are area where the graphene-PMMA film is cracked. (b) is a TEM image of several holes in the Si_3N_4 membrane, graphene is suspended over those holes (graphene drums). The TEM image in (c) shows an area of a graphene drums. (d) is a SAED of a graphene drums, the diaphragm diameter is 870 nm. (e) Is the cross section of the yellow dashed line in (d). Scale bars: (a) 200 µm, (b) 2 µm, (c) 10 nm and (d) 2 nm^{-1}.*

4.1.3 CVD Graphene on copper directly transferred on TEM grids.

Quantifoil are a 300 mesh gold grid covered with an amorphous carbon (a-C) thin film. This film is perforated by an array of circular holes of 1 µm in diameter. Graphene is grown on a copper foil by CVD, purchased from Graphene supermarket. Copper and graphene are placed on a bath of copper etchant: $(NH_3)_4S_2O_8$ at $2.5x10^{-2}$ $mol.L^{-1}$ for 30 hours. Once the copper foil is completely etched, graphene is visible on the surface of the solution. Gold quantifoil grids or Si_3N_4 membranes are plunged in the solution and brought under the floating graphene. While the grid is gently surfaced, graphene sticks to the grid. It is dried on a hot plate in air at 100°C for 15', rinsed in DI water and let to dry in air.

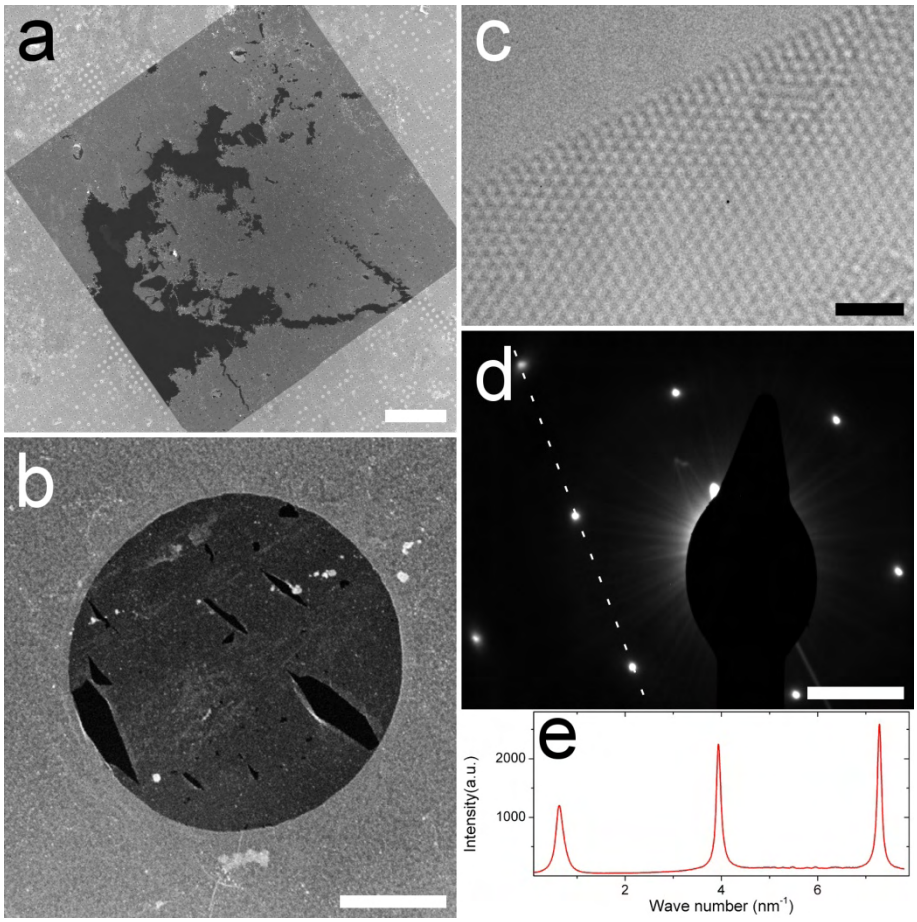

Figure 4.4. *Graphene grown on a copper foil and transferred onto gold quantifoil and Si_3N_4 grids with a resist-free technique. (a) SEM image of a Si_3N_4 grid covered with graphene. (b).SEM image of suspended graphene grown by CVD and directly transferred onto gold quantifoil grid. (c) is a SACTEM image of suspended graphene deposited onto gold quantifoil grid. Taken with a Titan^3 from FEI operating at 80kV. (d) is a SAED of suspended graphene deposited on a Si_3N_4 grid. (e) Is the cross section of the white dashed line in (d) Scale bars: (a) 100 µm, (b) 500 nm, (c) 2 nm and (d) 2 nm^{-1}.*

The coverage rate of graphene transferred by this method is as high as 80% (Figure 4.4a). A SEM image in Figure 4.4b shows a hole of a gold quantifoil grid covered with graphene, graphene has been mechanically torn during the transfer. Figure 4.4c is a SACTEM image showing the edge of one of these mechanically torn graphene. The intensity ratio $\frac{I_{[0\bar{1}10]}}{I_{[1\bar{2}10]}}$ in the SAED (Figures 4.4d and e) confirm that graphene is monolayer.

4.2 Electron beam induced etching of graphene.

Unless further precisions, the following experiments are conducted on copper TEM grids covered with graphene grown on nickel by CVD. Irradiations are performed with elec-

trons accelerated at 20 kV. Water vapor was injected near the irradiation by a gas injection system (GIS) of the SEM.

4.2.1 Principle.

EBIE is a patterning technique using a focused electron beam to etch mater at a nano-scale resolution. Gas assisted EBIE combines a focused electron beam and a gas injected near the irradiated area. A focused electron beam of a FEG SEM has energies ranging from 1 to 30 keV. The spatial distribution of the electron beam is well described by a Gaussian. The full width at half maximum (FWHM) of the focused electron beam intensity is a few nanometers. Precursor gas is injected in the close vicinity of the irradiated area.

Precursor molecules from the injected gas adsorb, desorb and diffuse at the surface of the sample (see Figure 4.5). The electron beam dissociates those molecules and several processes can occur, depending on the precursor. If products of the reaction are non volatile, a deposit forms and grows under the electron beam. This phenomenon is called gas assisted electron beam induced deposition (EBID). Dissociated molecules can also react with the surface and produce volatile compounds, resulting in the etching of the reactive surface, it is called gas assisted electron beam induced etching (EBIE).

A precursor molecule can be dissociated by primary electrons of the incident beam but also by secondary (SE) or backscattered electrons (BSE). SEs are generated by the interaction between primary electrons and mater of the substrate. Energy of SE is of a few eV and their escape depth is only a few nanometers. [27] BSEs are primary electrons reflected by elastic collisions in the substrate, their energy peak is situated close to the energy of primary electrons. [27] Their escape depth is dependent on their energy, ranging from 30 nm to 10 μm for 1keV and 30keV respectively in silicon. [27]. SE and BSE can lead to non local etching.

Gas assisted EBIE will be used to etch graphene. The capability to etch graphene will be discussed in the next paragraph.

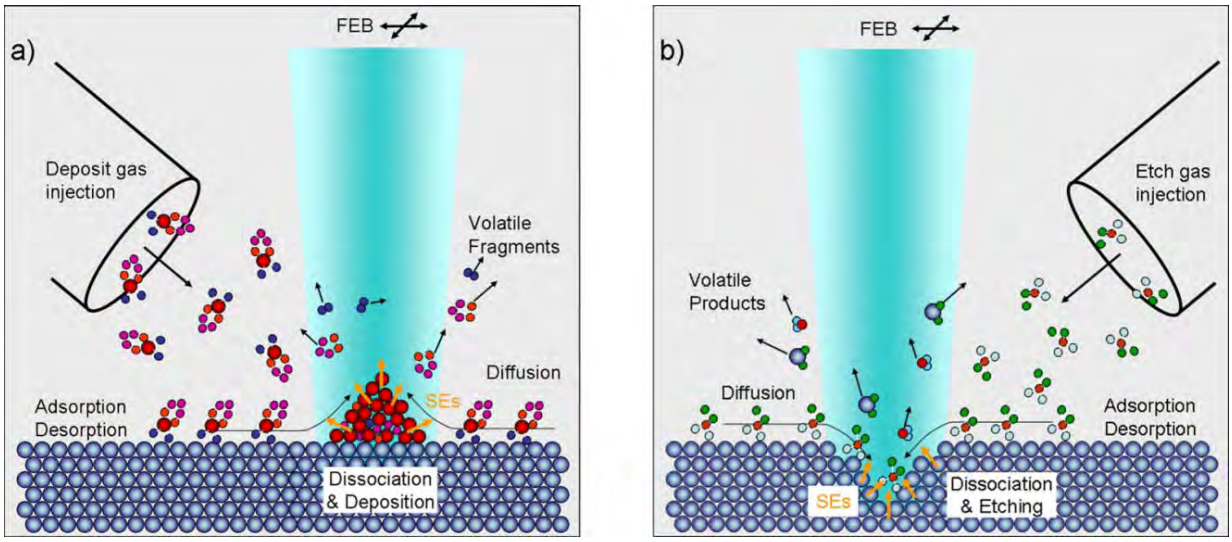

Figure 4.5. *Schematics illustrating the processes involved in gas assisted electron beam induced deposition (a) and etching (b). Adapted from [27].*

4.2.2 EBIE patterning of graphene.

Cut on graphene consists on irradiating several points along a straight line. Two conditions are considered. One irradiation is performed without injecting any gas in the chamber and each point irradiated receives an electronic dose of 20 $C.mm^{-2}$. The other irradiation is performed while water vapor is injected near the irradiated area with a GIS. The vertical distance between the nozzle of the GIS and the surface is about 100 µm, the electronic dose is 4 $C.mm^{-2}$ and the pressure decreased by one order of magnitude to about $5x10^{-6}$ mbar during the gas injection.

Figure 4.6 shows SEM images after irradiations on graphene. No etching is observed for irradiation without water vapor (Figure 4.6a). When water vapor was injected in the chamber (see Figure 4.6b) a series of coalescing holes are visible on the graphene.

Water assisted EBIE of graphene is shown, in following, the major parameters that influence etching of graphene will be discussed.

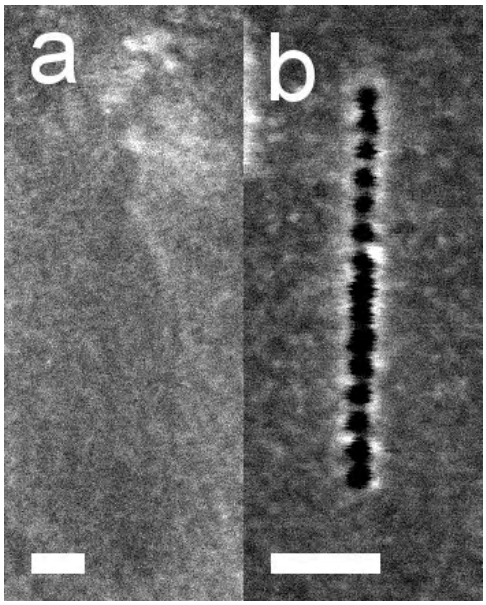

Figure 4.6. *Evidence for gas assisted EBIE on graphene. SEM images of two series of irradiations (a) without water vapor and (b) with water vapor. Electronic doses per holes are 20 C.mm^{-2} for (a) and 4 C.mm^{-2} for (b). The width of the cut is 12 nm. Scale bar: 50 nm.*

Electrons with incident energy of 20 keV can transfer a maximum energy by a head-on collision with a C atom of 3.7 eV [28, 29]. This is less than the T_d energy in graphene (17 eV) or in its edge (15 eV)[17]. It can explain why no etching is visible for graphene irradiated with electron accelerated at 20 kV. However if water vapor is injected on the irradiated area, etching occurs. This is evidence that the electron beam activates a chemical reaction between water molecules and the carbon of graphene. The situation is similar for STM lithography of graphite, while in vacuum the minimum voltage to etch graphene is 8.5 V, [15] this threshold decreases to 2-3 V in presence of atmospheric water. [12, 13, 16]

4.2.3 Parameters influencing water assisted EBIE of graphene.

The irradiation dose is the charge per unit area received during the beam rastering of the surface:

$$D = \frac{I \times t}{S} \tag{4.1}$$

Where I is the current of the beam (A), t is the pixel time (s) and S the surface (m²) irradiated by the electrons.

Beam current has been evaluated with a Faraday cup in a SEM chamber. The current is 150±10 pA at 5kV acceleration and 280±15 pA at 20kV. For a single irradiation, the electron beam irradiates the same area during t. The electron density distribution is assimilated to a radial Gaussian around the optical axis. For a radial Gaussian profile, S it is chosen as the maximum surface etched by EBIE at 5 kV on graphene. Indeed, as t increases, the size of the hole in graphene increases and seems to saturate (Figure 4.7). This surface is S=1,500 nm^2, it is about 200 times more than the surface of the beam size (7 nm^2).

To perform dose vs. etched surface experiments, graphene was irradiated for various exposure time (t). 2, 5 and 20 kV acceleration tensions have been used. The surface of the holes has been measured on SEM images with the software ImageJ.

The results are presented in the plot of Figure 4.7. For each acceleration tensions, the data follow a power law with an exponent of 0.5 for 2 and 5 kV and an exponent of 0.6 for 20kV. On the 5 kV data, a saturation is visible for doses higher than 80 $C.mm^{-2}$, the etched area is about 1,500 nm^2. This behavior is observable neither for 20 kV nor for 2 kV. A dependence with electron energy is observed, the higher the electron energy, the smaller the etched area.

A square root dependence has been founded between the etched area and the electronic dose. At 5kV for the lowest electronic doses (Figure 4.7d and e) the holes are surrounded by a white area which could be deposited contaminants or amorphized graphene. When the electronic dose increases, the size of the amorphized zone is constant in contrary to the size of the etched area. In consequence, for electronic dose higher than 5 $C.mm^{-2}$, the amorphized area has been etched. In the following, etched lines are performed at doses equivalent to 5-50 C. mm^{-2} to reduce the amorphized area. The dependence with electron energy suggests that a hole can be etched with a lower electronic dose at 2 kV than at 5 or 20kV. Reducing the acceleration tension of the beam could improve the technique by lowering the electronic dose that is needed to etch graphene.

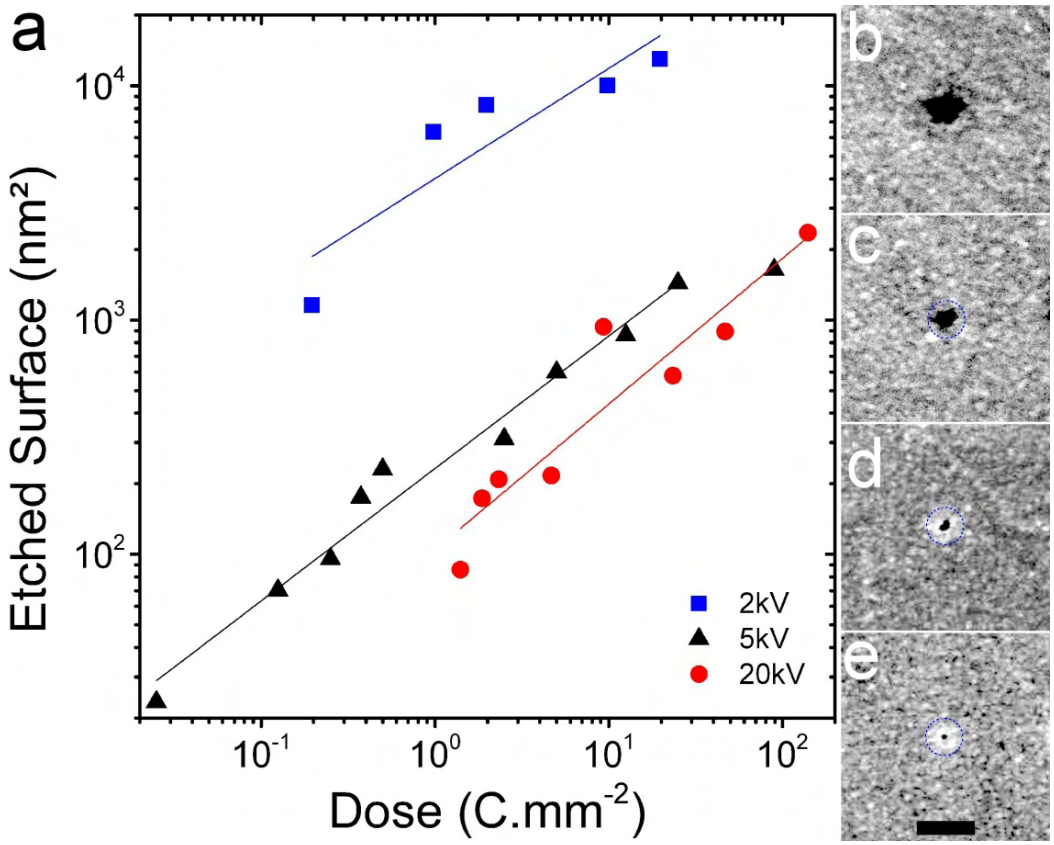

Figure 4.7. *Etched area versus electronic dose. Holes were performed by EBIE on FLG at several electrons energy (2, 5 and 20 keV). The surface etched versus the electronic dose is plotted in a log-log scale. Blue squares for 2 kV, black triangles for 5 kV and red disks for 20kV. Lines are the linear fit of the data. The values of the slopes obtained by linear fit are 0.5, 0.5 and 0.6 for 2, 5 and 20 kV respectively. (b-e) holes with decreasing dose, (b) 35.8; (c) 2; (d) 0.2 and (e) 0.1 C.mm^{-2} acceleration tension is 5 kV. In (c-d) a dashed blue circle represents the irradiated area, a disk with an area of 1,500 nm². Scale bar is 100 nm.*

The effect of the electronic dose on the etched surface is thus characterized for a spot mode or a single irradiation. The following study will focus on how to use spot mode irradiation to produce continuous cuts. The parameters that control the electron beam for EBIE/EBID are the probe size (Ps), the pitch factor (R) and the pixel time (t). A line is etched by making a succession of irradiations in spot mode separated by the pitch. The pitch (p) is defined as the product of the probe size by the pitch factor. Each spot irradiation is maintained during the pixel time.

In order to determine the effective size of the electronic beam, several etching following lines have been performed. The probe size value has been set to an arbitrary value (14 nm) and the pitch factor has been varied from 0.2 to 2.

High pitch factor values produce separated holes as shown in Figure 4.8a. For intermediate pitch factor value, holes are tangent, see Figure 4.8b. And for small pitch factors, the etching is a continuous line with smooth edges, see Figure 4.8c. The real probe size (d) is:

$$d = d_e \times R_c \tag{4.2}$$

With:

d_e The probe size used for the experiments (14 nm)

R_c the pitch factor value for which holes are tangent to each other.

Several experiments led to a value of the probe size:

$d = 13 \pm 1\ nm$

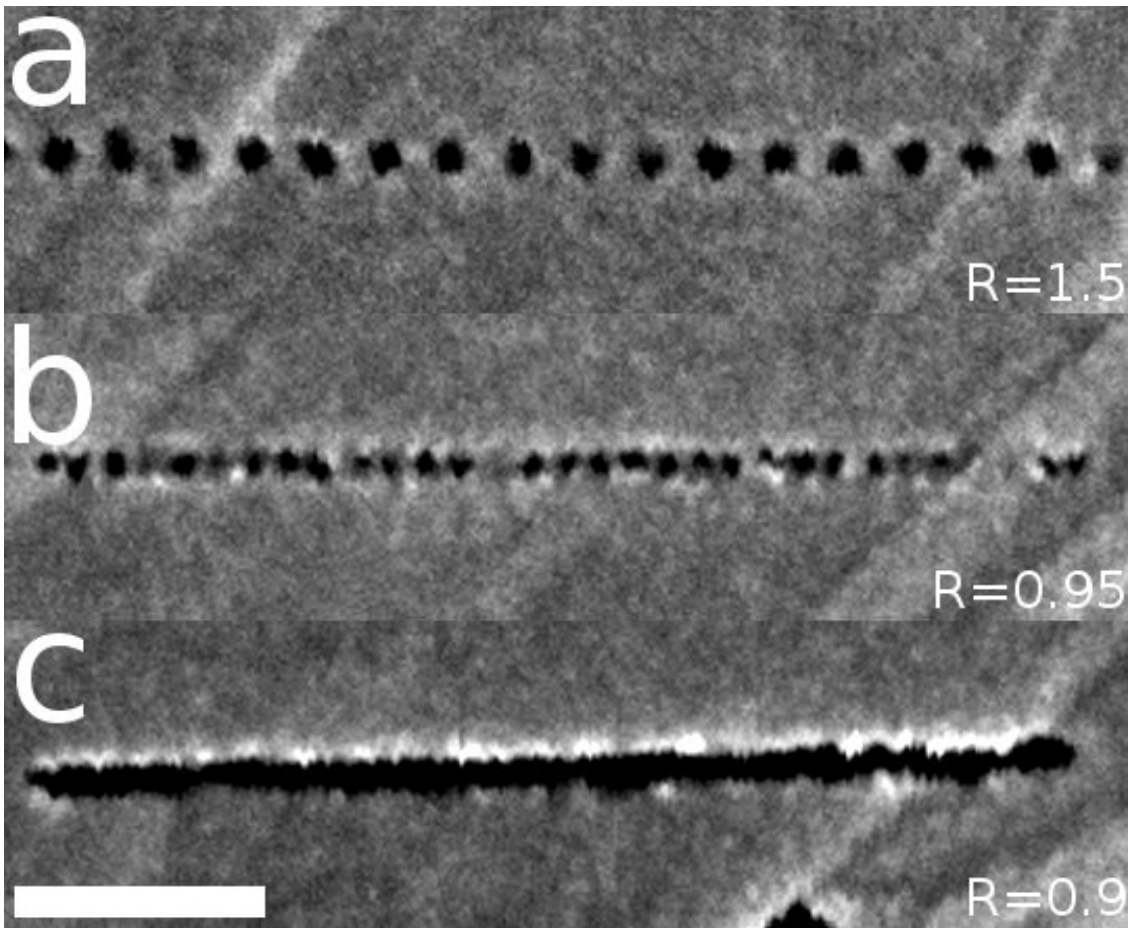

Figure 4.8. *SEM images for EBIE patterns etched in a suspended graphene for pitch factor (a) R>1 lead to a series of separated spots with a diameter Φ=15 nm. (b) R~1 corresponds to tangents spots. (c) Continuous etched line is obtained for R<1. Scale bars are 100 nm.*

For etched lines, a linear electronic dose is defined:

$$D_L \equiv \frac{I \times t}{L} = \frac{I \times t}{P_S \times R} \tag{4.3}$$

Where L is the length of the etched line, P_S the probe size and R the pitch factor.

When the pitch between successive holes is too large, an unwanted roughness is introduced, as illustrated in Figure 4.9. In this schematic representation, each disk represents an EBIE hole in spot mode. The successive disks are shifted of 1/2, 1/4 and 1/20 of their diameter, corresponding to pitch factor of 0.5, 0.25 and 0.05 respectively. The edge roughness is defined by the distance between two parallel lines in which fit the corrugated edges, represents 7.5% for a pitch factor of 0.5, i.e. 1-2 nm. The roughness is reduced to 1.5% for R=0.25 (3 Å) and to 0% for R=0.05. Clearly, a more uniform edge is obtained with smaller pitch values.

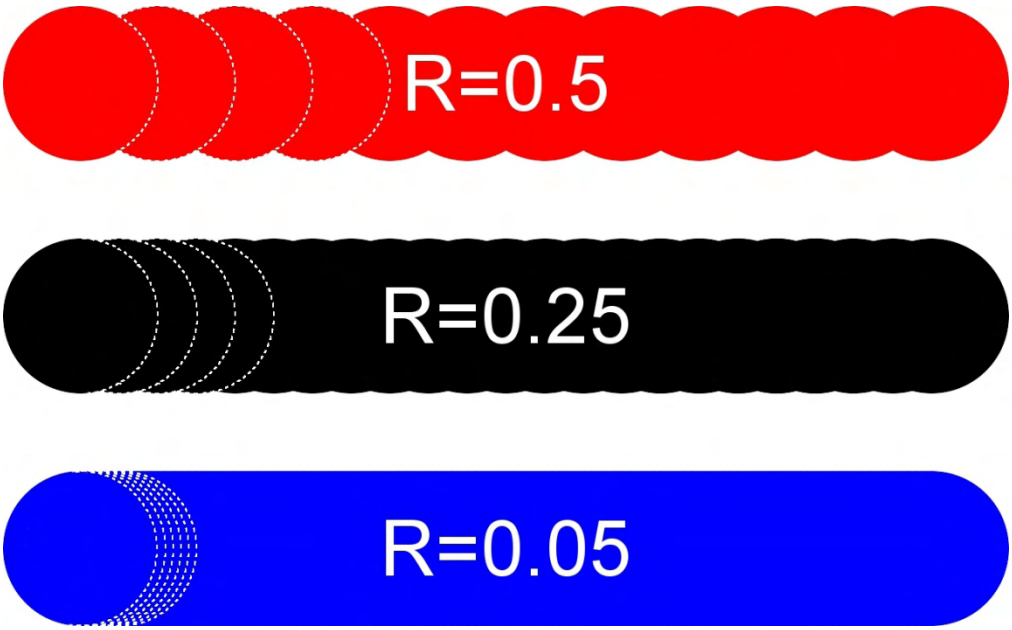

Figure 4.9. *Comparison between several pitch factor values. The disks represent holes created by a spot mode EBIE. The disks are then spaced by 1/2, 1/4 and 1/20 of the diameter. This simulates an EBIE etch following a line with a pitch factor of R=0.5 (red disks); 0.25 (black disks) and 0.05 (blue disks).*

Reducing the pitch factor results in an increase of the electronic dose if the pixel time remains unchanged. Such a high dose damages graphene. Therefore, experiments were con-

ducted to estimate the minimum pixel time that still etch FLG. For R=0.05, the minimum pixel time is about 0.1s. These values correspond to a linear electronic dose of $4\ 10^{-2}$ C.m^{-1}. However, this value has been obtained on a FLG and is very dependent on the flake thickness.

4.2.4 Influence of adsorbates on EBIE etch rates.

Two types of irradiations have been performed on FLG. Firstly, water vapor has been injected near the irradiated area, two lines have been irradiated with pitch factor of 0.5 and an electronic dose of $8.5\text{x}10^{-2}$ C.cm^{-1}. Second, water vapor has not been injected, the vacuum was about 10^{-7} mTorr and a rectangle has been irradiated by imaging mode of the SEM, the electronic dose is unknown.

Figure 4.10a is a SEM image of these two electrons irradiations. The lines are white, unlike etched graphene that appears black like in Figure 4.8. In the top part of the left irradiated line of the Figure 4.10a, a SEM rectangle scan is visible, that has the same white deposit aspect. Graphene, which has been irradiated with a very low electronic dose (low magnification SEM image) presents a wooly aspect.

Under e-beam irradiation, graphene undergoes two processes which are in competitions: etching and deposition. For the rectangle irradiated in the absence of injected water, an EBID process dominates and leaves a deposit on the graphene surface. Although water vapor is injected, two lines were irradiated, an EBID phenomenon is visible in Figure 4.10a. The irradiations conditions are similar to the one used for the trenches in Figure 4.8 except that the SEM grid was used just after receiving it in the previous experiment and store in ambient conditions for the experiment described here. Graphene has been contaminated by the air atmosphere and the electron beam bound a material to the graphene during the irradiation.

In order to identify the nature of the contaminants, a square of 1x1 μm² has been irradiated with a high electronic dose (Figure 4.10b) and analyzed in EDX. The presence of cop-

per, aluminum, traces of iron and carbon were the only detectable elements. In the absence of other identifiable elements, we assume that the contamination comes from ambient hydrocarbons and the deposited material is probably a carbonaceous one. [30] Etching graphene with EBIE thus need an efficient method to clean its surface.

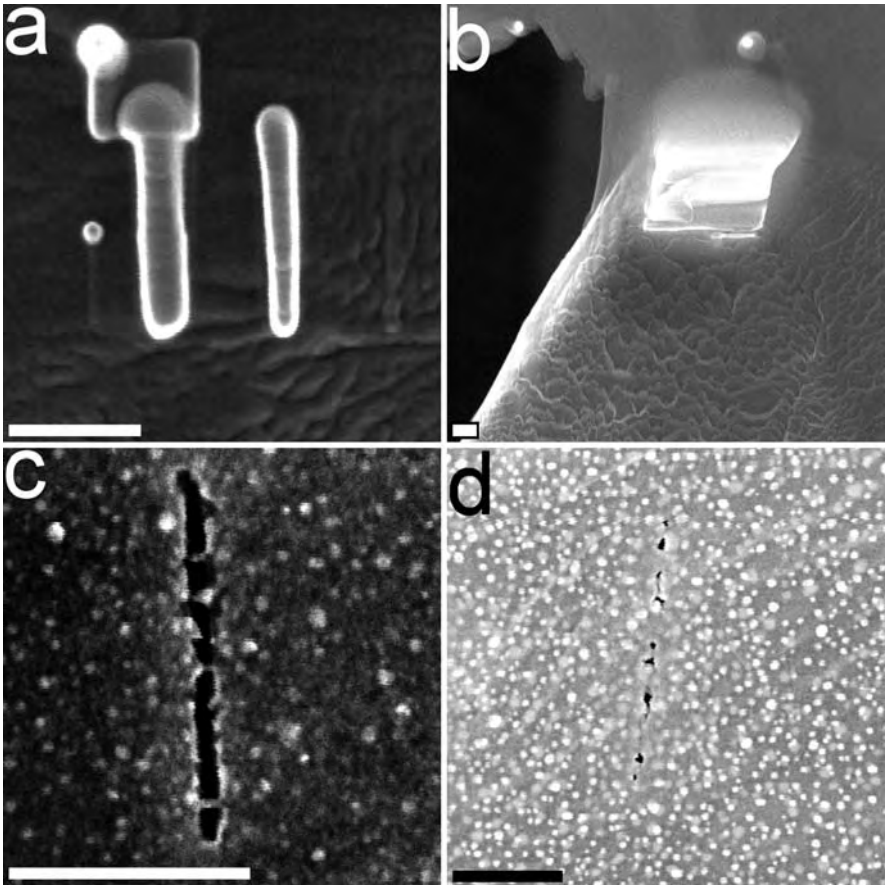

Figure 4.10. *Cleaning of graphene. (a) SEM images of a graphene suspended on a copper grid irradiated by an electron beam following two lines in presence of water Vapor with an electronic dose of 8.5x10^{-2} C.cm^{-1} and a pitch factor of R=0.5. (b) SEM image of suspended graphene, a 1x1 µm² square has been irradiated, no gas was injected, the electronic dose was 150 C.cm^{-2} and pitch factor, R=0.7. (c-d) SEM image of EBIE cut on thin graphite after an annealing in a flow of Ar and H_2 with a flow of (c) 50 cm^3.min^{-1} for each gases and (d). Ar:100 and H_2:75 cm^3.min^{-1} at a temperature of (c) 300°C for 3h and (d) 400°C for 6h. The electronic doses were (c) 8.5x10^{-2} C.cm^1 with a pitch factor of R=0.5 and (d) 0.15 C.cm^1 with a pitch factor of R=0.3. Scale bars : 200 nm.*

In order to evaluate the efficiency of thermal annealing in removing adsorbates, two samples have been prepared. The samples are contaminated grid, the first has been annealed at 300°C for 3h in a flow of argon and dihydrogen (50 cm^3.min^{-1} for each) and the second for a longer time at higher temperature (400°C for 6h in a flow of argon and dihydrogen 100

and 75 $cm^3.min^{-1}$ respectively). Irradiations following lines have been performed on the samples in presence of water vapor. The sample one has been etched with an electronic dose of $8.5x10^{-2}$ $C.cm^{-1}$ and a pitch factor of R=0.5, for the second sample, the dose was 0.15 $C.cm^1$ and the pitch factor, R=0.3.

On the first sample, Figure 4.10c shows an EBIE trench which is continuous but for the second sample (Figure 4.10d), EBIE produced dashed cut. An annealing in reducing atmosphere removes contaminants of the graphene surface. This cleaning allows EBIE of graphene, EBID of carbonaceous material is no longer the dominant process in annealed graphene. The annealing performed in the first sample (300°C for 3h with a flow of argon and dihydrogen of 50 $cm^3.min^{-1}$ for each gas) has successfully cleaned a graphite surface which was contaminated by carbonaceous material

However, after annealing, Nanoparticles of various sizes are also visible on the sample, with a higher density for the sample two, which has been annealed at a higher temperature and greater time than the sample one. The particles produced by annealing can even hinder the etching of graphene if their density is too high. As shown by Figure 4.10d annealing at 400°C for 6h avoid continuous etching of graphene. The work by Lin et al [6] conclude that annealing in forming gas clean the graphene but increasing the temperature over 250°C does not improve the cleaning.

EBIE on graphene has been shown to etch graphene when water is injected and the effect of electronic dose on the etched area is now known, the following will aim to show the potential of EBIE on graphene in term of etched shape.

4.2.5 Crystallographic orientation of the etching.

EBIE of graphene is a chemical reaction at the gas/solid interface between water and the carbon of graphene activated by the electron beam. Hydrogenation of graphene, which is also a chemical etching, shows crystallographic selectivity: cut lines are parallel to either zigzag or armchair directions of graphite. In hydrogenation of graphene, catalytic particles can

freely diffuse on the graphite surface and are able to follow the most energetically favorable path. In the case of EBIE, the cutting direction is imposed by the beam rastering. If this direction follows the crystallographic orientations, it could results in a better – smoother – etching.

Graphene has been irradiated following lines with an electronic dose of $6x10^{-2}$ $C.m^{-1}$ and a pitch factor of 0.8. Lines are orientated with respect to a graphite step with relative angles from 0 to 38°.

Figure 4.11a shows a graphite step marked with a dashed white line. No clear dependence of the edge roughness with the orientation seems to appear in the cuts shown in Figure 4.11.

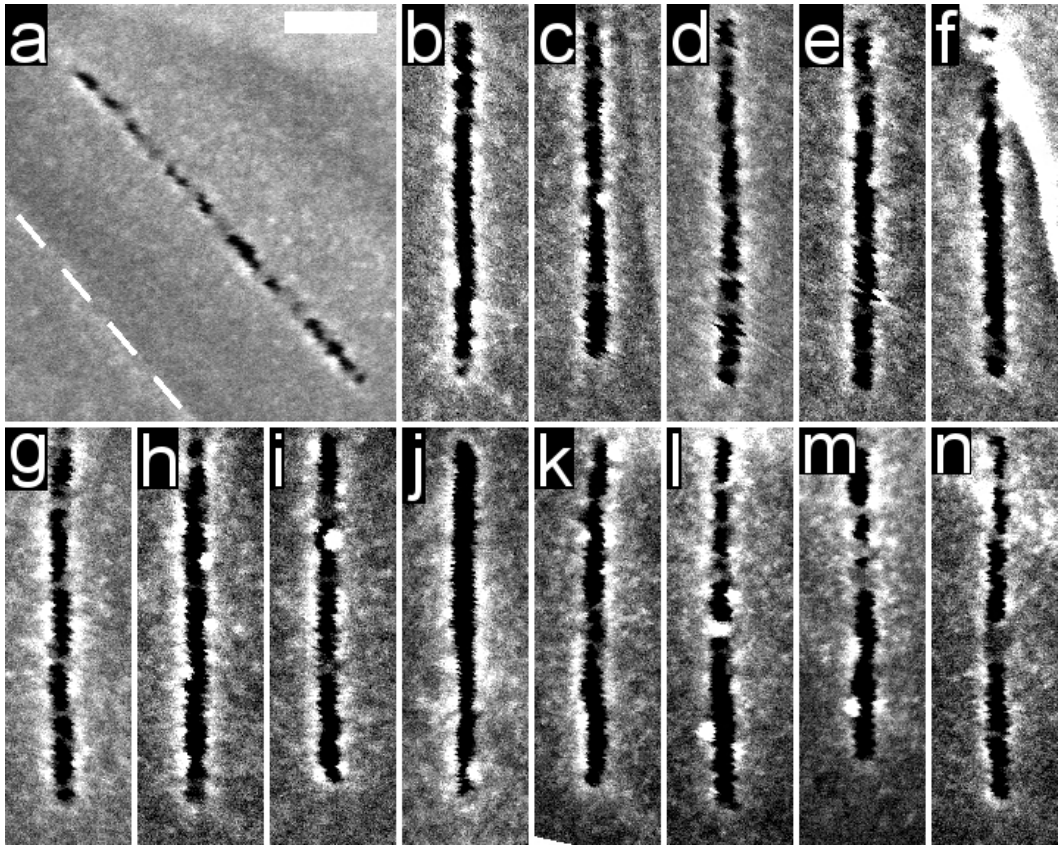

Figure 4.11. *Effect of the orientation of the etching. Electronic doses were $6x10^{-2}$ $C.m^{-1}$ for a pitch factor of 0.8. (a) Cut is parallel to a step in the FLG (along the white dashed line). (b-n) cuts make an angle with respect to the direction of the cut in (a). The values of the angles are (b) 3°, (c) 8°,.(d) 10°, (e) 13°, (f) 16°, (g) 19°, (h) 22°, (i) 25°, (j) 28°, (k) 30°, (l) 32°, (m) 36° and (n), 38°. Scale bar is 50 nm.*

The step on the FLG is a strong indication of an armchair or zig-zag edge. Several parameters can hide a dependence on the crystallographic orientation, like the carbonaceous contaminants, since the sample has not been annealed. The domains size of graphene corresponds to the crystallographic domains of nickel, some cut are potentially on different domains. The latest samples that we produced, graphene CVD on copper transferred on Si_3N_4 membranes would solve these issues and a new analysis of crystallographic orientation will have to be done.

4.2.6 Long distance etching.

One of the requirements of the etching technique is to be able to etch graphene over micrometric scale with nanometric resolution for the shape, this feature is discussed here. A 1 μm long cut has been etch, it fits between two line separated by 15 nm (Figure 4.12b). This cut has been done on a suspended graphene, etched by EBIE following a line. Electronic dose was $5.4x10^{-2}$ $C.m^{-1}$ and the pitch factor, 0.8. The etching speed was 250 $nm.min^{-1}$. This trench shows that the objectives of long range etching are reached.

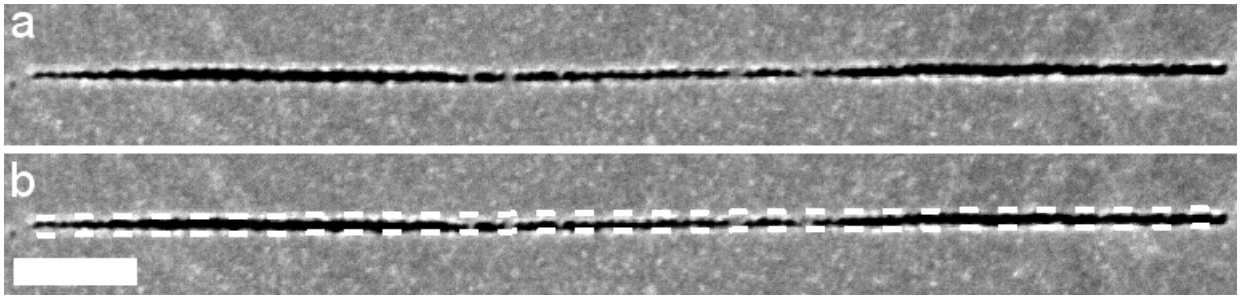

Figure 4.12. *SEM image of EBIE long cut. (a) is a SEM image of a EBIE cut performed on graphite. (b) is the same image with two parallel dashed lines separated by 15 nm. Electronic dose was $5.4x10^{-2}$ $C.m^{-1}$, pitch factor was 0.8 and it took 4 min to be etched. Scale bar is 100 nm.*

4.2.7 Fabrication of a junction between two lines.

To produce more complex shape with EBIE, two trenches have to be connected, this is the purpose of this paragraph. A series of three junctions were etched. A junction is composed of two lines forming an angle of 45°. The overlapping of the junction is schematized in

Figure 4.13. The junction in Figure 4.13a has no overlapping, for the junction in Figure 4.13b a line is vertically (down) shifted of 20 nm with respect to the other line and a junction with a line horizontally (left) shifted of 20 nm is shown in Figure 4.13c. Cuts have been performed by EBIE on suspended graphene, with an electronic dose of and 8.6×10^{-2} C.m^{-1} and a pitch factor of 0.5.

The broken lines are not perfectly continuous. There is a gap of non etched graphite between the two lines. In the SEM image of Figure 4.13a, A 15 nm gap of non etched material or redeposited contaminant is visible. If the two lines are set so that there is an overlapping of the ending and starting line the gap reduces to 10 nm for a vertical gap (Figure 4.13b) and even 7 nm for a horizontal gap (Figure 4.13c). Overlap the etched lines reduces the gap but do not suppress it.

This sample has not been annealed, carbonaceous contaminants are probably on the surface. This is perhaps the phenomenon observed when two lines forming an angle of 45° are being etched by EBIE. Further improvement of the technique will probably need to reduce the contaminant amount by annealing the graphite.

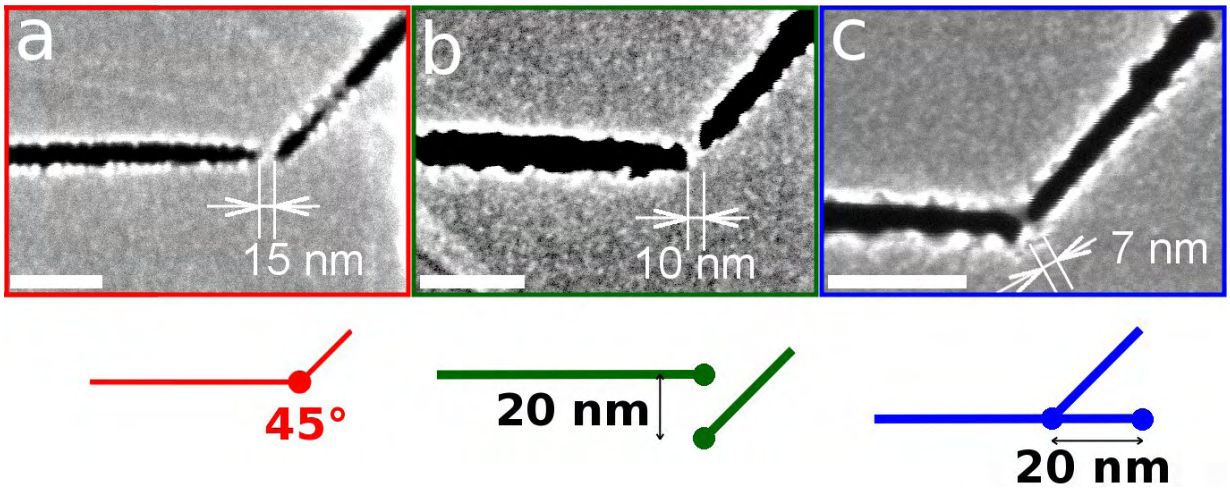

Figure 4.13. *SEM images of ribbon with funnels. (a), (b) and (c): SEM images of two connected EBIE trench. Schematics of the etching ordered on the EBIE software is shown bellow each images. Pitch factor and doses are 0.5 and 8.6×10^{-2} C.m^{-1}. Scale bars are 100 nm.*

4.2.8 Thickness of the FLG.

The samples used to study EBIE of graphene are multilayer this experiment compares cut performed on thick and thin FGL. Suspended graphene has been etched by EBIE. On two distinct areas, two series of cut have been produced. The first series was etched with electronic dose of $1.1x10^{-1}$ $C.m^{-1}$ and the second with $4.5x10^{-2}$ $C.m^{-1}$. The grids have not been annealed.

The first series of etching is shown in Figure 4.14a. Edges are very rough, the maximum edge roughness is 15 to 20 nm. The formation of white beads is also observed on the edges. This etching led to the formation of trenches that are not traversing all the FLG. The SEM image of the second series of etching, shown in Figure 4.14b have edges maximum roughness of 5 nm, very few beads are visible and their diameter is smaller than in the case of the first series. Etchings led to cut over all the thickness of the FLG.

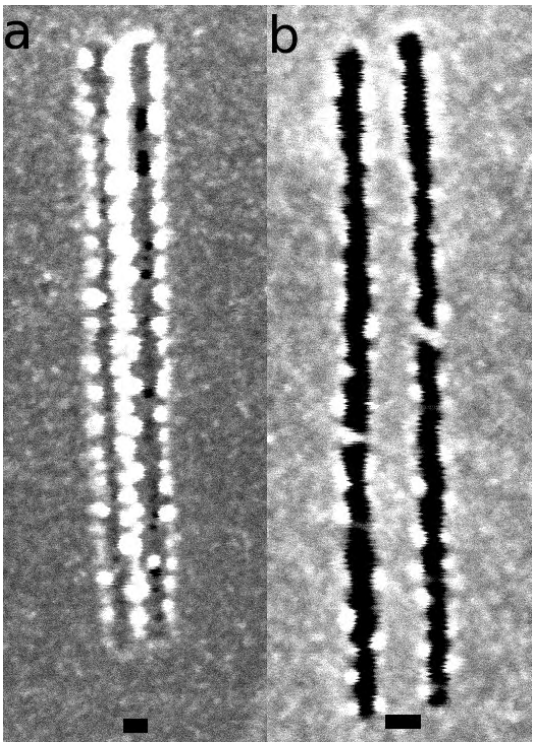

Figure 4.14. *EBIE etching on thick and thin FLG. EBIE cut in Figure (a) has been done on a thick FLG, the electronic dose was $1.1x10^{-1}$ $C.m^{-1}$. Figure (b) is an EBIE trench performed with a dose of $4.5x10^{-2}$ $C.m^{-1}$ on a thinner graphite than (a). Electron beam was 20 kV and water vapor was used. Scale bars are 20 nm.*

The first series of etching produced trenches while the second series produced cuts. However the electronic dose for the second series ($4.5x10^{-2}$ C.m^{-1}) is 2.5 times smaller than the one used for the first series ($1.1x10^{-1}$ C.m^{-1}). Since the amount of adsorbates is similar, this difference in the etching is attributed to a difference in the thickness of the FLG. The FLG used for the first series is probably much thicker than the one of the second series. Extra layers added to graphene monolayer quickly reduce the edge quality of the EBIE cut edges. A solution to this effect is to selectively use graphene grown on copper foil instead of Ni-grown graphene. Since such samples were not initially available, we have selected the thinnest possible areas of Ni-grown graphene transferred on grids. The two parallel cut performed in Figure 4.14 make a GNR with a 25 nm width over a 350 nm length.

4.2.9 Thin graphene ribbons.

In this paragraph the production of as thin as possible GNRs by etching two parallel cuts in graphene is discussed. Suspended graphene has been etched by EBIE in pairs of parallel lines. The distance separating the etched lines has been decreased: the separations are 50 nm, 30 nm and 20 nm, electronic doses were 4.5, 9 and 4.5 $x10^{-2}$ C.m^{-1} for the first, second and third pairs respectively. The fourth pair has been made on another grid with those parameters, separation of 40 nm and electronic dose of $1.2x10^{-2}$ C.m^{-1}.

Figures 4.15 shows SEM images of the pairs of etched lines that results in the formation on nanoribbons. The first GNR has a width of 25 nm and a length of 350 nm. The cuts are not fully continuous. The second pair produced a 15x450 nm GNR which stands alone only on the upper part of the image on a length of about 100 nm. The bottom part of the ribbon is stuck on the right border of graphene edge. The third pair did not produce any ribbon, only a large trench is visible. Finally the fourth pairs produced a 20x400 nm GNR.

If the nominal separation between two lines is too small (20 nm, third Figure 4.15c) the two etched line will merge in a unique and large cut. By increasing this nominal separation to 30 nm, a 15 nm wide ribbon is produced, (Figure 4.15b) it breaks and folds on an edge of the FLG film. A nominal separation of 50 nm produced a genuine ribbon with a width of

25 nm and a length of 350 nm. However this ribbon is still connected by nano-bridges to the rest of the graphene in few points. These bridges are possibly redeposition of amorphous carbon, originating from the EBIE product or the contamination of the grid. The fourth pair has been performed on another grid that was cleaner. A separation of 40 nm successfully produced a ribbon of 20 nm in width and 400 nm in length.

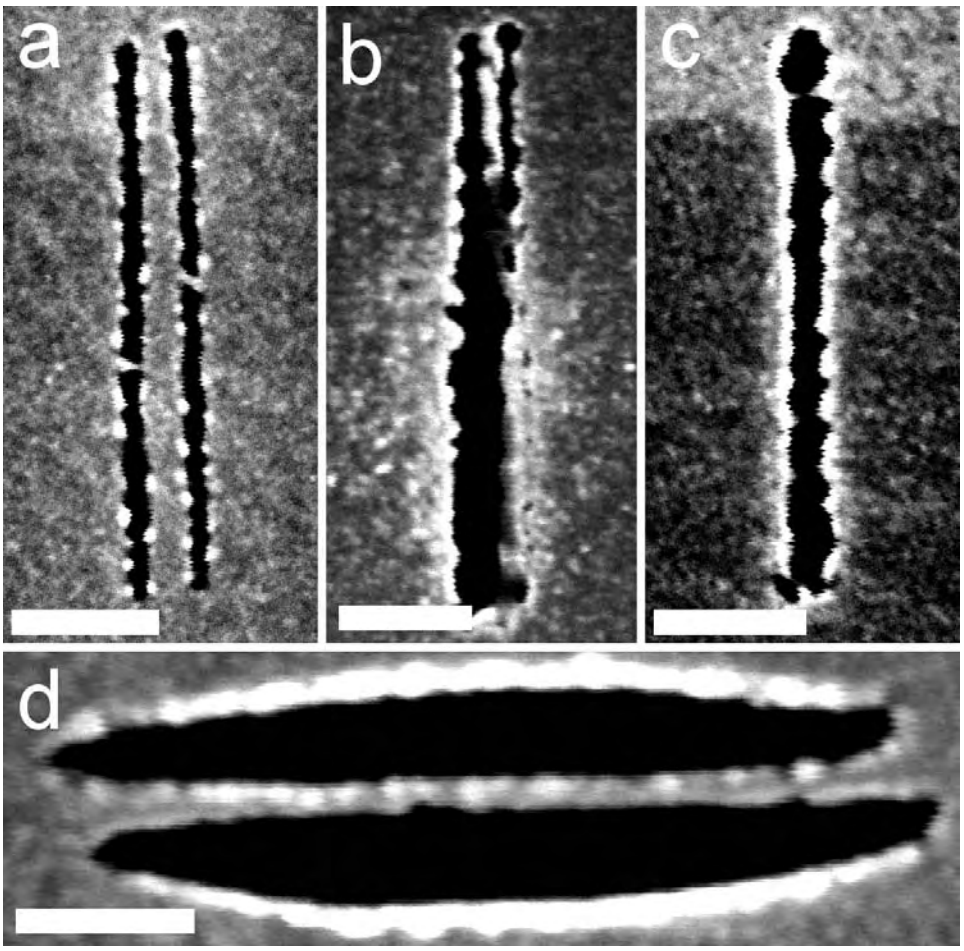

Figure 4.15. *SEM images of thin GNR produced by two parallel cut with a nominal separation of (a) 50 nm, (b) 30 nm (c) 20 nm and (d) 40 nm. The width and length of the GNRs are (a) 25x350 nm, (b) 15x110 nm and (d) 20x400 nm. The two cuts in (d) merged and produced a unique large cut. Electronic doses are (d): 1.2x10^{-2} C.m^{-1}, (a): 4.5x10^{-2} C.m^{-1}, (b): 9x10^{-2} C.m^{-1} and (c): 4.5x10^{-2} C.m^{-1}. Electron beam are 5 kV for (d) and 20kV for (a), (b) and (c). Pitch factors are 0.5. Scale bars are 100 nm.*

We have shown that EBIE can almost achieve the objectives of this work with a resolution of few nanometers on micrometer range. Further experiments will have to be done specially by improving the graphene source to a monolayer graphene grown by CVD on a cop-

per foil associated to a transfer as clean as possible. Such a sample could improves the resolution achieved by water assisted EBIE. Due to a too low resolution, the edge roughness cannot be studied by SEM. In the next section, SACTEM is used to characterize the edge roughness and crystallinity quality of graphene edge cut by water assisted EBIE.

4.3 Structural analysis of graphene cut by EBIE.

Unless further precisions, the following experiments are conducted on copper TEM grids covered with graphene grown on nickel by CVD. Irradiations are performed with electrons accelerated at 20 kV. Water vapor was injected near the irradiation by the gas injection system (GIS) of the SEM.

4.3.1 Roughness and structural analysis of EBIE cut graphene edges.

This paragraph characterizes the roughness of EBIE cut edges of graphene. A comparison with cut made in graphene by catalytic hydrogenation is discussed. Suspended graphene has been etched by EBIE in a SEM. The etching has been performed following a line with an electron dose of 2.5×10^{-1} C.m^{-1}. The sample has been then imaged in a SACTEM operating at 100 kV. The sample has not been annealed. The maximum edge roughness is defined as the distance between two parallels line in which the edge fits.

Figure 4.16a and b are SACTEM images of segments of EBIE cuts. The widths of the cuts are about 10 nm. The edges have a maximum roughness of 0.5 and 1.3 nm over a length of 10 and 35 nm for Figures 4.16a and b respectively. The RMS roughness is 0.4 nm over a length of 25 nm for Figure 4.16b.

The edge roughness found for the graphene edge cut by EBIE is similar to the roughness found by Schäffel et al.[24] For graphene edges cut by catalytic hydrogenation and CNT opening. [31] 0.5 to 1 nm over a length of 15 nm for CNT and 1 to 1.6 nm for maximum roughness and 0.25 nm for RMS roughness over a 24 nm long edge.

The roughness of edges produced by EBIE is very similar to the roughness of catalytic hydrogenation of graphite or intense sonication of CNT, which are actually the techniques giving the smoothest edges of patterned graphene. EBIE as major advantages as performing the etching with an arbitrary shape, no contamination of the surface with metallic particles and being compatible with suspended graphene monolayer.

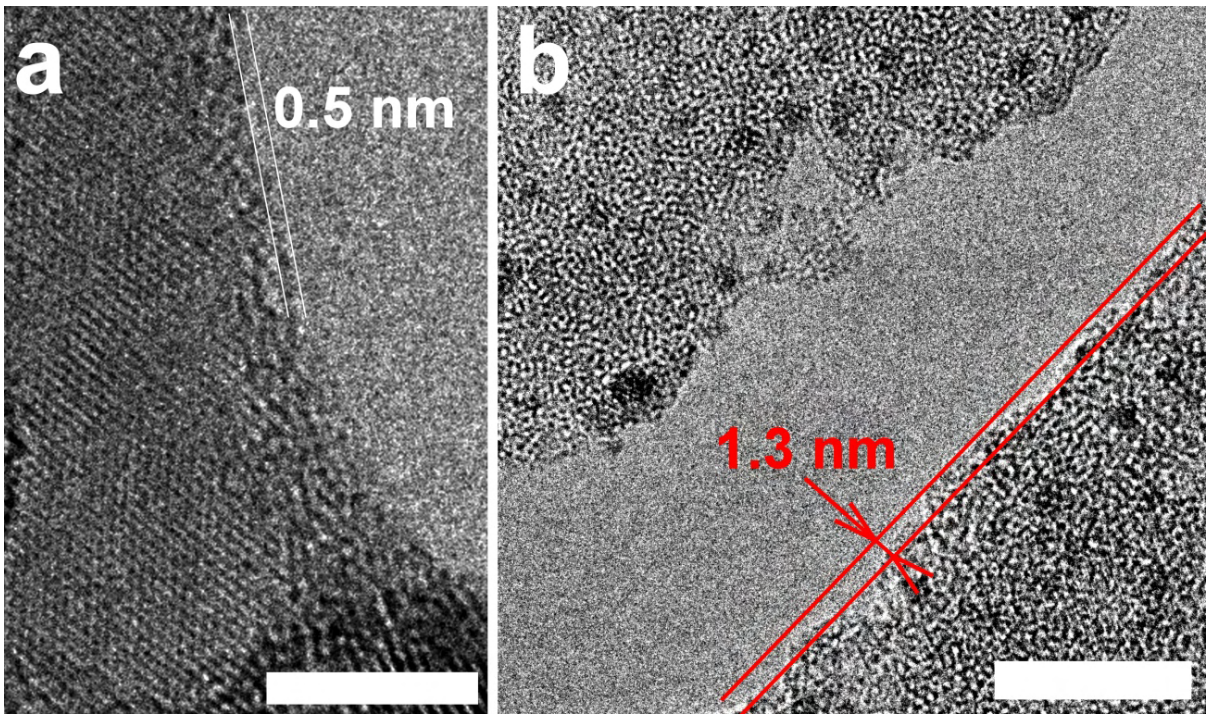

Figure 4.16. *Edge roughness. The maximum edge roughness defined as the distance between two parallel lines (red) in which fit the edge. TEM operated at 100 kV. Scale bars are 10 nm.*

4.3.2 Crystalline quality of EBIE cut graphene.

One additional parameter which can seriously decrease the electronic transport quality in graphene etched by EBIE is the lattice amorphization by the electron beam. In the following, some evidences of the lattice preservation near EBIE cuts are provided.

Suspended graphene has been etched by EBIE along a line with an electronic dose of 2.5×10^{-1} C.m^{-1}. The sample has not been annealed. The graphene close to a cut has been analyzed by electron diffraction. A SAED of an area including the cut (see Figure 4.17a) is shown in Figure 4.17b. As the sample has not been annealed, it is covered with amorphous

carbon, similarly to the samples of Figure 4.16. However, the crystallinity of the graphene is confirmed by the SAED which exhibits the two periodicity of the graphene lattice. The selected area contains the cut and a part of the edges, it is not an evidence that graphene is still crystalline on the edge of the EBIE cut but that there is crystalline graphene in an area of about 60 nm around the EBIE cut.

A FFT of an image of a cut is shown in Figure 4.17c. It clearly exhibits the 2.13 Å periodicity, this is another evidence that there is crystalline graphite around the EBIE cut. If one looks carefully at the Figure 4.16b, graphene lattice is even visible in the direct image, superposed with the amorphous contaminant. The graphene lattice is visible in an area very close to the cut, but amorphous contaminants make it difficult to precisely determine the distance over which amorphization occurred.

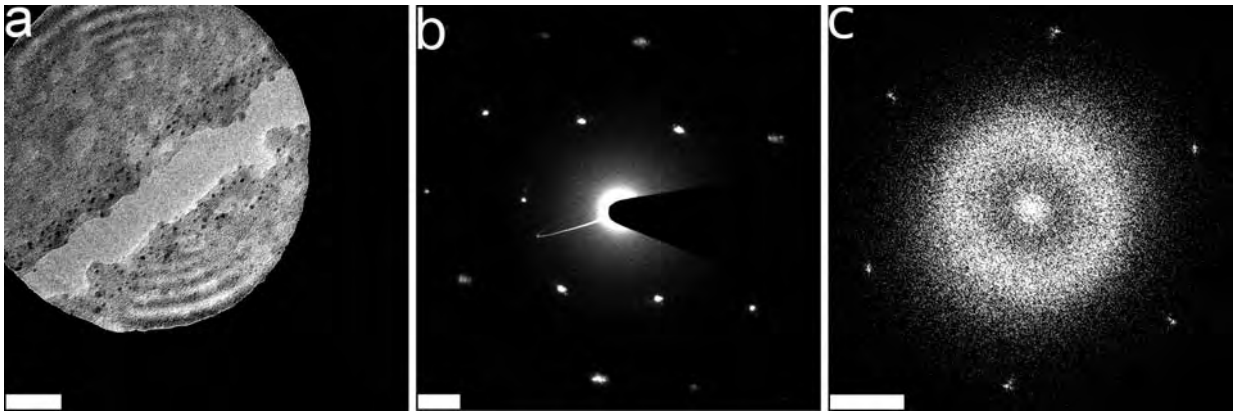

Figure 4.17. *Diffraction and FFT of areas close to an EBIE cut. (a) TEM images of an EBIE cut. the central disk is the selected area for the electron diffraction of (b). (b) SAED of the EBIE cut shown in (a). (c) FFT of an image of the cut shown in (a). Scale bars are (a) 20 nm, (b) and (c) 2 nm^{-1}.*

Suspended graphene has been etched by EBIE along a line with an electronic dose of $2.5x10^{-1}$ $C.m^{-1}$. The sample has not been annealed. The grid has been studied in a SACTEM, using the greatest condenser diaphragm and focusing the 100 kV TEM beam close to the EBIE cut, a hole has been made and enlarged under the e-beam.

In Figure 4.18a, the SACTEM image shows an EBIE cut (top right) and the surrounding graphene. In the direct image, mostly amorphous material is visible, but the FFT of the en-

tire image (Figure 4.18b) shows that the pattern of crystalline graphene is visible. Two domains are distinguishable. Figure 4.18c shows the hole made by focusing the TEM beam. It is quite isotropic in shape (circular). After enlarging this hole by imaging it with a spread TEM beam, its shape become anisotropic. The hole is visible at the bottom left of the EBIE cut in the main image (Figure 4.18a). Long straight edges are visible, making several relative angles of 120° and 30° (Figure 4.18d).

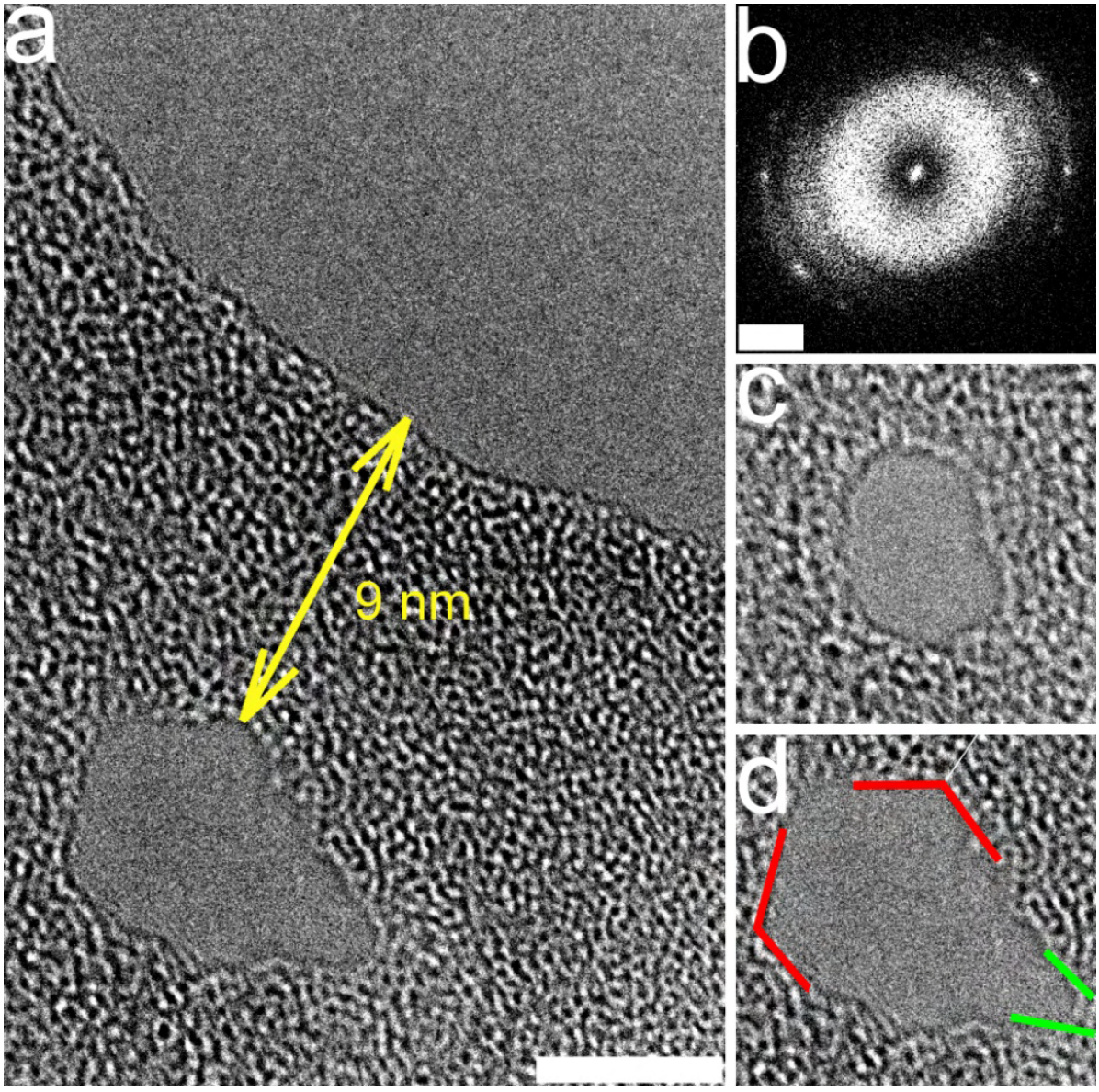

Figure 4.18. *(a) is a SACTEM image of an EBIE cut. The EBIE cut is in the upper right corner of the image. A hole created near the EBIE cut by focusing the TEM beam and enlarged with a spread beam is visible at about 9 nm from the EBIE cut. (b) FFT of the image (a). (c) hole before it enlargement. (d) hole after enlargement 120° (red) and 30° (green) edges are shown. Scale bar are (a), (c) and (d) 5 nm; (b) 2 nm^{-1}.*

Angles of 120° and 30° visible on the enlarged hole are typical of a graphene lattice. 120° can separates two zig-zag or armchair edges while 30° angle can be a change from zig-zag to armchair or the contrary. The shape is very similar to the hole obtained by the group of Zettl. [17] This resemblance may be interpreted as graphene is crystalline under an amorphous layer of carbonaceous covering it. The closest edge from the EBIE cut is at a distance of 9 nm, this is the maximum amorphization distance that can be deduced from this experiment. Again, the amorphization distance can be less than 9 nm but the hole could not have been created closer to the trench. The graphene sample was not annealed and its surface was covered with an amorphous carbonaceous material. In the following experiment an annealing has been performed on graphene.

Suspended graphene has been etched by water assisted EBIE, the electronic dose was $2x10^{-2}$ $C{\cdot}m^{-1}$ and the pitch factor R=0.05. After the cut, the sample has been annealed 2h in air at 200°C followed by 2h at 250°C in Ar and H_2 flux of 300 and 75 $cm^3.min^{-1}$ respectively. The sample has been then introduced in a SACTEM, the EBIE cut and its edges have been imaged.

The trench is 100 nm long and 15 nm in width. In the SACTEM image of Figure 4.19 graphene lattice is clearly visible in the direct image, this crystalline area is separated from the EBIE trench by a 1.5 nm band which appears amorphous in the direct SACTEM image. This 1.5 nm band can be contamination of the very reactive edges or amorphization due to the EBIE process. From this data we conclude that the EBIE process does not amorphize the graphene edges or that the amorphization length is less than 1.5 nm.

Therefore EBIE can produce GNR with smooth edges at small scale and very limited if any amorphization of the graphene lattice. However long range EBIE cuts have a different behavior.

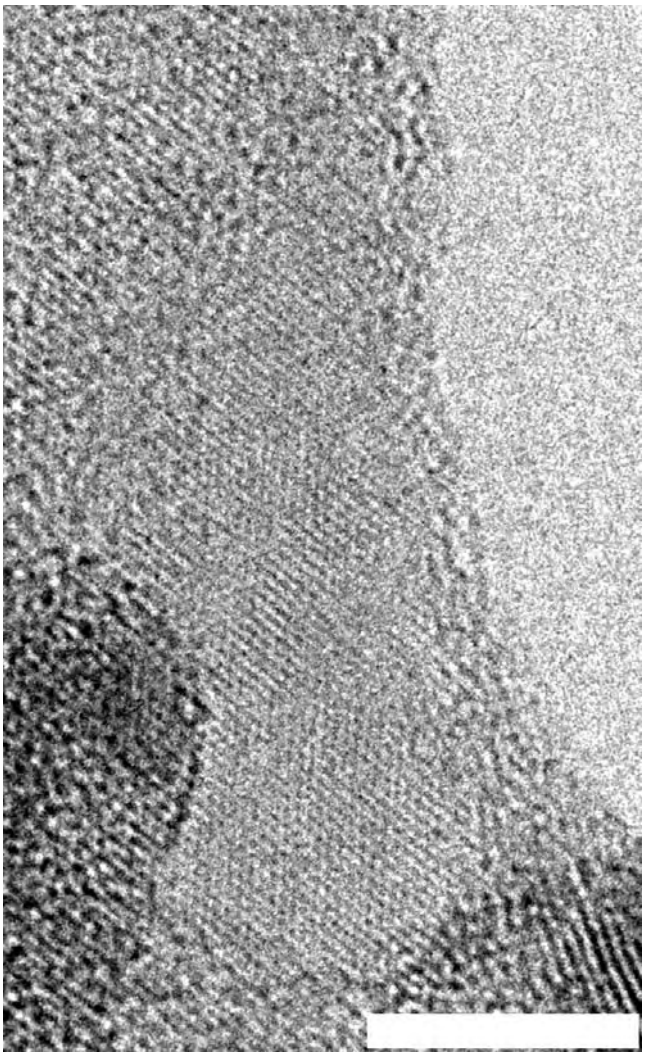

Figure 4.19. *SACTEM image of a graphene edge cut by EBIE. The EBIE cut is visible on the top right of the image. Scale bar is 5 nm.*

4.3.3 EBIE Edge roughness at long range.

The previous paragraphs examine the local edge fluctuations and structural quality. However devices performances will also depend on the mesoscale quality of the GNR.

Figure 4.20a has been reconstructed from several SACTEM images of a single EBIE cut. The cut is 230 nm long and its width varies from 10 to 20 nm. Along the total length of the cut, the maximum roughness is 6 nm for the left edge and 8 nm for the right edge. The RMS roughnesses are 1.3 and 2.0 nm for the left and right edges respectively. 4 or 5 larges protuberances are visible along the cut edges, we attribute these protuberances to redeposition of

carbonaceous material, [30] they result in increasing the roughness. This EBID process could decorate the intrinsic EBIE edges with carbonaceous material and dramatically increase edges roughness. In the center of the cut, two protuberances are almost joint. Before imaging the trench, these two protuberances were bridging across the cut but were cut by the 100 keV electron beam while the graphene edges were not enlarged using the same electronic dose conditions.

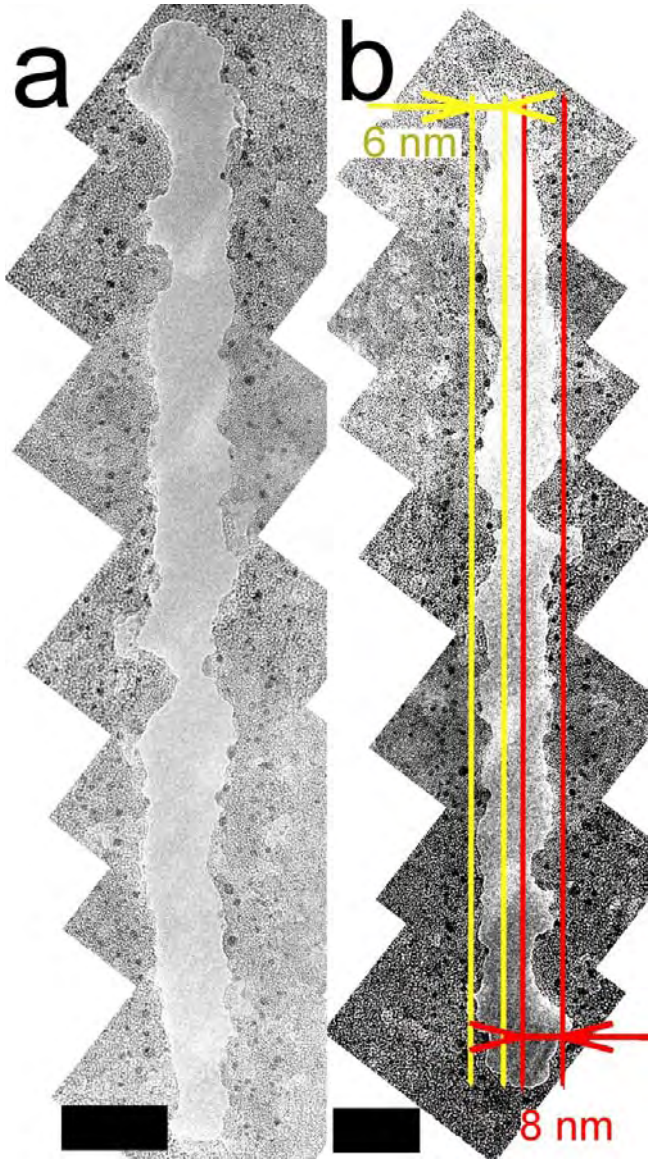

Figure 4.20. *Roughness analysis. (a) Reconstructed SACTEM image of a long EBIE cut. (b) Is the reproduction of (a), two couples of parallel lines were added to highlight the left (yellow lines) and right (red lines) edges roughness. TEM operated at 100 kV. Scale bars are 20 nm.*

If the EBID process is increasing the edges roughness, it has to be limited. In order to achieve the targeted maximum roughness of less than 1 nm, a solution to avoid EBID is to limit carbonaceous sources, this is the object of the next paragraph.

4.3.4 Cleaning of graphene.

In order to assess the effect of absorption of ambient hydrocarbon on graphene, a FLG grown by CVD on a nickel substrate has been transferred on a copper TEM grid by a resist-free technique, [25] it has been stored in ambient conditions for several weeks. The sample has been then annealed in forming gas (Ar/H_2 300/75 $cm^3.min^{-1}$) at 400°C during 4h. SACTEM images have been taken before and after annealing.

Figure 4.21a shows a SACTEM micrograph taken before annealing. The direct image shows only an amorphous organization on the surface. Barely visible spots referring to the graphene lattice are visible in the FFT. After an annealing in forming gas, a second SACTEM image has been taken and is shown in Figure 4.21b. The graphene lattice is now clearly visible in the direct image and the FFT shows four sets of 6 spots attributed to four graphene domains within the image frame.

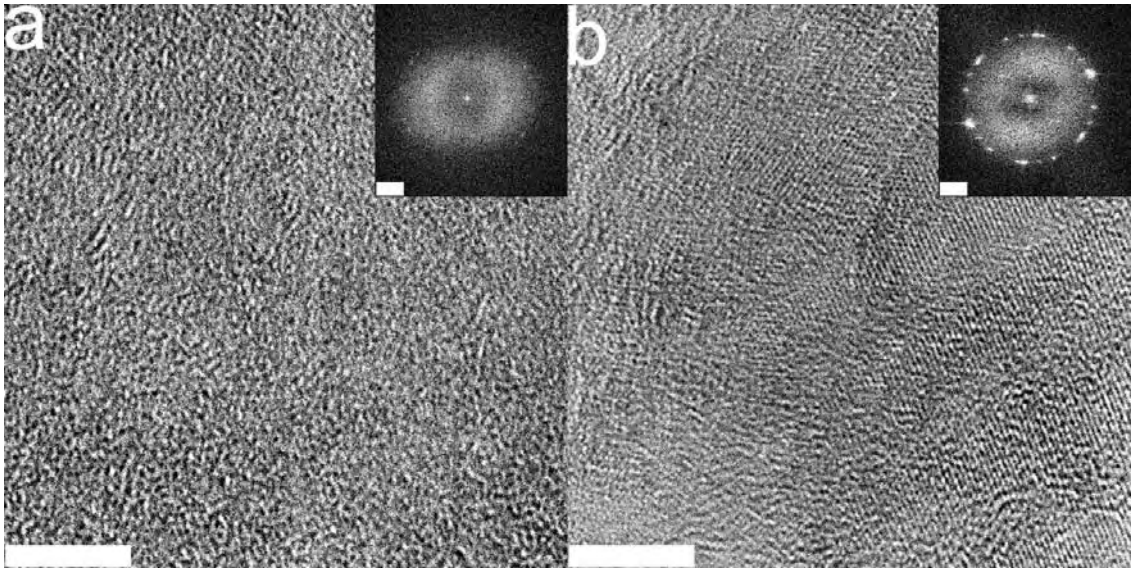

Figure 4.21. *SACTEM images of a FLG on a copper TEM grid. Inset: FFT of the entire image. The graphene surface is imaged as received in (a) or after an annealing in forming gas (Ar/H_2 300/75 $cm^3.min^{-1}$) at 400°C during 4h in (b). Scale bars: 5 nm for mains images and 2 nm^{-1} for insets.*

The annealing process clearly removes adsorbates from the graphene surface. Although formal identification was not possible, we associated them to a contamination from air hydrocarbons that can be removed by an annealing in forming gas. A grid stored in ambient air is recontaminated within a few hours. Storage of a grid under dry N_2 atmosphere limits contamination for a few days at least.

Two samples were used for the following experiments. The first sample was a TEM copper grid covered with a FLG grown by CVD on a nickel surface. The second sample was a TEM gold grid Quantifoil covered with a monolayer graphene grown by CVD on a copper foil and directly transferred by the technique described in paragraph 4.1.3.

Although annealing is effective to remove contaminants, extended treatment leads to a massive diffusion of metallic particles (Figures 4.10). The copper support is probably the origin of particles contamination. The first sample has been annealed in forming gas (Ar/H_2 300/75 $cm^3.min^{-1}$) at 300°C during 3h. Figure 4.22a shows a SACTEM image of the sample one. On the FLG, copper nanoparticles are visible with various diameters, 1 to 20 nm. The edges of an EBIE trench in the middle of the image are almost invisible, hidden by the nanoparticles. When using a copper TEM grid, particles diffuse readily during the annealing in forming gas. These particles, the density of which is quite high, are disturbing for the entire process of etching and producing GNRs.

The second sample has been annealed in forming gas (Ar/H_2 300/75 $cm^3.min^{-1}$) at 300°C during 3h. Figure 4.22b is a SACTEM image of the sample on a gold quantifoil grid. Almost no nanoparticles are visible and their diameter is below 5 nm. An EBIE cut visible in the bottom right of the image shows a very good edge roughness, 1.1 nm over a 22 nm length. A gold quantifoil grid avoids massive diffusion of nanoparticles. The sample two, avoided different contaminations which has been identified. The contamination from air atmosphere is cleaned by an annealing in forming gas and a storage in N_2 atmosphere. No particles diffused on the sample because the grid was not made of copper. The contamination due to volatile carbonaceous compound released by the EBIE process and the contamination due to

the injected water vapor were removed by a second annealing treatment. The result is that the edge roughness found is small. These samples will have to be investigated to set the intrinsic potential of EBIE.

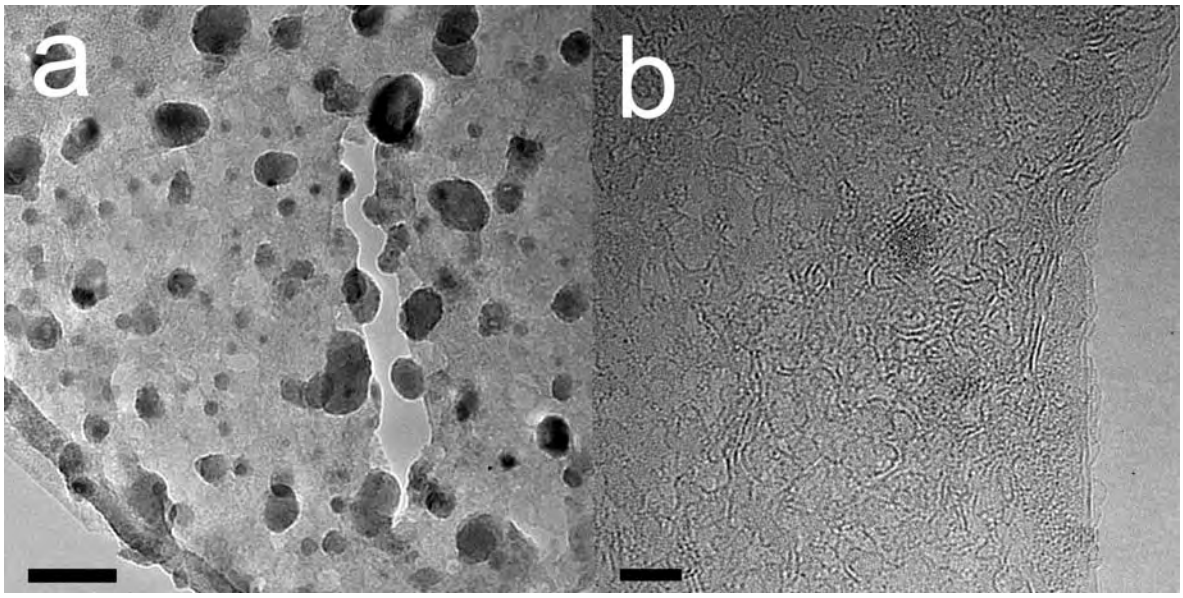

Figure 4.22. Metallic particles on annealed graphene. (a) is a TEM image of a graphene grown by CVD on a nickel surface transferred on a copper TEM grid. (b) is a TEM image of a graphene grown by CVD on a copper surface transferred on a gold TEM grid. The samples have been annealed in forming gas at 300°C for 2 h. Scale bars: (a) 30 nm, (b) 4 nm.

Transfer on gold and Si_3N_4 membranes is currently under investigation that grid sustain high temperature, as it is the case for graphene in inert atmosphere, a more efficient annealing in higher (~700°C) temperature will be explored.

4.4 Conclusion.

L'analyse structurale du graphene découpé par EBIE a révélé une très faible amorphisation et une rugosité des bords sur une petite distance de moins de 1 nm. Le recuit du graphene est essentiel pour le nettoyage de sa surface contaminée par des adsorbats, cette

The structural analysis of graphene etched by EBIE revealed a very limited amorphisation and an edge roughness at small scale around 1 nm. Annealing of graphene is essential for cleaning it from adsorbates, but it is also a well known technique for smoothing

technique est également utilisée pour redresser des bords rugueux. [32-34] Les grilles MET utilisées pour cette étude n'ont pas permis de recuit trop important à cause de la diffusion de particules de cuivre. Cependant, du graphène CVD transféré sur des grilles MET Si_3N_4 ou des quantifoils en or permettront un recuit plus poussé de monocouches de graphène.

edges even at the atomic scale. [32-34] The TEM grid on which this study has been led does not allow intensive annealing because of copper diffusing. However CVD graphene transferred from Copper foil to Si_3N_4 membrane or gold quantifoil TEM grid will allow a further study of annealing of the sample and provide monolayer graphene.

4.5 References

[1] Novoselov, K. S.; Geim, A. K.; Morozov, S. V.; Jiang, D.; Zhang, Y.; Dubonos, S. V.; Grigorieva, I. V.; Firsov, A. A. "**Electric field effect in atomically thin carbon films**". *Science* (**2004**) *Vol. 306*, p. 666-669.

[2] Chen, Z. H.; Lin, Y. M.; Rooks, M. J.; Avouris, P. "**Graphene nano-ribbon electronics**". *Physica E* (**2007**) *Vol. 40*, p. 228-232.

[3] Han, M. Y.; Ozyilmaz, B.; Zhang, Y. B.; Kim, P. "**Energy band-gap engineering of graphene nanoribbons**". *Phys. Rev. Lett.* (**2007**) *Vol. 98*, p. 4.

[4] Ishigami, M.; Chen, J. H.; Cullen, W. G.; Fuhrer, M. S.; Williams, E. D. "**Atomic Structure of Graphene on SiO2**". *Nano Lett.* (**2007**) *Vol. 7*, p. 1643-1648.

[5] Moser, J.; Barreiro, A.; Bachtold, A. "**Current-induced cleaning of graphene**". *Appl. Phys. Lett.* (**2007**) *Vol. 91*, p. 3.

[6] Lin, Y. C.; Lu, C. C.; Yeh, C. H.; Jin, C. H.; Suenaga, K.; Chiu, P. W. "**Graphene Annealing: How Clean Can It Be?**". *Nano Lett.* (**2012**) *Vol. 12*, p. 414-419.

[7] Sols, F.; Guinea, F.; Neto, A. H. C. "**Coulomb blockade in graphene nanoribbons**". *Phys. Rev. Lett.* (**2007**) *Vol. 99*, p. 4.

[8] Han, M. Y.; Brant, J. C.; Kim, P. "**Electron Transport in Disordered Graphene Nanoribbons**". *Phys. Rev. Lett.* (**2010**) *Vol. 104*, p. 4.

[9] Dujardin, E.; Thio, T.; Lezec, H.; Ebbesen, T. W. "**Fabrication of mesoscopic devices from graphite microdisks**". *Appl. Phys. Lett.* (**2001**) *Vol. 79*, p. 2474-2476.

[10] Dayen, J. F.; Mahmood, A.; Golubev, D. S.; Roch-Jeune, I.; Salles, P.; Dujardin, E. "**Side-gated transport in focused-ion-beam-fabricated multilayered graphene nanoribbons**". *Small* (**2008**) *Vol. 4*, p. 716-720.

[11] Lemme, M. C.; Bell, D. C.; Williams, J. R.; Stern, L. A.; Baugher, B. W. H.; Jarillo-Herrero, P.; Marcus, C. M. "**Etching of Graphene Devices with a Helium Ion Beam**". *ACS Nano* (**2009**) *Vol. 3*, p. 2674-2676.

[12] Albrecht, T. R.; Dovek, M. M.; Kirk, M. D.; Lang, C. A.; Quate, C. F.; Smith, D. P. E. "**Nanometer-scale hole formation on graphite using a scanning tunneling microscope**". *Appl. Phys. Lett.* (**1989**) *Vol. 55*, p. 1727-1729.

[13] Tapaszto, L.; Dobrik, G.; Lambin, P.; Biro, L. P. "**Tailoring the atomic structure of graphene nanoribbons by scanning tunnelling microscope lithography**". *Nat. Nanotechnol.* (**2008**) *Vol. 3*, p. 397-401.

[14] Weng, L. S.; Zhang, L. Y.; Chen, Y. P.; Rokhinson, L. P. "**Atomic force microscope local oxidation nanolithography of graphene**". *Appl. Phys. Lett.* (**2008**) *Vol. 93*, p. 3.

[15] Kondo, S.; Lutwyche, M.; Wada, Y. "**Nanofabrication of layered materials with the scanning tunneling microscope**". *Applied Surface Science* (**1994**) *Vol. 75*, p. 39-44.

[16] McCarley, R. L.; Hendricks, S. A.; Bard, A. J. "**Controlled nanofabrication of highly orientated pyrolitic-graphite with the scanning tunneling microscope**". *J. Phys. Chem.* (**1992**) *Vol. 96*, p. 10089-10092.

[17] Girit, C. O.; Meyer, J. C.; Erni, R.; Rossell, M. D.; Kisielowski, C.; Yang, L.; Park, C. H.; Crommie, M. F.; Cohen, M. L.; Louie, S. G.; Zettl, A. "**Graphene at the Edge: Stability and Dynamics**". *Science* (**2009**) *Vol. 323*, p. 1705-1708.

[18] Song, B.; Schneider, G. F.; Xu, Q.; Pandraud, G.; Dekker, C.; Zandbergen, H. "**Atomic-Scale Electron-Beam Sculpting of Near-Defect-Free Graphene Nanostructures**". *Nano Lett.* (**2011**) *Vol. 11*, p. 2247-2250.

[19] Li, X. L.; Wang, X. R.; Zhang, L.; Lee, S. W.; Dai, H. J. "**Chemically derived, ultrasmooth graphene nanoribbon semiconductors**". *Science* (**2008**) *Vol. 319*, p. 1229-1232.

[20] Kawai, T.; Okada, S.; Miyamoto, Y.; Hiura, H. "**Self-redirection of tearing edges in graphene: Tight-binding molecular dynamics simulations**". *Physical Review B* (**2009**) *Vol. 80*, p. 033401.

[21] Poumirol, J.-M.; Cresti, A.; Roche, S.; Escoffier, W.; Goiran, M.; Wang, X.; Li, X.; Dai, H.; Raquet, B. "**Edge magnetotransport fingerprints in disordered graphene nanoribbons**". *Physical Review B* (**2010**) *Vol. 82*, p. 041413.

[22] Tomita, A.; Tamai, Y. "**Optical microscopic study on catalytic-hydrogenation of graphite**". *J. Phys. Chem.* (**1974**) *Vol. 78*, p. 2254-2258.

[23] Ci, L.; Xu, Z. P.; Wang, L. L.; Gao, W.; Ding, F.; Kelly, K. F.; Yakobson, B. I.; Ajayan, P. M. "**Controlled Nanocutting of Graphene**". *Nano Res.* (**2008**) *Vol. 1*, p. 116-122.

[24] Schaffel, F.; Wilson, M.; Bachmatiuk, A.; Rummeli, M. H.; Queitsch, U.; Rellinghaus, B.; Briggs, G. A. D.; Warner, J. H. "**Atomic Resolution Imaging of the Edges of Catalytically Etched Suspended Few-Layer Graphene**". *ACS Nano* (**2011**) *Vol. 5*, p. 1975-1983.

[25] Regan, W.; Alem, N.; Aleman, B.; Geng, B. S.; Girit, C.; Maserati, L.; Wang, F.; Crommie, M.; Zettl, A. "**A direct transfer of layer-area graphene**". *Appl. Phys. Lett.* (**2010**) *Vol. 96*, p. 3.

[26] Meyer, J. C.; Geim, A. K.; Katsnelson, M. I.; Novoselov, K. S.; Obergfell, D.; Roth, S.; Girit, C.; Zettl, A. "**On the roughness of single- and bi-layer graphene membranes**". *Solid State Commun.* (**2007**) *Vol. 143*, p. 101-109.

[27] Utke, I.; Hoffmann, P.; Melngailis, J. "**Gas-assisted focused electron beam and ion beam processing and fabrication**". *J. Vac. Sci. Technol. B* (**2008**) *Vol. 26*, p. 1197-1276.

[28] Banhart, F. "**Irradiation effects in carbon nanostructures**". *Rep. Prog. Phys.* (**1999**) *Vol. 62*, p. 1181-1221.

[29] Egerton, R. F.; Li, P.; Malac, M. "**Radiation damage in the TEM and SEM**". *Micron* (**2004**) *Vol. 35*, p. 399-409.

[30] Meyer, J. C.; Girit, C. O.; Crommie, M. F.; Zettl, A. "**Hydrocarbon lithography on graphene membranes**". *Appl. Phys. Lett.* (**2008**) *Vol. 92*, p. 3.

[31] Xie, L. M.; Wang, H. L.; Jin, C. H.; Wang, X. R.; Jiao, L. Y.; Suenaga, K.; Dai, H. J. "**Graphene Nanoribbons from Unzipped Carbon Nanotubes: Atomic Structures, Raman Spectroscopy, and Electrical Properties**". *Journal of the American Chemical Society* (**2011**) *Vol. 133*, p. 10394-10397.

[32] Jia, X. T.; Hofmann, M.; Meunier, V.; Sumpter, B. G.; Campos-Delgado, J.; Romo-Herrera, J. M.; Son, H. B.; Hsieh, Y. P.; Reina, A.; Kong, J.; Terrones, M.; Dresselhaus, M. S. "**Controlled Formation of Sharp Zigzag and Armchair Edges in Graphitic Nanoribbons**". *Science* (**2009**) *Vol. 323*, p. 1701-1705.

[33] Yang, R.; Zhang, L. C.; Wang, Y.; Shi, Z. W.; Shi, D. X.; Gao, H. J.; Wang, E. G.; Zhang, G. Y. "**An Anisotropic Etching Effect in the Graphene Basal Plane**". *Adv. Mater. 22*, p. 4014-4019.

[34] Nemes-Incze, P.; Magda, G.; Kamaras, K.; Biro, L. P. "**Crystallographically selective nanopatterning of graphene on SiO(2)**". *Nano Res.* (**2010**) *Vol. 3*, p. 110-116.

CHAPTER 5

EBIE patterning of graphene nanoribbons for electronic transport measurements.

Dans ce chapitre nous allons appliquer la technique EBIE de fabrication de nanorubans développée et caractérisée au chapitre 4 dans le cas très spécifique du graphene déposé sur Si/SiO_2 et contacté électriquement en vue de mesures de transport électronique.

Pour effectuer la caractérisation électronique des rubans de graphène, une configuration en transistor à effet de champ avec grille arrière permet de modifier la densité des porteurs de charge dans le graphène et donc de sonder son spectre énergétique tout en laissant le graphène disponible pour sa caractérisation ð Z copie en sa structuration en GNR par EBIE. Cette

In this chapter we will apply the EBIE technique for manufacturing nano-ribbons, developed and characterized in Chapter 4, in the very specific case of graphene devices deposited on Si/SiO_2 and electrically contacted for electronic transport measurements.

In order to perform the characterization of the electronic properties of graphene, a configuration of field effect transistor with a back-gate can be designed to tune the density of the charge carriers and thus probe the energy spectrum while leaving the graphene available for its characterization in Raman spectroscopy, near-field microscopy and its patterning in the shape of GNR by EBIE. This back-gate is con-

grille arrière, est constituée par le silicium [100] fortement dopé du substrat et couvert d'une couche diélectrique de 285 nm de silice thermique. Le graphène est déposé par exfoliation micromécanique [1, 2] qui produit le graphène de meilleure qualité pour l'électronique à ce jour. [3, 4] Le graphène est contacté par des électrodes macroscopiques puis mis en forme de nanorubans par EBIE (Figure 5.1).

La première section présente les substrats et les techniques de contact électrique du graphène. La lithographie électronique utilisant du PMMA a été utilisée car elle présente l'avantage d'être simple à mettre en œuvre. Cependant elle implique de couvrir le graphène d'une résine qui contamine durablement le graphène. [5, 6] Une technique alternative a été développée pour contacter le graphène sans contamination: le stencil qui consiste à placer un pochoir de la forme des électrodes sur le graphène et à évaporer un métal à travers.

La deuxième section présente la gravure par EBIE de graphène déposé sur un substrat Si/SiO_2. Les paramètres étudiés au chapitre 4 sont repris dans la situation du graphène supporté sur silice. Toutefois, l'examen de la qua-

stituted by the heavily doped Si[100] substrate, covered with a dielectric layer of 285 nm of thermally grown silica. Graphene is deposited by micro exfoliation, [1, 2] which produces the best graphene quality for electronics until now. [3, 4] The graphene is contacted by macroscopic electrodes and is then patterned into connecting constrictions and a nano-ribbon shape by EBIE (Figure 5.1).

The first section of the Chapter presents the substrates and the techniques used for contacting electrically the graphene. Electron beam lithography using PMMA was used because it has the advantage of being simple to implement. However, it implies covering the graphene with a resist that irreversibly contaminates graphene. [5, 6] A technique has been developed contacting the graphene without contamination: the stencil, which consists in aligning a shadow mask with the shape of the electrodes over the graphene and to evaporate a metal directly through it.

The second section presents the etching of graphene supported on a Si/SiO_2 substrate by EBIE. The parameters studied in Chapter 4 are adapted to the situation of graphene supported on silica. However, considering the quality of

lité de la gravure nous imposera de modifier la configuration des composants de graphène.

the etching, the configuration of the device had to be changed.

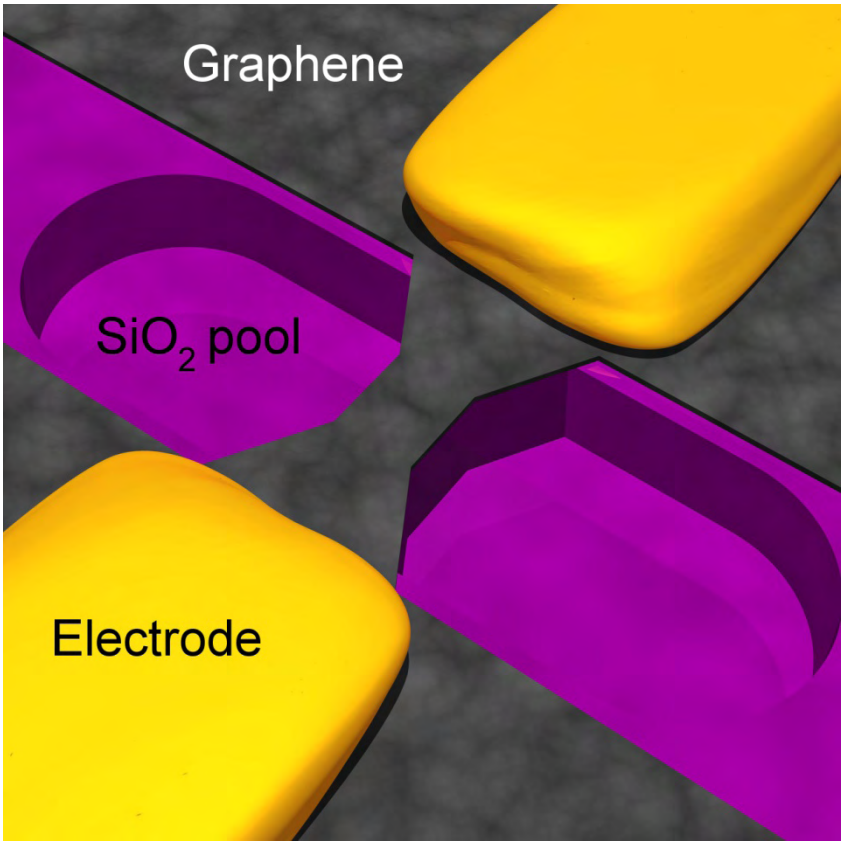

Figure 5.1. Schéma représentant du graphène déposé sur un substrat Si/SiO_2 contacté par des électrodes et gravé en forme de nanoruban par EBIE.

Figure 5.1. *Schematic representation of graphene deposited on a Si/SiO_2 substrate contacted by electrodes and patterned in the shape of nano-ribbon.*

Dans la troisième section, la modification apportée au substrat pour suspendre localement le graphène est exposée. Des réseaux de trous sont creusés dans la silice avant de déposer le graphène pour localement le suspendre, comme montré sur le schéma de la Figure 5.1. La gravure EBIE est alors effectuée sur le graphène localement

In the third section, the change in the substrate in order to locally suspend graphene is explained. Arrays of trenches are etched in the silica before depositing graphene to locally suspend it, as schematized in Figure 5.1. EBIE etching is then performed to cut the locally suspended graphene. The graphene cuts show two morphological differences compared to those obtained in

suspendu mais les tranchées obtenues présentent deux différences morphologiques par rapport à celles obtenues dans le chapitre 4. Ces tranchées sont beaucoup plus larges et au delà d'une dose électronique limite, la gravure du graphène est totalement inefficace. L'origine de ces deux phénomènes est décrite et des mesures pour retrouver des gravures morphologiquement similaires à celles obtenu dans le chapitre 4 sont exposées. Finalement des conditions sont rassemblées qui permettent de former des rubans similaires à ceux obtenus sur grille TEM (30x200 nm) mais localement suspendu. Finalement, le chapitre se conclue avec la démonstration de l'intégration complète de ces différentes techniques et présente un ruban de graphène localement suspendu, isolé du reste du graphène et contacté par des électrodes métalliques.

Chapter 4. The cuts are much broader and, beyond a certain electronic dose, etching of graphene is totally ineffective. The origins of these two phenomena are described and the technique is adapted to etch again cuts with a morphology similar to those obtained in Chapter 4. Finally the conditions are found to pattern ribbons similar to those obtained on TEM grid (30x200 nm for example) but for graphene locally suspended on a back-gated substrate. Finally, the chapter concludes with a demonstration of the full integration of these different techniques and steps and provides a locally suspended graphene ribbon device, isolated from the graphene and contacted by metallic electrodes.

5.1 Sample preparation.

5.1.1 Graphene deposition, substrate.

The technique used to deposit graphene is the mechanical exfoliation of graphite. [1, 2] Although very empirical and limited to small graphene samples, this graphene production technique still provides the best graphene quality for electronic transport. [3, 7]

Beyond the identification of graphene samples, this configuration of graphene supported on a dielectric layer on top of the degenerated silicon surface is well-suited for elec-

tronic transport measurement. Indeed the conductive substrate can be used as a back-gate electrode on which an applied voltage with respect to one of the graphene contact results in the controllable doping of graphene with electrons or holes carriers. However, such thick substrates are not suitable for TEM investigations performed in chapter 4. In the following we will therefore revisit the EBIE fabrication protocol and use SEM to assess of the results on supported graphene match the observation on suspended graphene.

5.1.2 Electrical contact made by EBL.

Graphene is contacted by electron beam lithography combined with metal evaporation. The substrates used during this work were fabricated by A. Miranda and M. Rubio-Roy. Briefly, a PMMA layer is spin coated on the sample and the exposure to a rastered electron beam allows to define the electrode pattern to be metalized. Metallization is performed by thermal evaporation or e-beam sputtering. The metalized PMMA is lifted off in acetone. An example of FLG contacted with two metallic contacts is shown in Figure 5.2.

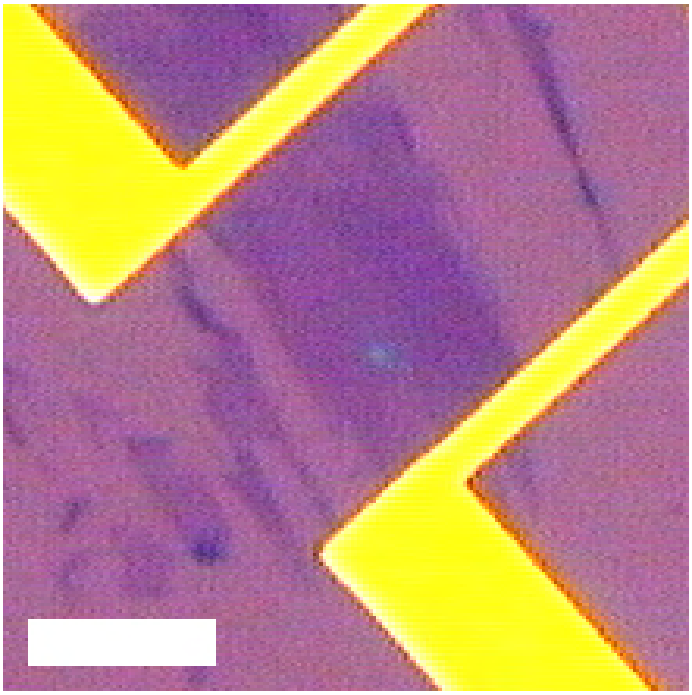

Figure 5.2. *Optical image of a FLG deposited on a Si/SiO_2 substrate and Contacted with Ti/Pd (5/50 nm). Scale bar: 10 µm.*

However it has already been shown in chapter 4 that PMMA contaminates graphene. [5, 6] This technique is applied for contacting sample because it results in samples of high enough quality for mesoscale transport measurements. However, anticipating adsorbate–related limitation of EBIE, another technique has been investigated and is discussed in the next paragraph.

5.1.3 Electrical contact made by Stencil.

Stenciling [8, 9] is a resist less, UHV compatible surface patterning method in which a Si_3N_4 membrane is patterned with an apertured motif through which metal, for example, can be directly evaporated. [10] The stencil shadow mask is placed on the substrate, aligned with the graphene sample and metal vaporized through the stencil, transfer the pattern such as electrodes onto the substrate (Figure 5.3a).Depending on the pattern feature size, stencil is fabricated by optical or e-beam lithography or by direct etching, with a xenon difluoride assisted FIB. The membranes used in this work were fabricated by C. Soldano using the FIB fabrication method.

The first step consist in aligning the stencil membrane with the graphene flake (Figure 5.3a). Since our supported graphene flakes are only a few micrometers in size, we have developed a dedicated alignment tool (Figure 5.3b). It consists in a video microscope combined with a dual motorized stage. The substrate with graphene rests on the bottom stage that can be aligned in X and Y directions with the microscope optical axis. The membrane is mounted on an apertured disk and manipulated with the top stage that has 6 degrees of freedom: X,Y and Z translations, parallel rotation and out of plane rotation that ensures the parallelism of the membrane and the substrate surfaces.

The graphene flake is brought on the focus plane. The stencil is brought in the field of view of the microscope and moved down closer to the substrate. Electrode motif is positioned at the desired location on the graphene flake, as shown in Figure 5.3b. The membrane is lowered towards the substrate (**z** axis) until contact is reached. Finally the membrane is fixed to the substrate with bees' wax, which solidifies very fast without noticeable shearing

during cooling induced. The complete membrane/substrate block is introduced in the metallization bench to produce electrodes. The stencil is then simply detached.

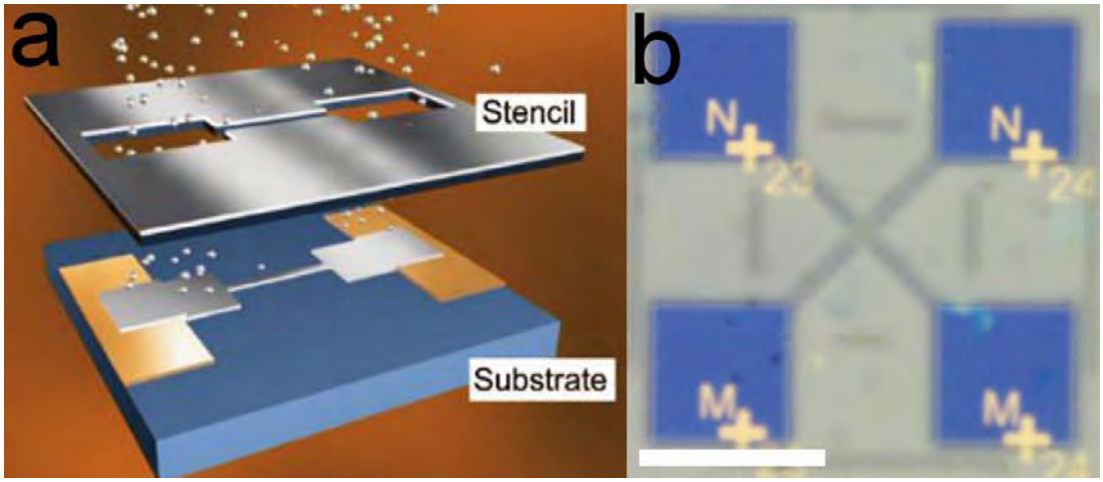

Figure 5.3. *(a) Schematics illustrating the stencil deposition technique. Adapted from [8]. (b) Optical image of a Si_3N_4 membrane positioned onto a substrate. In this case, the membrane is transparent, allowing to see the substrate too. Scale bar, 100 μm.*

Figure 5.4a shows an AFM image of a graphene sheet connected with aluminum electrodes by the stencil technique. In this sample, the electrodes are in Hall bar configuration with two current electrodes (largest electrodes) and four voltage leads (lateral probes). Figure 5.4 b represents the cross section of the electrodes. All the electrodes profiles are similar, with a thickness ranging from 144 and 147 nm. The voltage electrode width is typically 900 nm while the spacing is about 2 μm.

The stencil alignment is a critical process because of the size of the area between the external electrodes compared to the maximal area of the graphene flakes that can be routinely obtained. The distance between the edges of the electrodes is about 8x4 μm² for a Hall bar pattern while the flakes surface is typically 10x5 μm². The repeatability of optical alignment with this technique is estimated in 1 or 2 μm. The superposition shown in Figure 5.4b shows a very good homogeneity in the thickness and width of the electrodes deposited by stencil. Stencil technique shown that metallic electrodes can be deposited on a graphene flake without using any resist contaminant or ion irradiation. One of the limitations is the fragility of

the Si_3N_4 membranes. In Figure 5.4a, the two electrodes in the top of the image are short-circuited because metal was evaporated through a crack between two electrodes pattern.

Stencil is a fully compatible UHV [11] technique for contacting graphene, opening the way for an ultraclean technology for graphene.

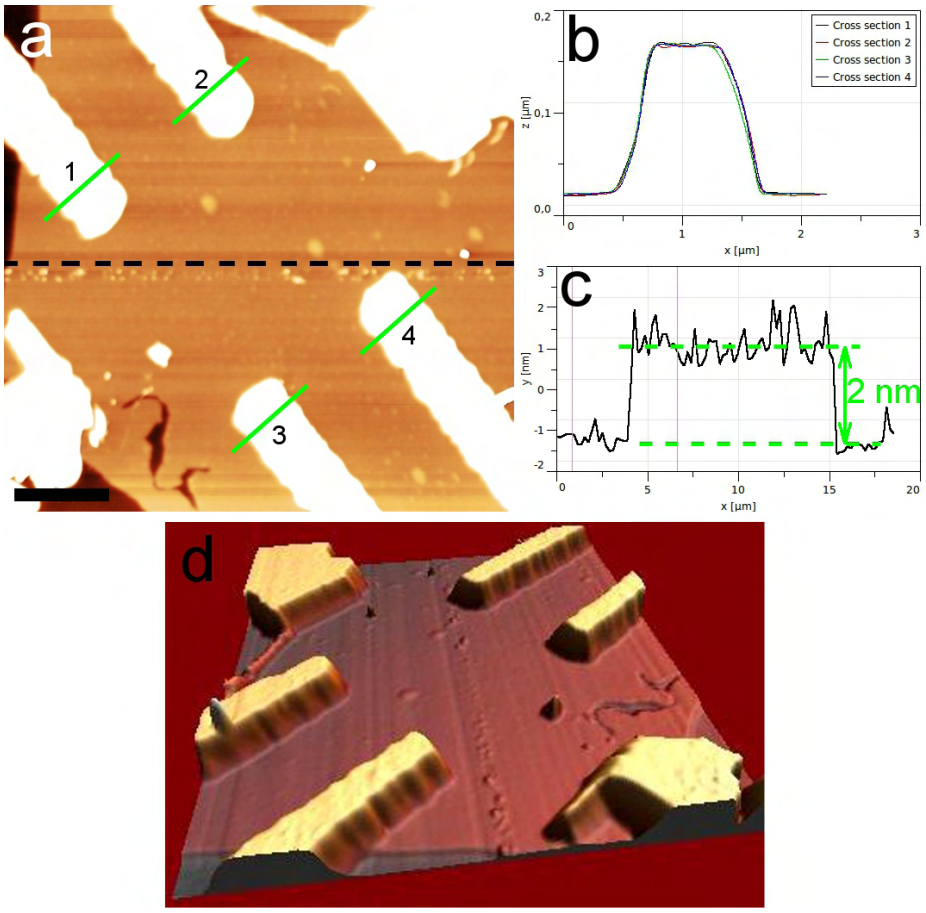

Figure 5.4. *Electrodes deposited on a graphene flake by the stencil technique. (a) AFM image of Al electrodes deposited on a FLG flake by the stencil technique. (b) AFM cross section of the electrodes along the green lines in image (a). (c) Cross section of the graphene flakes of an AFM image taken before electrodes deposition (not shown). (d) is a 3D view of (a). Scale bar: 2 µm. vertical color scale: 40 nm.*

5.2 EBIE on graphene supported by a Si/SiO_2 substrate.

5.2.1 EBIE of supported FLG without water vapor.

In chapter 3, the presence of water on graphene deposited on Si/SiO_2 has been discussed. This paragraph aims to etch this supported graphene by EBIE with this adsorbed water as precursor source. In the absence of water vapor injected, e-beam etching has been

performed on graphite flakes deposited on SiO_2 surface. The acceleration tension was 5 kV and the electronic dose, 50 $C.mm^{-2}$. The residual pressure was about 1 to $5x10^{-7}$ mbar. SEM and AFM images of the holes have been recorded. Figure 5.5 is an AFM image and its cross section through the graphite flake. Although no gas was injected near the irradiated surface, a hole is visible at the surface of the FLG. This hole has a diameter of 750 nm and a depth of 3 to 4 nm. Along a cross section, as shown in Figure 5.5, the depth is the height difference between the graphite surface and the bottom of the hole.

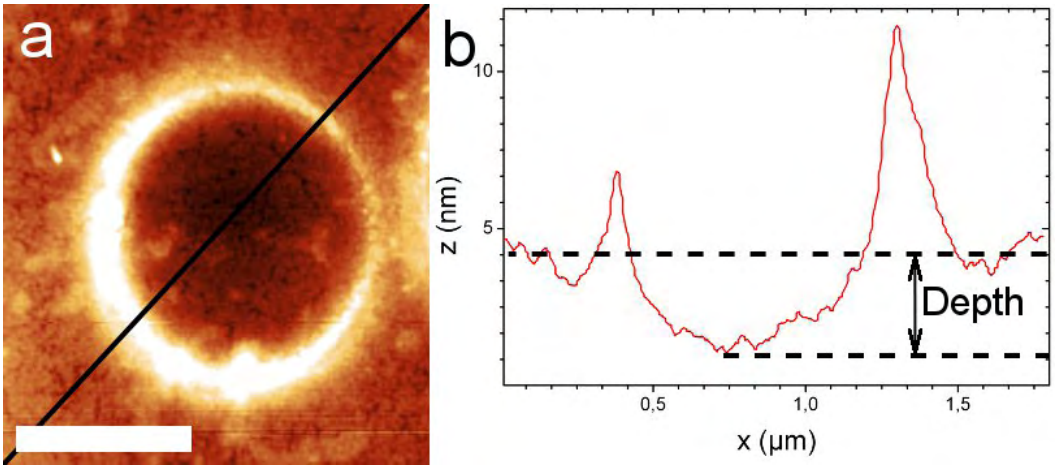

Figure 5.5. *Electron irradiation in spot mode of a supported FLG on SiO_2. (a): AFM Image of a FLG deposited on a silica surface. The irradiation has been made in the center of the image with a dose of 50 $C.mm^{-2}$ and an acceleration tension of 5 kV, no gas was injected. (b) is a cross section of the black line in (a), the depth of the hole is shown. Vertical color scale: 10 nm. Scale bar: 500 nm.*

This hole is different from water vapor assisted EBIE cut obtained on TEM grid (see chapter 4). While the probe size of the electron beam is only a few nanometers, this hole etched on graphite has a diameter of 750 nm. Furthermore, around this hole, some material has accumulated a phenomenon that was not observed on suspended graphene. These facts suggest a different mechanism of etching than the one reported in chapter 4. Since no water has been injected but a marked modification of the surface is observed, an experiment has been conducted to understand this behavior.

Graphite flakes with two different thicknesses (50 and 130 nm) have been exposed to e-beam in spot mode. Series of holes have been etched for a varying exposure time (t) or doses. The depth of the holes has been measured by AFM and is shown in Figure 5.6a.

Since we have demonstrated in chapter 4 that graphene is not etched by e-beam in the absence of water, we investigated the evolution of the silica beneath the observed depletion. For this, graphite flakes have been removed by sonication after e-beam irradiation,: the substrate has been sonicated for 15 minutes in each NMP, acetone and IPA baths. A second series of AFM images have been taken and the depth of the holes has been measured again. Figures 5.6a and b show an example of holes before (a) and after (b) sonication. In Figure 5.6c the depth of the holes measured by AFM is plotted versus the irradiation dose before (full disks and squares) and after (empty disks and squares) sonication for two different graphite flake, one is 50 nm thick (circles) and the other is 130 nm thick (squares).

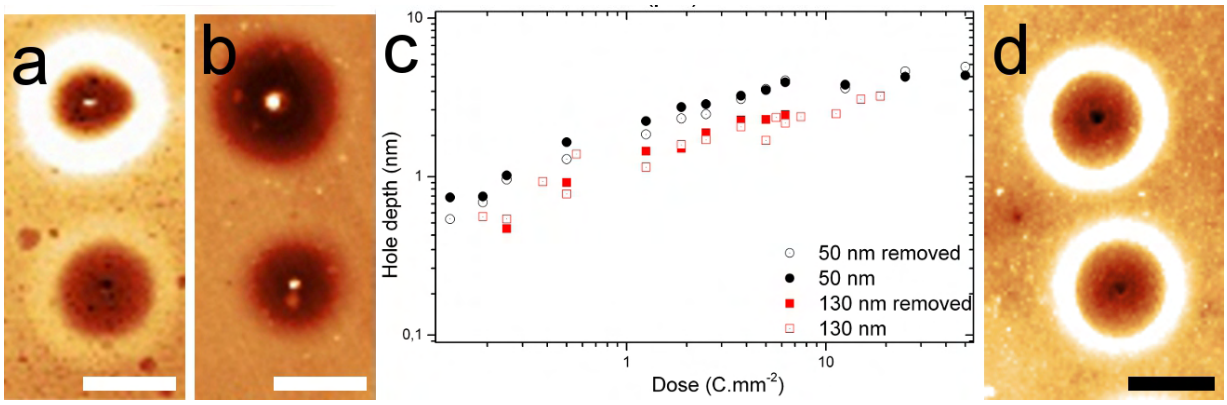

Figure 5.6. *AFM analysis of holes made on graphite supported on a SiO_2 surface. (a) and (b) are AFM images of a graphite flake deposited on a Si/SiO_2 substrate. It has been irradiated by an electron beam without any gas injected in the chamber, AFM Images have been taken before (a) and after (b) graphite removal by sonication. In the (c) graph is plotted the depth of holes versus the electronic dose for two graphite flake, the thickness of which was 50 nm (black circle) and 130 nm (red square). The depth was measured by AFM before (empty circles and squares) and after (filled disks and squares) graphite removal by sonication. (d) Electron irradiation of silica without graphite, unknown dose, the beam was not fully focused on the surface. Acceleration tension was 5 kV for all irradiations. Vertical color scale is 10 nm. Scale bars are 500 nm.*

The hole depths before and after removing the graphite flake are matching for each thicknesses but the depth corresponding to the 50 nm flake is deeper than the one for the thicker sample (130 nm) (Figure 5.6c). This suggests that the SiO_2 itself has been etched and the graphite remained conformal to the SiO_2 surface. Graphene follows the shape of the

etched silica underneath, agreeing with the literature, which has reported that graphene has the same roughness than the underneath substrate when it is deposited on silica, mica [12] or BN. [13]

Silica can be reduced under low energy electron beam. [14] It is also confirmed in Figure 5.6d where holes have been made in bare silica by 5kV irradiations in spot mode. This reduction can explain the formation of holes on silica by an electron beam irradiation at 5 kV.

It has been reported that electron irradiation induces defects such as the conversion of sp^2 carbon into sp^3 species. [15, 16] Defects can also be induced because of residual O_2 [17] or H_2O (see chapter 3). These residual molecules could etch graphene by EBIE process but the amount of molecules is too low and only localized damages occurs. Following the results in chapter 4, we have therefore introduced water vapor in the chamber.

5.2.2 EBIE of supported FLG with water vapor.

Electron beam irradiations in presence of water vapor precursor have been performed on 30 nm thick graphite flakes deposited on a SiO_2 substrate. Arrays of holes have been etched using the spot mode. The acceleration tension was 5 kV, with electronic doses from 1 to 50 $C.mm^{-2}$. The Gas Injection System (GIS) was positioned at 250 μm from the sample surface, allowing for a selective flow of water vapor in the vicinity of the rastered beam. When the reactant is injected in the chamber, the vacuum level was degraded by one order of magnitude (~10^{-6} mbar). As graphene is supported in contrast to chapter 4, a new etched surface versus electronic dose relation will be experimented. SEM and AFM images of the holes have been then recorded.

SEM image in Figure 5.7a shows a hole presenting two distinct features: a circle with a diameter of about 350 nm in diameter and a smaller hole (50 nm) with straight edges and anisotropic angles. The two distinct holes are confirmed by the AFM image in Figure 5.7b, a crater-like ring of raised material is characterized by an aspect-ratio of about 1%, defined as

the quotient of the depth over the diameter of the hole. This hole is similar to the one in Figure 5.5a. Secondly, a smaller diameter hole is observed in the center (darker area in the middle of Figure 5.7b). It is observed that the depth of the second hole is 25 nm nevertheless it is probably deeper since the AFM tip cannot scan the bottom of the hole due to the finite tip solid angle . The aspect ratio of this second hole is about 25%.

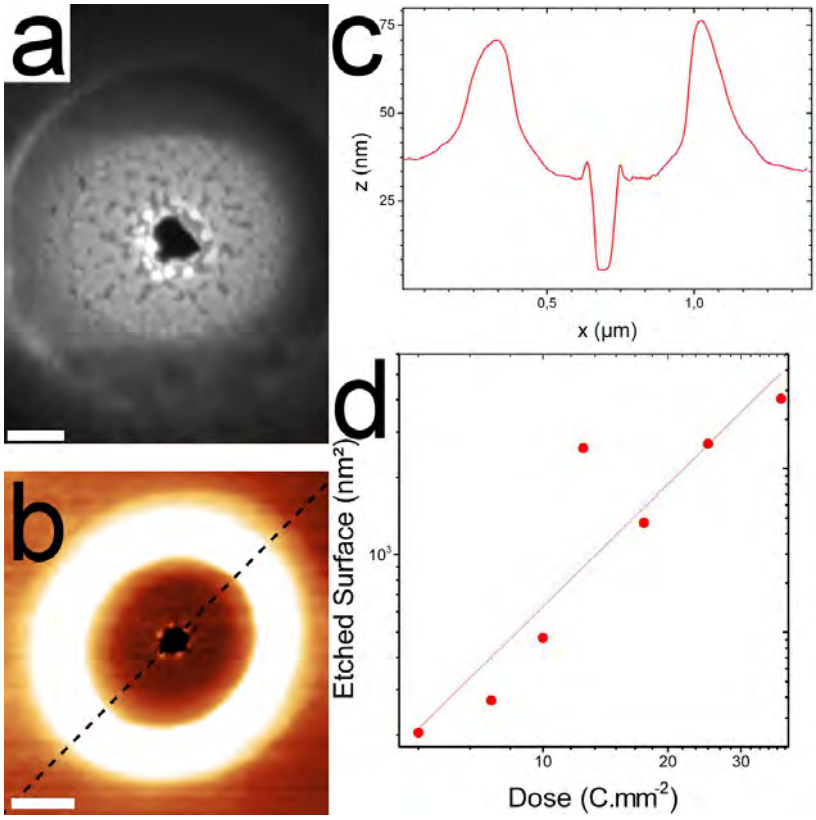

Figure 5.7. *(a) is a SEM image of water assisted EBIE in spot mode on a micromechanically exfoliated graphite deposited on a Si/SiO_2 substrate. The electronic dose for (a) is 50 C.mm^{-2} (b): AFM Image of a FLG deposited on a silica surface. An irradiation was made in the center of the image with a dose of 40 C.mm^{-2} and an acceleration tension of 5 kV, water vapor was injected. (c) is a cross section of the black line in (b). (d) log-log plot of the etched surface versus electronic dose for graphite supported on a Si/SiO_2 substrate. The linear fit has a slope of 1.6 µm^4.C^{-1}. Vertical color scale: (a) 30 nm Scale bars are 200 nm for (a) and 50 nm for (c).*

The high aspect-ratio (~25%) suggests a different dynamics. The graphite flake is about 30 nm thick. Our interpretation is that the electrons reduce silica and form a hole with a low aspect ratio of about 1%. However, because water is injected near the irradiated area graphite has also been etched, leading to the formation of a smaller hole (90 nm in diameter) with a high aspect ratio (25%).

The shape of the small and high depth/diameter aspect ratio hole shown in Figure 5.7d is anisotropic, with long straight edges. This shape is reminiscent to that of graphene holes enlarged by a TEM electron beam (80 keV) by Girit et al. [18].This anisotropy is also reminding the hexagonal holes obtained by Hiura. [17]

Figure 5.7d is a log-log plot of graphite etched area versus the electronic dose. The data follow a linear trend with a slope of 1.6 $\mu m^4.C^{-1}$. The etched area of supported graphene varies as $D^{1.6}$ whereas the etched area of suspended graphene varies as $D^{0.5}$ (Figure 4.7). The significant difference implies that EBIE is more efficient on supported graphene and can be attributed to the presence of the silica underneath the graphene. The substrate produces backscattered electrons (BSE) that contribute to increase the effective electronic dose beyond the nominal value. Additionally backscattered electrons are not confined in the narrow and normal electron beam (unlike incidents electrons) and could significantly increase the etched area.

In gas assisted EBIE process, the etching process is induced by primary, backscattered and secondary electrons. The energy of primary and backscattered electrons is a few tens of keV, while the energy of secondary electrons is only a few eV. The primary electrons are focused and interact with graphene in the probe size only. Only the SE produced within a few nanometers from the surface even far from the incident point can escape and induce some EBIE. However BSE produced within the interaction volume will induce EBIE on their way back out. Since these electrons emerge in all directions, they produce damages in a very wide area, away from the impact point.

5.2.3 Water assisted EBIE of lines in FLG on SiO_2.

The etching of lines in supported graphene has been investigated. Water vapor has been injected in the SEM chamber, the electronic dose was 0.11 $C.m^{-1}$ and the pitch factor 0.5. The etching speed was 900 $nm.min^{-1}$.

The resulting cut is shown in Figure 5.8, it presents a very complex morphology. The graphene flake is visible in the top left and bottom right corners separated by the cut in the middle of the image in Figure 5.8b. While the electron beam size is only a few nanometers in diameter, graphene has been completely etched on a width of 500 nm and is partially etched on two bands on either side of about 200 nm in width, in which a series of narrow ribbons (width of 50±20 nm) perpendicular to the etch direction are visible. In the center of the cut, the contrast is white with a sudden change to black in the middle.

This pattern is the generalization of Figure 5.7b in which the etching process has been induced by primary and backscattered electrons, the latter ones being responsible for the significant 900 nm wide broadening of the cut.

The etching quality is highly dependent on the suppression of the backscattered electrons. A solution to lower the influence of BSEs is to locally suspend graphene, which is explored in the following.

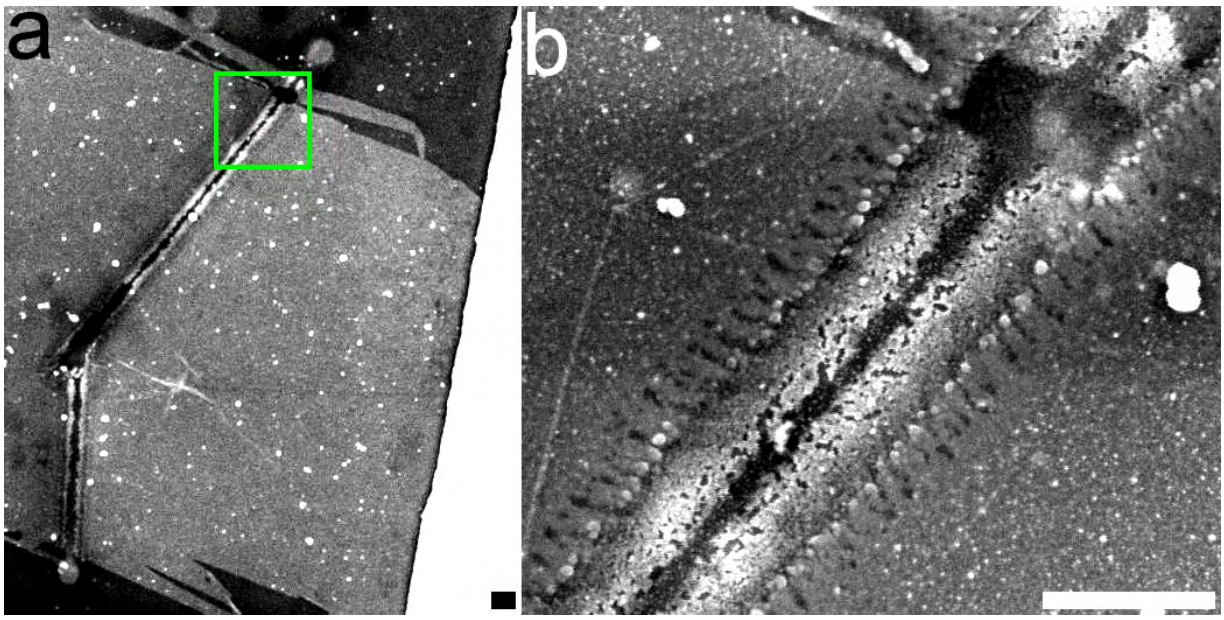

Figure 5.8. *EBIE etching of graphene on SiO_2. (a) is a SEM image of a graphene flake supported on a Si/SiO_2 substrate. An EBIE trench has been performed on it, the zoom of the green square is visible in the b) image. Water vapor was injected in the SEM chamber acceleration tension was 20 kV and dose, 0.11 $C.m^{-1}$. Scale bars are 500 nm.*

5.3 EBIE on locally suspended graphene.

5.3.1 Modification of the Substrate for locally suspends graphene.

One should point out that pools beneath graphene have been fabricated before [3, 4] or after [19, 20] graphene deposition. We have selected the first approach in order to limit the contamination on graphene. Arrays of pools (1x5 μm², Figure 5.9) have been defined on the silicon oxide surface by photolithography. Oxide has been etched by a solution of buffered HF on a depth of 200 to 250 nm. Graphene is deposited on this substrate by micromechanical exfoliation.

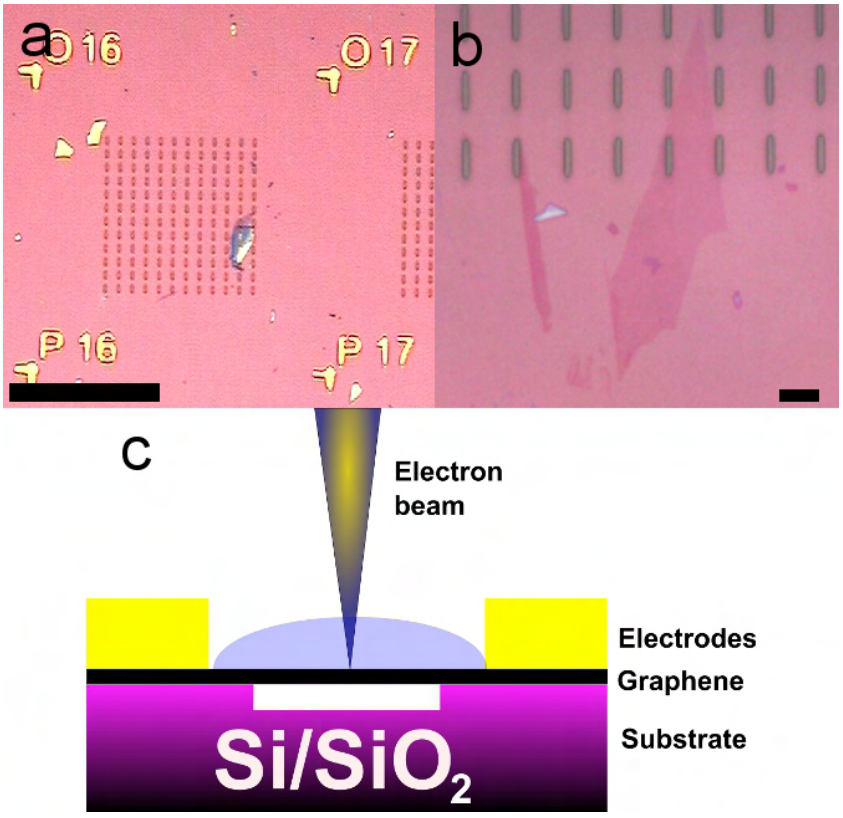

Figure 5.9. *(a) and (b) Optical image of a Si/SiO_2 substrates with pools, graphene has been deposited by micromechanical exfoliation. (b) Schematic view of a Si/SiO_2 substrate with pools. A locally suspended graphene flake connected with metallic electrodes is cut by water assisted EBIE. Scale bar are (a) 100 μm and (b) 5 μm.*

5.3.2 EBIE pattern of locally suspended graphene.

Graphene has been deposited on a pre-patterned substrate by the micromechanical exfoliation technique. 1 μm long cuts has been performed by water assisted EBIE on the sus-

pended part of the graphene flakes with an electronic dose of $6x10^{-2}$ C.m^{-1} and acceleration tension of 20 kV, the resulting cut is visible in Figure 5.10.

The first observation is that the etching has been successful and the cut has a length of 1 μm for a width of 150 nm. The maximum edge roughness is 20 nm and the area around the edge of the cut is uniformly dark. One can notice, though, that the rest of the suspended graphene has a wooly aspect and a brighter contrast.

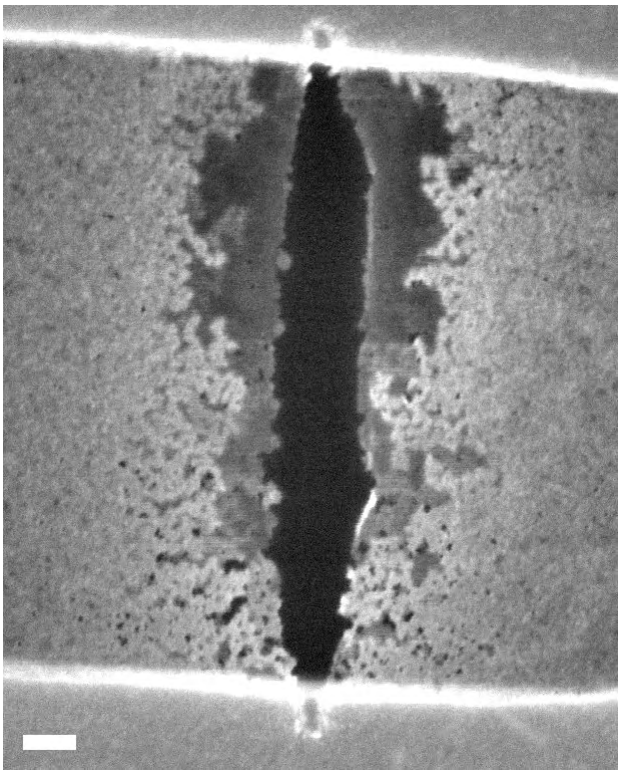

Figure 5.10. *Water assisted EBIE cut on a locally suspended graphene. Electronic dose is $6x10^{-2}$ C.m^{-1} and acceleration tension, 20 kV. Scale bar is 100 nm.*

Although graphene has been suspended, the EBIE cuts have not exactly the same aspect than the cuts performed on graphene suspended on TEM grid in chapter 4. The aspect of the trench is very different from the supported graphene in Figure 5.8. The trench is about ten times larger than the electron beam size, an interpretation of this enlargement as well as a technique to avoid enlargement of the EBIE trench will be provided in the paragraph 5.3.4. The change in SEM contrast around the trench is a manifestation of a modification of the graphene surface, this phenomenon will be described in the following paragraph.

5.3.3 Silicon sputtering and redeposition.

For this entire section, Si/SiO_2 substrates were used. The oxide thickness was 285 nm and pools were patterned on them with a depth of 200 to 250 nm. Graphene has been deposited onto them by micromechanical exfoliation. A water assisted EBIE has been performed on a locally suspended graphene flake along three lines with an electronic dose of $9x10^{-2}$ $C.m^{-1}$ for each line.

Figure 5.11a shows two of the three cuts around which an area of about 1.5 μm is dark, the rest of the pool is very bright with a wooly aspect as described for image 5.10. Only two cuts are visible on the SEM image because the third irradiation did not etch graphene.

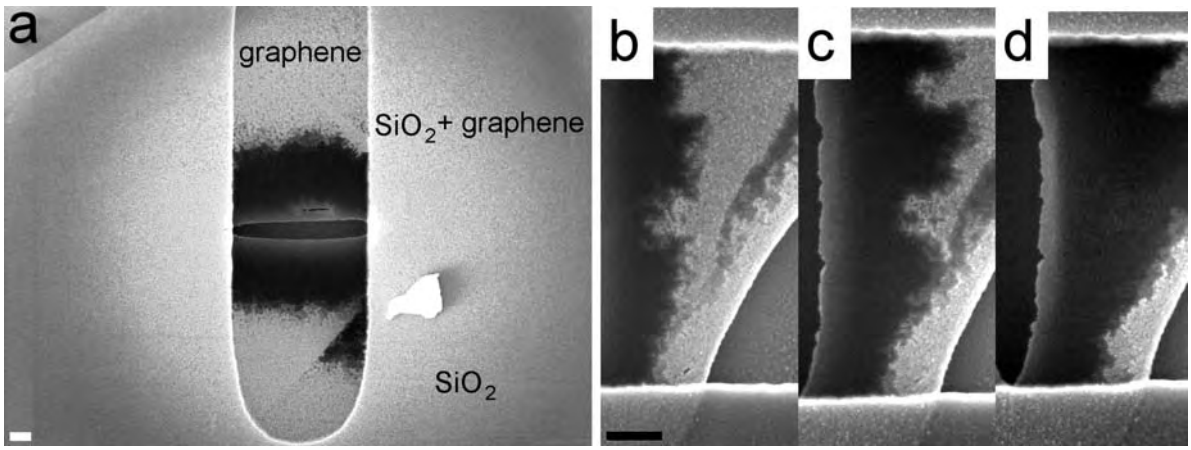

Figure 5.11. *SEM images of EBIE trenches. All the samples are locally suspended graphene over pools of a Si/SiO_2 substrate, with an oxide thickness of 285 nm and a pool depth between 200 and 250 nm. (a) SEM image of an EBIE cut made with an electronic dose of $9x10^{-2}$ $C.m^{-1}$. (b-d) This sequence of images has been taken after an EBIE etching with an electronic dose of (b) $9x10^{-2}$ $C.m^{-1}$, (c) $18x10^{-2}$ $C.m^{-1}$ and (d) $27x10^{-2}$ $C.m^{-1}$. Scale bars are 200 nm.*

Although EBIE patterning the cuts graphene as in the case of freely suspended graphene, it seems that a secondary phenomenon results in the limitation of the etching efficiency. To further investigate this point three EBIE lines have been etched along the same segment on locally suspended graphene and monitored by SEM (Figure 5.140b-d). The extension of the dark area appearing after the first etching increases with the successive electronic doses.

We think that silica is vaporized from the bottom of the pool by the electron beam irradiation and contaminates the graphene surface. To test this hypothesis, a locally suspended graphene flake is irradiated following two lines in the presence of xenon difluoride (XeF_2) injected by the GIS with electronic doses of 2 and $4x10^{-2}$ $C.m^{-1}$ and imaged by SEM. On the same sample, lines have been etched in the same area in presence of water until the EBIE process was blocked. Finally a cut was etched in the presence of XeF_2 again with an electronic dose of $2x10^{-2}$ $C.m^{-1}$. SEM images of the successive step are collected in Figure 5.12. After an irradiation under a flux of XeF_2, the graphene remains intact but severe damages are visible through it, on the bottom of the pool (shown by the black arrow). The etching of silica in the bottom of the pool is extensive. The water assisted EBIE step that has etched graphene is shown in Figure 5.12b. Graphene present the same apparent modification described above and it is no longer possible to etch it by water assisted EBIE. An etching by XeF_2 assisted EBIE shown in Figure 5.12c violently tore graphene apart.

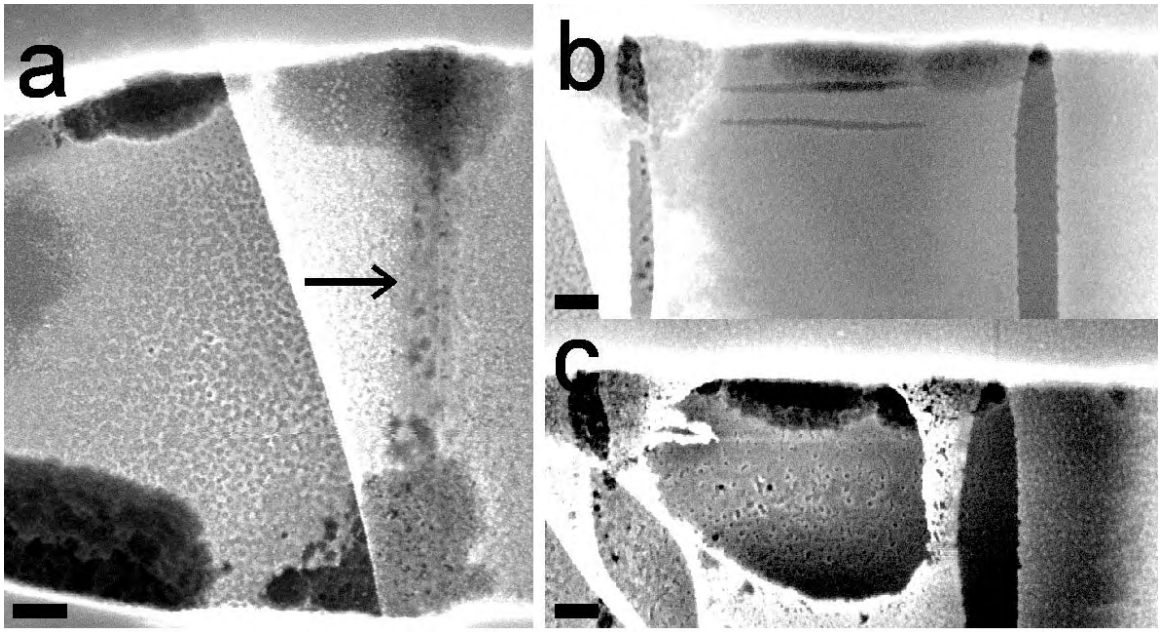

Figure 5.12. *XeF_2 assisted EBIE of graphene. (a): SEM image of a graphene locally suspended which has been irradiated twice ($2x10^{-2}$ and $4x10^{-2}$ $C.m^{-1}$) with a flux of XeF_2. (b) is a SEM image of the same graphene flake etched by water assisted EBIE until etching become impossible. (c): The same area after an etching by XeF_2 assisted EBIE along a line with an electronic dose of $2x10^{-2}$ $C.m^{-1}$. Scale bars are 100 nm.*

From this series of EBIE irradiations we can conclude that pristine graphene is not etched by XeF_2 assisted EBIE (with electronic dose smaller than $4x10^{-2}$ $C.m^{-1}$). However, silica and/or silicon in the bottom of the pool are clearly etched by XeF_2. [21, 22] We also confirm that there is a maximal electronic dose after which water assisted EBIE of locally suspended graphene is blocked. However, a subsequent XeF_2 assisted EBIE seriously alter the graphene sheet. It thus appears that during the water assisted EBIE patterning of graphene, the e-beam reaches the bottom of the pool where silica is sputtered onto the bottom side of the graphene surface. When the graphene is coated with silica, the etching is blocked unless one reacts with the silica sheath with XeF_2 under the e-beam which results in the complete destruction of the suspended material.

In Figure 5.13 we show that dual H_2O/ XeF_2 EBIE protocol could be successfully used to produce a graphene ribbon of 140 nm in width and 300 nm in length (Figure 5.13a) and eventually to fabricate the graphene lead. However, in the final state shown in Figure 5.13b, the ribbon morphology is not controlled. Moreover, the suspended ribbon is most certainly amorphized, fluorinated [23] or even mostly composed of an undefined Si/C/F/O material.

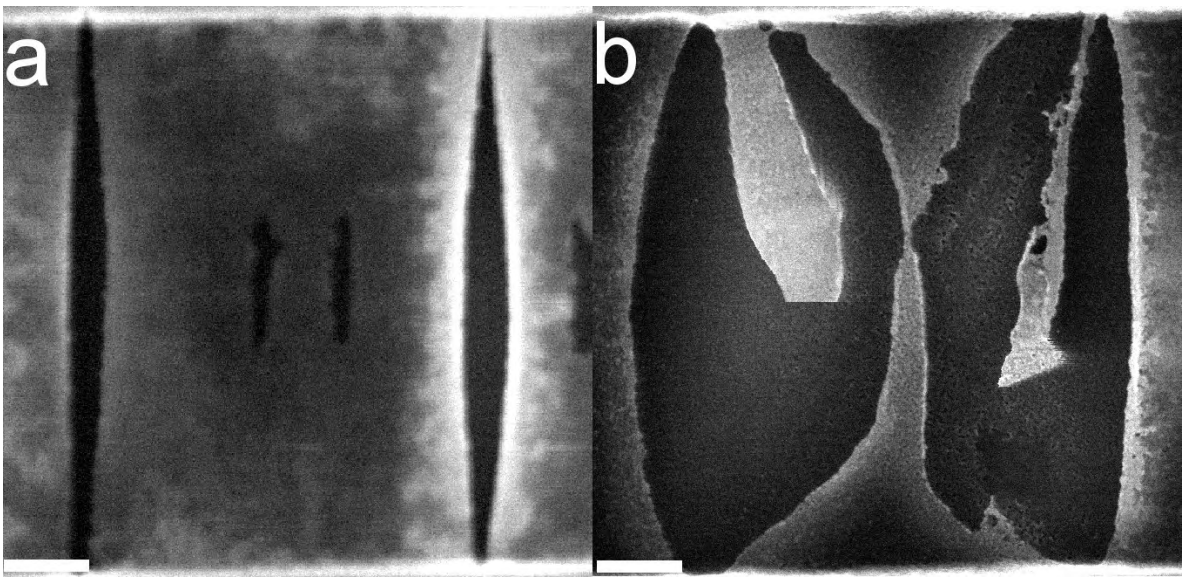

Figure 5.13. *Suspended graphene nanoribbon. (a): a 150 nm wide ribbon. Finishing the ribbon shown in (a) by water and xenon difluoride assisted EBIE, (b) is a SEM image of a ribbon with two funnels. The ribbon is 60 to 80 nm in width. There is a constriction of 60 nm long and 15 nm wide. Scale bars are 200 nm.*

As a consequence, silica or silicon sputtering onto graphene should be avoided. This can be reached by fabricating deeper pools, which is in progress. The next paragraph will investigates the cause of the enlargement of the EBIE cut on locally suspended graphene observed in Figure 5.10.

5.3.4 Mechanical strains in a graphene sheet.

Locally suspended graphene has been etched by water assisted EBIE along the 1 μm pool width. The electronic dose was $9x10^{-2}$ $C.m^{-1}$.Figure 5.14 shows that the cut is 350 nm wide and edge roughness is about 25 nm over a length of 400 nm or more. The extremities of the cut, magnified in Figure 5.7b have a parabolic shape. This shape and width are in great contrast with those of the cuts obtained on fully suspended graphene (see chapter 4). For such a dose, the cut width is about 15 to 20 nm and the RMS roughness is smaller than 2 nm over hundreds of nanometers. This cut broadening behavior appears on all micromechanically exfoliated graphene deposited on Si/SiO_2 substrates, although the width of the trench can be larger (Figure 5.15a).

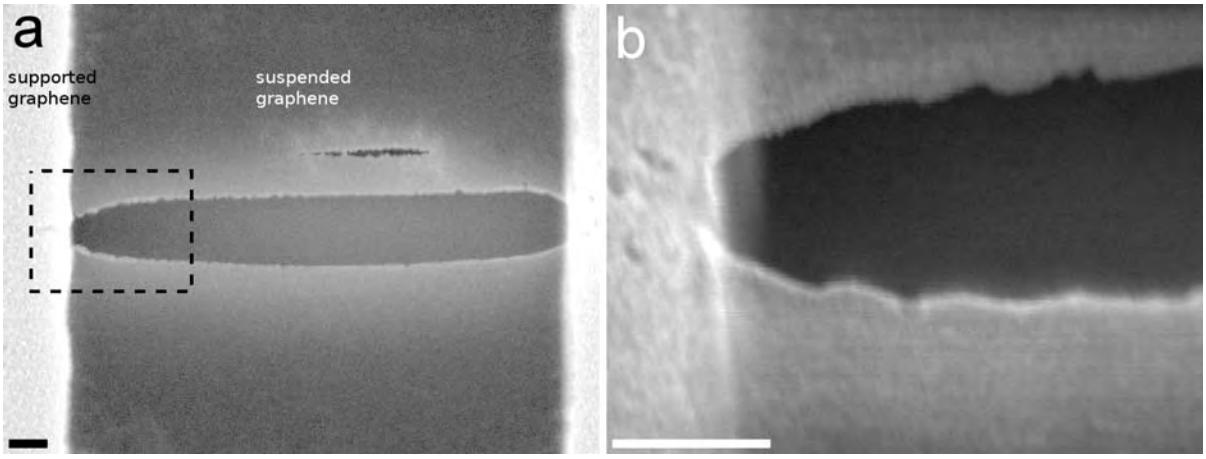

Figure 5.14. *(a) SEM image of graphene suspended over a pool of a Si/SiO_2 substrate. It has been etched by water assisted EBIE. The acceleration tension was 20 kV and the electronic dose $9x10^{-2}$ $C.m^{-1}$. (b) is a zoom of the black dashed square in (a). Scale bars: 100 nm.*

A series of three water assisted EBIE cuts at an electronic dose of $9x10^{-2}$ $C.m^{-1}$ have been performed on locally suspended graphene Figure 5.15 shows the succession of EBIE cuts. The first etching leads to a very large cut of 500 to 650 nm in width as seen in Figure 5.15a

with partially folded edges. The width of the second cut is only 150 nm and the third cut performed between the two first ones has a width of 30 nm.

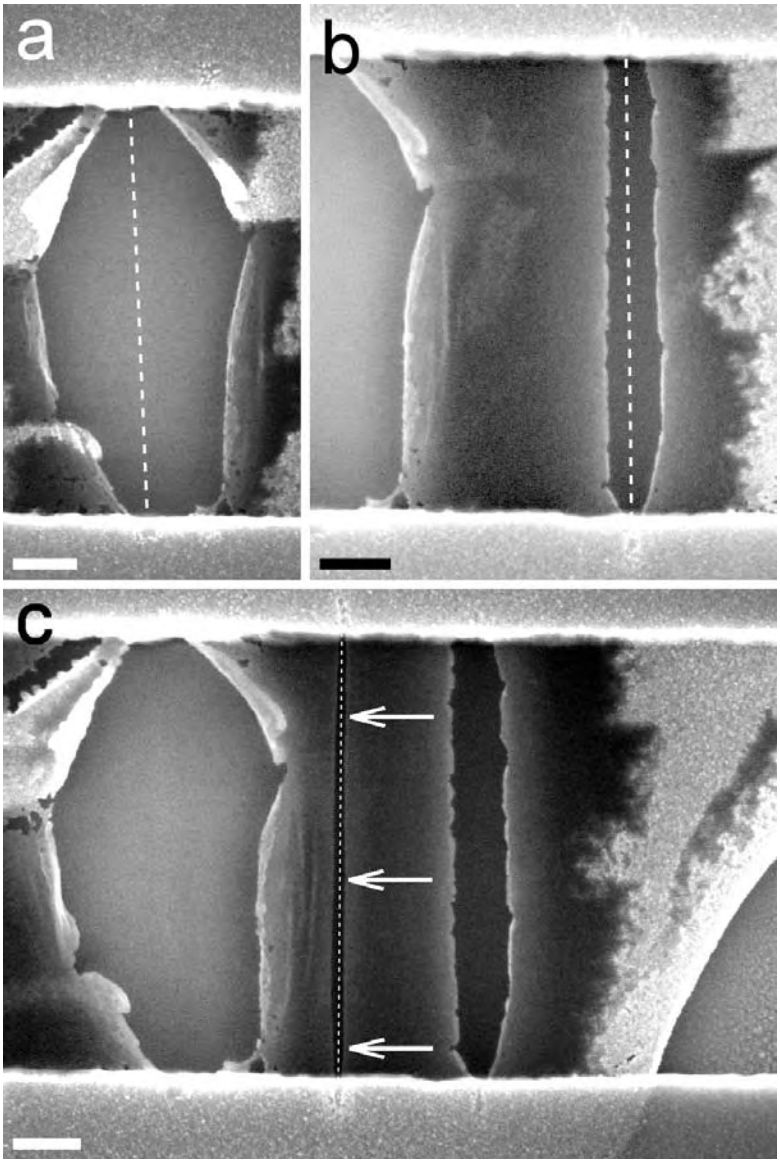

Figure 5.15. *SEM images of a series of EBIE cuts on locally suspended graphene. All the cuts are made by water assisted EBIE with an electronic dose of $9x10^{-2}$ $C.m^{-1}$ and a voltage acceleration of 20 kV. The first cut is shown in (a). The second cut is done at the right of the first cut, visible in (b). White arrows show the third cut, visible in (c) which has been done between the two previous cuts. Scale bar are 200 nm.*

The shape of the first cut suggests that the graphene is initially under a high in plane strain. Upon etching, the edges are released and the strain on the graphene sheet is significantly reduced. The second cut done next to the first one, (Figure 5.15b) has a width much smaller (150 nm). Figure 5.15c demonstrates that the third etching, performed between these

two first cuts, recovers a width of 30 nm, which is close to the value obtained on freely suspended graphene on TEM grids (15-20 nm). This indicates that the built in tension of the graphene sheet has been fully relaxed by the first two cuts allowing to retrieve the optimal EBIE conditions.

Another experiment that corroborates this interpretation is shown in Figure 5.16a, two parallel cuts have been etched by water assisted EBIE on locally suspended graphene. The first cut has a width of 150 nm, while it is reduced to 80 nm for the second.

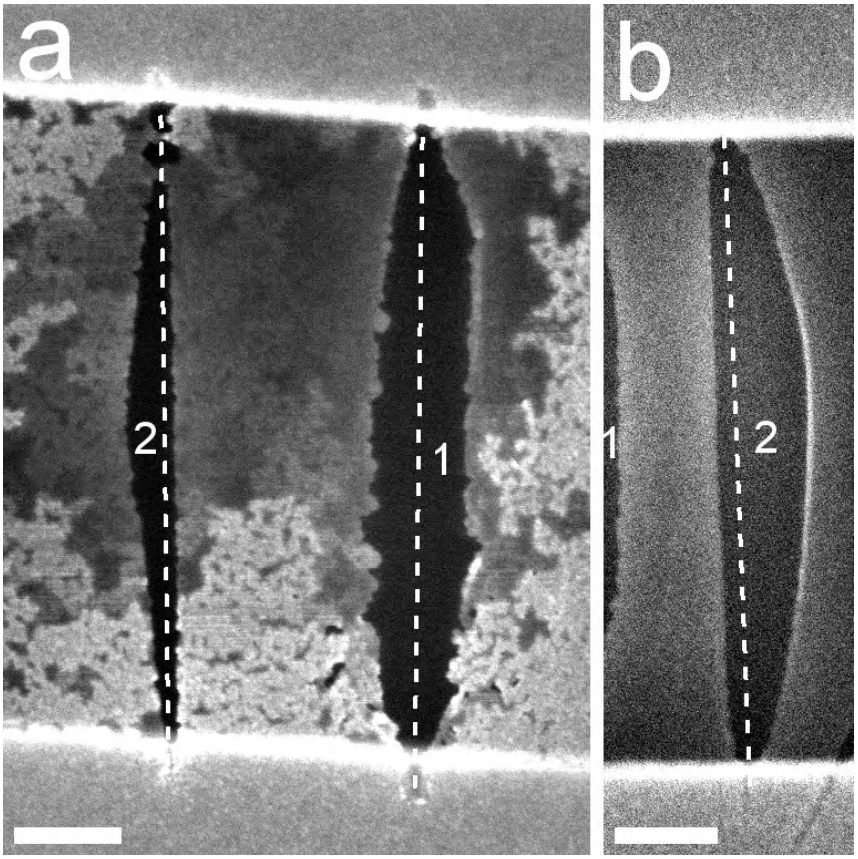

Figure 5.16. *Asymmetric EBIE cut. SEM images of water assisted EBIE cuts on locally suspended graphene. The numbers on images indicates the order of etching. Electronic doses were (a) $6x10^{-2}$ C.m^{-1} and (b) $3x10^{-2}$ C.m^{-1}. In both images acceleration tension was 20 kV. Scale bars are 200 nm.*

Noticeably, a clear asymmetry in the shape of the second cut can be observed. This effect is also visible in a similar experiment shown in Figure 5.16b. We observed that the broadening of the cut on one side can be up to 3-4 times longer than on the other side. Both Figure 5.16a and b illustrate that the broadening is reduced on the side facing the first cut. In

the case of etching performed between two cuts (Figure 5.15c) or between a cut and a freely suspended edge of the graphene flake (Figure 5.15b), this asymmetry disappears. All these evidences can be qualitatively accounted for by considering a strained graphene. The strain could be induced initially by the micromechanical exfoliation technique. The successive peeling between the elastic glued adhesive tape surfaces could build up a strain that could be transferred to the deposited graphene. The buffer layer evoked in chapter 3 [24] could contribute to the preservation of the built-in strains by promoting the adhesion of the graphene to the silica. The weight of the 1x5 μm suspended graphene over the pools could also contribute to this strain along the long axis of the pools.

In order to get some confirmation on which shape would results from a line cutting in a strained film, we have used some very simple finites elements numerical simulations using the structural mechanics module of the software COMSOL. The locally suspended graphene has been modelized by a 2D rectangle of 1x5 μm with strain of equal intensity imposed on the four edges. The etching has been modelized by a 600x20 nm^2 rectangle hole in the graphene sheet. The thickness, the Young's modulus and the Poisson coefficient of graphene were chosen to 0.35 nm, $1x10^{12}$ Pa [25] and 0.165 [25] respectively. The sheet was left to relax and Figure 5.17 shows the results of the simulation.

A built-in strain of 35 $N.m^{-1}$ had to be set on the edges in order to get a 150 nm resulting width as observed in Figure 5.10. Interestingly, the simulation leads a parabolic shape of the cut similar to the experiment. This very preliminary approach seems to confirm that the built-in strain could account for the relaxed shape of the cuts in the case of locally suspended graphene but more detail should be taken into consideration. The strain obtained is very close to the breaking strength of graphene, 41 $N.m^{-1}$ [25] but the weight of the suspended graphene has not been included. The dependence on the thickness of the film is critical but difficult to define. It thus appears that a more quantitative mechanical modeling will be necessary to fully interpret our observations.

Our experimental observations are in striking contrast with the absence of strained Raman data acquired on micromechanically exfoliated graphene. [26]

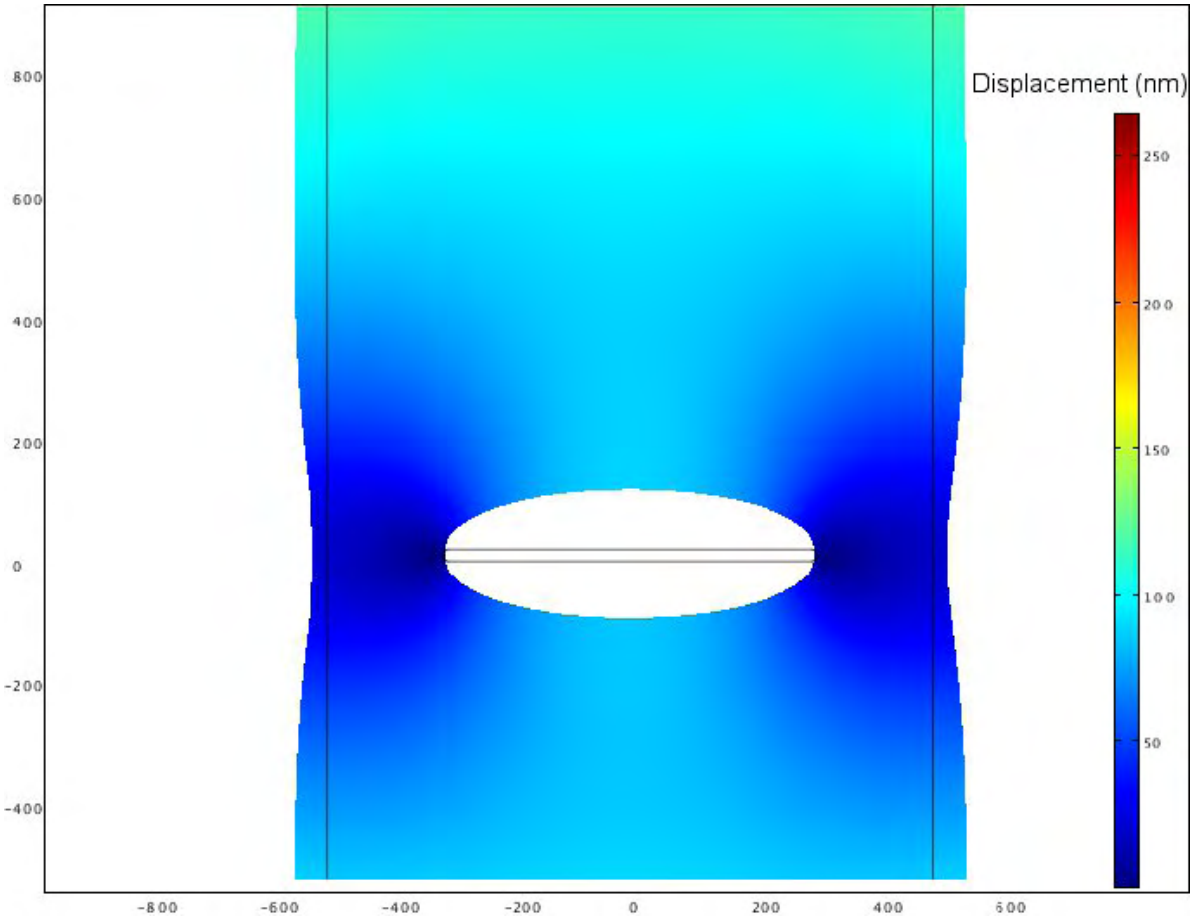

Figure 5.17. *Simulated displacement of a cut in a strained film. X and Y axis are in nm, black solid line is the contour of the non strained film. Color scale represents the displacement of the loaded film.*

5.4 Complete patterning of GNR devices on locally suspended graphene.

Figure 5.18 is an illustration of our achievements, a locally suspended graphene has been etched by water assisted EBIE at an electronic dose of 2×10^{-2} C.m^{-1}. Two cuts separated by 750 nm have been etched to release the build-in strain. Between these cuts, a graphene nanoribbon with two contacting wedges has been etched (Figure 5.18a). The two first cuts have width of 45 and 15 nm. The ribbon has a width of 30 nm over a length of 200 nm.

A locally suspended graphene deposited by micromechanical exfoliation on a Si/SiO_2 substrate (285 nm of oxide thickness) has been contacted with Ti/Pd electrodes deposited by e-beam lithography. Graphene has been etched by water assisted EBIE along Two parallel cuts to relax the build-in tensions and a GNR with two contact wedges has been etched between these cuts. The GNR has been isolated from the rest of the graphene sheet by etching long cuts on the supported graphene. A false color SEM of the GNR device is shown in Figure 5.520b. The SiO_2 surface (violet) is visible where graphene does not cover the substrate and where it has been etched. The GNR is connected to the leads (yellow) by a contact wedges and the left part of the starting graphene sheet has been cutaway. After the first nanofabrication attempt seen in Figure 5.18b, contacts between the GNR and the rest of the suspended graphene flake persists. However, the GNR has been fully isolated by a second EBIE cut.

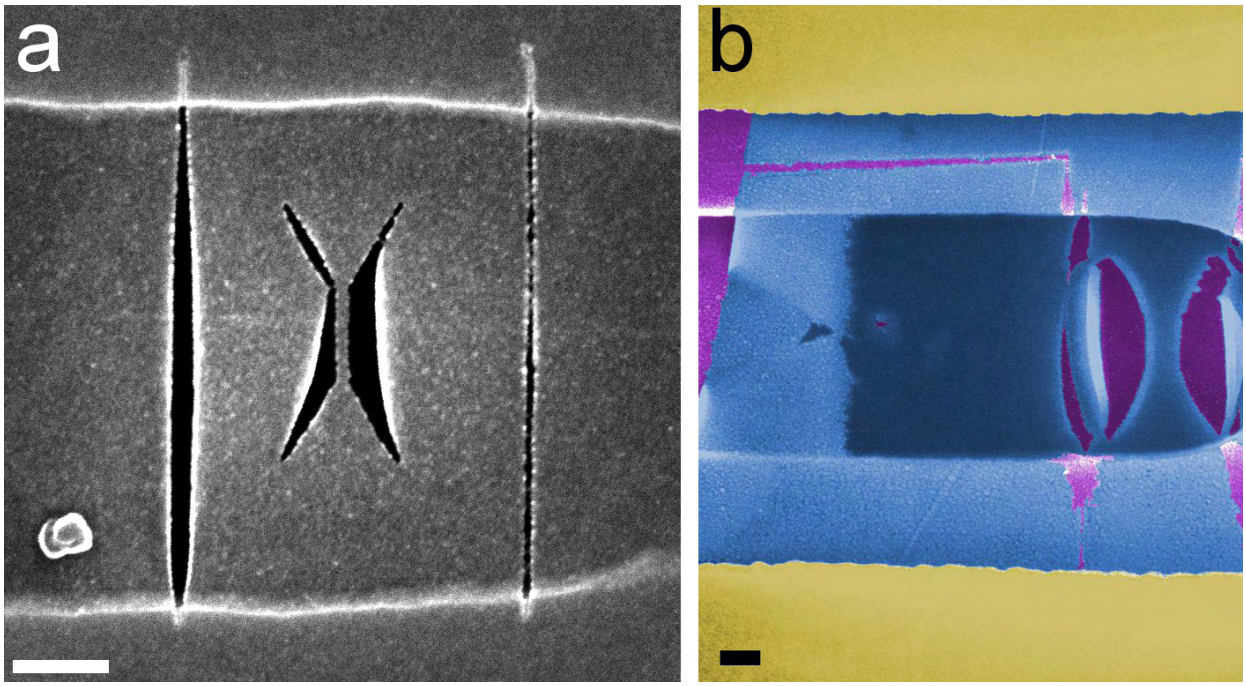

Figure 5.18. *(a) SEM image of a 30x200 nm graphene ribbon etched by water assisted EBIE on a locally suspended graphene. Electronic dose was $2x10^{-2}$ $C.m^{-1}$ (b) Graphene nano-ribbon etched by EBIE and contacted by metallic electrodes. Colorized SEM image of metallic leads (yellow-brown), supported (blue), suspended graphene (dark blue) and silica surface (violet). Acceleration tension 20 kV. Scale bars are 200 nm.*

5.5 Conclusion.

La technique EBIE caractérisée au chapitre 4 a montré un potentiel pour fabriquer des nano-rubans de graphène tout en préservant leur qualité structurale. Dans le dernier chapitre de cette thèse, nous avons appliqué cette technique sur du graphène en configuration de dispositif électronique. La vaporisation de silice du fond des piscines limite actuellement la technique, mais la fabrication, déjà en cours, de substrats avec des piscines plus profondes, devrait permettre de limiter ce phénomène. Le graphène localement suspendu est en tension mécanique, ce qui est contradiction avec des études Raman [26]. Une amélioration de la simulation de la forme de découpes formées dans un film dont nous avons présenté un embryon ici devrait permettre de calculer les tensions présentes dans un feuillet de graphène de manière complémentaire à la spectroscopie Raman.

En relâchant ces tensions, un nanoruban de graphène de 30 nanomètre de large connecté à des électrodes et isolé du reste du feuillet de graphène a aussi été fabriqué, constituant l'aboutissement de ce travail.

The EBIE technique, characterized in chapter 4, has shown a potential to produce nano-graphene ribbons while pre-serving their structural quality. In this last chapter, we have applied this technique to a graphene configuration suitable for electronic device. Vaporization of silica from the bottom of pools currently limit the technique, but the manufacturing, already underway, of substrates with deeper pools should limit this phenomenon. Locally suspended graphene is mechanically strained, which is inconsistent with Raman studies [26]. Improved simulation of the shape of the cuts formed in a strained film which we have presented here should allow to calculate these strains in graphene sheet in a complementary manner with Raman spectroscopy.

By releasing these strains, we have etched a 30 nanometer wide graphene nanoribbon. A ribbon connected to electrodes and isolated from the rest of the graphene sheet has also been fabricated, constituting the culmination of this work.

5.6 References

[1] Novoselov, K. S.; Geim, A. K.; Morozov, S. V.; Jiang, D.; Zhang, Y.; Dubonos, S. V.; Grigorieva, I. V.; Firsov, A. A. "**Electric field effect in atomically thin carbon films**". *Science* (**2004**) *Vol. 306*, p. 666-669.

[2] Novoselov, K. S.; Jiang, D.; Schedin, F.; Booth, T. J.; Khotkevich, V. V.; Morozov, S. V.; Geim, A. K. "**Two-dimensional atomic crystals**". *Proc. Natl. Acad. Sci. U. S. A.* (**2005**) *Vol. 102*, p. 10451-10453.

[3] Bolotin, K. I.; Sikes, K. J.; Jiang, Z.; Klima, M.; Fudenberg, G.; Hone, J.; Kim, P.; Stormer, H. L. "**Ultrahigh electron mobility in suspended graphene**". *Solid State Commun.* (**2008**) *Vol. 146*, p. 351-355.

[4] Du, X.; Skachko, I.; Barker, A.; Andrei, E. Y. "**Approaching ballistic transport in suspended graphene**". *Nat. Nanotechnol.* (**2008**) *Vol. 3*, p. 491-495.

[5] Ishigami, M.; Chen, J. H.; Cullen, W. G.; Fuhrer, M. S.; Williams, E. D. "**Atomic Structure of Graphene on SiO2**". *Nano Lett.* (**2007**) *Vol. 7*, p. 1643-1648.

[6] Lin, Y. C.; Lu, C. C.; Yeh, C. H.; Jin, C. H.; Suenaga, K.; Chiu, P. W. "**Graphene Annealing: How Clean Can It Be?**". *Nano Lett.* (**2012**) *Vol. 12*, p. 414-419.

[7] Blake, P.; Brimicombe, P. D.; Nair, R. R.; Booth, T. J.; Jiang, D.; Schedin, F.; Ponomarenko, L. A.; Morozov, S. V.; Gleeson, H. F.; Hill, E. W.; Geim, A. K.; Novoselov, K. S. "**Graphene-based liquid crystal device**". *Nano Letters* (**2008**) *Vol. 8*, p. 1704-1708.

[8] Vazquez-Mena, O.; Villanueva, G.; Savu, V.; Sidler, K.; van den Boogaart, M. A. F.; Brugger, J. "**Metallic Nanowires by Full Wafer Stencil Lithography**". *Nano Lett.* (**2008**) *Vol. 8*, p. 3675-3682.

[9] Gross, L.; Schlittler, R. R.; Meyer, G.; Vanhaverbeke, A.; Allenspach, R. "**Fabrication of ultrathin magnetic structures by nanostencil lithography in dynamic mode**". *Appl. Phys. Lett.* (**2007**) *Vol. 90*, p. 3.

[10] Rangelow, I. W.; Shi, F.; Hudek, P.; Kostic, I.; Hammel, E.; Löschner, H.; Stengl, G.; Cekan, E. "**Silicon stencil masks for masked ion beam lithography proximity printing**". *Microelectronic Engineering* (**1996**) *Vol. 30*, p. 257-260.

[11] Guo, H.; Martrou, D.; Zambelli, T.; Dujardin, E.; Gauthier, S. "**Development of UHV dynamic nanostencil for surface patterning**". *The Review of scientific instruments* (**2008**) *Vol. 79*, p. 103904.

[12] Lui, C. H.; Liu, L.; Mak, K. F.; Flynn, G. W.; Heinz, T. F. "**Ultraflat graphene**". *Nature* (**2009**) *Vol. 462*, p. 339-341.

[13] Dean, C. R.; Young, A. F.; Meric, I.; Lee, C.; Wang, L.; Sorgenfrei, S.; Watanabe, K.; Taniguchi, T.; Kim, P.; Shepard, K. L.; Hone, J. "**Boron nitride substrates for high-quality graphene electronics**". *Nat. Nanotechnol.* (**2010**) *Vol. 5*, p. 722-726.

[14] Tanuma, S.; Kimura, T.; Nishida, K.; Hashimoto, S.; Inoue, M.; Ogiwara, T.; Suzuki, M.; Miura, K. "**Quantitative evaluation of surface damage onSiO(2)/Si specimen caused by electron beam irradiation**". *Appl. Surf. Sci.* (**2005**) *Vol. 241*, p. 122-126.

[15] Teweldebrhan, D.; Balandin, A. A. "**Modification of graphene properties due to electron-beam irradiation**". *Appl. Phys. Lett.* (**2009**) *Vol. 94*, p. 3.

[16] Childres, I.; Jauregui, L. A.; Foxe, M.; Tian, J. F.; Jalilian, R.; Jovanovic, I.; Chen, Y. P. "**Effect of electron-beam irradiation on graphene field effect devices**". *Appl. Phys. Lett.* (**2010**) *Vol. 97*, p. 3.

[17] Hiura, H. "**Generation of circular and hexagonal microholes in a graphite surface**". *J. Mater. Res.* (**2001**) *Vol. 16*, p. 1287-1292.

[18] Girit, C. O.; Meyer, J. C.; Erni, R.; Rossell, M. D.; Kisielowski, C.; Yang, L.; Park, C. H.; Crommie, M. F.; Cohen, M. L.; Louie, S. G.; Zettl, A. "**Graphene at the Edge: Stability and Dynamics**". *Science* (**2009**) *Vol. 323*, p. 1705-1708.

[19] Bunch, J. S.; van der Zande, A. M.; Verbridge, S. S.; Frank, I. W.; Tanenbaum, D. M.; Parpia, J. M.; Craighead, H. G.; McEuen, P. L. "**Electromechanical resonators from graphene sheets**". *Science* (**2007**) *Vol. 315*, p. 490-493.

[20] Garcia-Sanchez, D.; van der Zande, A. M.; Paulo, A. S.; Lassagne, B.; McEuen, P. L.; Bachtold, A. "**Imaging mechanical vibrations in suspended graphene sheets**". *Nano Lett.* (**2008**) *Vol. 8*, p. 1399-1403.

[21] Randolph, S. J.; Fowlkes, J. D.; Rack, P. D. "**Focused electron-beam-induced etching of silicon dioxide**". *J. Appl. Phys.* (**2005**) *Vol. 98*, p. 6.

[22] Matsui, S.; Ichihashi, T.; Mito, M. "**Electron-beam induced selective etching and deposition technology**". *J. Vac. Sci. Technol. B* (**1989**) *Vol. 7*, p. 1182-1190.

[23] Robinson, J. T.; Burgess, J. S.; Junkermeier, C. E.; Badescu, S. C.; Reinecke, T. L.; Perkins, F. K.; Zalalutdniov, M. K.; Baldwin, J. W.; Culbertson, J. C.; Sheehan, P. E.; Snow, E. S. "**Properties of Fluorinated Graphene Films**". *Nano Lett.* (**2010**) *Vol. 10*, p. 3001-3005.

[24]Mahmood, A. **Towards graphene based mono-molecular electronics: Stuctural and electrical characterization.** PhD thesis, Université Paul Sabatier Toulouse III, (**2009**).

[25] Lee, C.; Wei, X.; Kysar, J. W.; Hone, J. "**Measurement of the Elastic Properties and Intrinsic Strength of Monolayer Graphene**". *Science* (**2008**) *Vol. 321*, p. 385-388.

[26] Berciaud, S.; Ryu, S.; Brus, L. E.; Heinz, T. F. "**Probing the Intrinsic Properties of Exfoliated Graphene: Raman Spectroscopy of Free-Standing Monolayers**". *Nano Lett.* (**2009**) *Vol. 9*, p. 346-352.

Conclusion.

L'objectif principal de ce travail de thèse est l'intégration de méthode de dépôt de graphène sur substrat isolant, de contact électrique et de structuration multi-échelle depuis la dizaine de micromètres jusqu'à la dizaine de nanomètres en limitant au maximum la contamination et l'amorphisation que nous nous sommes attaché à caractériser par microscopie électronique. Par ailleurs, l'extension de ce travail étant destiné à une ingénierie du graphène jusqu'à l'échelle moléculaire voire atomique, il est essentiel que l'ensemble des méthodes de structuration, contact et caractérisation soit compatible avec un futur environnement en ultravide.

Dans un premier temps, cet objectif nous a conduit à caractériser la monocouche de graphène sur substrat isolant par des méthodes spectrosco-

The main objective of this work is the integration of methods like deposition of graphene on insulating substrate, electrical contact and multi-scale patterning of graphene, from tens of micrometers to tens of nanometers with a minimal contamination and amorphization that we characterized by electron microscopy. Moreover, the extension of this work is intended for engineering graphene to atomic or molecular scale, it is essential that all the structuring methods, contact and characterization are compatible with a future UHV environment.

At first, this goal has led us to characterize the monolayer graphene on insulating substrate by spectroscopic methods such as

piques, comme la spectroscopie Raman, et microscopiques, comme la microscopie à force atomique ou la microscopie électronique. Bien qu'il soit désormais admis que le graphène déposé sur un substrat de silice thermique ait, dans des conditions ambiantes, une épaisseur apparente variable d'au moins 0.5-1.0 nm, aucune étude détaillée ne donnait des conditions de mesure AFM fiables ni ne cherchaient l'origine de cette épaisseur supérieure à la distance interplanaire du graphite (0.345 nm). Nous avons montré qu'une des causes de la forte variabilité des mesures AFM en mode intermittent était liée à des conditions d'imagerie pour lesquelles la consigne d'amplitude de vibration de la pointe AFM, Asp excède une valeur seuil et à une humidité relative ambiante comprise entre 40 et 60%. La formation d'un ménisque d'eau entre la pointe et la surface solide résulte alors en une situation stable d'imagerie de la silice, hydrophile, mais une situation d'imagerie instable de la surface de graphène, de sorte que la hauteur apparente du graphène est alors surestimée de 0.7 nm. Pour éviter cet artefact, l'amplitude de vibration de la pointe AFM doit être réduite en-deçà des valeurs menant à l'instabilité afin de garantir que le ménisque d'eau soit préservé en cours d'imagerie aussi si bien sur la silice

Raman spectroscopy and microscopic, such as atomic force microscopy or electron microscopy. Although it is now accepted that graphene deposited on a thermal silica substrate has, in ambient conditions, a variable apparent thickness of at least 0.5-1.0 nm, no detailed study gave reliable neither AFM measurement conditions nor seeking the origin of the greater thickness than the interplanar spacing of graphite (0.345 nm). We have shown that the causes of the high variability of AFM measurements in intermittent mode was related to imaging conditions for which the amplitude setpoint of oscillation of the AFM tip, Asp exceeds a threshold value and a relative humidity between 40 and 60%. Forming a meniscus of water between the solid tip and the surface results in a stable imaging over silica, which is hydrophilic, but unstable situation imaging over the graphene surface, so that the apparent height of graphene is overestimated by 0.7to 1.0 nm. To avoid this artifact, the amplitude of oscillation of the AFM tip must be reduced below the values leading to instability to ensure that the water meniscus is preserved during imaging on the silica as

que sur le graphène. Il ne reste alors plus qu'une source de surestimation systématique de l'épaisseur de la monocouche de graphène, la présence d'adsorbats sous le mono-feuillet. Ceux-ci peuvent être éliminés par recuit et un environnement ultravide.

La deuxième technique de caractérisation utilisée est la spectroscopie Raman. Nous avons utilisé l'intensité intégrée du pic G du graphène pour une identification sans ambigüité du nombre de couches composant un dépôt de graphène. Ensuite, nous nous sommes intéressés à l'exaltation du signal Raman, et en particulier celle du pic D, comme moyen de suivre des défauts, dès leurs premières apparitions en cours de nanostructuration du graphène. Pour cela, des prismes et nanobâtonnets cristallins d'or ont été déposés sur ou sous du graphène monocouche. Nous avons observé que les nanobâtonnets exaltaient l'intensité des pics G et G' par des facteurs respectifs de 1.5 et 3.5. La présence de nanobâtonnets au voisinage immédiat du graphène a provoqué une exaltation de l'intensité du pic D du graphène. Toutefois, l'exaltation n'est pas très reproductible, nombre de facteurs n'étant pas maitrisés comme par exemple le dopage du graphène. Bien qu'il soit intéressant de tester ce phénomène en présence d'un bord dé-

well as on the graphene. There remains a source of systematic overestimation of the thickness of the monolayer graphene, in the presence of adsorbates on single sheet. These can be removed by annealing and a UHV environment.

The second technique used for characterization of graphene is the Raman spectroscopy. We used the integrated intensity of the G peak of graphene for unambiguously identify the number of layers of a graphene flake. Then we are interested in the exaltation of the Raman signal and in particular that of the D peak, as a means to track defects, since their first appearances during the nanostructuring of graphene. To do this, prisms and crystal gold nanorods were deposited on or in the graphene monolayer. We observed that the nanorods exalted peak intensity of the G and G 'by factors of 1.5 and 3.5 respectively. The presence of nanorods in the immediate vicinity of graphene caused also an enhancement of the intensity of the D peak of graphene. However, the exaltation is not very reproducible, many factors are not mastered like for example the doping of graphene. Alt-

coupé de graphène, cette approche n'a pas été poursuivie dans l'état d'avancement actuel de compréhension de l'exaltation du signal Raman et notamment de sa faible reproductibilité.

La fabrication, à terme, de structures de graphène multi-échelle dédiées au transport électronique jusqu'aux dimensions moléculaires ou atomiques requerra une méthode d'imagerie du graphène avec une résolution atomique sur substrat isolant. Pour cela, les premières tentatives d'imager du graphène sur silice thermique par AFM non contact en modulation de fréquence en ultravide ont été entreprises. Toutefois, malgré nos efforts, le graphène a été systématiquement détruit lors de l'imagerie. Nous soupçonnons que l'interaction est trop faible entre le graphène et le substrat dont la rugosité nominale (<1 nm) reste par ailleurs trop importante par rapport à l'amplitude d'oscillation de la pointe (quelques nanomètres). D'autres substrats, parmi ceux connus pour permettre une imagerie nc-AFM résolue - KBr, saphir monocristallin et mica - ont été examinés et du graphène monocouche y a été déposé avec succès. Cependant, le contraste optique du graphène monocouche sur ces substrats transparents est extrêmement faible, de sorte que malgré

hough it will be interesting to test this phenomenon in the presence of a graphene cut edge, this approach was not pursued in the current status of understanding of the exaltation of the Raman signal and mainly its low reproducibility.

Manufacturing multi-scale structures of graphene dedicated to electron transport to the molecular or atomic dimensions require an imaging method of graphene with atomic resolution on insulating substrate. For this, the first attempts to image graphene on thermal silica by non-contact AFM in frequency modulation in UHV were undertaken. However, despite our efforts, graphene has been systematically destroyed during imaging. We suspect that the interaction is weak between graphene and the substrate the roughness of which (<1 nm) is also too large compared to the oscillation amplitude of the tip (a few nanometers). Other substrates, including those known to allow imaging in nc-AFM at the atomic or submolecular resolution were examined: KBr, monocrystalline sapphire and mica. Monolayer graphene has been successfully deposited on those substrates. However, the

des recherches aussi longues que vaines, il n'a pas été possible de retrouver le graphène déposé par nc-AFM.

De cette série de trois approches de caractérisation, il apparaît donc que la technique d'exfoliation de graphite fournit du graphène de qualité mais qui est trop peu abondant sur les substrats et trop sujet à contamination lors du dépôt. C'est pourquoi il semble essentiel de développer des méthodes propres, compatibles avec l'ultravide, de transfert du graphène cru par CVD sur films métalliques.

Le travail central de cette thèse qui est présenté aux chapitres 4 et 5, est la structuration directe du graphène par faisceau d'électrons en présence d'un réactif : l'eau. Pour cela, nous avons choisi deux configurations: du graphène multicouche (1 à 10) et suspendu sur des grilles TEM a été utilisé pour mettre au point la gravure de graphène par EBIE et étudier par microscopie électronique la qualité structurale et la propreté du graphène après gravure. Ensuite, notre approche a été appliquée à une configuration plus proche du composant électronique, c'est-à-dire supporté ou

optical contrast of graphene monolayer on the transparent substrates is extremely low, so that despite searches in vain as long as it has not been possible to find graphene deposited nc-AFM.

In this series of three approaches to characterize the graphene, it appears that the technique of graphite exfoliation of graphite provides the best quality but with a too low yield and too sensitive to contamination. This is why it seems essential to develop specific methods compatible with the ultrahigh vacuum, transfer of graphene by CVD on raw metal films.

The central work of this thesis, presented in Chapters 4 and 5, is the patterning of graphene by a focused electron beam in the presence of a reagent: water. For this aim, we chosen two configurations, one is a multilayer graphene (1-10 layers) suspended on TEM grids which was used to develop EBIE of graphene and study its structural quality in an electron microscope after etching. For the second sample, EBIE has been applied to a configuration closer to an electronic component, that is to say, supported

partiellement supporté sur un substrat possédant une grille arrière.

Une première série de travaux a montré la faisabilité de la gravure de graphène avec des électrons de faible énergie (2 à 20 keV) en présence de vapeur d'eau. Les découpes ainsi obtenues ont des largeurs de 10 à 20 nm. La gravure d'une ligne s'effectue par une succession de points d'irradiation espacés régulièrement. Le rapport de cet espacement au diamètre d'un trou (~15 nm) doit être faible (~0.05) pour graver une ligne continue avec des bords aussi lisses que possible. Un paramètre limitant l'efficacité de gravure est la contamination du graphène par des d'espèces carbonées qui s'oppose à l'éjection de matière lors de l'irradiation réactive. Un recuit et un stockage en atmosphère inerte est alors indispensable et permet de partiellement résoudre ce problème qui ne devrait être limité en environnement ultravide. Nous avons étudié en détail les stratégies de gravure permettant de réaliser des motifs complexes à plusieurs segments. et montré qu'il est parfaitement possible de réaliser des découpes de 15 nm de large sur de longues distances (1 μm), ce qui est indispensable lors de la structuration du graphène entre quelques micromètres et la dizaine de nanomètres. Enfin, nous avons montré qu'il est pos-

or partially supported on a substrate possessing a backgate.

A first series of studies has demonstrated the feasibility of graphene etching with low energy electrons (2-20 keV) in the presence of water vapor. The cuts obtained have widths of 10 to 20 nm. Etching a line is done by a succession of regularly spaced spots of irradiation. The ratio of the spacing to the diameter of a hole (~ 15 nm) must be low (~ 0.05) for etching a continuous line with the edges as smooth as possible. A parameter limiting the effectiveness of the etching is the contamination of graphene by carbonaceous species. Annealing and storage in an inert atmosphere is therefore essential and can partially solve this problem, which should be limited by a full UHV environment process. We studied in detail the strategies for achieving cuts with an arbitrary and complex pattern. We shown that it is possible to make cuts of 15 nm wide over long distances (1 μm), demonstrating the multiscale characteristic of this technique. Finally, we have shown that it is possible to produce on a routine basis, of graphene

sible de produire, de manière routinière, des nanorubans de graphène de 20-30 nm de large et plusieurs centaines de nanomètres de long par gravure de deux découpes parallèles. La largeur minimale réalisée est de 20 nm pour 250 nm de long. Nous avons alors entrepris la caractérisation des bords de gravure par microscopie électronique à transmission avec correction d'aberrations qui révèle la très bonne qualité de la découpe par rapport aux techniques actuelles. La rugosité de bord intrinsèque à courte distance (~30 nm) est de 1.3 nm et la rugosité RMS est de 0.4 nm. L'imagerie directe à résolution atomique a montré que le bord de la gravure n'était amorphisée que sur une largeur maximale de 1.5 nm, soit quelques cycles aromatiques. Par ailleurs, il apparaît que la rugosité de bord à longue distance (> 200 nm) résulte de la redéposition de contaminants adsorbés dont l'élimination a été obtenue par recuit de l'échantillon à 250°C en atmosphère réductrice.

Enfin, notre protocole EBIE de gravure des nanorubans de graphène a été appliqué à du graphène supporté par un substrat Si/SiO_2. Deux phénomènes liés à la présence du substrat apparaissent. Sous l'irradiation électronique en présence d'eau, la silice est gravée et une modification substantielle de la morphologie du substrat est

nanoribbons of 20-30 nm in width and several hundred nanometers long by etching two parallel cuts. The minimum width of 20 nm is performed for 250 nm long. We then undertook the characterization of the etched edges by transmission electron microscopy with aberration correction, which reveals the high quality of the cut compared to current techniques. Intrinsic edge roughness at short distance (~ 30 nm) is 1.3 nm and the RMS roughness is 0.4 nm. The direct imaging at atomic resolution showed that the edge of EBIE cuts was amorphized at a maximum length of 1.5 nm, a few aromatic rings. Moreover, it appears that the edge roughness at long distance (> 200 nm) results from a redeposition of adsorbed contaminants whose elimination was obtained by annealing the sample at 250 ° C in a reducing atmosphere.

Finally, our EBIE protocol for etching graphene nanoribbons has been applied to graphene supported by a Si/SiO_2 substrate. Two phenomena related to the presence of the substrate appear. Under electron irradiation in the presence of water, silica is etched

observée. De plus, les électrons rétrodiffusés par la silice élargissent la gravure à plus de 500 nm contre seulement 15-20 nm lorsque le graphène est suspendu. Nous avons donc modifié notre méthode de préparation du graphène afin de le suspendre localement, à 250 nm au-dessus de la silice, ce qui a permis de résoudre ce problème. Toutefois, dans ces conditions, la silice est encore vaporisée du fond de la tranchée et le graphène ainsi partiellement suspendu sur une aire de 1x5 micromètres subi des tensions mécaniques qui élargissent significativement les gravures. Nous nous sommes affranchis de cette tension par la gravure de deux découpes de part et d'autre du motif à réaliser qui retrouve alors la largeur optimum de 30 nm. Ainsi, nous avons démontré qu'il était possible de graver des nanorubans de graphène localement suspendu de 30 nm de large et 200 nm de long par la technique EBIE. Ces nanorubans, réalisés sur des substrats avec une grille arrière ont été contactés par des électrodes métalliques et leur caractérisation en magnéto-transport est possible.

L'objectif de ce travail qui était de développer une méthode de structuration multi-échelle du graphène en évitant la contamination et l'amor-

and a substantial change in the morphology of the substrate is observed. In addition, backscattered electrons in silica extend the etching over 500 nm against only 15-20 nm when graphene is suspended. So we changed our method of preparation of graphene to locally suspend, above a 250 nm deep silica pool, this approach solved this problems. However, under these conditions, silica is still sputtered from the bottom of the trench and partially suspended graphene on an area of a 1x5 micrometers is mechanically strained which significantly enlarge the cuts. We relax this tension by etching two cuts on both sides of the pattern to achieve cut with a typical width of 30 nm. Thus, we have shown that it is possible to perform locally suspended graphene nanoribbons wide of 30 nm and long of 200 nm by EBIE. These nanoribbons, on substrates with backgate were contacted by metallic electrodes and magneto-transport characterization is possible.

The objective of this work was to de-

phisation du mono-feuillet atomique a été, en grande partie, réalisé. La technique de découpe par EBIE en présence de vapeur d'eau est désormais fiable. La qualité des nanorubans semble atteindre celles des autres techniques les plus avancées et l'étude systématique structurale et fonctionnelle des nanorubans ainsi produits est désormais possible. Il est cependant important de noter que la principale limitation à cette approche qui ressort à la fois des expériences de spectroscopie Raman exaltée par les colloïdes d'or, de nos tentatives d'imagerie en nc-AFM et de l'analyse par microscopie électronique à haute résolution des découpes par EBIE est la nécessité impérative de produire, contacter puis structurer le graphène en éliminant au maximum toute source de contamination. D'une manière générale, l'environnement ultravide devra, à terme, être choisi pour les composants. Toutefois, la priorité est de produire le graphène sans adsorbat. Le transfert sans résine du graphène produit par CVD sur métaux que nous avons commencé à développer pourra répondre à ces exigences, à conditions de prévoir un recuit à haute température en atmosphère réductrice ou sous ultravide et donc sur des substrats ne diffusant pas. Dans le cadre des études par TEM à haute résolution, les premiers essais sur des grilles

velop a method of multi-scale structuration of graphene avoiding contamination and amorphization of single-atomic sheet, it has been largely achieved. The water assisted EBIE is now reliable. The quality of the edges of cuts performed by this technique seems to reach those of the best actual techniques and systematic structural and functional study of GNR is now possible. It is important to note that the main limitation to this approach emerges from all the characterization experiences of Raman signal exaltation by gold colloids, attempt of nc-AFM imaging and analysis of the cuts by high resolution electron microscopy is the imperative to produce, then contact the graphene by eliminating any source of contamination. Generally, the UHV environment will eventually have to be chosen for the components. However, the priority is to produce graphene without adsorbate, transfer without resist of graphene produced by CVD on metals that we have started to develop can meet these requirements, if a high-temperature annealing in a reducing atmosphere or ultrahigh vacuum is doable. In the studies using high-resolution TEM, the first

en or montrent une faible diffusion des particules métalliques. Si cette qualité est confirmée, le graphène CVD, de grande extension latérale, pourra être déposé sur des substrats atomiquement plans pour reprendre sa caractérisation en nc-AFM.

Concernant l'EBIE, si les preuves de principes de l'efficacité de cette approche ont été démontrées au cours de ces travaux, une optimisation de la stratégie de gravure des motifs complexes est nécessaire. En particulier l'affinement du choix de la tension d'accélération, du gaz réactif, de la méthode d'accumulation de la dose de gravure devront être encore étudiés. Enfin, il est évident que l'EBIE ne fournit pas encore des structures de graphène à la structure de bords maitrisée à l'échelle atomique. La conjonction d'un redressement des bords par courant Joule ou manipulation d'atomes dans un STM pourrait permettre d'atteindre les objectifs ultimes de structuration du graphène. [1, 2]

Enfin, dans le cas des composants électroniques à base de nanorubans de graphène, l'approche des rubans partiellement suspendus est propice aux mesures de transport. Les mesures de transport électronique des nanorubans de graphène gravés par EBIE peuvent être planifiées ainsi : A basse température faire varier la tension de

annealing tests on gold grids show a more moderate diffusion of metallic particles. If this quality is confirmed CVD graphene of large lateral extent, may be deposited on substrates atomically flat to resume its characterization by nc-AFM.

Concerning EBIE, if the evidence of effectiveness principles of this approach have been demonstrated in this work, an optimization strategy of the etching is required. In particular refinement of the selection of the acceleration voltage, the reactive gas, the method of storage of the etching rate will still be studied. Finally, it is clear that EBIE does not yet provide structures of graphene edges at the atomic scale. The combination of a recovery of edges by Joule heating or manipulation of atoms in STM could achieve the ultimate goals of the graphene patterning. [1, 2]

Finally, in the case of electronic components based on graphene nanoribbons, the approach of partially suspended ribbon is ideal for transport measurements. Elec-

la grille arrière dont on peut en déduire le dopage et la mobilité des porteurs de charge. Cette expérience devrait être répétée avec des rubans de largeur différente afin de savoir à partir de quelle largeur le transport électronique passe à un régime de blocage de coulomb. Cette étude permettrait une nouvelle caractérisation de la qualité de gravure du par EBIE.

Toutefois, la question de la vaporisation de silice imposera d'approfondir la gravure du substrat. Par ailleurs, la relaxation de la tension mécanique observée dans nos échantillons sera essentielle à la préservation des structures de graphène suspendu. L'intégration de la méthode de contact par stencil complètera notre approche d'une production de nanorubans entièrement compatible avec l'UHV.

tronic transport measurements of graphene nanoribbons etched by EBIE can be scheduled as follows: At low temperatures varying the voltage of the gate to tune the doping and deduce the mobility of charge carriers. This experiment should be repeated with ribbons of different widths to see from electron transport what ribbon which lead to Coulomb blockade regime. This study would be a new characterization of the quality of the etching by EBIE.

However, the question of vaporization of silica requires further etching the substrate. In addition, the relaxation of the tension observed in our samples is essential for the preservation of suspended graphene structures. The integration of the contacting method using a stencil complements our approach to the production of nanoribbons fully compatible with UHV.

Références

[1] Jia, X. T.; Hofmann, M.; Meunier, V.; Sumpter, B. G.; Campos-Delgado, J.; Romo-Herrera, J. M.; Son, H. B.; Hsieh, Y. P.; Reina, A.; Kong, J.; Terrones, M.; Dresselhaus, M. S. "**Controlled Formation of Sharp Zigzag and Armchair Edges in Graphitic Nanoribbons**". *Science* (**2009**) *Vol. 323*, p. 1701-1705.

[2] Moser, J.; Barreiro, A.; Bachtold, A. "**Current-induced cleaning of graphene**". *Appl. Phys. Lett.* (**2007**) *Vol. 91*, p. 3.

[1] Jia, X. T.; Hofmann, M.; Meunier, V.; Sumpter, B. G.; Campos-Delgado, J.; Romo-Herrera, J. M.; Son, H. B.; Hsieh, Y. P.; Reina, A.; Kong, J.; Terrones, M.; Dresselhaus, M. S. "**Controlled Formation of Sharp Zigzag and Armchair Edges in Graphitic Nanoribbons**". *Science* (**2009**) *Vol. 323*, p. 1701-1705.

[2] Moser, J.; Barreiro, A.; Bachtold, A. "**Current-induced cleaning of graphene**". *Appl. Phys. Lett.* (**2007**) *Vol. 91*, p. 3.

[1].Jia, X. T.; Hofmann, M.; Meunier, V.; Sumpter, B. G.; Campos-Delgado, J.; Romo-Herrera, J. M.; Son, H. B.; Hsieh, Y. P.; Reina, A.; Kong, J.; Terrones, M.; Dresselhaus, M. S. "**Controlled Formation of Sharp Zigzag and Armchair Edges in Graphitic Nanoribbons**". *Science* (**2009**) *Vol. 323*, p. 1701-1705.

[2].Moser, J.; Barreiro, A.; Bachtold, A. "**Current-induced cleaning of graphene**". *Appl. Phys. Lett.* (**2007**) *Vol. 91*, p. 3.

Summary:

Graphene is one of the most promising candidates to build future electronic devices. Its peculiar electronic properties derive from its atomic structure and are characterized by a two-dimensional electron gas at macroscopic scale and molecular states at the nanometer scale. This thesis work aims at patterning graphene monolayer over this entire range of length scales to produce arbitrarily shaped graphene nanoribbons (GNR) continuously connected to graphene pads. The three main objectives consist in (i) producing, contacting and patterning graphene monolayer down to features size of about 10 nm for a ribbon length of several hundreds of nanometers, (ii) integrating all steps while minimizing contamination to ultimately reach UHV-compatible samples and (iii) etching GNRs while preserving the high crystallinity of graphene and minimizing its amorphization.

The first part will focus on the characterization of the graphene monolayer itself by ambient AFM topography and Raman spectroscopy. We show that these techniques suffer from a poor reproducibility of the height measurement and a limited sensitivity to low defect density. However, the source of AFM instabilities is identified as the presence of a water meniscus. Stable operating conditions are found and yield reproducible height measurements. In order to enhance the Raman signal of defects in graphene, we investigate the intensity evolution near crystalline gold nanorods placed close to graphene edges.

The second part describes in detail how GNR can be etched directly in graphene using a low energy (1-20 keV) electron beam in the presence of water vapor. We show that electron beam induced etching (EBIE) can produce < 20 nm-wide GNRs with length of hundreds of nanometers or micrometer-long trenches to isolate the GNR form the graphene sheet. A particular attention is paid to the characterization of the structural quality of the GNR edges. A spherical aberration corrected TEM analysis demonstrates that the graphene lattice is intact at less than 2 nm from the EBIE-cut edges.

The last part is dedicated to the application of our promising EBIE method to the fabrication of contacted GNR electronic field-effect devices. We show that graphene devices supported on silica are significantly amorphized by backscattered electrons. A new design of devices made of locally suspended graphene is proposed and makes it possible to produce GNRs (typically 30x200 nm) connected to electrodes on a back-gated substrate.

This work opens the way to electrical transport measurements of GNR and, beyond, GNR-based complex structures and constitutes the first step towards an integrated atomic technology of molecular graphene devices.

Keywords: Graphene, E-Beam Induced Etching, AFM, aberration-corrected TEM, Raman spectroscopy molecular electronics

---

Résumé:

Le graphène est l'un des candidats les plus prometteurs pour la fabrication des futurs dispositifs électroniques. Ses remarquables propriétés électroniques découlent de sa structure atomique et sont caractérisés par un gaz bidimensionnel d'électrons à l'échelle macroscopique et des états moléculaires à l'échelle nanométrique. Cette thèse a pour but de structurer le graphène sur une large gamme d'échelle de longueurs pour produire des nano rubans de graphène (GNR) connectés à des électrodes de graphène. Les trois principaux objectifs sont (i) produire, contacter et structurer des GNR jusqu'à une largeur de 10 nm et une longueur de plusieurs centaines de nanomètres, (ii) planifier toutes les étapes de ce processus tout en minimisant la contamination pour obtenir, à terme, des échantillons compatibles avec l'ultravide et (iii) graver des GNRs tout en préservant la qualité cristallographique du graphène et minimisant son amorphisation.

La première partie est dédiée à la caractérisation du graphène monocouche par des analyses topographiques AFM et spectroscopiques Raman. Nous montrons que ces techniques sont limitées, l'une, par une faible reproductibilité de la mesure de la hauteur apparente et l'autre, par une faible sensibilité aux défauts peu denses. Cependant, l'origine de l'instabilité de la mesure AFM a été identifiée comme résultant de la présence d'un ménisque d'eau. Des conditions de fonctionnement stable ont été trouvées et conduisent à des mesures de hauteur apparente reproductibles. Pour augmenter le signal Raman dû aux défauts dans le graphène, nous avons suivi l'évolution de l'intensité du signal dans le voisinage de nano-bâtonnets d'or cristallins placés près des bords du graphène.

Une seconde partie décrit en détail comment nous avons directement gravé des GNR dans le graphène en utilisant un faisceau électronique de faible énergie (1-20 keV) en présence de vapeur d'eau. Nous montrons que la gravure induite par un faisceau électronique (EBIE) produit des GNRs de moins de 20 nm de large et longs de plusieurs centaines de nanomètres ou des tranchées longues de plusieurs micromètres permettant d'isoler un GNR du feuillet de graphène. Une attention particulière a été portée à la caractérisation de la qualité structurale des bords des GNR. La microscopie électronique en transmission avec correcteur d'aberrations montre que le graphène est intact à moins de 2 nm d'un bord de découpe EBIE.

La dernière partie est dédiée à l'application de cette technique EBIE prometteuse pour fabriquer des GNR contactés électriquement dans un dispositif à effet de champ. Nous montrons que des dispositifs de graphène sur silice sont amorphisés de manière significative par des électrons rétrodiffusés. Un nouveau dispositif a été conçu et réalisé qui consiste à suspendre localement le graphène et a permis de fabriquer des GNR (typiquement 30x200 nm) connectés par des électrodes sur un substrat possédant une grille arrière.

Ce travail ouvre la voie pour la mesure de transport électronique dans des GNR et, au-delà sur des structures plus complexes basées sur les GNRs. Il constitue la première étape vers une technologie atomique intégrée pour des dispositifs d'électronique moléculaire à base de graphène.

Mots clés: Graphène, Gravure induite par faisceau électronique, AFM, MET avec correcteur d'aberrations, Spectroscopie Raman et électronique moléculaire.